行政院國家科學委員會補助專題研究計畫 ■ 成 果 報 告
□期中進度報告

冷媒流量和熱通量振盪引起之暫態新冷媒和 FC-72 流動沸騰研究(三)

計畫類別：■ 個別型計畫　　□ 整合型計畫
計畫編號：NSC 96－2221－E－009－133－MY3
執行期間：民國 98 年 08 月 01 日 起至民國 99 年 07 月 31 日

計畫主持人：林清發 教授
共同主持人：
計畫參與人員：陳建安 博士生
許書豪、熊宏嘉、林永龍、楊政陞 碩士生

成果報告類型(依經費核定清單規定繳交)：□精簡報告　■完整報告

本成果報告包括以下應繳交之附件：
□赴國外出差或研習心得報告一份
□赴大陸地區出差或研習心得報告一份
□出席國際學術會議心得報告及發表之論文各一份
□國際合作研究計畫國外研究報告書一份

處理方式：除產學合作研究計畫、提升產業技術及人才培育研究計畫、列管計畫及下列情形者外，得立即公開查詢
□涉及專利或其他智慧財產權，□一年□二年後可公開查詢

執行單位：國立交通大學機械工程研究所

中　華　民　國　九十九　年　　十　　月　　日

摘要

本研究以實驗方式探討冷媒流量或熱通量週期性振盪對流動沸騰熱傳(含飽和、次冷流動沸騰及蒸發熱傳)及相關氣泡特徵和蒸發流譜之影響。主要針對 HFCs 冷媒(R-134a，R-407C 及 R-410A)在雙套管中與 FC-72 在矩形管中的飽和及次冷態流動沸騰進行實驗。除外，也將對這三種 HFC 冷媒在雙套管中的蒸發熱傳進行量測。雙套管的間隙大小對沸騰和蒸發熱傳的影響將深入探討。雙套管測試段則由玻璃外管及加熱內銅管組成來量測熱傳係數及流場觀測。一電橋式加熱棒置於銅管內部提供熱通量加熱狹窄流道內流動之冷媒。矩形管測試段其加熱段為一置於矩形管底部之圓盤型銅板，以模擬電子冷却情形，加熱段之上方設計有壓克力視窗以利沸騰現象觀測。

首先第一部分，提出 HFCs 冷媒(R-134a，R-407C 及 R-410A)在雙套管中與 FC-72 在矩形管中，在冷媒流量週期性振盪對飽和、次冷流動沸騰及蒸發熱傳之測試結果。從所量測之實驗結果發現，當所施加之熱通量接近穩態流動沸騰成核所需的起始熱通量時，會有間歇性流動沸騰現象產生。而在次冷流動沸騰下，間歇性流動沸騰現象會發生的實驗參數範圍則是更小。隨著增加所施加之熱通量，則會由間歇性流動沸騰現象轉換成持續流動沸騰現象。此外，冷媒流量週期性振盪對經由時間平均的沸騰曲線及熱傳係數幾乎沒有影響。並且，壁溫、氣泡特徵和蒸發流譜會隨著冷媒流量週期性振盪，而有相同頻率的震盪。再者，在持續流動沸騰下長週期或大振幅時會導致壁溫、氣泡特徵振盪更為強烈。從流場觀測之結果顯示在第一個半週期時氣泡脫離尺寸隨著質通量減小而增加、氣泡脫離頻率隨著質通量減小而減小，但是氣泡成核址密度則隨著質通量減小而增加，在第二個半週期時則有相反趨勢。冷媒流量週期性振盪時氣泡脫離尺寸和氣泡成核址密度比氣泡脫離頻率更佔有主導影響因素，所以會造成隨著質通量減小而壁溫下降、熱傳係數上升與單相強制對流時相反的趨勢。但是，振盪週期對於氣泡特徵的影響是不明顯的。除此之外，在中間乾度時經由冷媒流量週期振盪，則會造成蒸發流譜由成核沸騰主導轉換成液膜所主導呈週期性改變。最後，我們把這個實驗中間歇性流動沸騰現象所占有的實驗參數範圍資料作分析，求出間歇性流動沸騰之邊界經驗式。

接著第二部分，提出 HFCs 冷媒(R-134a，R-407C 及 R-410A)在雙套管中與 FC-72 在矩形管中，在熱通量週期性振盪對飽和、次冷流動沸騰及蒸發熱傳之測試結果。從所量測之實驗結果發現，當所施加之平均熱通量接近穩態流動沸騰成核所需的起始熱

通量時，會有間歇性流動沸騰現象產生。而在次冷流動沸騰下，間歇性流動沸騰現象會發生的實驗參數範圍則是更小。隨著增加所施加之平均熱通量，則會由間歇性流動沸騰現象轉換成持續流動沸騰現象。此外，熱通量週期性振盪對經由時間平均的沸騰曲線及熱傳係數幾乎沒有影響。並且，壁溫、氣泡特徵和蒸發流譜會隨著熱通量週期性振盪，而有相同頻率的震盪。再者，在持續流動沸騰下長週期或大振幅時會導致壁溫、氣泡特徵振盪更為強烈。從流場觀測之結果顯示在第一個半週期時氣泡脫離尺寸隨著熱通量減小而減小、氣泡脫離頻率隨著熱通量減小而減小、氣泡成核址密度隨著熱通量減小而減小，在第二個半週期時則有相反趨勢。除此之外，在中間乾度時經由熱通量週期振盪，則會造成蒸發流譜由成核沸騰主導轉換成液膜所主導週期性改變。最後，我們把這個實驗間歇性流動沸騰現象所占有的實驗參數範圍資料作分析，求出間歇性流動沸騰之邊界經驗式。

關鍵字: 週期性流動沸騰，週期性蒸發熱傳，冷媒 R-134a，冷媒 R-407C，冷媒 R-410A，FC-72，氣泡特徵，蒸發熱傳流譜，狹窄雙套管，流量振盪，熱通量振盪

ABSTRACT

Experiments have been conducted here to investigate how the imposed time periodic refrigerant flow rate or heat flux oscillation affects the saturated and subcooled flow boiling heat transfer and associated bubble characteristics for refrigerants R-134a, R-407C and R-410A and for dielectric coolant FC-72. Besides, the evaporation heat transfer of R-134a flow in the same duct are examined. The test section for the horizontal annular duct consists of an outer pipe made of Pyrex glass and an inner heated copper pipe, intending to measure the boiling heat transfer coefficient and to facilitate the visualization of boiling processes. A cartridge heater is installed inside the inner pipe to provide the required heat flux to the refrigerant flow in the narrow annular duct. In the study the gap of the duct is varied from 1.0 to 5.0 mm with the mean refrigerant mass flux, saturated temperature, imposed heat flux and mean vapor quality respectively ranging from 100 to 600 kg/m^{2}s, 5 to 15℃, 0 to 45 kW/m^2 and 0.05 to 0.95. The inlet subcooling is varied from 3 to 6℃. In particular, attention is focused on the time periodic flow boiling characteristics affected by the mean levels, amplitudes and periods of the flow rate or heat flux oscillation.

Some results have been obtained and are reported here. In the first part of the present study, experiments have been carried out to investigate the effects of the imposed time periodic refrigerant flow rate oscillation in the form of nearly a triangular wave on the saturated and subcooled flow boiling and evaporation heat transfer and associated bubble characteristics of refrigerants R-134a, R-407C and R-410A and for dielectric coolant FC-72. The results indicate that when the imposed heat flux is close to that for the onset of stable flow boiling, intermittent flow boiling appears in which nucleate boiling on the heated surface only exists in a partial time interval of each periodic cycle. But the intermittent boiling prevails in narrower ranges of the experimental parameters in the subcooled flow boiling. At somewhat higher heat flux persistent boiling prevails. Besides, the refrigerant flow rate oscillation is found to negligibly affect the time-average boiling curves and heat transfer coefficients. Moreover, the heated wall temperature, bubble departure diameter and frequency, active nucleation site density, and evaporating flow pattern are noted to oscillate periodically in time as well and at the same frequency as the imposed mass flux oscillation. Furthermore, in the persistent boiling the resulting T_w oscillation is stronger for a longer period and a larger amplitude of the mass flux oscillation. And for a larger amplitude of the mass flux oscillation, stronger temporal oscillations in d_p, f and n_{ac} are noted. Specifically, in the first half of the periodic cycle in which the mass flux decreases with time the departing bubbles are larger and the departure rate is lower but

the active nucleation site density is higher. The opposite is the case in the second half of the cycle in which the mass flux increases. The effects of the mass flux oscillation on the departing bubble size and active nucleation site density dominate over the bubble departure frequency, causing the heated wall temperature to decrease and heat transfer coefficient to increase at reducing G in the flow boiling, opposing to that in the single-phase flow. But the bubble characteristics are only mildly affected by the period of the mass flux oscillation. However, a short time lag in the T_w oscillation is also noted. Finally, flow regime maps are provided to delineate the boundaries separating different boiling regimes for the R-134a saturated and subcooled flow boiling in the annular duct.

Moreover, at the intermediate vapor quality changes in the evaporating flow patterns between that dominated by the nucleation bubbles and liquid film resulting from the refrigerant flow rate oscillation take place cyclically. Furthermore, after the time lag the heated pipe wall temperature decreases and the evaporation heat transfer gets better as the mass flux decreases in the first half of the periodic cycle. In the second half of the cycle in which the mass flux increases the opposite processes occur. These unusual changes of the heating surface temperature and heat transfer coefficient with the mass flux oscillation are attributed to the strong effects of the mass flux oscillation on the state of the refrigerant at the duct inlet and hence on the changes of the vapor quality and liquid film thickness in the evaporating flow.

In the second part of the present study, experiments are conducted to investigate how the imposed time periodic heat flux oscillation also in the form of nearly a triangular wave on the refrigerants R-134a, R-407C and R-410A and for dielectric coolant FC-72 saturated and subcooled flow boiling and evaporation heat transfer and associated bubble characteristics in a horizontal narrow annular duct. The results also show that when the mean imposed heat flux is close to that for the onset of stable flow boiling, intermittent flow boiling appears in which nucleate boiling on the heated surface only exists in a partial interval of each periodic cycle. But the intermittent boiling appears in narrower ranges of experimental parameters in the subcooled flow boiling. At somewhat higher heat flux persistent boiling prevails. Besides, the heat flux oscillation does not noticeably affect the time-average boiling curves and heat transfer coefficients. Moreover, the heated wall temperature, bubble departure diameter and frequency, active nucleation site density, and evaporating flow pattern are found to oscillate periodically in time as well and at the same frequency as the imposed heat flux oscillation. Furthermore, in the persistent boiling the resulting oscillation amplitudes of the heated surface temperature, heat transfer coefficient and bubble parameters, such as d_p, f and n_{ac}, get larger for a longer period and a larger

amplitude of the imposed heat flux oscillation and for a higher mean imposed heat flux. A significant time lag in the T_w oscillation is noted. In the first half of the periodic cycle in which the heat flux decreases with time, after the time lag the heated wall temperature decreases with time, so does the bubble parameters. The opposite processes occur in the second half of the cycle in which q increases with time. Finally, flow regime maps are provided to delineate the boundaries separating different boiling regimes for the R-134a saturated and subcooled flow boiling in the annular duct.

Moreover, at the intermediate vapor quality changes in the evaporating flow patterns between that dominated by the nucleation bubbles and by the liquid film resulting from the heat flux oscillation take place cyclically. Furthermore, after the time lag the heated pipe wall temperature decreases and the evaporation heat transfer gets worse as the heat flux decreases in the first half of the periodic cycle. In the second half of the cycle in which the heat flux increases the opposite processes occur. These changes of the heating surface temperature and heat transfer coefficient with the heat flux oscillation are attributed to the strong effects of the heat flux oscillation on the changes of the vapor quality and liquid film thickness in the evaporating flow.

Keywords : Time periodic flow boiling, Time periodic evaporation, Heat transfer, R-134a, R-407C, R-410A, FC-72, Bubble characteristics, Evaporating flow pattern, Flow rate oscillation, Heat flux oscillation, Mini-channel

CONTENTS

ABSTRACT(CHINESE) **i**

ABSTRACT(ENGLISH) **iii**

CONTENTS **vi**

NOMENCLATURE **x**

CHAPTER 1 INTRODUCTION **1**

1.1 Motivation 1

1.2 Literature Review 2

1.2.1 Stable flow boiling heat transfer 2

1.2.2 Time Dependent Flow Boiling Heat Transfer 4

1.2.3 Flow Patterns and Bubble Characteristics 6

1.2.4 Correlation Equations for Flow Boiling Heat Transfer 7

1.3 Objective of the Present Study 8

CHAPTER 2 EXPERIMENTAL APPARATUS AND PROCEDURES **13**

2.1 Refrigerant Flow Loop 13

2.2.1 Test Section (Annular Duct) 14

2.2.2 Test Section (Rectangular Duct) 15

2.3 Water Loop for Preheater 16

2.4 Water-Glycol Loop 16

2.5 Programmable DC Power Supply 17

2.6 Photographic System 17

2.7 Data Acquisition 18

2.8 Experimental Procedures 18

CHAPTER 3 DATA REDUCTION **32**

3.1 Single-Phase Heat Transfer Coefficient 32

3.2 Two-Phase Heat Transfer Coefficient 33

3.3 Flow Boiling Bubble Characteristics 35

3.4 Uncertainty Analysis 36

CHAPTER 4 Time Periodic Saturated Flow Boiling Heat Transfer of

R-134a and Associated Bubble Characteristics in a Narrow Annular Duct due to Flow Rate Oscillation **38**

4.1 Single-Phase Heat Transfer 38

4.2 Time-Average Boiling Curves and Heat Transfer Coefficient 39

4.3 Time Dependent Flow Boiling Heat Transfer Characteristics 40

4.4 Intermittent Flow Boiling 42

4.5 Bubble Characteristics in Time Periodic Flow Boiling 43

4.6 Concluding Remarks 47

CHAPTER 5 Time Periodic Subcooled Flow Boiling Heat Transfer of R-407C and Associated Bubble Characteristics in a Narrow Annular Duct due to Flow Rate Oscillation **72**

5.1 Single-Phase Heat Transfer 72

5.2 Stable and Time-average Saturated Flow Boiling Curves and Heat Transfer Coefficients 73

5.3 Time Periodic Flow Boiling Heat Transfer Characteristics 74

5.4 Intermittent Flow Boiling 77

5.5 Time Periodic Bubble Characteristics in Saturated Flow Boiling 77

CHAPTER 6 Time Periodic Evaporation of R-410A in Narrow Annular Duct due to Mass Flux Oscillation **147**

6.1 Single-Phase Heat Transfer 148

6.2 Stable and Time-average Evaporation Heat Transfer Coefficients 149

6.3 Time Periodic Evaporation Heat Transfer Characteristics 150

6.4 Characteristics of Time Periodic R-410A Evaporating Flow 152

CHAPTER 7 Transient Saturated Flow Boiling of FC-72 over a Small Heated Copper Plate **213**

7.1 Single-phase Liquid Convective Heat Transfer 213

7.2 Stable and Time-average Saturated Flow Boiling Curves and Heat Transfer Coefficient 214

7.3 Transient Flow Boiling Heat Transfer Characteristics 216

7.4 Transient Bubble Characteristics in Saturated Flow Boiling 218

7.5 Correlation Equations 221

CHAPTER 8 Time Periodic Saturated Flow Boiling Heat Transfer of R-134a and Associated Bubble Characteristics in a Narrow Annular Duct due to Heat Flux Oscillation 334

8.1 Time-Average Boiling Curve and Heat Transfer Coefficient 335

8.2 Time Dependent Flow Boiling Heat Transfer Characteristics 335

8.3 Intermittent Flow Boiling 336

8.4 Effect of Heat Flux Oscillation at Extremely Short and Long Periods 337

8.5 Effect of Heat Flux Oscillation Amplitude 338

8.6 Bubble Characteristics in Time Periodic Flow Boiling 338

8.7 Concluding Remarks 341

CHAPTER 9 Time Periodic Saturated Flow Boiling of R-410A in a Narrow Annular Duct due to Heat Flux Oscillation 364

9.1 Time-average Saturated Flow Boiling Curves and Heat Transfer Coefficients 365

9.2 Time Periodic Flow Boiling Heat Transfer Characteristics 365

9.3 Intermittent Boiling 366

9.4 Effect of Heat Flux Oscillation at Extremely Short and Long Periods 367

9.5 Effect of Heat Flux Oscillation Amplitude 368

9.6 Time Periodic Bubble Characteristics in Saturated Flow Boiling 368

CHAPTER 10 Time Periodic Evaporation of R-410A in Narrow Annular Duct due to Heat Flux Oscillation 424

10.1 Stable and Time-average Evaporation Heat TransferCoefficients 425

10.2 Time Periodic Evaporation Heat Transfer Characteristics 425

10.3 Effect of Heat Flux Oscillation at Extremely Short and Long Periods 427

10.4 Effect of Heat Flux Oscillation Amplitude 427

10.5 Characteristics of Time Periodic R-410A Evaporation Flow 428

CHAPTER 11 Transient Oscillatory Saturated Flow Boiling of FC-72

Over a Small Heated Copper Plate **489**

11.1 Single-phase Liquid Convective Heat Transfer 490

11.2 Stable and Time-average Saturated Flow Boiling Curves and Heat Transfer Coefficient 491

11.3 Transient Saturated Flow Boiling Heat Transfer Characteristics 492

11.4 Intermittent Boiling 493

11.5 Effects of Heat Flux Oscillation at Very Short and Long Periods 494

11.6 Bubble Characteristics 495

11.7 Correlation Equations 499

CHAPTER 12 CONCLUDING REMARKS **657**

12. Concluding Remarks 657

12.1.1 Concluding remarks for mass flux oscillation 657

12.1.2 Concluding remarks for heat flux oscillation 658

REFERENCES **661**

NOMENCLATURE

A	heat transfer area of the annular duct, m^2
A_{Tw}	amplitude of the heated wall temperature oscillation, ℃
Bo	Boiling number, $Bo=\frac{q}{G \cdot i_{fg}}$, dimensionless
$\overline{Bo}$	time-average Boiling number, $\overline{Bo}=\frac{q}{\overline{G} \cdot i_{fg}}$, dimensionless
c_p	specific heat, J/kg℃
D	diameter of duct, m
D_h	hydraulic diameter, m, $D_h = 4A_c/P = (D_o - D_i)$
d_P	bubble departure diameter, m
f	bubble generation frequency
f_f	friction factor
F_f	fluid-dependent parameter
Fr	Froude number, $Fr=\frac{G^2}{\rho_l^2 \cdot g \cdot D_h}$, dimensionless
g	acceleration due to gravity, m/s^2
G, $\overline{G}$	instantaneous and time-average mass fluxes, kg/m^2s
h	heat transfer coefficient, W/m^2℃
i_{fg}	enthalpy of vaporization, J/kg
I	measured current from DC power supply, A
Ja_1	Jakob number based on ΔT_{sat}, $Ja_1=\frac{\rho_l \cdot C_p \cdot \Delta T_{sat}}{\rho_g \cdot i_{fg}}$, dimensionless
Ja_2	Jakob number based on ΔT_{sub}, $Ja_2 = \frac{\rho_l \cdot C_p \cdot \Delta T_{sub}}{\rho_g \cdot i_{fg}}$, dimensionless
k	thermal conductivity, W/m℃
L	heating length of the annular duct, m
N_{ac}	active nucleation site density, n/m^2

N_{conf} Confinement number, $N_{conf}=\frac{(\sigma/(g\Delta\rho))^{0.5}}{D_h}$, dimensionless

Nu Nusselt number, $Nu=\frac{hD_h}{k}$, dimensionless

P system pressure, kpa

Pr Prandtl number, $Pr=\frac{\mu \cdot C_p}{k}$, dimensionless

q, $\bar{q}$ instantaneous and time-average imposed heat flux, W/m^2

Q heat transfer rate, W

R radius of duct, m

Ra Rayleigh number, $g\beta\Delta TH^3/\alpha\nu$

$\overline{Re}$ time-average Reynolds number of liquid flow, $\overline{Re}=\frac{\bar{G}D_h}{\mu_l}$, dimensionless

Re_l Reynolds number of liquid in two phase flow, $Re_l=\frac{GD_h(1-x)}{\mu_l}$, dimensionless

t_p period of mass flux and heat flux oscillation, sec

T temperature,℃

T_{sat}, $\bar{T}_{sat}$ instantaneous and time-average saturated temperature of refrigerant, ℃

t_{lf} liquid film thickness, μm

V measured voltage from DC power supply, V

W mass flow rate

We_l Weber number based on liquid, $We_l=\frac{G^2 \cdot D}{\rho_l \cdot \sigma}$, dimensionless

X_{tt} Martnelli parameter

x vapor quality

z coordinate (downstream coordinate for annular duct flow), mm

Greek Symbols

ΔG amplitude of mass flux oscillation, kg/m^2s

Δq amplitude of heat flux oscillation, W/m^2

ΔT	temperature difference, ℃
ΔT_{sat}	wall superheat, $(T_w - T_{sat})$, °C
$\Delta \overline{T}_{sat}$	time-average wall superheat, $(\overline{T}_w - \overline{T}_{sat})$, °C
δ	gap size, mm
μ	viscosity, $N \cdot s / m^2$
ρ	density, kg/m^3
$\Delta\rho$	density difference, $\Delta\rho = \rho_l - \rho_g$, kg/m^3
σ	surface tension, N/m
α	void fraction, dimensionless
ε	mean absolute error, $\varepsilon = \frac{1}{N}\sum_{1}^{N}\left\lvert\frac{\text{predicted value-experimental value}}{\text{experimental value}}\right\rvert$, %
λ	fraction of data predicted to within ±30%, %

Subscripts

ave	average
exp	experimental value
fg	difference between liquid phase and vapor phase
g	vapor
i, o	inside and outside diameter of the smooth pipe
l	all-liquid nonboiling heat transfer
m	average value for the two phase mixture or between the inlet and exit
n	net power input to the refrigerant
p	preheater
r	refrigerant side
s	heater surface
sat	saturated flow boiling
sub	subcooled flow boiling

tp	two-phase
w	duct wall

CHAPTER 1

INTRODUCTION

1.1 Motivation

It is well known that refrigerant R-22 is one of the most widely used working fluids in air-conditioning systems. However, the use of the chlorofluorocarbons refrigerants (CFCS) such as CFC-11, CFC-12, CFC-113, CFC-114, CFC-115 and the hydrochlorofluorocarbons refrigerants (HCFCs) such as R-22 have resulted in the destruction of the ozone layer in the arctic area and the global warming. Thus the Montreal Protocol signed in 1987 only allowed the use of the CFCs up to 1996 and the HCFCs are going to be phased out in 2020. Therefore, the substitution of CFCs and HCFCs becomes urgent. The hydrofluorocarbons refrigerants (HFCs) such as R-134a, R-407C, R-410A, R-410b and R-507 have been considered to be suitable and some are currently in use.

Refrigerant R-410A has zero ozone depletion potential and is recognized as the main replacement to R-22. It is a high pressure and near-azeotropic binary mixture refrigerant consisting of 50 wt% of R-32 and 50 wt% of R-125. This near-azeotropic mixture has a very small temperature glide (0.1 ^{o}C) and behaves like a single component refrigerant. The operating conditions of refrigerants R-410A, R-407C and R-134a are compared in Table 1.1.

In the past, the use of variable frequency compressors in air-conditioning and refrigeration systems to meet the changing heat load is found to significantly improve their energy efficiencies. It is important to note that the two-phase flow in these systems is subject to time varying refrigerant flow rate and heat flux. The use of compact heat exchangers to promote the thermal performance of these systems is beneficial because of their low thermal resistance, very high ratio of surface area to volume, and lower total mass of working fluids.

Additionally, it is also well known that the IC junction temperature must be kept under 85℃ to avoid being damaged and to maintain its normal operation. The use of the direct liquid cooling accompanying with phase change can greatly increase the heat

removal rate, but the power dissipation in IC chips are often time dependent in practical operation. Therefore, the transient oscillatory flow boiling resulting from varying heat load needs to be explored.

In view of the possible enhancement of heat transfer in small channels, we require to develop smaller and more compact evaporators and condensers. Despite the great effort has been paid to the investigation of single- and two-phase flow and heat transfer in small channels from the heat transfer research community, the detailed heat transfer mechanisms in the small-channel flow boiling remain controversial. A detailed understanding of the phase-change processes in-small channel flow subject to time varying coolant flow rate or imposed heat flux is essential in thermal design for electronics cooling and air-conditioning and refrigeration systems. Although considerable research has been carried out in the past for the two-phase flow and heat transfer under the condition of fixed flow rate and imposed heat flux, the corresponding research for the transient oscillatory flow rate or imposed heat flux remains largely unexplored. In the present study an initial attempt is made to unravel how the characteristics of flow boiling and associated heat transfer and bubble motion in a narrow annular channel are affected by given time periodic refrigerant flow rate or imposed heat flux oscillation.

1.2 Literature Review

In sizing the small channels, Kandlikar and Grande [1] proposed that D_h >3mm for the conventional channels, 200μm< D_h <3mm for the mini-channels, 10μm < D_h <200μm for the micro-channels, 0.1μm < D_h <10μm for the transitional channels, 1μm < D_h <10μm for the transitional micro-channels, 0.1μm < D_h <1μm for the transitional nano-channels, and $D_h \leq 0.1\mu m$ for the molecular nano-channels. On the other hand, Kew and Cornwell [2] introduced a dimensionless group named as the Confinement number, $N_{conf} = \frac{(\sigma/(g\Delta\rho))^{0.5}}{D_h}$, which represents the importance of the restriction of the flow by the small size of the channel. They showed that when N_{conf} >0.5, the effects of the channel size become very important.

1.2.1 Stable Flow Boiling Heat Transfer

The literature on stable flow boiling heat transfer is reviewed at first. Here the stable flow boiling denotes the boiling subject to constant imposed flow rate and heat flux. It is

well known that boiling heat transfer for flow inside channels can be regarded as a combination of convective heat transfer from the wall to the liquid and nucleate boiling at the wall. In convection-dominated flow boiling, the heat transfer coefficient is independent of the wall heat flux but increases with increasing mass flux and vapor quality. On the contrary, in nucleation-dominated flow boiling the boiling heat transfer coefficient is independent of the mass flux and vapor quality. However, it increases with the heat flux and is sensitive to the refrigerant saturation pressure level.

Hsieh et al. [3] examined the stable flow boiling heat transfer and associated bubble characteristics of R-410A in a horizontal annular duct. They showed that raising the imposed heat flux can increase the boiling heat transfer coefficient. Wang et al. [4] compared the two-phase heat transfer characteristics of refrigerants R-22 and R-410A. Their results indicate that the evaporative heat transfer coefficients for R-410A are about 10-20% higher than that for R-22. Ebisu and Torikoshi [5] examined the evaporative heat transfer for R-410A, R-407C and R-22. They showed that evaporative heat transfer coefficient of R-410A was about 20% higher than that of R-22 up to the vapor quality of 0.4, while the heat transfer coefficients of R-410A and R-22 became almost the same at the quality of 0.6.

Fujita et al. [6] studied flow boiling heat transfer and pressure drop for refrigerant R-123 in a horizontal small-diameter tube (D_h=1.12 mm). They showed that the flow boiling was dominated by bubble nucleation in the small tube rather than the forced convective evaporation because of very weak influences of the mass velocity and vapor quality. Hsieh et al. [7] investigate the effect of the channel size on R-407C saturated flow boiling heat transfer in a narrow annular duct. The gap of the duct is fixed at 1.0 mm and 2.0 mm. They reported that the saturated flow boiling heat transfer coefficient increased with a decrease in the duct gap. Besides, Lie & Lin [8,9] examined the flow boiling heat transfer and associated bubble characteristics of R-134a in the same duct (D_h = 2&4 mm). The effects of the refrigerant mass flux and saturated temperature on the boiling heat transfer coefficient were found to be small.

Flow boiling of refrigerants R-11 and R-123 in a small horizontal copper tube (D_h=1.95 mm) investigated by Bao et al. [10] showed that the heat transfer coefficients were independent of the refrigerant mass flux and vapor quality, but were a strong function of the heat flux. Nucleate boiling was noted to be the dominant mechanism over a wide

range of flow conditions. A similar study from Tran et al. [11] examined flow boiling of refrigerant R-12 in small circular and rectangular channels (D_h=2.46, 2.4 mm). Two distinct two-phase flow regions were noted, convective boiling dominant region at lower wall superheat (< 2.75K) and nucleate boiling dominant region at higher wall superheat (> 2.75K). Kandlikar and Steinke [12] noted that for a high liquid-vapor density ratio (ρ_l/ρ_g), the convective effects dominated as the vapor quality increased. This led to an increasing trend in the boiling heat transfer coefficient at increasing vapor quality. A high Boiling number results in a higher nucleate boiling contribution, which tends to decrease as the vapor quality increases. This leads to a decreasing trend in heat transfer coefficient with increasing vapor quality. Oh et al. [13] examined flow boiling heat transfer characteristics of R-134a in a capillary tube heat exchanger (D_h=2, 1, 0.75 mm). Their data showed that the heat transfer in the forced convection dominated region was more influenced by the mass flux than by the Boiling number and the heat transfer coefficient was controlled by the Reynolds number.

Yin et al. [14] investigated the subcooled flow boiling heat transfer for refrigerant R-134a flowing in a horizontal annular duct. The gap of duct is 5.16 mm. They found that boiling heat transfer is insignificantly affected by the mass flux, imposed heat flux and refrigerant saturation temperature. But a decrease in the inlet subcooling results in much better heat transfer. Chen et al. [15] investigate how the channel size affects the subcooled flow boiling heat transfer of refrigerant R-407C in a horizontal narrow annular duct(D_h = 1.0 and 2.0 mm). They indicated that the temperature overshoot at ONB is relatively significant. Besides, the subcooled flow boiling heat transfer coefficient increases with a reduction in the duct gap, but decreases with an increase in the inlet liquid subcooling.

1.2.2 Time Dependent Flow Boiling Heat Transfer

In examining two-phase flow instabilities in a circular channel (D_h=9.525mm), Comakli et al [16] found that the periods and amplitudes of the pressure drop and density wave type oscillations decreased with decreasing mass flow rate and increased with decreasing inlet temperature. Recently, some detailed characteristics associated with these intrinsic instabilities were investigated through experimental measurement and theoretical modeling. An experimental investigation of thermal instabilities in forced convection boiling of R-11 in a vertical annular channel (D_h =17 mm) was conducted by Kakac et al. [17]. Two-phase homogeneous model along with the thermodynamic equilibrium

assumption were used to predict the condition leading to the thermal oscillation. And their predicted periods and amplitudes of the oscillations were in a good agreement with their measured data. In a continuing study for R-11 in a horizontal tube of 106 cm long, Ding et al. [18] examined the dependence of the oscillation amplitude and period on the system parameters and located the boundaries of various types of oscillations on the steady-state pressure-drop versus mass flux characteristic curves.

Wang et al. [19] noted that the boiling onset in a upward flow of subcooled water in a vertical tube of 7.8-m long connected with a liquid surge tank could cause substantial flow pressure and density-wave oscillations. These boiling onset oscillations were attributed to a sudden increase of pressure-drop across the channel and a large fluctuation in the water flow rate at the onset of nucleate boiling. This in turn results from the feedback of the pressure-drop and flow rate by the system, causing the location of the boiling onset to move in and out of the channel. Experimental investigation on the critical heat flux was conducted under the forced flow oscillation condition by Ozawa et al. [20]. They found that the reduction of the CHF from the steady state value was larger for increases in the amplitude and period of the flow oscillation.

Kotaoka et al. [21] investigated transient flow boiling of water over a platinum wire subject to an exponentially increasing heat input. The wire diameter and length respectively vary from 0.8 to 1.5 mm and from 3.93 to 10.4 cm. Two types of transient boiling were observed. In A-type (heating period is 20 ms, 50 ms or 10 s) boiling, the transient maximum critical heat flux increases with decreasing heating period at constant flow velocity. Whereas in the B-type (heating period is 5ms, 10ms, or 14ms) boiling, the transient maximum critical heat flux decreases first with the period and then increases. Two-phase flow and heat transfer in a small tube of 1 mm in the internal diameter using R-141b as the working fluid were studied by Lin et al. [22]. At a low heat flux input, a relatively constant wall temperature was obtained. Besides, forced convection evaporation occurs towards the outlet end of the tube and the fluctuations in the wall temperature are small. With a high heat flux input, however, significant fluctuation in the wall temperature can appear. This is caused by a combination of time varying heat transfer coefficient and time varying local pressure and fluid saturation temperature.

The dynamic behavior for a horizontal boiling channel connected with a surge tank for liquid supply has also received some attention. Mawasha and Gross [23] used a

constitutive model containing a cubic nonlinearity combined with a homogeneous two-phase flow model to simulate the pressure-drop oscillation. Their prediction is matched with the measured data. Later, the channel wall heat capacity effects were included [24] to allow the wall temperature and heat transfer coefficient to vary with time.

1.2.3 Flow Patterns and Bubble Characteristics

To elucidate the flow boiling heat transfer mechanisms in small channels, we require to delineate the prevailing flow regimes. Cornwell and Kew [25] examined various flow regimes for boiling of refrigerant R-113 in a vertical rectangular multi-channel with D_h = 1.03 and 1.64 mm. Based on visualization of the flow and measurement of the heat transfer, three flow regimes have been suggested, namely, the isolated bubble, confined bubble and annular-slug bubble flows. In the isolated bubble regime, heat transfer coefficient depends on the heat flux and hydraulic diameter. In the confined bubble regime, heat transfer coefficient depends on the heat flux, mass flux, vapor quality and hydraulic diameter. While in the annular-slug bubble regime, heat transfer coefficient depends on the mass flux, vapor quality and hydraulic diameter.

However, bubble characteristics such as bubble departure frequency, growth, sliding and departure size are known to play an important role in flow boiling heat transfer. Visualization of subcooled flow boiling of upward water flow in a vertical annular channel (D_h=19 mm) by Situ et al. [26] suggested that generally the bubble departure frequency increased as the heat flux increased. The averaged bubble growth rate drops sharply after lift-off. An experimental analysis was carried out by Thorncroft et al. [27] to investigate the vapor bubble growth and departure in vertical upflow and downflow boiling of FC-87. They found that the bubble growth rate and bubble departure diameter increased with the Jacob number(increasing $\triangle T_{sat}$) and decreased at increasing mass flux in both the upflow and downflow. Hsieh et al. [3] examined saturated flow boiling heat transfer and associated bubble characteristics of R-410A in a horizontal annular duct. They concluded that a higher refrigerant mass flux results in a smaller bubble departing size and a higher bubble departure frequency.

Kandlikar [28] examined the subcooled flow boiling of water in a rectangular horizontal channel. They noted that the bubble growth was slow at high subcooling and the departure diameter decreased as the flow rate increased. The influence of the heat flux on

the waiting time between two cycles is much weaker. Chang et al. [29] studied the near-wall bubble behavior for water in a vertical rectangular channel with one-side heated (D_h=4.44 mm). They showed that the size of coalesced bubbles decreased for an increase in the mass flux and the mass flux only exhibited a strong effect on the bubble size. Del Balle and Kenning [30] examined the subcooled flow boiling for water in a rectangular vertical channel and found that the maximum bubble diameter was independent of the heat flux. Yin et al. [14] examined the bubble characteristics associated with subcooled flow boiling of refrigerant R-134a in a horizontal annular duct (D_h=10.31 mm). They noted that the bubble departure frequency was suppressed by raising the mass flux and subcooling of R-134a, and only the subcooling showed a strong effect on the bubble size. The study of water boiling in a horizontal rectangular channel with one side heated (D_h=40 mm) conducted by Maurus et al. [31] found that the waiting time between two bubble cycles decreased significantly at increasing mass flux. An experimental study on bubble rise path after the departure from a nucleation site for water in a vertical upward tube (D_h=20 mm) by Okawa et al. [32] suggested that the inertia force significantly influenced the onset of bubble detachment and the shear force induced a lift force to detach the bubble from the wall.

1.2.4 Correlation Equations for Flow Boiling Heat Transfer

An early general correlation model for the flow boiling in channels was proposed by Chen [33]. He divided the boiling heat transfer coefficient into two parts: a microconvective (nucleate boiling) contribution estimated by the pool boiling correlations and a macroconvective (non-boiling forced convection) contribution estimated by the single-phase correlation such as the Dittus-Boelter equation [34]. In order to account for the diminished contribution of nucleate boiling, as the convective boiling effects increased at a higher vapor quality he introduced the enhanced factor E and suppression factor S to respectively accommodate the forced convective and nucleate boiling contributions. Gungor and Winterton [35] modified the Chen's correlation and proposed the correlations for the enhanced and suppression factors. A new correlation from Liu and Winterton [36] introduced an asymptotic function to predict the heat transfer coefficient for vertical and horizontal flows in tubes and annuli. Zhang et al. [37] modified the Chen's correlation to predict the heat transfer in mini channels. Besides, Tran et al. [11] modified the heat transfer correlation of Lazarek and Black [38] with the Reynolds number of the flow

replaced by the Weber number to eliminate viscous effects in favor of the surface tension. Similar correlations were proposed by Fujita et al. [6].

Kandlikar [39] proposed a general correlation for saturated flow boiling heat transfer inside horizontal and vertical tubes. The correlation was based on a model utilizing the contributions due to nucleate boiling and convective mechanisms. In a following study [40,41], he developed correlations to predict transition, laminar and deep laminar flows in minichannels and microchannels. A new correlation for boiling heat transfer in small diameter channels was proposed by Kew and Cornwell [2]. The correlation was divided by three flow regimes based on the values of the Confinement number. Some empirical correlation equations proposed in the literature for flow boiling heat transfer coefficients in the small channels were summarized in Table 1.2.

1.3 Objective of the Present Study

In recent years, environmental concerns over the use of CFCs as working fluids in refrigeration and air-conditioning systems have led to the development of alternative refrigerants. Among these alternatives, refrigerants R-134a, R-407C and R-410A are often used as substitutes for refrigerant HCFC-22. But the above literature review clearly indicates that the unsteady flow boiling heat transfer of HFC refrigerants in small diameter channels resulting from time varying mass flux and/or heat flux remains largely unexplored. In this study, the R-134a flow boiling and evaporation heat transfer in an annular duct with a small gap between the inner and outer ducts subject to a time periodic mass flux and/or heat flux oscillation with a constant imposed heat flux and/or mass flux are investigated. The effects of the imposed heat flux, gap size, vapor quality, amplitude and period of the mass flux and/or heat flux oscillation, inlet subcooling, and saturation temperature of refrigerant R-134a on the temporal boiling heat transfer characteristics will be examined in detail. Particularly, flow visualization is conducted to examine the bubble characteristics associated with the time periodic flow boiling, intending to improve our understanding of the unsteady flow boiling processes in the narrow channel.

Table 1.1 Comparison of some properties of three HFCs refrigerants for air-conditioning and refrigeration applications

Refrigerant	**R-410A**	**R-134a**	**R-407C**
Component	HFC-32/125	HFC-134a	HFC-32/125/134a
Wt %	50/50%	100 %	23/25/52%
Comparison with R-22	1. near-azeotropic refrigerant. 2. the working pressure is five times than R-22. 3. the frication pressure drop is smaller.	1. the lower working pressure. 2. the frication pressure drop is larger in the same capability of freezing.	1. zeotropic refrigerant, and the components charge easy. 2. the working pressure is same with R-22.
The energy efficiency ratio relative to R-22	94~100	72~90	90~97
Molecule quality	72.6	102.3	85.62
Remark	1. the design of system must to consider the strong and optimum elements.	1. the volume of operating system becomes larger. 2. the air-out volume of compress is larger.	1. the solutions of variation of R-407C components.
Green-house effect (100 years)	1725	1300	1526
Toxicity limit (kg/m^3)	0.44	0.25	0.31
Boiling point (℃)	-52.7 R32 (-51.8℃) / R125 (-48.5℃)	-26.2	-43.6 R32 (-51.8℃) / R125 (-48.5℃) / R134a (-26.2℃)
Temperature glides	＜1 ℉	—	10 ℉

Table 1.2 Heat transfer correlations for flow boiling in small channels

Reference	Fluid	Heat Transfer Coefficient Correlations	Application Range
Lazarek and Black [38]	R-113	$h_{tp} = 30\,\mathrm{Re}_l^{0.857}\, Bo^{0.714}(k_l / D)$	$D: 3.1mm$ $G: 125-750\,kg/m^2 s$ $q: 14-380\,kW/m^2$ $\mathrm{Re}: 860-5500$ $Bo: 2.3\times10^{-4}-76\times10^{-4}$ $P: 1.3-4.1bar$
Y. Fujita et al. [6]	R-123	$h_{tp} = 0.884G^{0.143}q^{0.714}$	$D: 1.12mm$ $G: 50-400\,kg/m^2 s$ $q: 5-20\,kW/m^2$ $\mathrm{Re}: 135-1070$ $P: 1.1-1.2bar$ $x: -0.2-0.9$ $Bo: 3\times10^{-4}-8.9\times10^{-4}$
Z.Y. Bao et al. [10]	R-11, R-123	$h_{tp}/h_l = 1+3000Bo^{0.86}+1.12(x/(1-x))^{0.75}(\rho_l/\rho_g)^{0.41}$	$D: 1.95mm$ $G: 50-1800\,kg/m^2 s$ $q: 50-200\,kW/m^2$ $\mathrm{Re}: 860-5500$ $P: 2-5bar$ $x: -0.3-0.9$ $\Delta T_{sat}: 5-15^oC$
T.N. Tran et al. [11]	R-12, R113	$h_{tp} = \left(8.4\times10^{-5}\right)\left(Bo^2We_l\right)^{0.3}\left(\frac{\rho_l}{\rho_g}\right)^{-0.4}$ for $\Delta T>2.75^{\circ}C$	$D: 2.46mm, 2.92mm; D_h = 2.4mm$ $G: 44-832\,kg/m^2 s$ $q: 7.5-129\,kW/m^2$ $P_r: 0.045-0.2$ $Bo: 2\times10^{-4}-23\times10^{-4}$ $\Delta T_{sat}: 2.8-18.2^oC$

Table 1.2 Continued

Reference	Fluid	Heat Transfer Coefficient Correlations	Application Range
Z. Liu and R.H.S. Winterton [36]		$h_{tp}^{\ 2} = (Fh_l)^2 + (Sh_{pool})^2$ $h_l = 0.023(k_l/D)\,\mathrm{Re}_l^{\ 0.8}\,\mathrm{Pr}_l^{\ 0.4}$ $h_{pool} = 55P_r^{\ 0.12}(-\ln P_r)^{-0.55}M^{-0.5}q$ $F = (1 + x\,\mathrm{Pr}_l(\rho_l/\rho_g - 1))^{0.35}$ $S = (1 + 0.55F^{0.1}\,\mathrm{Re}_l^{\ 0.16})^{-1}$	$D: 2.95 - 32mm$ $G: 12.4 - 8179.3\,kg/m^2s$ $q: 0.35 - 2620\,kW/m^2$ $\mathrm{Re}: 568.9 - 87500$ $\mathrm{P}_r: 0.0023 - 0.895$ $x: 0 - 0.948$ $Fr: 2.66\times10^{-4} - 2240$ $\mathrm{Pr}_l: 0.83 - 9.1$
W. Zhang et al. [37]	R-11, R-123	$h_{tp} = S\cdot h_{pool} + F\cdot h_l$ $S = 1/\left(1 + 2.53\times10^{-6}\,\mathrm{Re}_l^{\ 1.17}\right)$ $h_{pool} = 0.00122\left(\frac{k_l^{\ 0.79}c_{pl}^{\ 0.45}\rho_l^{\ 0.49}}{\sigma^{0.5}\mu_l^{\ 0.29}i_{fg}^{\ 0.24}\rho_g^{\ 0.24}}\right)(T_w - T_{sat})^{0.24}\Delta P_{sat}^{\ 0.75}$ $F = Max\left(0.64\left(1 + \frac{C}{X_{tt}} + \frac{1}{X_{tt}^{\ 2}}\right)^{0.5}, 1\right)$	$D_h = 0.78 - 6mm$ $G = 23.4 - 2939\,kg/m^2s$ $q = 2.95 - 2511\,kW/m^2$ P=0.101-1.21MPa

Table 1.2 Continued

Reference	Fluid	Heat Transfer Coefficient Correlations	Application Range
S.G. Kandlikar [40]		$h_{tp}/h_l = \text{maximun} \quad \text{of} \begin{matrix}[h_{tp}/h_l]_{NBD} \\ [h_{tp}/h_l]_{CBD}\end{matrix}$ Nucleate boiling dominant region $[h_{tp}/h_l]_{NBD} = 0.6683(\rho_l/\rho_g)^{0.1} x^{0.16}(1-x)^{0.64} f(Fr_l)$ $+1058Bo^{0.7}F_f(1-x)^{0.8}$ Convection boiling dominant region $[h_{tp}/h_l]_{CBD} = 1.1360(\rho_l/\rho_g)^{0.45} x^{0.72}(1-x)^{0.08} f_2(Fr_l)$ $+667.2Bo^{0.7}F_f(1-x)^{0.8}$ $f(Fr_l) = \begin{matrix}(25Fr_l)^{0.3} \ for \quad Fr_l < 0.04 \ for H.-tube \\ 1 \ for \quad Fr_l > 0.04 \ for H.\&V.-tube\end{matrix}$	$D: 8.1-20mm \qquad G: 123-1523 kg/m^2 s$ $q: 0.8-82.1 kW/m^2 \qquad P: 1.6-14.8 bar$ $x: 0-0.868 \qquad Bo: 0.035\times10^{-4}-24.02\times10^{-4}$

CHAPTER 2

EXPERIMENTAL APPARATUS AND PROCEDURES

The experimental apparatus used in the present study to investigate the characteristics of time periodic saturated flow boiling, subcooled flow boiling and evaporation heat transfer of refrigerants R-134a in a horizontal narrow annular duct is schematically shown in Fig. 2.1. The apparatus consists of three main loops, namely, a refrigerant loop, a water-glycol loop and a hot-water loop for preheater, along with a data acquisition system and a 100V-50A programmable DC power supply (Chroma 62012P-100-50). Refrigerant R-134a is circulated in the refrigerant loop. We need to control the temperature and flow rate in the water-glycol loop to obtain enough cooling capacity for condensing the refrigerant vapor and for maintaining the refrigerant liquid at a preset temperature. The liquid refrigerant in the narrow duct is heated by passing a DC current through the inner pipe in the test section from the programmable DC power supply. To unravel the bubble characteristics in the boiling of refrigerant on the heating surface, a high-speed movie camera connected to a photographic microscope is set up beside the test section to observe the boiling flow.

2.1 Refrigerant Flow Loop

The main components in the refrigerant loop include an oil-free variable-speed refrigerant pump, an accumulator, a mass flow meter, a test section, a condenser, a sub-cooler, a receiver, a filter/dryer, and four sight glasses. An AC motor is used to control the refrigerant mass flow rate through the change of the inverter frequency. Figure 2.2 schematically shows the control loop for the mass flux oscillation. Specifically, the temporal oscillation of the coolant flow rate can be implemented by an optional external control of the inverter through a programmable DC current or voltage signal sequence. The time-average refrigerant flow rate can also be adjusted by regulating a by-pass valve installed in the by-pass flow path. The refrigerant at the outlet of the refrigerant pump is kept subcooled to avoid any vapor flow through the mass flow meter. The flow meter (Micro motion RFT9739) has an accuracy of ±1%. The preheater is used to heat the

refrigerant to a specified refrigerant state before entering the test section. The vapor generated in the test section is reliquefied in an oversized condenser/subcooler in the cold water-glycol loop. Leaving the subcooler, the liquid refrigerant flows back to the receiver at the bottom of the system. An accumulator is connected to a high-pressure nitrogen tank to dampen the fluctuations of the flow rate and pressure. The filter/dryer is used to filter the impurities and noncondensable gas possibly existing in the loop. Varying the temperature and flow rate of the water-glycol mixture flowing through the condenser and subcooler allows us to control the pressure of the refrigerant loop. Two absolute pressure transducers are respectively installed at the inlet and exit of the test section with a resolution up to ± 2kPa. All the refrigerant and water temperatures are measured by copper-constantan thermocouples (T-type) with a calibrated accuracy of ±0.2℃. The test section is thermally insulated with a polyethylene insulation layer of 19.5 mm thick so that heat loss from it can be reduced significantly.

2.2.1 Test Section (Annular Duct)

The boiling of refrigerant R-134a in an annular duct with a small clearance between the inner and outer pipes is explored. As schematically shown in Fig. 2.3, the test section of the experimental apparatus is a horizontal annular duct with the outer pipe made of Pyrex glass to permit the visualization of boiling processes in the refrigerant flow. The outer Pyrex glass pipe is 160-mm long and 4-mm thick with inside diameter of 20 mm. Both ends of the pipe are connected with a copper tube of the same size by means of flanges and are sealed by O-rings. The inner smooth pipe has 10.0, 16.0 or 18.0 mm nominal outside diameter (the pipe wall thickness is 1.0, 1.5 or 2.5 mm) and is 0.41 m long, so that the hydraulic diameter of the annular duct D_h is 10.0, 4.0 or 2.0 mm (corresponding to the gap size of 5.0, 2.0 or 1.0 mm for the duct). Note that the outside surface of the inner pipe is polished by fine sandpaper. In order to insure the gap between the ducts being uniform, we first measure the average outside diameter of the inner pipe and the mean inside diameter of the Pyrex glass pipe by digital calipers having a resolution of 0.001mm. The absolute accuracy of the measurement is in the range of 0.01 mm. Then we photo the top and side view pictures of the annular ducts and measure the average distance between the inside surface of the Pyrex glass pipe and the outside surface of the inner tube, with an absolute accuracy also in the range of 0.01mm. From the above procedures the duct gap is

ascertained and its absolute uncertainty is estimated to be 0.019 mm. It is also noted that the flow enters the duct long before the heated section so that the entrance effects on the boiling are small. An electric cartridge heater of 160 mm in length and 7.5 mm or12.5 mm in diameter with a maximum power output of 800W is inserted into the inner pipe. Furthermore, the pipe has an inactive heating zone of 10-mm long at each end and is insulated with Teflon blocks and thermally nonconducting epoxy to minimize heat loss from it. Thermal contact between the heater and the inner pipe is improved by coating a thin layer of heat-sink compound on the heater surface before the installation of the heater. Then, 8 T-type calibrated thermocouples are electrically insulated by covering their beads with an electrically nonconducting thermal bond before they are fixed on the inside surface of the inner pipe so that the voltage signals from the thermocouples are not interfered by the DC current passing through the cartridge heater. The thermocouples are positioned at three axial stations along the smooth pipe. At each axial station, two to four thermocouples are placed at top, bottom, or two sides of the pipe circumference with 180° or 90° apart. The outside surface temperature T_w of the inner pipe is then derived from the measured inside surface temperature by taking the radial heat conduction through the pipe wall into account. Figure 2.4 shows the detailed thermocouple locations at each axial station and the arrangement of the cartridge heater.

2.2.2 Test Section (Rectangular Duct)

The test section mainly consists of a circular copper plate flush mounted on the bottom of the horizontal rectangular channel. The rectangular flow-channel includes a gradually diverging section, the main test section, and a gradually converging section (Fig. 2.6). They are all made of stainless steel plate. The installation of the inlet and exit sections intends to avoid the sudden change in the cross section of the channel. The test section is 20 mm in width, 5 mm in height, and 150 mm in length, and hence the aspect ratio of the test section is 4.0. The heated plate is placed around the geometric center of the bottom plate of the test section. A ladder-shaped acrylic window is installed on the upper lid of the test section right above the heated plate. The temperature and pressure of the FC-72 flow at the inlet and exit of the test section are measured by the calibrated thermocouples and pressure transducers, as schematically shown in Fig. 2.6.

The copper plate module schematically shown in Figs. 2.8 and 2.9 includes a hollow

cylindrical Teflon block, a cylindrical Teflon bolt, a copper plate, two pieces of mica plates, a Teflon plate, and an electric-heater. The diameter of the copper plate is 10 mm and the plate is 2 mm thick and is heated by passing DC current through the electric-heater. Besides, three thermocouples are fixed at the back surface of the copper plate to estimate the temperature of the upper surface of the copper plate and another two thermocouples are fixed at the top and bottom surface of the electric-heater to measure their surface temperatures. The locations of the thermocouples at the backside of the copper plate and at the electric-heater surface are shown in Fig. 2.9. The mica plates are placed between the heater and copper plate and between the heater and Teflon plate, intending to prevent the leaking of the DC current to the copper plate. The detailed structure of the module is shown in Fig. 2.10. The magnitude of heat loss from each surface of the cylindrical-hollow Teflon block can be evaluated from the temperature measured at selected locations in the block. Locations of the thermocouples are schematically shown in Fig. 2.11.

2.3 Water Loop for Preheater

In order to maintain the preset refrigerant temperature and vapor quality at the test section inlet, a water loop is used to preheat the refrigerant before it arrives at the inlet. The water loop for the preheater system includes a double-tube heat exchanger, having a heat transfer area of $0.12m^2$, a 125-liter hot water container with three 2.0-kW heaters in it, and a 0.5-hp water pump which can deliver the hot water at specified temperature and flow rate to the preheater. In the preheater the hot water passes through the outer pipe while the liquid refrigerant flows in the inner pipe. The water flow rate is controlled by an AC motor through the change of the inverter frequency and by the by-pass valve. The connecting pipe between the preheater and test section is thermally insulated with a 5-cm thick polyethylene layer to reduce the heat loss from the pipe.

2.4 Water-Glycol Loop

The water-glycol loop is designed for condensing the refrigerant vapor and for subcooling the liquid refrigerant. The water-glycol loop is cooled by a water cooled R-22 refrigeration system. The cooling capacity is 3.5-kW for the water-glycol mixture at -20℃. The cold water-glycol mixture at a specified flow rate is driven by a 0.5-hp pump to the condenser as well as to the subcooler. A by-pass loop is provided to adjust the flow rate. By

adjusting the mixture temperature and flow rate, the bulk temperature of the refrigerant in the subcooler can be controlled at a preset level.

2.5 Programmable DC Power Supply

As described above, the inner pipe in the test section is heated by a 800-W cartridge heater. A 100V-50A programmable DC power supply (Chroma 62012P-100-50) delivers the required electric current to the cartridge heater. The steady or transient oscillatory power input to the cartridge heater is transmitted through a GPIB interface to a personal computer. In order to measure the D.C. current, a precision ammeter (KYORITSU AC/DC DIGITAL CLAMP METER) is arranged in series connection with the electric circuit. Besides, a YOKOGAWA data recorder is used to measure the voltage drop across the test heater assembly. A Yokogawa (WT210) digital power meter is used to measure the DC current through the cartridge heater with an accuracy of ±1%. Thus the power input to the heater can be calculated. Figure 2.12 schematically shows the detailed heat flux control loop for the required heat flux oscillation.

2.6 Photographic System

The photographic apparatus established in the present study to record the bubble characteristics in the time periodic saturated flow boiling, subcooled flow boiling and evaporation in the annular duct consists of an IDT X-Stream^{TM} VISION XS-4 high speed CMOS digital camera, a Mitutoyo micro lens set, a 3D positioning mechanism, a Personal computer, and a Nikon digital camera. The high-speed digital camera can take photographs up to 143,307 frames/s with an image resolution of 512×16. Here, a recording rate of 10,000 frames/s with the highest image resolution of 512×256 is adopted to obtain the images of the bubble ebullition processes in the flow boiling. The digital camera shutter speed can be as short as 1/4000 second in taking the overview of the flow images. The data for some bubble characteristics are collected in the regions around the middle axial location (z = 80 mm). Note that the symbol z denotes the axial coordinate measuring from the inlet of the heated test section. After the experimental system reaches a statistically steady state, we start recording the boiling activity. The high-speed digital camera can store the images which are later downloaded to the personal computer. Then, the time variations of the space-average bubble departure diameter and frequency and active nucleation site

density in a periodic cycle are calculated by viewing more than 1,000 frames at each time instant.

2.7 Data Acquisition

The data acquisition system includes a recorder (Yokogawa MX-100), a 24V-3A power supply, and a controller. The water flowmeter and differential pressure transducer need the power supply as a driver to output an electric current of 4 to 20 mA. The data signals are collected and converted by a hybrid recorder (Micro Motion RFT9739). The converted signals are then transmitted to a host computer through a GPIB interface for further calculation.

The system automatically monitors all the T-Type thermocouples, pressure transducers, differential pressure transducer and mass flowmeters. The thermodynamic and transport properties of the refrigerants are obtained by a manual from AlliedSignal Co. Ltd. and by the ASHRAE handbook [82].

2.8 Experimental Procedures

Before a test is started, the temperature of the refrigerant R-134a under investigation in the test section is compared with its saturation temperature corresponding to the measured saturation pressure and the allowable difference is kept in the range of 0.2-0.3K. Otherwise, the system is re-evacuated and then re-charged to remove the air existing in the refrigerant loop. A vacuum pump is used to evacuate noncondensable gases in the system to a low pressure of 0.067 pa in the loop. In the test for the time periodic flow boiling the refrigerant at the inlet of the test section is first maintained at the liquid state ($x = 0$) and its temperature is kept at the time-average saturated temperature corresponding to the time-average refrigerant pressure or at the preset subcooled temperature by adjusting the water-glycol temperature and flow rate. While for the test of the time periodic evaporation the inlet vapor quality for the refrigerant is also controlled at the preset level. In addition, we adjust the thermostat temperature in the water loop to stabilize the refrigerant temperature at the test section inlet. Next, the temperature and flow rate of the hot-water loop for the preheater are adjusted to keep the vapor quality of R-134a at the test section inlet at the desired value. Then, we regulate the time-average refrigerant pressure at the test section inlet by adjusting the opening of the gate valve locating right after the exit of the

test section. Meanwhile, by controlling the inverter current of the AC motor connecting to the refrigerant pump, the refrigerant flow rate can be varied to procure the preset mean level and the chosen period and amplitude of the mass flux oscillation. More specifically, due to the flow intertia the refrigerant flow rate varies like a triangular wave. The imposed heat flux from the heater to the refrigerant is adjusted by varying the electric current delivered from the programmable DC power supply. By measuring the current delivered to and voltage drop across the heater and by photographing the bubble activity, we can calculate the heat transfer rate to the refrigerant and obtain the bubble characteristics. All tests are run at statistical state conditions. The whole system is considered to be at a statistical state after the initial transients in the starting stage of a test have died out. Then all the data channels are scanned every 0.05 second for a period of 360 seconds.

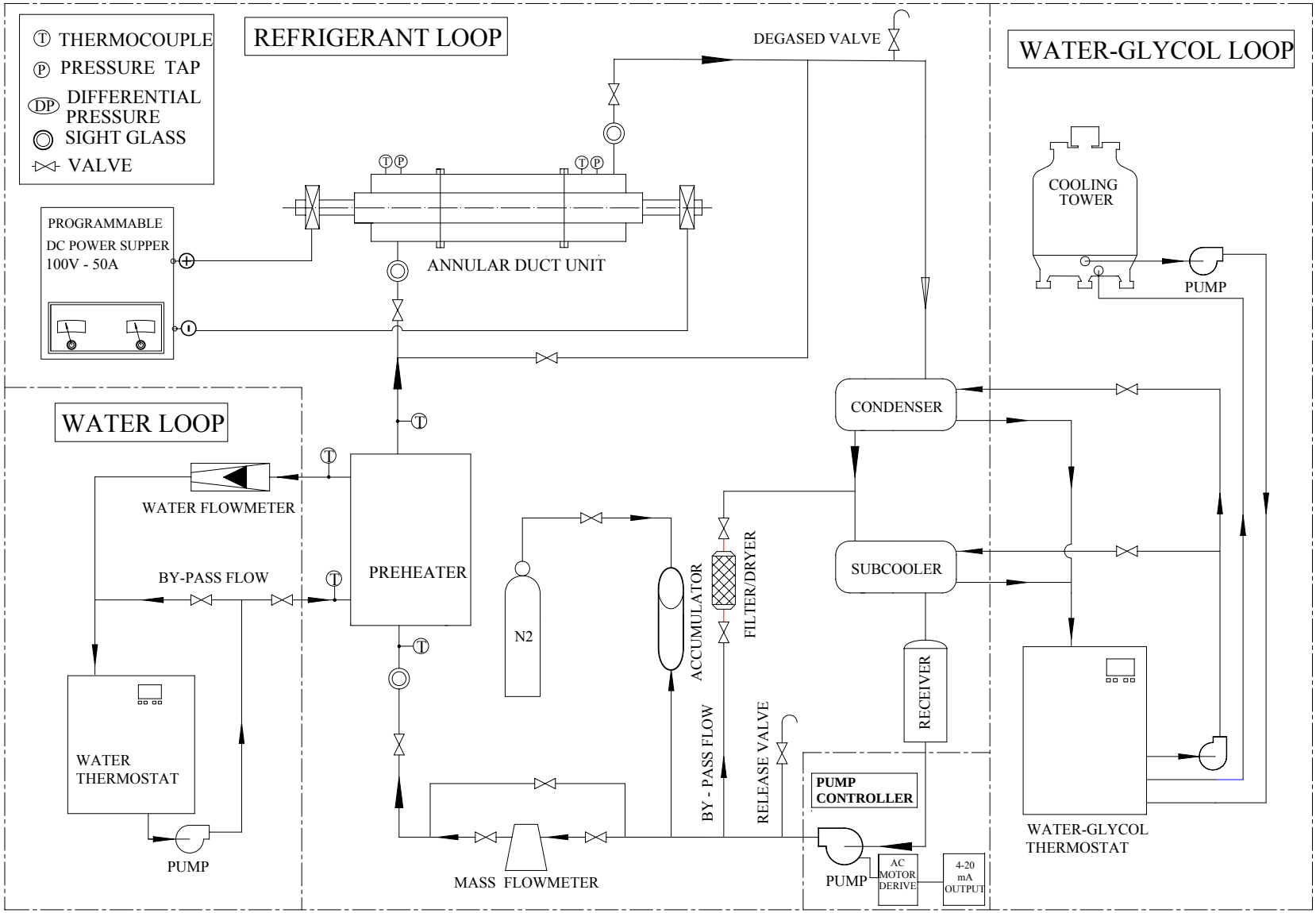


Fig. 2.1 Schematic of experimental system for flow boiling in annular

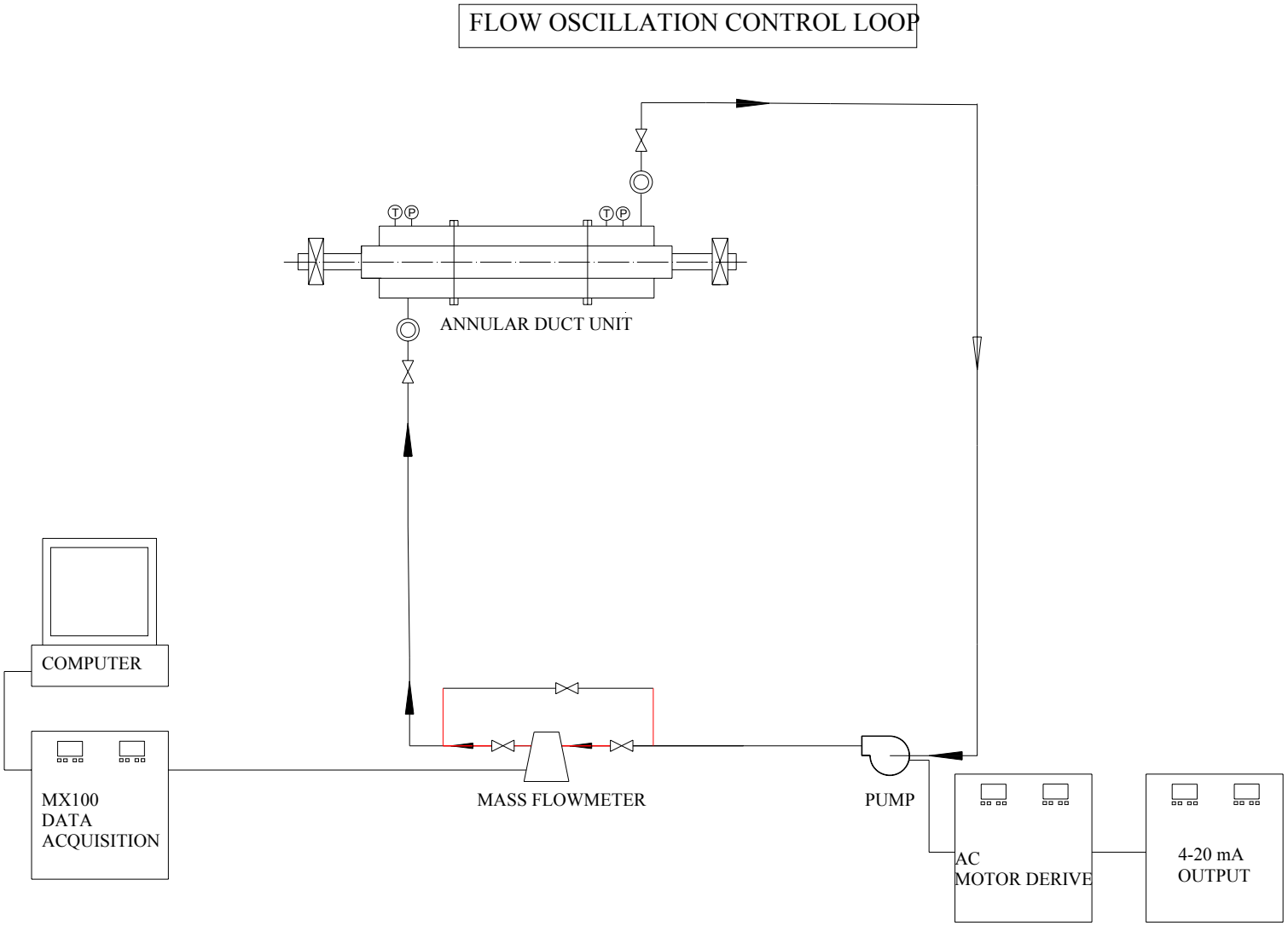
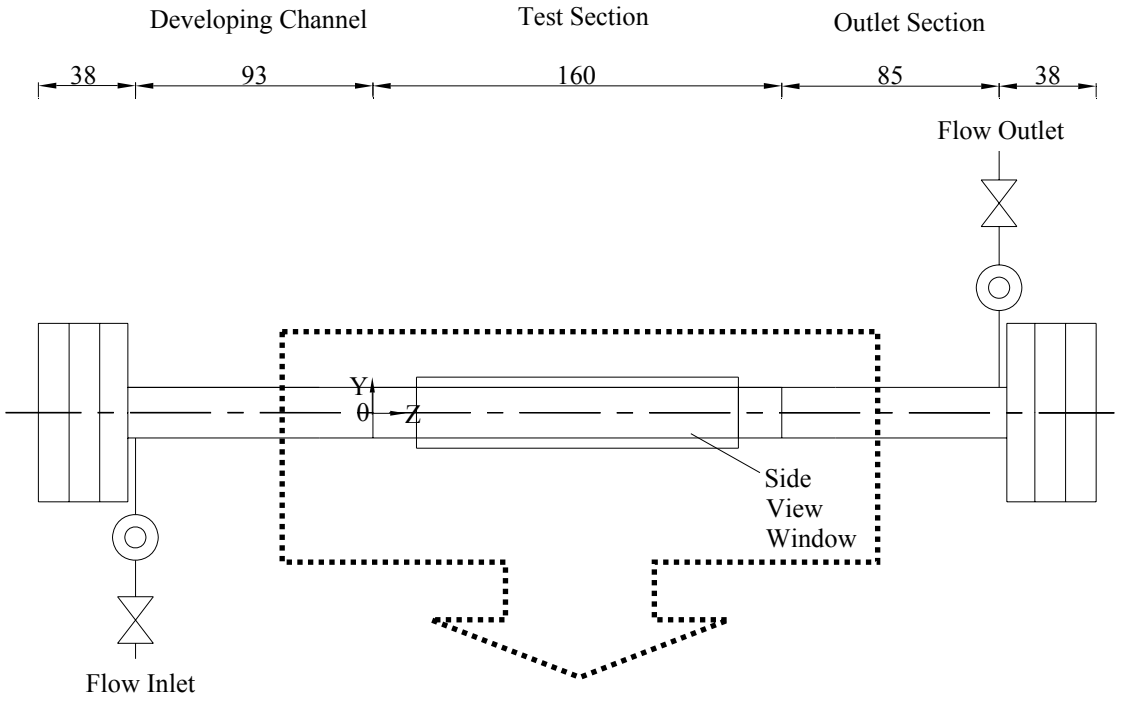


Fig. 2.2 Schematic of mass flux oscillation control loop.



Unit : mm

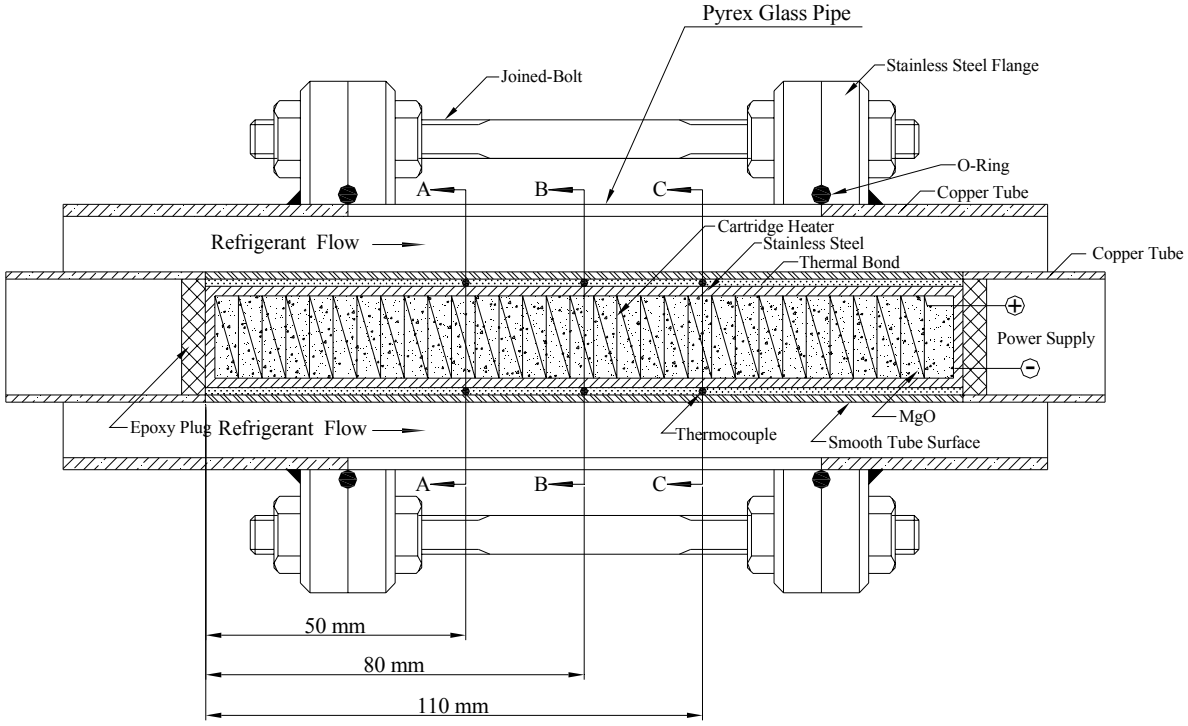
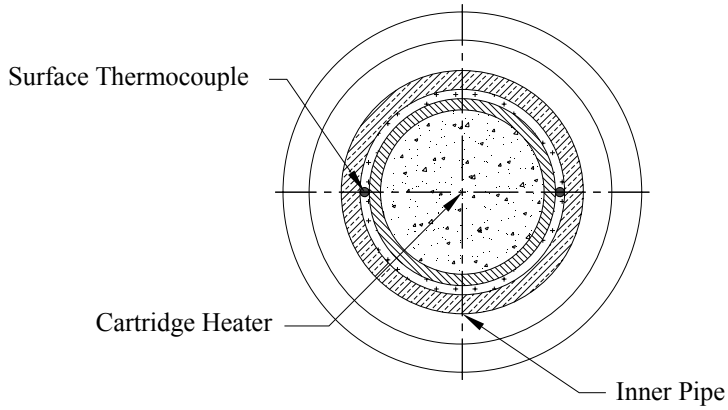
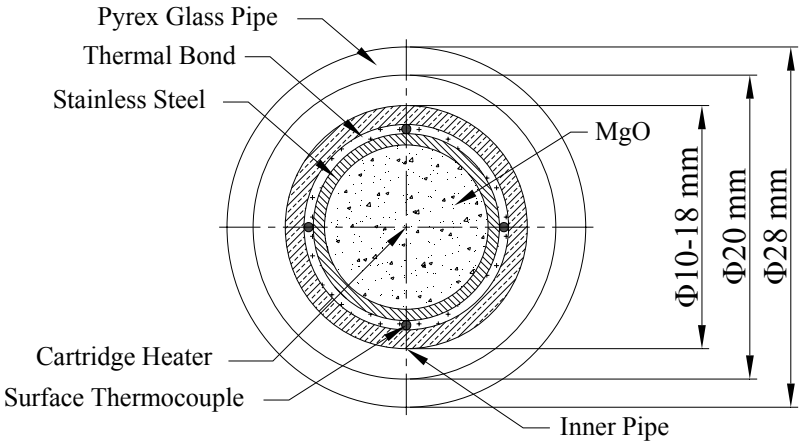


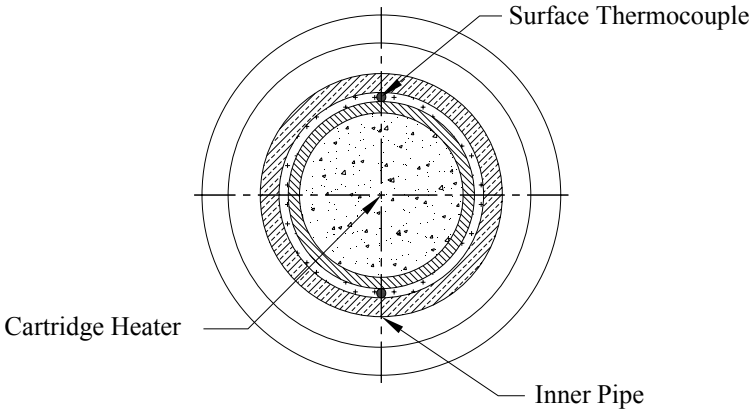
Fig. 2.3 The detailed arrangement of test section for annular duct.



SECTION VIEW A-A



SECTION VIEW B-B



SECTION VIEW C-C

Fig. 2.4 The cross-sectional view of the annular duct showing the heater and locations of the thermocouples.

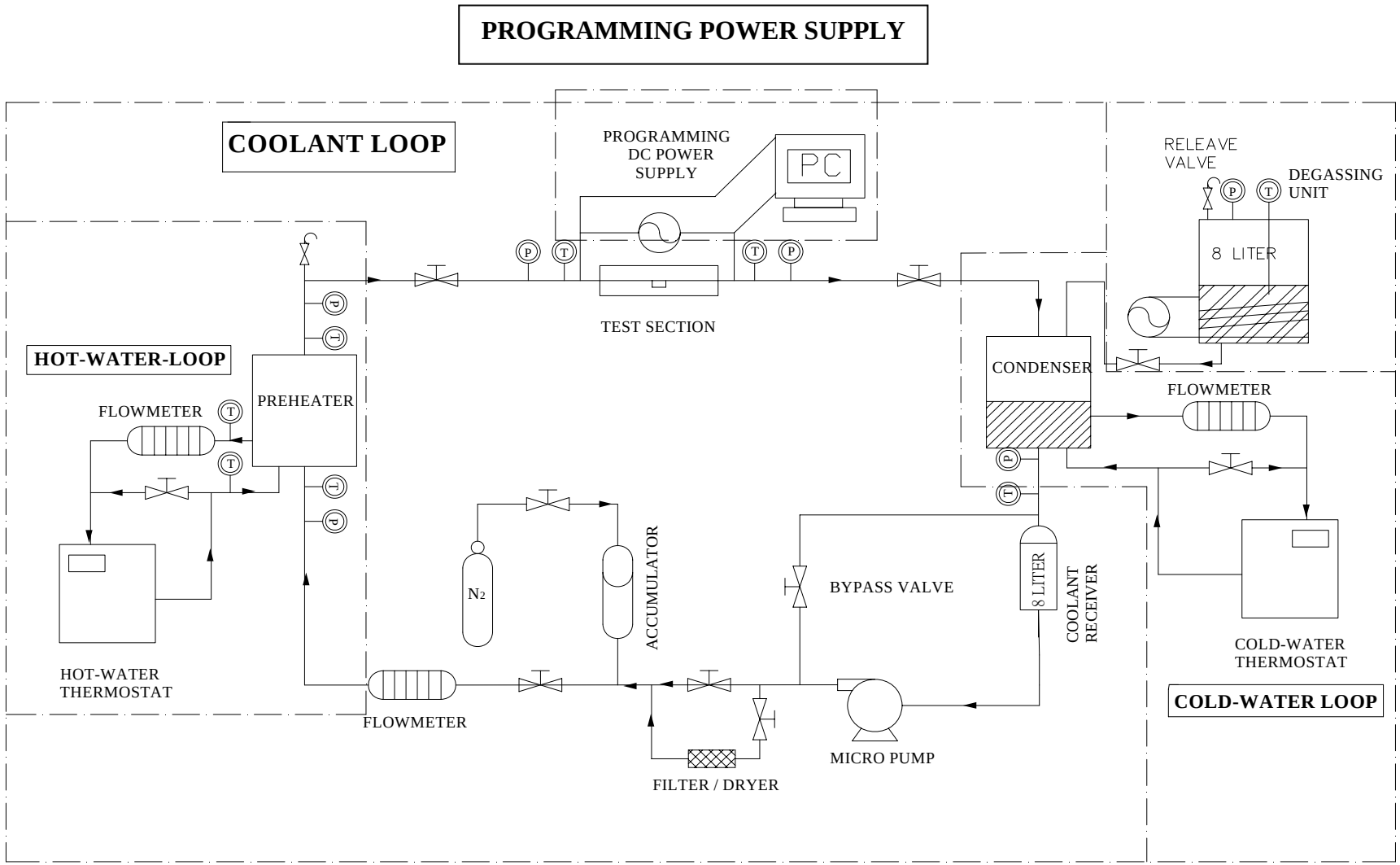


Fig. 2.5 Schematic diagram of experimental apparatus

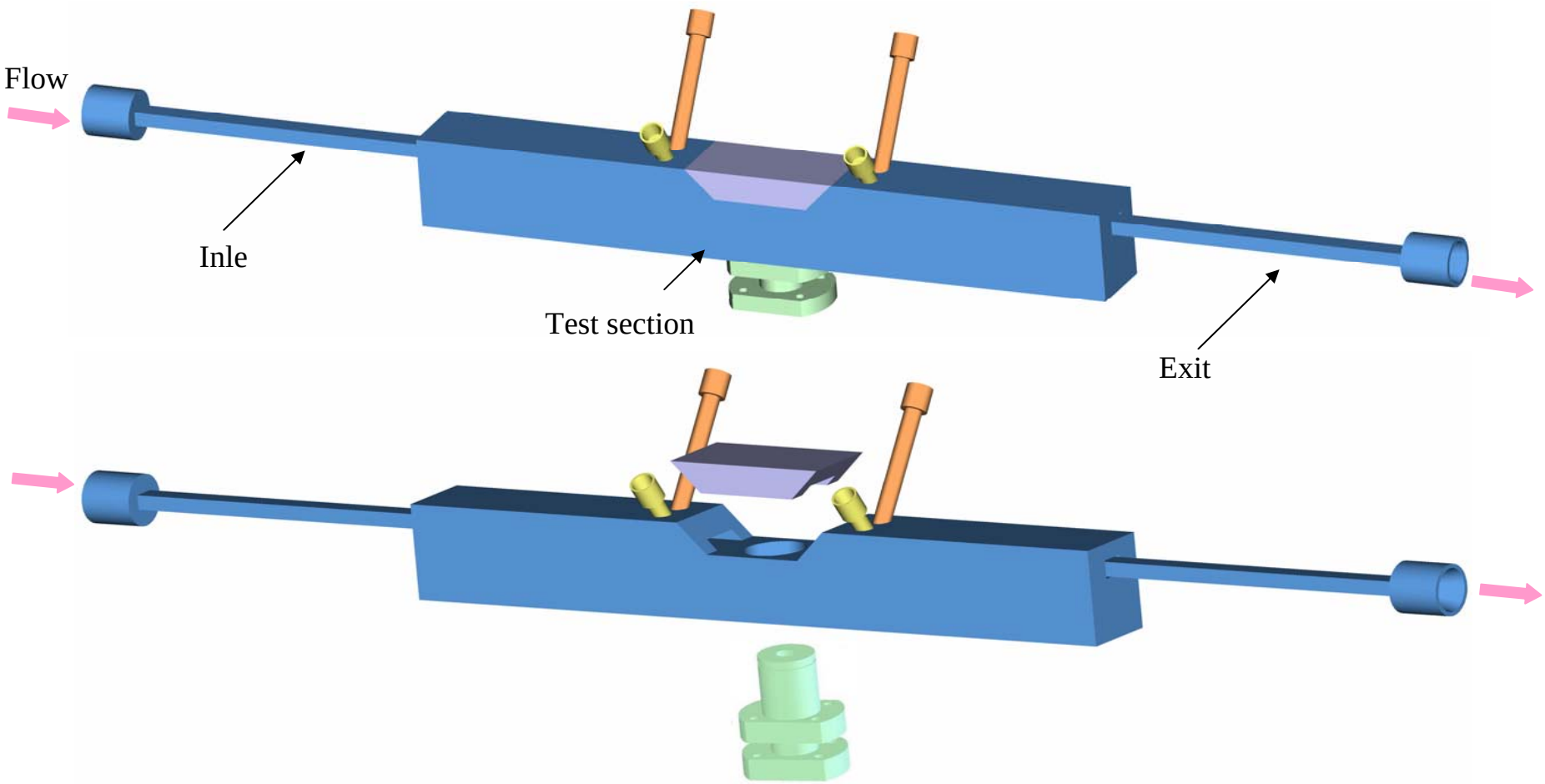


Fig. 2.6 Three-dimensional plots of test section along with inlet and outlet sections.

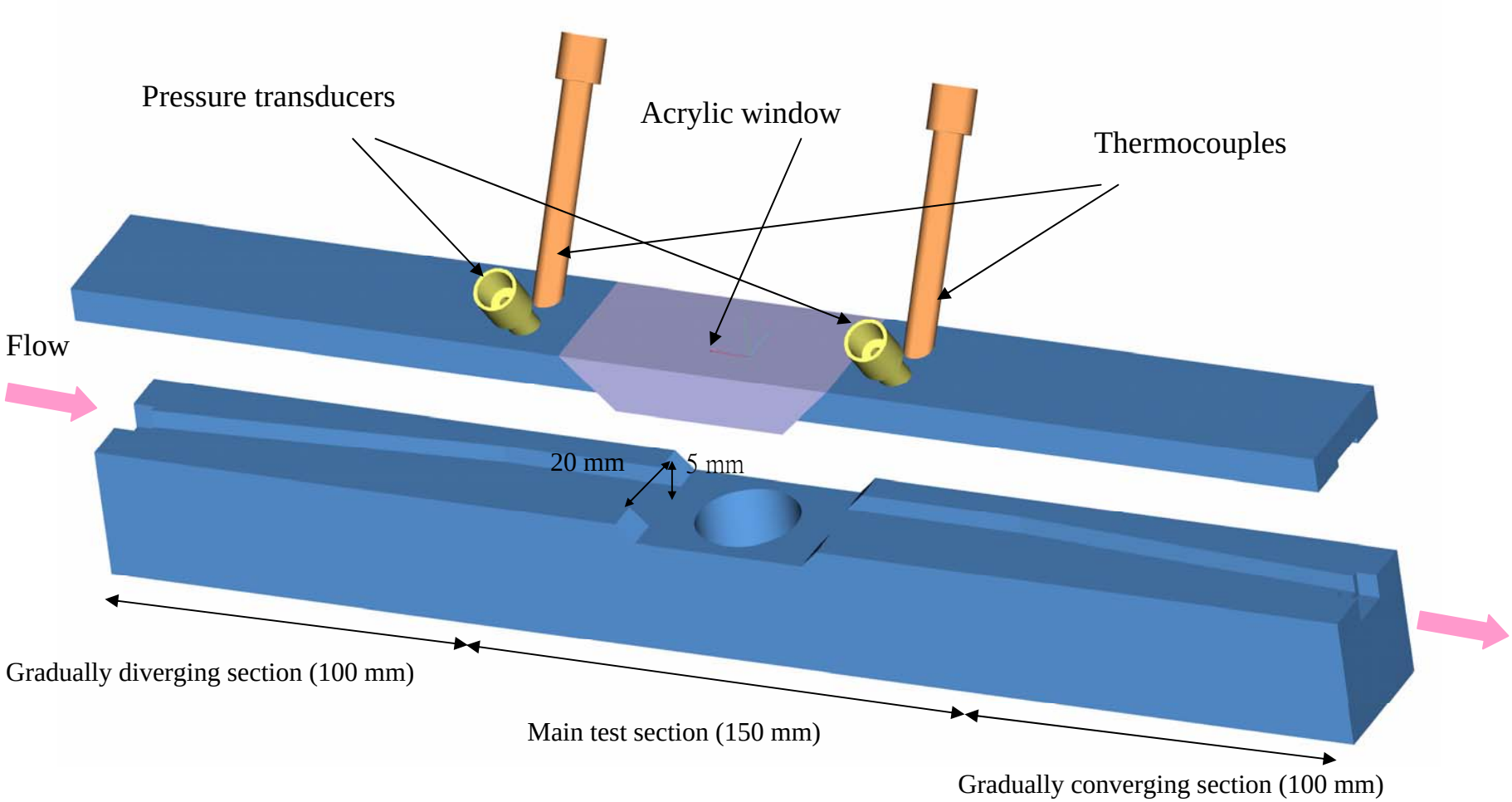


Fig. 2.7 Three-dimensional plots illustrating the test section in the rectangular flow channel.

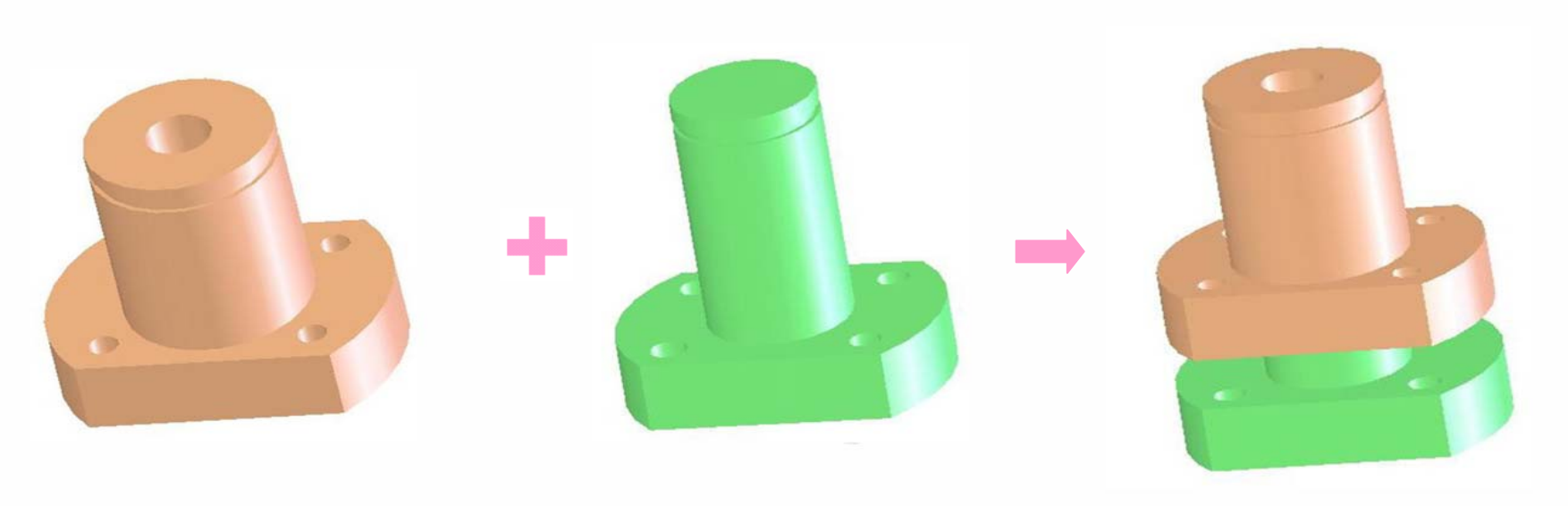
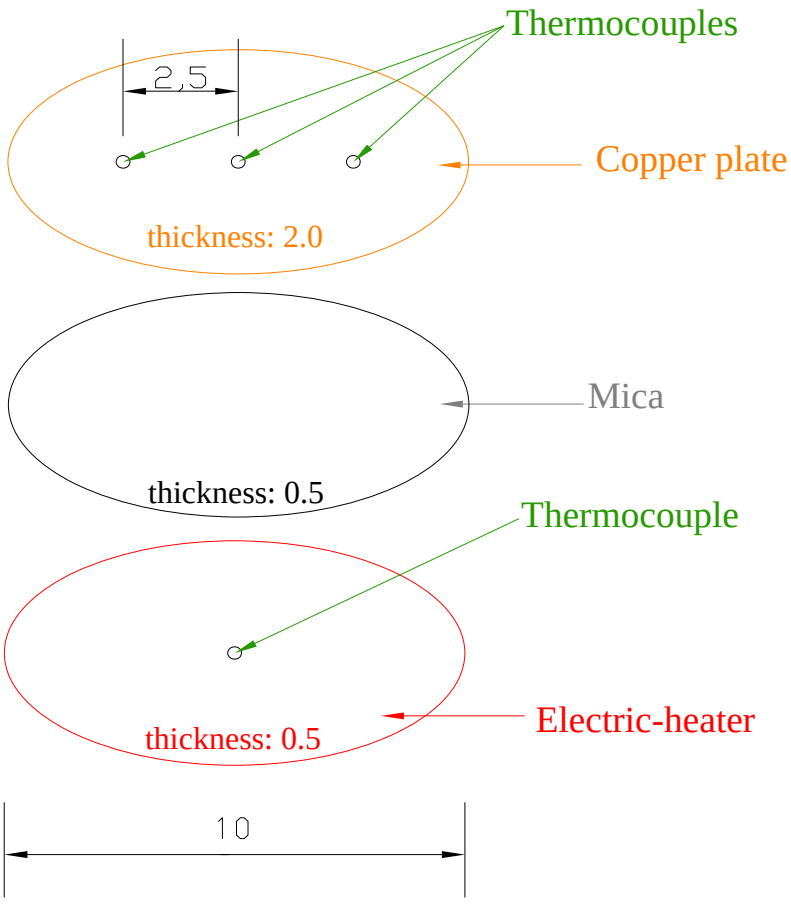


Fig. 2.8 Three-dimensional pictures showing (a) hollow cylindrical Teflon block and (b) cylindrical Teflon bolt.



(unit: mm)

Fig. 2.9 Locations of thermocouples.

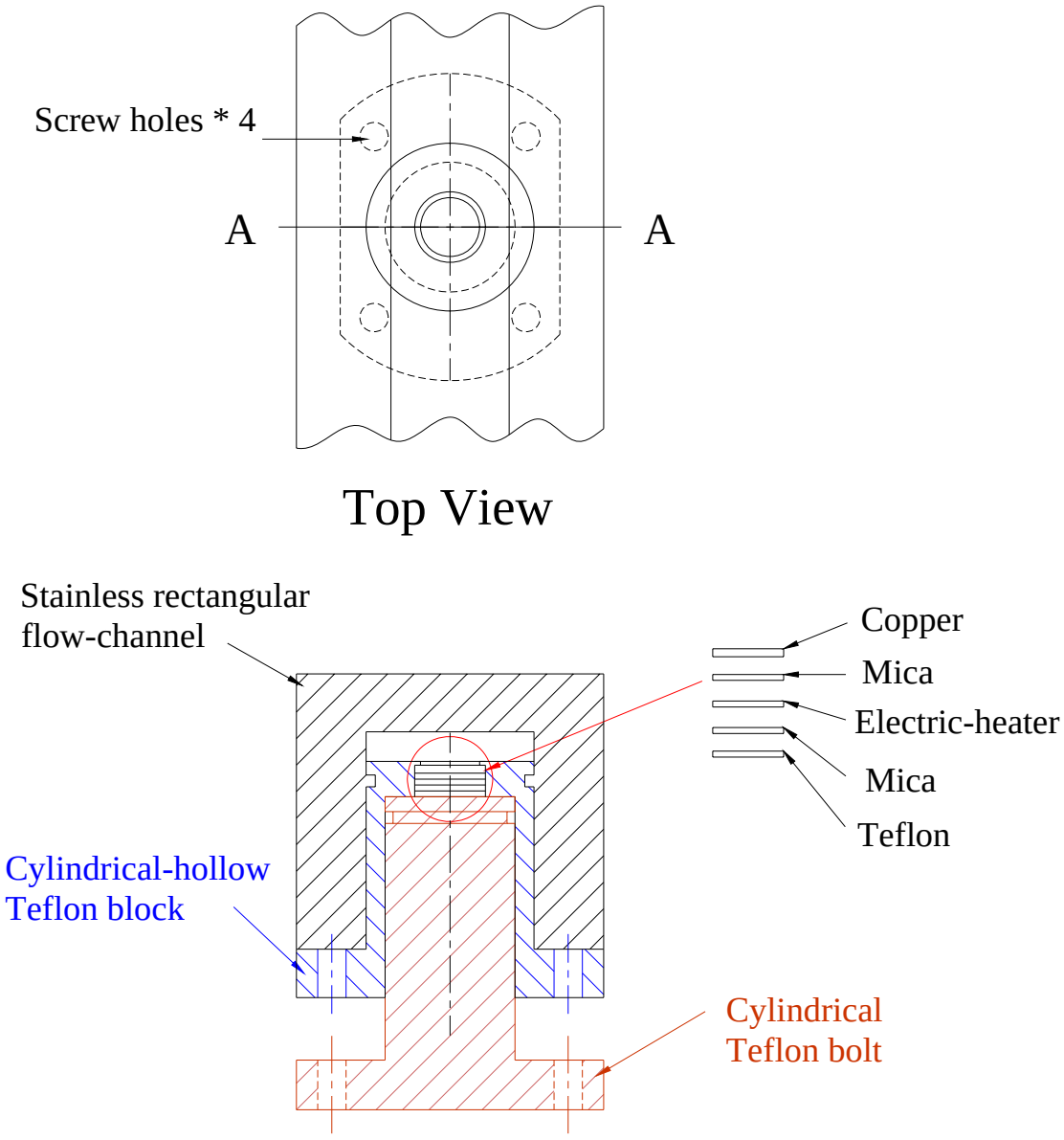


Fig. 2.10 Schematics of the copper plate module.

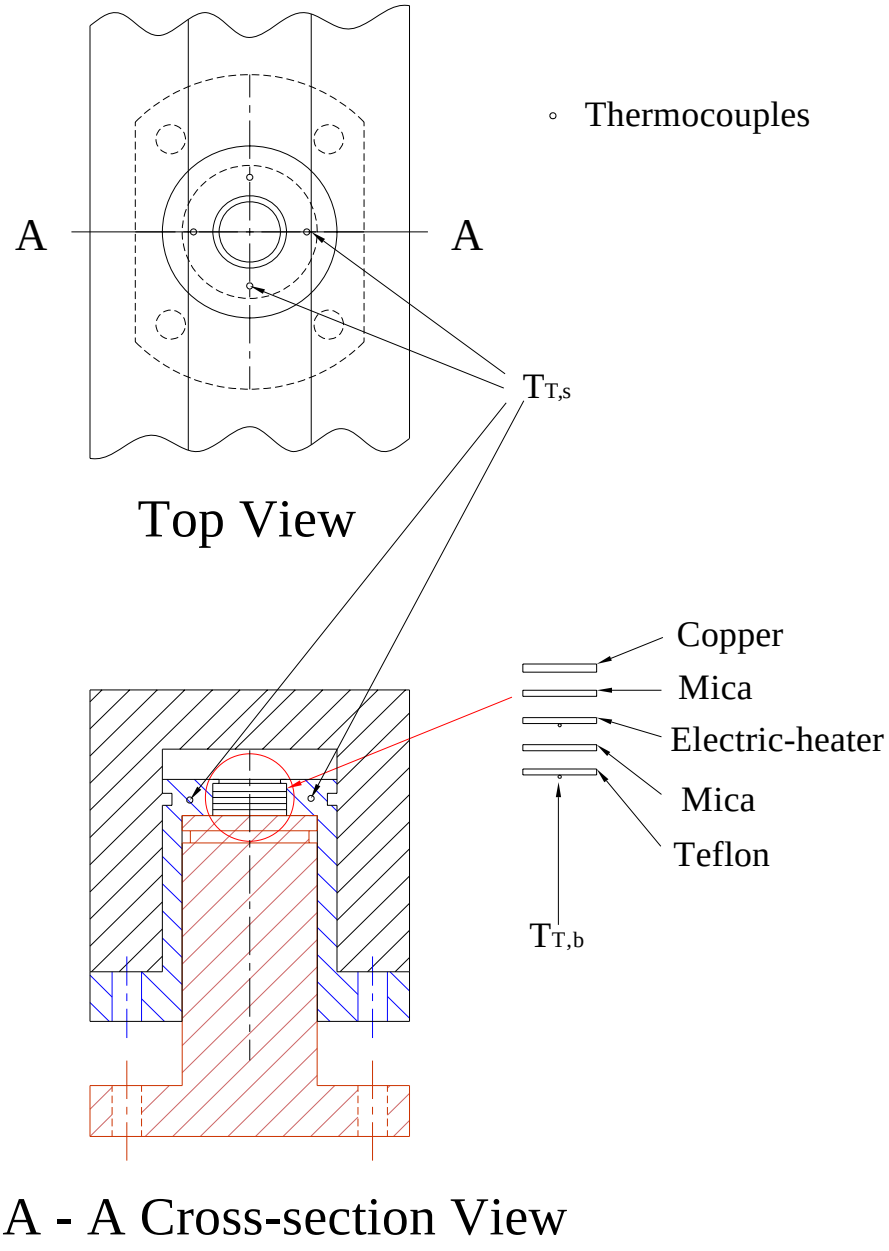


Fig. 2.11 Locations of the thermocouples inside the cylindrical-hollow Teflon block.

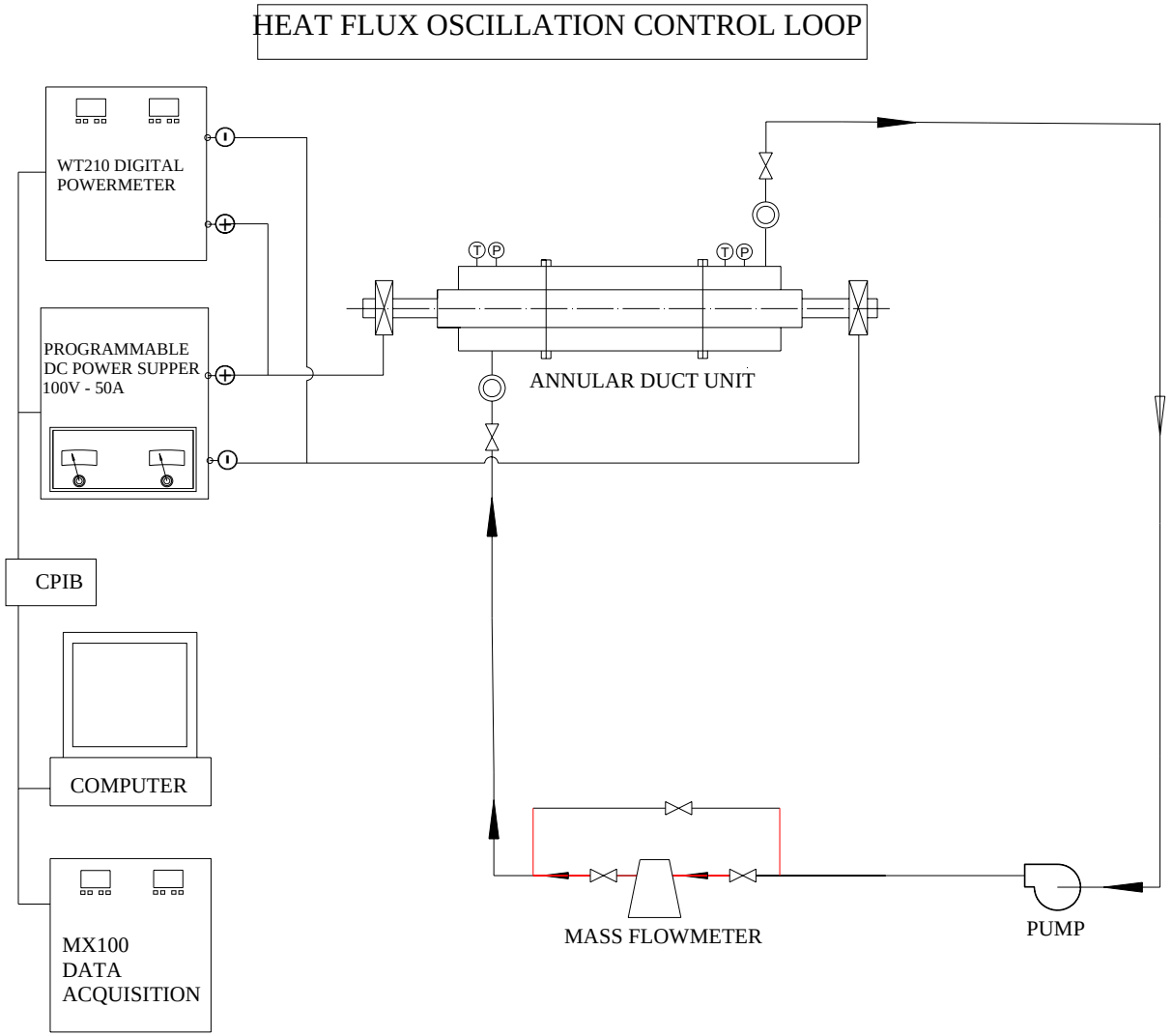


Fig. 2.12 Schematic diagram of heat flux oscillation control loop

CHAPTER 3

DATA REDUCTION

Data reduction analyses are needed in present study to deduce the time periodic subcooled, saturated flow boiling and evaporation heat transfer coefficients in the horizontal annular duct from the measured raw data.

3.1 Single-Phase Heat Transfer Coefficient

The imposed heat flux to the refrigerant flow in the annular duct is calculated on the basis of the total power input Q_t and the total outside heat transfer area of the inner pipe of the annular duct A_s. The total power input is computed from the product of the measured voltage drop across the cartridge heater and the electric current passing through it. Hence the net power input to the refrigerant flow in the test section Q_n is equal to (Q_t – Q_{loss}). The imposed heat flux at the outside surface of the inner pipe is then evaluated from the relation

$$q = Q_n / A_s \tag{3.1}$$

The total heat loss from the test section Q_{loss} is evaluated from the correlation for natural convection around a circular cylinder by Churchill and Chu [83]. Their correlation is

$$Nu_a = \left\{ 0.6 + \frac{0.387 Ra_D^{1/6}}{\left[1 + \left(0.559/\mathrm{Pr} \right)^{9/16} \right]^{8/27}} \right\}^2 \tag{3.2}$$

where

$$Ra_D = g\beta \left(\overline{T_{ins}} - T_a \right) D_{os}^{\ 3} \Big/ \alpha\nu \tag{3.3}$$

To reduce the heat loss from the test section, we cover the test section with a polyethylene insulation layer. We measured the mean temperature of the outside surface of the insulation layer $\overline{T_{ins}}$ and ambient temperature T_a. Hence $Q_{loss} = h_N \cdot \left(\overline{T_{ins}} - T_a \right) \cdot A_{os}$ where

A_{os} is the outside surface area of the insulation layer and $h_N = Nu_a \cdot D_{os}/k_a$. Note that D_{os} is the diameter of the insulation layer. The results from this heat loss test indicate that the heat loss from the test section is generally less than 1% of the total power input when single-phase liquid flow or two-phase boiling flow is in the duct.

The average single-phase convection heat transfer coefficient for the liquid refrigerant flow over the entire heated surface in the annular duct is defined as

$$h_l = \frac{Q_n}{A_s \cdot (\overline{T}_w - T_{r,ave})} \tag{3.4}$$

and

$$T_{r,ave} = \frac{T_{r,i} + T_{r,o}}{2} \tag{3.5}$$

where Q_n is the net power input to the liquid refrigerant in the annular duct and $T_{r,ave}$ is the average of the measured inlet and outlet temperatures of the refrigerant flow through the test section, which is taken as the average bulk liquid refrigerant temperature. Note that $\overline{T_w}$ denotes the average outside surface temperature of the inner pipe measured at the selected thermocouple locations. The outside surface temperature at each thermocouple location is deduced from the measured inside surface temperature of the inner pipe by subtracting the radial temperature drop due to the radial heat conduction in the pipe wall. Thus we have

$$T_w = T_{w,i} - Q_n \frac{\ln(D_o / D_i)}{2\pi k_w L} \tag{3.6}$$

3.2 Two-Phase Heat Transfer Coefficient

In the two-phase test, we also estimate the heat loss from the test section by measuring the outside surface temperatures of the polyethylene insulation layer and the ambient temperature. The measured heat loss from the test section is less than 0.5% for all cases and hence can be neglected.

The vapor quality of R-134a entering the test section inlet is evaluated from the energy balance for the preheater. Based on the temperature drop on the water side, the

heat transfer in the preheater is calculated from the relation,

$$Q_{w,p}=W_{w,p}c_{p,w}(T_{w,p,i}-T_{w,p,o}) \tag{3.7}$$

While the heat transfer to the refrigerant in the preheater is the summation of the sensible heat transfer (for the temperature rise of the refrigerant to the saturated value) and latent heat transfer (for the evaporation of the refrigerant),

$$Q_{w,p}=Q_{sens}+Q_{lat} \tag{3.8}$$

here

$$\begin{aligned} Q_{sens}&=W_r c_{p,r}(T_{r,sat}-T_{r,p,i}) \\ Q_{lat}&=W_r i_{fg} x_{p,o} \end{aligned} \tag{3.9}$$

The above equations can be combined to evaluate the refrigerant quality at the exit of the preheater that is considered to be the same as the vapor quality of the refrigerant entering the test section. Specifically,

$$x_{in}=x_{p,o}=\frac{1}{i_{fg}}\left[\frac{Q_{w,p}}{W_r}-c_{p,r}\left(T_{r,sat}-T_{r,p,i}\right)\right] \tag{3.10}$$

The total change of the refrigerant vapor quality in the test section is then deduced from the net heat transfer rate from the electric heater to the refrigerant in the test section, thus

$$\Delta x=\frac{Q_n}{W_r i_{fg}} \tag{3.11}$$

The mean vapor quality for the evaporation of R-134a in the test section at the middle axial location Z=80 mm is

$$x_m=x_{in}+\frac{\Delta x}{2} \tag{3.12}$$

Finally, the circumferential average heat transfer coefficient for the evaporation of R-134a at the middle axial location in the test section is determined from the definition

$$h_{r,evp}=\frac{Q_n/A_s}{\left(T_w-\overline{T}_{sat}\right)} \tag{3.13}$$

The local subcooled and saturated flow boiling heat transfer coefficients at the middle axial location are respectively defined as

$$h_{r,sub} = \frac{Q_n / A_s}{\left(T_w - \overline{T}_{sat}\right)} \tag{3.7}$$

and

$$h_{r,sat} = \frac{Q_n / A_s}{\left(T_w - \overline{T}_{sat}\right)} \tag{3.8}$$

3.3 Bubble Characteristics in Flow Boiling

To explore the bubble characteristics in the flow boiling, we move further to estimate the average bubble departure diameter and frequency and the average active bubble nucleation site density in a periodic cycle on the heating surface for the cases dominated by the bubbly flow. Specifically, for a given case the average bubble departure diameter is determined by measuring the diameters of departing bubbles on a small heated surface area and it is defined as

$$d_p = \frac{\sum d_p}{N} \tag{3.10}$$

where N is the number of measured bubbles. In this determination of d_p, N is not less than 3. Similarly, the mean bubble departure frequency is estimated by averaging the number of bubbles departing from the heated surface n_b over a certain period of time t_b at a few bubble departing sites N. Thus f_b is defined as

$$f_b = \frac{\sum f_b}{N} = \frac{\sum n_b / t_b}{N} \tag{3.11}$$

here N is also greater than 3. The average active nucleation site density is estimated by counting the number of bubble nucleation sites n_s over a small heated surface area A_s', and it is defined as

$$n_{ac} = n_s / A_s' \tag{3.12}$$

3.3 Uncertainty Analysis

Uncertainties of the heat transfer coefficients are estimated according to the procedures proposed by Kline and McClintock for the propagation of errors in physical measurement [84]. The results from this uncertainty analysis are summarized in Table 3.1

Table 3.1 Summary of the uncertainty analysis

Parameter	Uncertainty
Annular duct geometry	
Length, width and thickness (%)	±1.0%
Gap size (%)	±5.0%
Area (%)	±2.0%
Parameter measurement	
Temperature, T (℃)	±0.2
Temperature difference, △T (℃)	±0.28
System pressure, P (MPa)	±0.002
Mass flux of refrigerant, $\overline{G}$ (%)	±2
Amplitude of mass flux oscillation, $\Delta G/\overline{G}$ (%)	±4.8
Period of mass flux oscillation, t_p (sec)	±0.25
Imposed heat flux, $\overline{q}$ (%)	±4.5
Amplitude of mass flux oscillation, $\Delta q/\overline{q}$ (%)	±0.2
Period of mass flux oscillation, t_p (sec)	±0.25
Single-phase heat transfer	
Heat transfer coefficient, h_l (%)	±12.5
Subcooled flow boiling heat transfer	
Heat transfer coefficient, $h_{r,sub}$ (%)	±14
Saturated flow boiling heat transfer	
Heat transfer coefficient, $h_{r,sat}$ (%)	±14.5
Evaporation heat transfer	
Mean vapor quality, $\boldsymbol{x}_m$ (%)	±9.5
Heat transfer coefficient, $h_{r,evp}$ (%)	±14

CHAPTER 4

Time Periodic Saturated Flow Boiling Heat Transfer of R-134a and Associated Bubble Characteristics in a Narrow Annular Duct due to Flow Rate Oscillation

The present time periodic R-134a flow boiling experiment is performed for the mean refrigerant mass flux $\overline{G}$ varying from 100 to 600 kg/m^{2}s, imposed heat flux q from 0 to 45 kW/m^2, and mean system pressure $\overline{P}$ set at 414.6 kPa and 488.6 kPa (corresponding to the mean R-134a saturation temperature $\overline{T}_{sat}$ =10℃ and 15℃) for the gap of the duct δ = 1.0, 2.0 and 5.0 mm. Besides, the amplitude of the refrigerant mass flux oscillation ΔG is set at 0, 10, 20 and 30% of $\overline{G}$. Moreover, the period of the mass flux oscillation t_p is fixed at 20, 30, 60 and 120 seconds. The ranges of the parameters chosen above for the mass flux oscillation are in accordance with the practical operation of variable speed compressors in some air-conditioners and refrigerators subject to fast changing thermal load. In the following, attention will be mainly paid to examining the effects of the amplitude and period of the refrigerant mass flux oscillation on the time periodic R-134a flow boiling heat transfer performance. Note that for the limiting case of $\Delta G / \overline{G}$ = 0% we have saturated flow boiling of R-134a at a constant refrigerant mass flow rate in the test section, which is designated as 〝stable flow boiling〞 and has been investigated by Lie and Lin [21]. The measured boiling heat transfer data are expressed in terms of the boiling curve and boiling heat transfer coefficient. The thermal characteristics of the time periodic flow boiling is illustrated by the time variations of the instantaneous heated pipe wall temperature T_w and boiling heat transfer coefficient h_r. Moreover, selected flow photos and data deduced from the images of the boiling processes are presented to show the bubble characteristics in the boiling flow.

The time constant t_c associated with the response of the heated wall temperature to the time dependent refrigerant flow rate is an important physical quantity in the time periodic flow boiling. It is measured directly here from the time response of T_w subject to a step change in the mass flux for various q. The measured data show that t_c is about 16.0 seconds which is known to mainly result from the thermal inertia of the heated pipe wall.

4.1 Single-Phase Heat Transfer

Before beginning the flow boiling experiments, the single-phase convective heat transfer experiments are conducted for liquid R-134a. The measured single-phase convection heat

transfer coefficients are compared with the correlations proposed by Dittus-Boelter [74] and Gnielinski [85]. In the single-phase heat transfer tests the refrigerant mass flux is varied from 75 to 1,200 kg/m^{2}s for the annular gap of the duct δ = 1.0, 2.0 & 5.0 mm (corresponding to the Reynolds number of the refrigerant flow varying from 2,675 to 15,412) for the refrigerant saturated temperature T_{sat}=15℃ and inlet liquid subcooling ΔT_{sub}=4℃. Selected results from these tests are plotted in Figs. 4.1 and 4.2.

The Dittus-Boelter correlation is

$$Nu_l = 0.023 \cdot \mathrm{Re}^{0.8} \cdot \mathrm{Pr}^{0.4} \qquad \text{for } \mathrm{Re} > 10^4 \tag{4.1}$$

and the Gnielinski correlation is

$$Nu_l = \frac{(f_f/8)(\mathrm{Re}-1000)\,\mathrm{Pr}}{1+12.7\sqrt{f_f/8}\,(\mathrm{Pr}^{2/3}-1)} \qquad \text{for } 2{,}300 < \mathrm{Re} < 10^6 \tag{4.2}$$

where $f_f = (1.82 \times \log_{10} \mathrm{Re} - 1.64)^{-2}$ (4.3)

The results in Figs. 4.1 and 4.2 manifest that the present data for h_l can be well correlated by the Gnielinski correlation with a mean absolute error of 6.3%. Because of the lack of the unsteady turbulent forced convection heat transfer data in the open literature, direct validation of the present time periodic liquid heat transfer data is not possible.

4.2 Time-Average Boiling Curves and Heat Transfer Coefficient

At first, the time-average boiling curves and heat transfer coefficients measured at the middle axial location (z =80 mm) of the narrow annular duct for various amplitudes and periods of the refrigerant mass flux oscillation are shown in Fig. 4.3 for $\overline{T}_{sat}$ = 15℃ and $\overline{G}$ = 500 kg/m^{2}s. The results in Fig. 4.3 clearly indicate that the time-average boiling curves and heat transfer coefficients are not affected by the amplitude and period of the refrigerant mass flux oscillation to a significant degree. In fact, they are nearly the same as that for the stable boiling.

Then, the effects of the duct size on the time-average boiling curves are shown in Fig. 4.4(a). It is noted that the boiling curve shifts significantly to the left as the gap in the duct is reduced, indicating that the boiling heat transfer in the smaller duct is substantially better. It is also evident from the data that lower imposed heat flux and wall superheat are needed to initiate boiling on the heated surface for the smaller duct. This mainly results from the fact that for given $\overline{G}$, q and $\overline{T}_{sat}$ the mass flow rate through the duct is lower for a smaller gap. For the lower refrigerant mass flow rate the axial temperature rise of the refrigerant flow is faster, which, in turn, causes

earlier bubble nucleation for a smaller gap. Then, the data shown in Fig. 4.4(b) indicate that the saturated boiling heat transfer increases noticeably with a decrease in the channel gap. Since the shear stress of the flow acting on the heated surface in a smaller channel is higher, the bubbles on the heating surface can be more easily swept away from the heated surface. Moreover, the flow pattern change from the bubbly flow to the slug flow for δ = 1.0 mm occurs at a lower imposed heat flux than that for δ = 2.0 mm. These effects are thought to be the main reasons for the enhancement of flow boiling heat transfer when the channel size is reduced.

4.3 Time Dependent Flow Boiling Heat Transfer Characteristics

The time periodic flow boiling heat transfer characteristics for R-134a flow in the annular duct resulting from the periodic refrigerant mass flux oscillation are illustrated in Figs. 4.5 - 4.8 by presenting the time variations of the heated wall temperature and boiling heat transfer coefficients at the middle axial location in the statistical state for various $\overline{G}$, $\overline{T}_{sat}$, $\Delta G/\overline{G}$, t_p, q and δ. For clear illustration, the measured data for the time variations of the imposed refrigerant mass flux are also given here. The results manifest that when G oscillates periodically in time nearly like a triangular wave, significant temporal oscillations in T_w and h_r can occur. Note that the T_w and h_r oscillations are also periodic in time and are at the same frequency as the mass flux. Besides, the T_w and h_r oscillations get stronger for a higher amplitude and a longer period of the mass flux oscillation. However, the amplitude of the T_w oscillation varies nonmonotonically with the imposed heat flux. Note that single-phase forced convection prevails in the duct at a relatively low imposed heat flux. The data given in Figs. 4.5 - 4.8 further reveals that the T_w and h_r oscillations slightly lag the mass flux oscillation. This time lag apparently results from the thermal inertia of the heated pipe wall. Moreover for the single-phase convection at low q and in the first half of the periodic cycle in which the mass flux decreases with time, the wall temperature is found to rise with time, suggesting that the single-phase convection heat transfer over the heated surface is poorer at a lower G. The opposite process occurs in the second half of the cycle. It is further noted in the experiment that at a low q the wall temperature of the heating surface is lower than that required for the onset of nucleate boiling and no bubble nucleates from the heating surface. Hence heat transfer in the flow results completely from the single-phase forced convection. As the imposed wall heat flux is raised gradually, the wall temperature increases correspondingly. The corresponding T_w oscillation amplitude can be significant, as evident from the curve for q = 3.0 kW/m^2 in Fig. 4.5(c). At a certain higher wall temperature for a small increase in q bubbles start to nucleate from the heated surface at certain instant of time but bubble nucleation is not seen in the whole cycle. Thus, we have intermittent boiling in the flow in which nucleate boiling only exists in partial duration of the periodic cycle. The time instants for the start and termination of the nucleate boiling are marked on the curves

for T_w for the cases with the intermittent boiling. At this intermediate imposed heat flux the T_w oscillation is very weak. In fact, for most cases the amplitude of T_w oscillation is smaller than 0.2℃ which is below the random thermal disturbances from the background and is close to that in the stable boiling. For some increase in the imposed heat flux nucleate boiling persists over the entire period of the cycle and we have persistent flow boiling in the duct. It is of interest to note that at this higher q in the first half of the cycle in which G decreases with time, T_w also decreases with time, suggesting that the flow boiling heat transfer over the heated surface is better at a lower G, as supported by the data for h_r (Fig. 4.6). This trend is opposite to that for the single-phase convection. The results in Fig. 4.6 also show that the amplitude of h_r oscillation is not affected by the imposed heat flux in the persistent boiling to a noticeable degree. The appearance of the intermittent nucleate boiling and the improvement of boiling heat transfer by reducing G in the persistent boiling are somewhat unusual and will be examined later when the quantitative data for the bubble characteristics are presented.

In this transient oscillatory boiling flow the time variations of the refrigerant pressure at the inlet of the test section are also shown in Figs. 4.5 - 4.8 for selected cases. The results indicate that P_{in} oscillates nearly in phase with G and also in the form of triangular waves. A close inspection, however, reveals that the mass flux oscillates slightly behind the pressure. Besides, the corresponding oscillation in the refrigerant saturated temperature is found to vary from 0.2℃ to 1.1℃ for all cases tested here. Specifically, in the first half of the periodic cycle in which G decreases with time the R-134a saturated temperature also decreases with time. Thus the R-134a liquid at the test section inlet which is kept at a constant level is at a superheated state and we have flow boiling in a superheated liquid. The resulting boiling heat transfer is hence improved. While in the second half of the cycle the opposite processes take place and we have boiling in a subcooled liquid. The resulting boiling heat transfer is hence poorer.

Finally, we move further to present the data in Fig. 4.9 to elucidate the effects of the experimental parameters on the amplitude of the T_w oscillation over a wide range of the imposed heat flux covering the single-phase, intermittent and persistent boiling flow regimes. The results for each curve at the high mean refrigerant mass flux of 500 kg/m^{2}s shown in Fig. 4.9(a) clearly indicate that in the single-phase flow the oscillation amplitude of T_w increases significantly with the imposed heat flux for a given mass flux oscillation amplitude $\Delta G/\overline{G}$. Note that when the intermittent boiling appears the T_w oscillation starts to weaken substantially with the increase in the imposed heat flux. At a certain higher q but still in the intermittent boiling regime the T_w oscillation decays to a minimum point and then a further increase in q causes T_w to oscillate in a larger amplitude. This nonmonotonic variation of the T_w oscillation amplitude with q in the intermittent boiling can be attributed to the completely opposite trends in the T_w oscillation for

the single-phase and boiling flow. Specifically, T_w increases as G decreases in the single-phase flow but in the boiling flow T_w decreases as G decreases. Thus as the bubble nucleation starts to appear in the single-phase flow the T_w oscillation is weakened. This trend continues until the boiling flow dominates over the single-phase flow for a rise in q to a certain level. Then, the T_w oscillation gets stronger for a higher q. In the persistent boiling regime at high imposed heat flux the T_w oscillation gets gradually stronger for a higher q up to about q = 30 kW/m^2. Beyond that the wall temperature oscillation nearly levels off. It is worth to note from the data given in Fig. 4.9(a) that at the low $\bar{G}$ of 300 kg/m^{2}s the T_w oscillation decays noticeably with q in the persistent boiling. This stronger T_w oscillation at a lower $\bar{G}$ is attributed to the associated stronger boiling ebullition on the heated surface with the accompanying weaker single-phase convection. While at the intermediate $\bar{G}$ of 400 kg/m^{2}s the variation of the T_w oscillation amplitude with q is small in the persistent boiling regime. Specifically, at intermediate imposed heat flux in the intermittent and persistent boiling T_w oscillates in a larger amplitude at a lower $\bar{G}$ but the opposite trend prevails at high q in the persistent boiling. The results in Fig. 4.9 also indicate that the T_w oscillation is stronger for a higher amplitude and a longer period of the mass flux oscillation. At the low t_p of 20 seconds, which is only slightly larger than the time constant of the present system, the T_w oscillation is rather weak (Fig. 4.9(d)), reflecting that the heated wall is unable to respond instantly to the fast mass flux oscillation for a t_p around or below t_c. But the mean refrigerant mass flux exhibits a nonmonotonic effect on the amplitude of the T_w oscillation, as evident from the data in Fig. 4.9(a). Specifically, at intermediate imposed heat flux in the intermittent and persistent boiling T_w oscillates in a larger amplitude at a lower $\bar{G}$ but the opposite trend prevails at high q in the persistent boiling. However, the mean saturated temperature of the refrigerant shows a relatively insignificant effect on the amplitude of the T_w oscillation (Fig. 4.9(b)). It is also noted that for all cases tested in the persistent boiling for q$>$ 10.0 kW/m^2 the amplitude of the T_w oscillation is less that 10% of the wall superheat. But in the intermittent boiling A_{T_w} can be as high as 25% of ΔT_{sat}. Then, the data shown in Fig. 4.9(e) indicate that T_w oscillation increases noticeably with a increase in the channel gap in the persistent flow boiling for q$>$20.0 kW/m^2. At the lower q the effects of duct gap on the amplitude of the Tw oscilation is milder. Moreover, for given $\bar{G}$, $\Delta G/\bar{G}$, $\bar{T}_{sat}$, t_p and δ the variation of the amplitude of the T_w oscillation with the imposed heat flux is also nonmonotonic.

4.4 Intermittent Flow Boiling

It is of interest to note in the visualization of the boiling flow in the annular duct that over a certain intermediate range of the imposed heat flux the intermittent boiling appears. More specifically, in a typical periodic cycle of the refrigerant mass flux oscillation bubble nucleation

on the heated inner pipe is first seen at a certain time instant in the first half of the cycle as the imposed refrigerant mass flux decreases to a certain low level and the pipe wall temperature rises to exceed the wall superheat required for the onset of nucleate boiling. The boiling process continues for some time interval. At a certain later time instant in the second half of the cycle in which the imposed refrigerant mass flux increases and T_w decreases to the level below that required for the onset of nucleate boiling, bubble nucleation disappears and the boiling stops. Single-phase flow then prevails in the duct. The above processes of the intermittent flow boiling are repeatedly seen on the heated surface. The data in Fig. 4.9 clearly manifest that the appearance of the intermittent boiling substantially affects the intensity of the wall temperature oscillation. To be more clear, we mark the time instants at which boiling starts and stops in Figs. 4.5 and 4.6 on the curves for the cases with the presence of the intermittent boiling. The present data show that at a higher imposed heat flux and at a lower mean mass flux the onset of boiling is earlier and the termination of boiling is later. Besides, the instants for the boiling inception and termination are not affected by the period of the mass flux oscillation to a noticeable degree (Fig. 4.5). A flow regime map to delineate the boundaries separating different flow boiling regimes in terms of the Boiling number versus the relative amplitude of the mass flux oscillation is given in Figs. 4.10 and 4.11. The results show that the intermittent boiling prevails over a significantly wider range of the Boiling number for a higher amplitude of the mass flux oscillation and a lower mean saturated temperature of the refrigerant and for the mean refrigerant mass flux lowered from 500 to 400 kg/m^{2}s by comparing the curves for different $\overline{T}_{sat}$ and $\overline{G}$. But for $\overline{G}$ reduced further from 400 to 300 kg/m^{2}s the intermittent boiling dominates in a smaller range of the Boiling number except for $\Delta G/\overline{G}$ exceeding about 25%. Based on the present data for δ = 2.0 mm, the conditions leading to the appearance of the intermittent boiling can be empirically correlated as

$$(-4.65\times10^{-5}+1.55\times10^{-6}\overline{\mathrm{Re}}^{0.5}) \le \frac{\overline{\mathrm{Bo}}^{1.2}}{(\Delta G/\overline{G})^{2.5}} \le (2.99\times10^{-3}+5.23\times10^{-6}\overline{\mathrm{Re}}^{0.5}) \qquad (4.4)$$

where $\overline{\mathrm{Bo}}=\frac{q}{\overline{G}\cdot i_{fg}}$. More than 96 % of the present data falls within the above correlation.

4.5 Bubble Characteristics in Time Periodic Flow Boiling

The bubble characteristics associated with the stable saturated flow boiling of R-134a in the present narrow annular duct have been examined in our recent study [21]. These characteristics indicate that for the imposed heat flux exceeding that for onset of nucleate boiling the duct is dominated by the persistent boiling and a number of discrete bubbles nucleate from the cavities and slide along the heating surface. At a higher q the active bubble nucleation density increases

and a lot of coalescence bubbles appear. More coalescence bubbles are seen and they are confined by the duct walls to become slightly deformed for a further increase in q. At even higher q the duct is mainly filled with the coalescence bubbles. They also reported that at a higher refrigerant mass flux the bubble departure frequency was higher and the bubbles were smaller and in violent agitating motion. However, the active nucleation site density is lower at a higher mass flux. But at the lower mass flux the bubble coalescence is more important and a number of bigger bubbles form in the duct. Then, at a lower saturation temperature of the refrigerant the bubbles were found to grow bigger and depart at a lower rate, and the active nucleation site density is lower due to the higher surface tension and enthalpy of vaporization.

By and large, in the time periodic flow boiling investigated here the effects of the imposed heat flux and mean refrigerant mass flux and saturation temperature on the bubble behavior exhibit similar trends to that in the stable flow boiling. Hence, we fisrt illustrate here how the time periodic bubble characteristics are affected by the amplitude and period of the mass flux oscillation for the persistent boiling in Fig. 4.12 by presenting the photos of the boiling flow for the cases with the imposed heat flux well above that required for ONB in a small region around the middle axial location at eight selected time instants in a typical periodic cycle in the statistical state. In the figure the symbol " $t = t_o$ " signifies the time instant at which the instantaneous refrigerant mass flux is at the highest level and starts to decrease. The results indicate that for given q, $\overline{G}$, $\Delta G/\overline{G}$ and t_p the bubbles get bigger and become more crowded in the duct in the first half of the cycle in which the mass flux decreases. The opposite processes take place in the second half of the cycle in which the mass flux increases with time. These changes of the bubble characteristics with the instantaneous mass flux become more significant for an increase in the amplitude of the mass flux oscillation. Besides, the bubble coalescence occurs more frequently and more large bubbles appear in the duct for the cases with a longer period of the mass flux oscillation, as seen in Fig. 4.13. Then, the bubble behavior in the intermittent flow boiling for a case with a selected intermediate imposed heat flux is shown in Fig. 4.15. The results clearly indicate that initially in the beginning of the cycle the instantaneous mass flux decreases with time but is still well above $\overline{G}$ no bubbles nucleate from the heated surface. The flow is in single-phase state. Note that the bubbles start to nucleate from the heated surface at a certain time instant slightly before $t_0+3t_p/8$ at which the instantaneous mass flux is somewhat below $\overline{G}$. Note that the number and size of the bubbles increase noticeably with time in the second quarter of the periodic cycle for the continuing decrease of the mass flux. Then in the third quarter of the periodic cycle the number and size of the bubbles diminish noticeably with time due to the increase of the mass flux. The bubbles cease to nucleate from the heated surface at a certain time instant slightly before $t_0+6t_p/8$ when the mass flux slightly exceeds $\overline{G}$

and bubble nucleation stops completely. Single-phase flow again dominates. We have to wait until the end of the first quarter of the next cycle to see the bubble nucleation appearing on the heated surface. The above processes repeat in each cycle. The precise instants of time at which the onset and termination of nucleate boiling take place vary with the flow conditions.

To be more quantitative on the bubble characteristics in the time periodic R-134a flow boiling due to the mass flux oscillation, we estimate the bubble departure diameter and frequency and the number density of the active nucleation sites on the heating surface in a typical periodic cycle at the middle axial location for the persistent flow boiling from the images of the boiling flow stored in the video tapes. Selected results from this estimation are manifested in Figs. 4.16-4.19 by presenting the effects of the amplitude and period of the refrigerant mass flux oscillation on the time dependent bubble characteristics for $\bar{G}$ = 500 kg/m^{2}s. In these plots the small time lag in the T_w oscillation is ignored. The data in Fig. 4.16 indicate that as the refrigerant mass flux oscillates time periodically, the bubble departure diameter also varies time periodically and to some degree like a triangular wave as the mass flux oscillation. More specifically, the size of the departing bubbles increases significantly in the first half of the periodic cycle in which the mass flux decreases with time. While in the second half of the cycle an opposite process is noted when the mass flux increases with time. Besides, the results in Fig. 4.16(a) show that at the larger amplitude of the mass flux oscillation the time variation of the bubble departure diameter is somewhat stronger. Meanwhile, the bubble departure diameter oscillates slightly stronger at a higher imposed heat flux. Moreover, the results in Fig. 4.16(b) indicate that to a certain degree the bubble departure diameter varies stronger with time for a longer period of the mass flux oscillation. Specifically, the amplitude of the d_p oscillation increases about 30% for t_p raised from 20 seconds to 120 seconds. This large change in the d_p oscillation amplitude with t_p causes the significant variation of the T_w oscillation amplitude with t_p, as already seen in Fig. 4.16(d). Furthermore, increases in the mean refrigerant mass flux, saturation temperature and duct gap cause the departing bubbles to oscillate slightly stronger but do not change the wave form of the d_p variation with time (Figs. 4.16(c), (d) and 4.19(a)). It is worth mentioning that even the size of the largest departing bubble is below 0.3 mm which is much smaller than the diameter of the outer glass pipe in the test section (D_p= 20.0 mm). Thus the observation of the bubble size through the curved surface of the glass pipe is not expected to produce significant error.

How the temporal variation of the bubble departure frequency is affected by the mass flux oscillation is shown in Fig. 4.17. Note that the bubble departure frequency also varies like a triangular wave. Besides, for an oscillation mass flux the bubbles depart from the heated surface

at a decreasing rate in the first half of the periodic cycle in which the refrigerant mass flux reduces with time (Fig. 4.17(a)). Apparently, in the second half of the cycle in which the refrigerant mass flux increases the bubble departing rate rises. Moreover, the data in Fig. 4.17(a) indicate that at the larger amplitude of the mass flux oscillation the bubble departure frequency exhibits a stronger variation with time and at a higher q the oscillation in f is slightly stronger. Then, the results in Fig. 4.17(b) manifest that the bubble departure frequency is negligibly affected by the period of the mass flux oscillation. Obviously, reducing the duct gap causes a much larger variation of the bubble departure frequency with time (Fig. 4.19(b)). Finally, at higher $\overline{G}$ and $\overline{T}_{sat}$ the bubble departure frequency is in a stronger oscillation (Figs. 4.17(c) and (d)).

The time variations of the associated number density of the active nucleation sites affected by the mass flux oscillation presented in Fig. 4.18 clearly show that in the time periodic flow boiling the active nucleation site density also varies like a triangular wave. Besides, n_{ac} increases substantially with time in the first half of the periodic cycle in which the refrigerant mass flux decreases. The reverse process appears in the second half of the cycle in which the refrigerant mass flux rises. At the higher amplitude of the mass flux oscillation the temporal variation of n_{ac} is also stronger (Fig. 4.18(a)) and a higher imposed heat flux results in a slightly stronger oscillation in n_{ac}. But the effect of the period of the mass flux oscillation on the time variation of n_{ac} is small (Fig. 4.18(b)). But reducing the duct gap from 5.0 to 1.0 mm results in a much weaker time variation of n_{ac} (Fig. 4.19(c)). Finally, n_{ac} oscillates slightly stronger at a lower $\overline{G}$ and a higher $\overline{T}_{sat}$ (Figs. 4.18(c) and (d)).

Based on the data in Figs. 4.16-4.18 for δ = 2.0 mm, the dependence of the quantitative bubble characteristics on the R-134a mass flux oscillation can be approximately expressed as $d_p \propto G^{-a}$, $f \propto G^{b}$ and $n_{ac} \propto G^{-c}$, as shown in Fig. 4.20, when the short time lag in the T_w oscillation is neglected. Here the exponents a, b and c range respectively from 0.37 to 0.42 , 0.93 to 0.99 , and 0.46 to 0.65. Note that the latent heat transfer resulting from bubble nucleation in the persistent boiling q_b is proportional to d_p^3, f and n_{ac}, as discussed in the previous study [21, 22]. Thus, $q_b \propto G^{-d}$, here d varies from 0.58 to 0.98. This result clearly indicates that the flow boiling heat transfer gets better at decreasing refrigerant mass flux since q_b prevails in the boiling heat transfer. This in turn causes the heated wall temperature to decrease at decreasing refrigerant mass flux and vice versa in the time periodic flow boiling, as already seen from Fig. 4.5. Besides, the dominant effect of the mass flux oscillation on the boiling heat transfer comes from the very strong influences of the mass flux on the bubble departure size.

4.6. Concluding Remarks

The heat transfer data for the time periodic flow boiling of R-134a resulting from the refrigerant mass flux oscillation in the narrow annular duct have been presented here along with the bubble behavior. Effects of the mean level and oscillation amplitude and period of the refrigerant mass flux on the time periodic R-134a flow boiling have been investigated. The major results obtained here can be summarized in the following.

(1) The time-average boiling curves and heat transfer coefficients for the time periodic flow boiling of R-134a are not affected to a noticeable degree by the amplitude and period of the refrigerant mass flux oscillation.

(2) The heated pipe wall temperature, bubble departure diameter and frequency, and active nucleation site density also oscillate periodically in time and at the same frequency as the mass flux oscillation. Experiments also show that the resulting oscillation amplitudes of the wall temperature get larger for a longer period and a larger amplitude of the mass flux oscillation. Besides for a larger amplitude of the mass flux oscillation, stronger oscillations in the bubble characteristics, such as d_p, f and n_{ac}, are noted. But f and n_{ac} are only slightly affected by the period of the mass flux oscillation. A short time lag in the wall temperature oscillation is also noted. Moreover, the bubbles become smaller and more dispersed when the refrigerant mass flux increases with time. The opposite processes take place for a decreasing refrigerant mass flux. Furthermore, reductions in the size of the departing bubbles and active nucleation site density and augmentation in the bubble departure frequency result in the time duration in which the mass flux is rising. When the mass flux is sinking the opposite processes occur.

(3) Increases in the bubble departure size and active nucleation site density at decreasing refrigerant mass flux overwhelms the bubble departure frequency decrease with the mass flux. This in turn causes an increase in the latent heat transfer and a drop in the heated wall temperature at decreasing G, opposite to that in the single-phase flow.

(4) When the imposed heat flux over the heated surface is close to the heat flux corresponding to that for the onset of stable flow boiling, intermittent flow boiling appears. A flow regime map and an empirical correlation are given to delineate the boundaries separating different boiling flow regimes in the annular duct.

Table 4.1 Time scales for transient R-134a saturated flow boiling (δ = 1 mm)

Time scales		(sec)
Time constants for flow boiling on heated surface t_c	T_{sat} = 15℃	27.3 (Single-phase)
		17.2 (Saturated flow boiling)
	T_{sat} = 10℃	29.3 (Single-phase)
		20.1 (Saturated flow boiling)

Table 4.2 Time scales for transient R-134a saturated flow boiling (δ = 2 mm)

Time scales		(sec)
Time constants for flow boiling on heated surface t_c	T_{sat} = 15℃	26.0 (Single-phase)
		16.0 (Saturated flow boiling)
	T_{sat} = 10℃	28.1 (Single-phase)
		19.2 (Saturated flow boiling)

Table 4.3 Time scales for transient R-134a saturated flow boiling (δ = 5 mm)

Time scales		(sec)
Time constants for flow boiling on heated surface t_c	T_{sat} = 15℃	25.1 (Single-phase)
		15.2 (Saturated flow boiling)
	T_{sat} = 10℃	27.6 (Single-phase)
		19.1 (Saturated flow boiling)

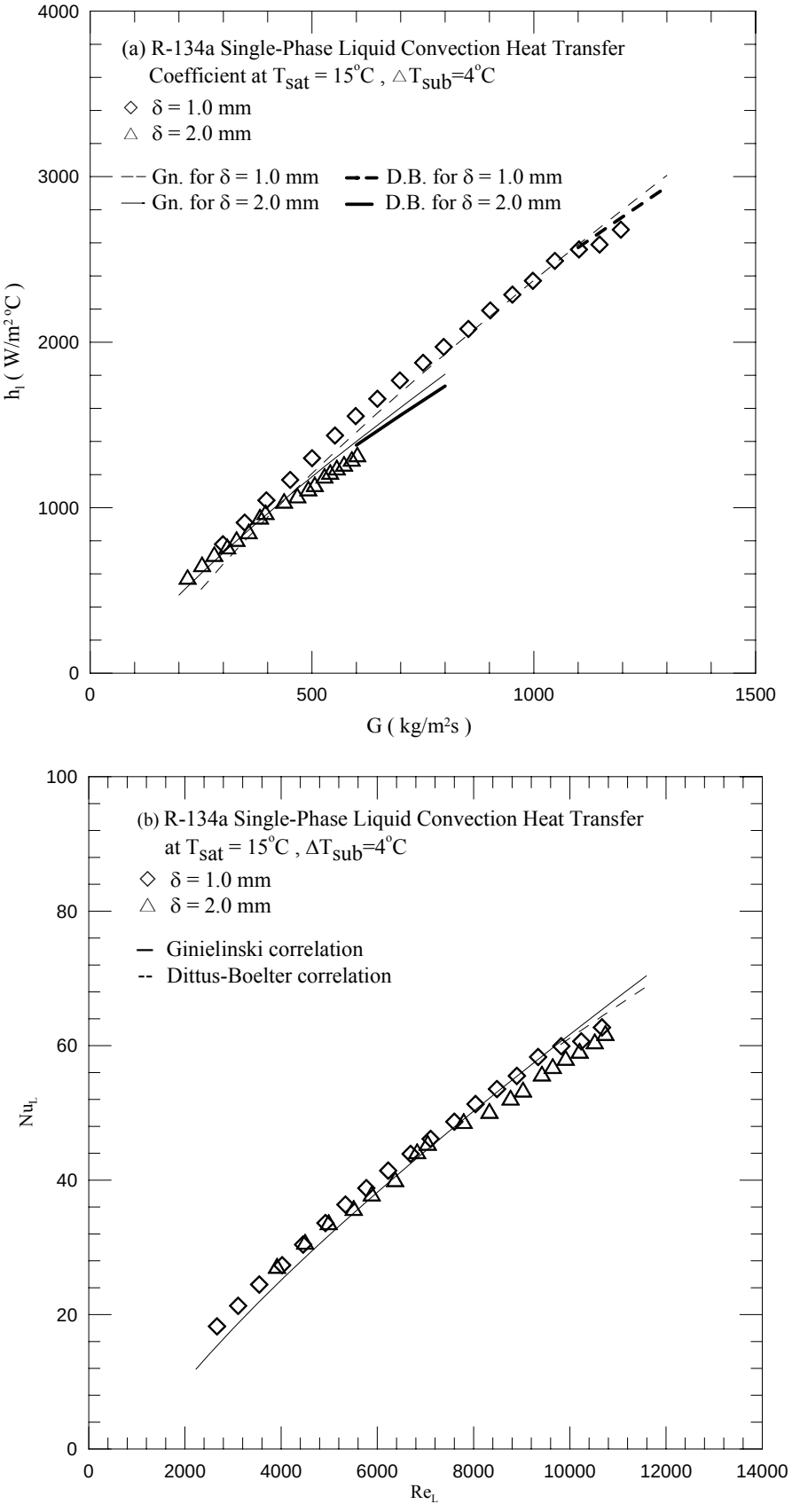


Fig. 4.1 Comparison of the present single-phase liquid convection heat transfer data h_l(a) and Nu_l(b) with the correlations of Gnielinski and Dittus-Boelter.

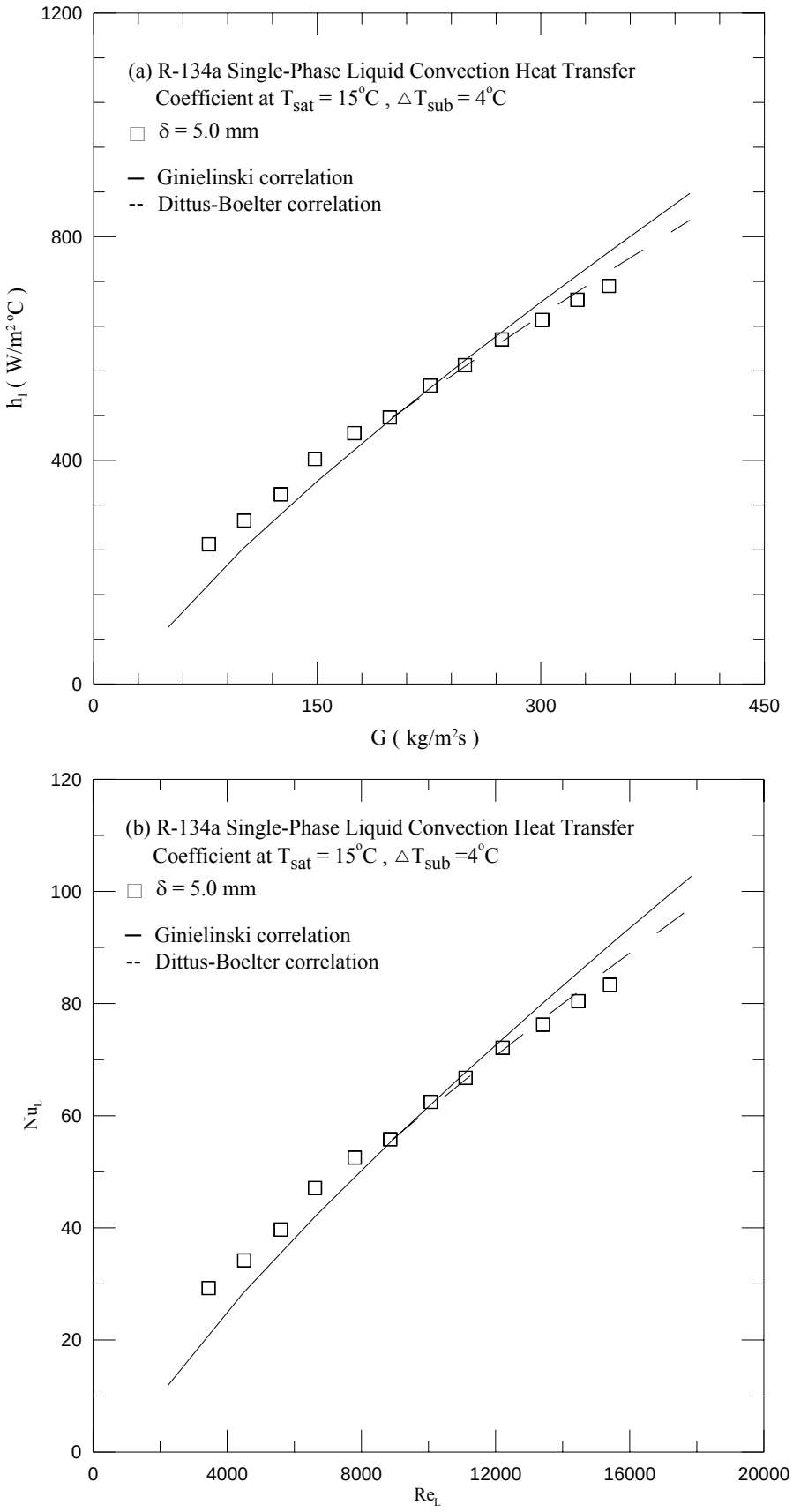


Fig. 4.2 Comparison of the present single-phase liquid convection heat transfer data h_l(a) and Nu_l(b) with the correlations of Gnielinski and Dittus-Boelter.

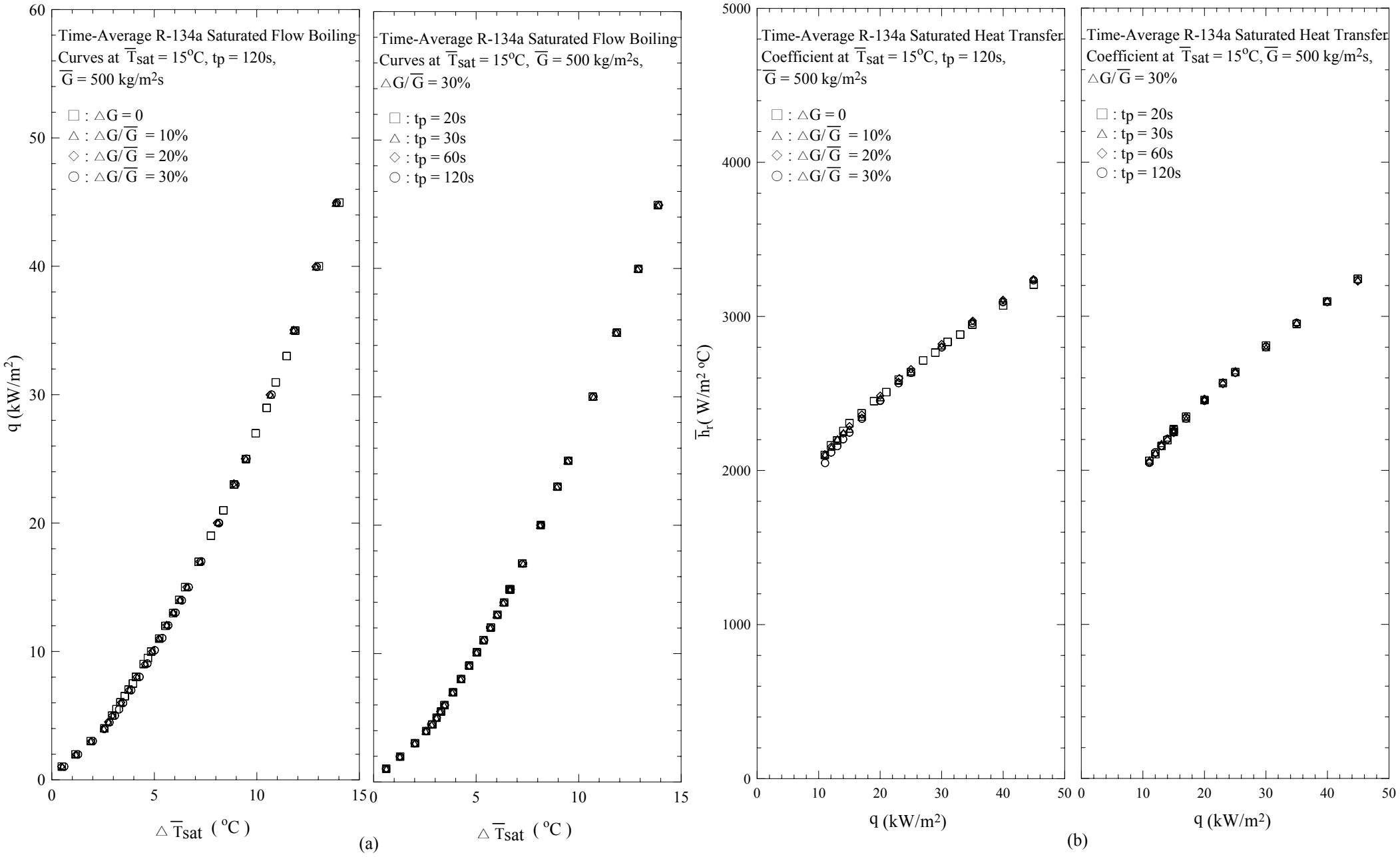


Fig. 4.3 Time-average R-134a flow boiling curves (a) and flow boiling heat transfer coefficients (b) for various $\Delta G/\overline{G}$ and t_p at δ = 2.0 mm.

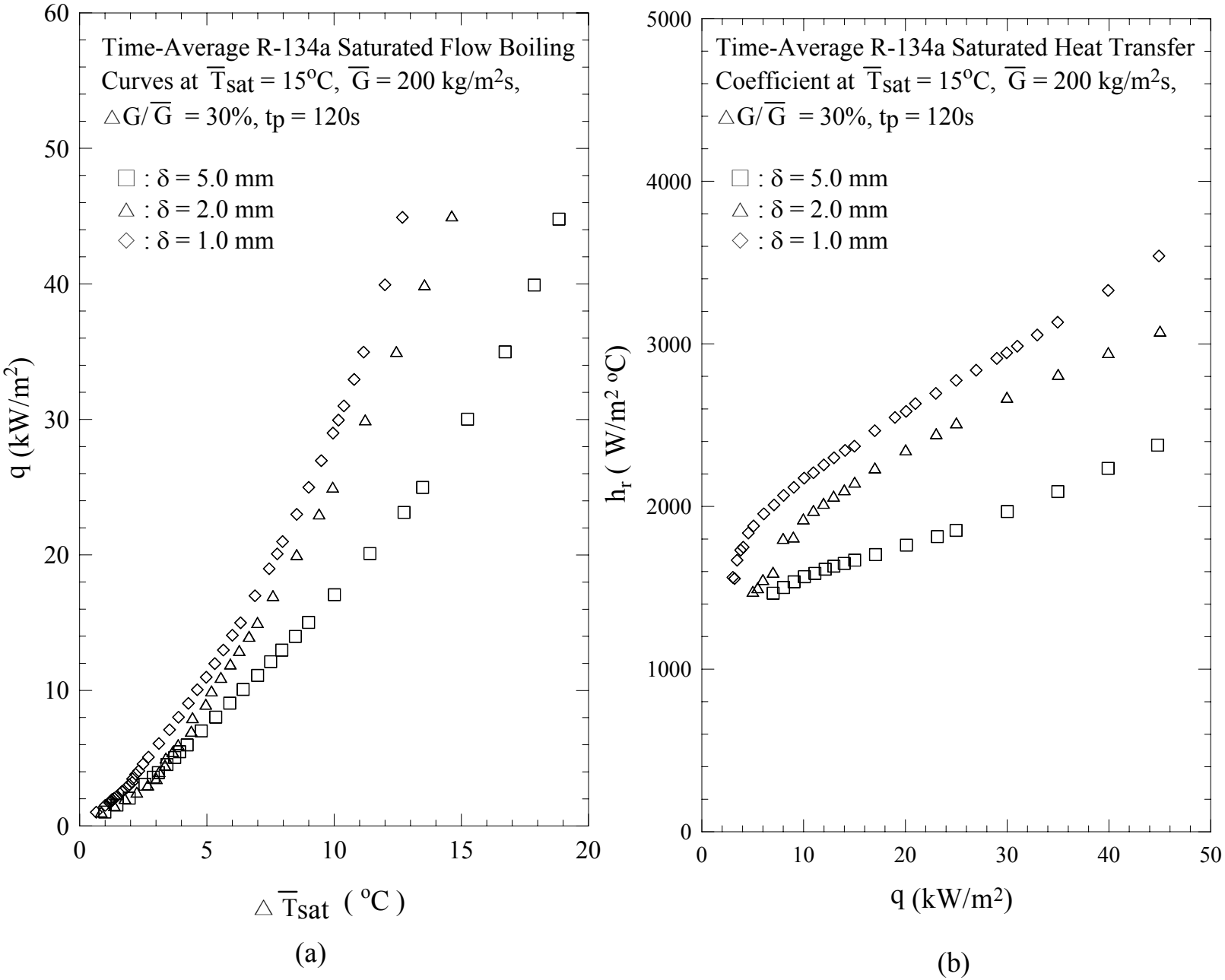


Fig. 4.4 Time-average R-134a flow boiling curves (a) and flow boiling heat transfer coefficients (b) for various gap sizes.

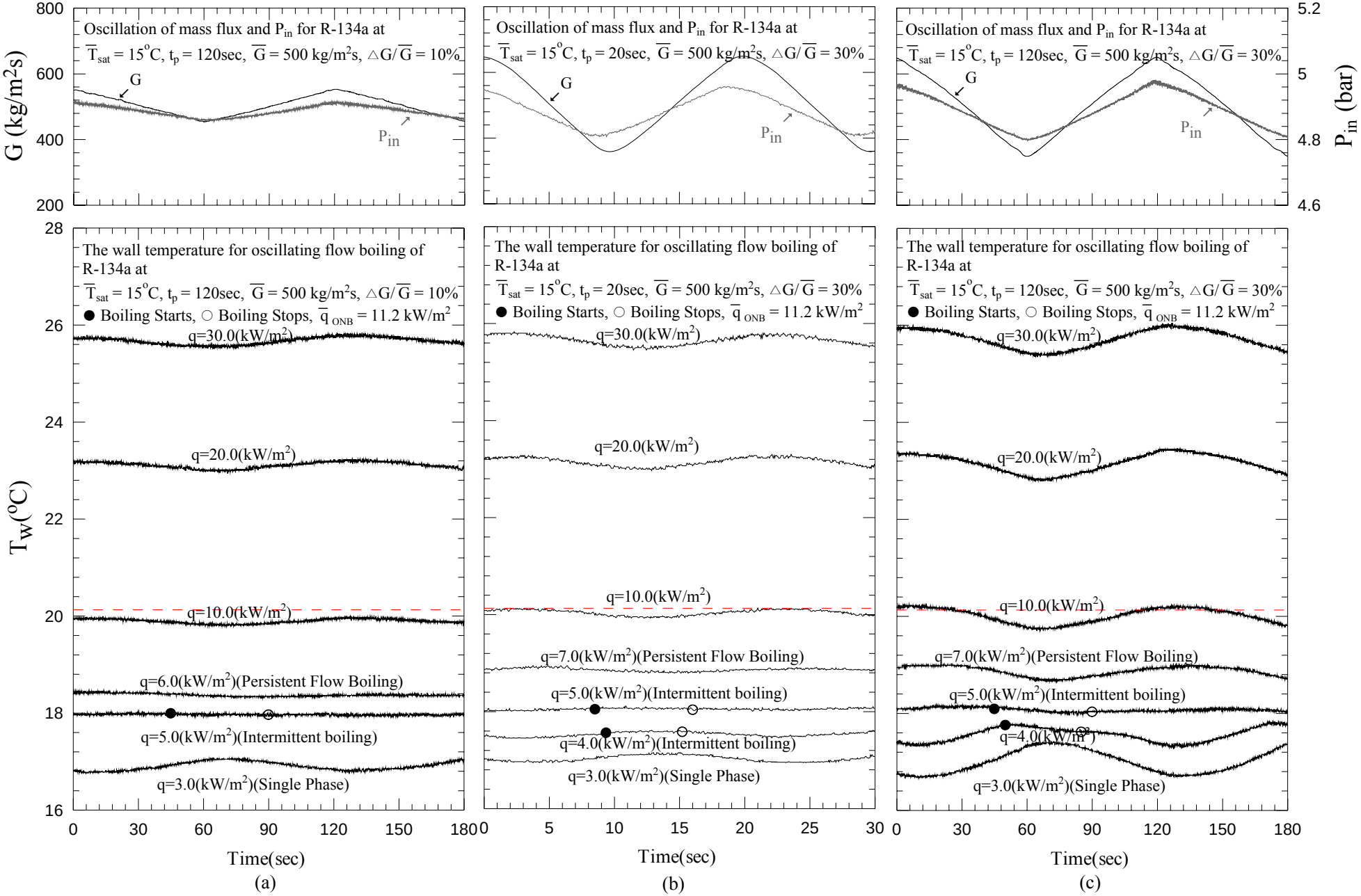


Fig. 4.5 Time variations of imposed mass flux, inlet pressure, and wall temperature at z = 80 mm for various q, $\Delta G/\overline{G}$ and t_p at δ = 2.0 mm.

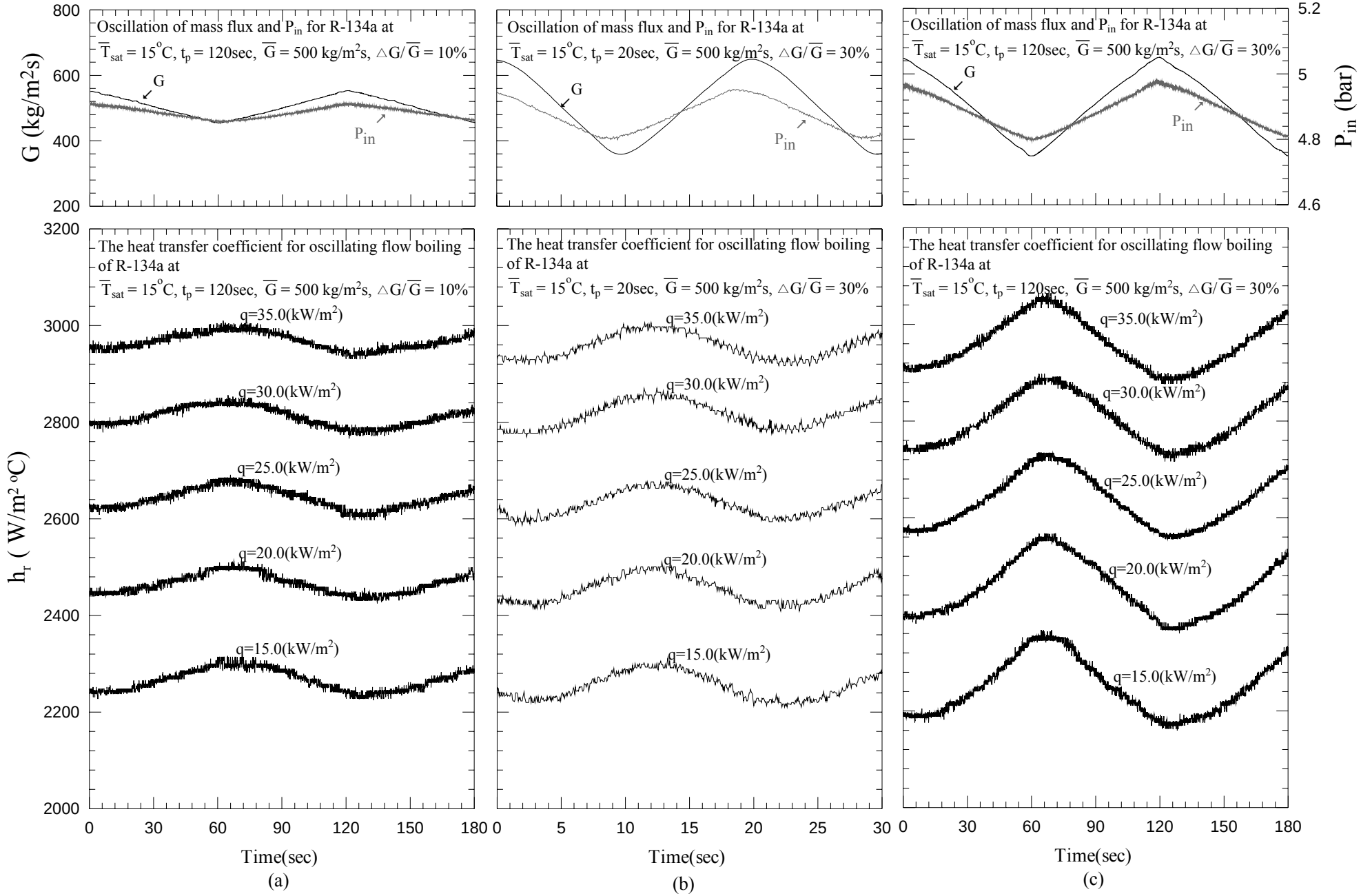


Fig. 4.6 Time variations of imposed mass flux, inlet pressure, and heat transfer coefficient at z = 80 mm in persistent boiling for various q, $\Delta G/\overline{G}$ and t_p at δ = 2.0 mm.

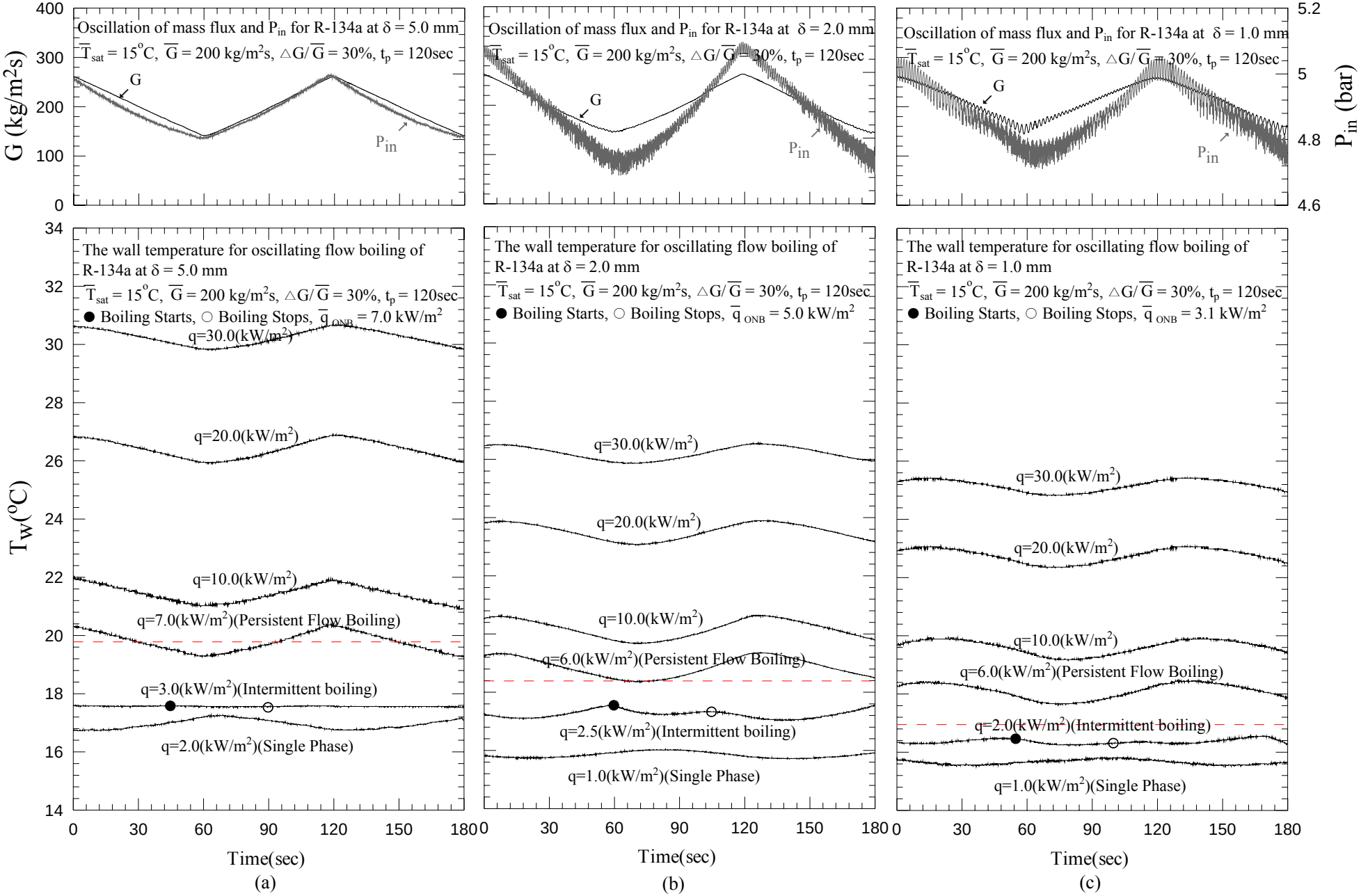


Fig. 4.7 Time variations of imposed mass flux, inlet pressure, and wall temperature at z = 80 mm for various gap sizes.

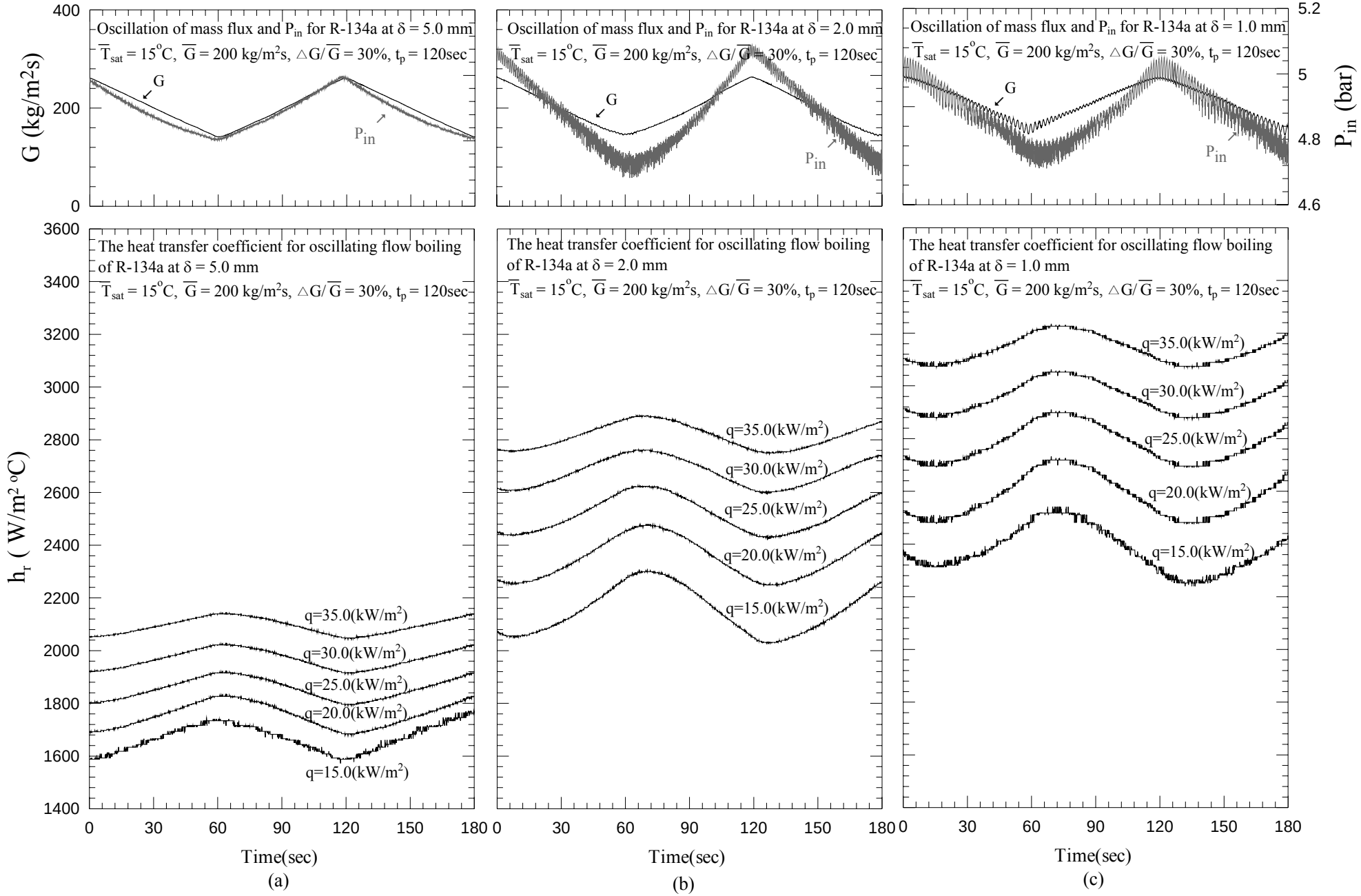


Fig. 4.8 Time variations of imposed mass flux, inlet pressure, and heat transfer coefficient at z = 80 mm in persistent boiling for various gap sizes.

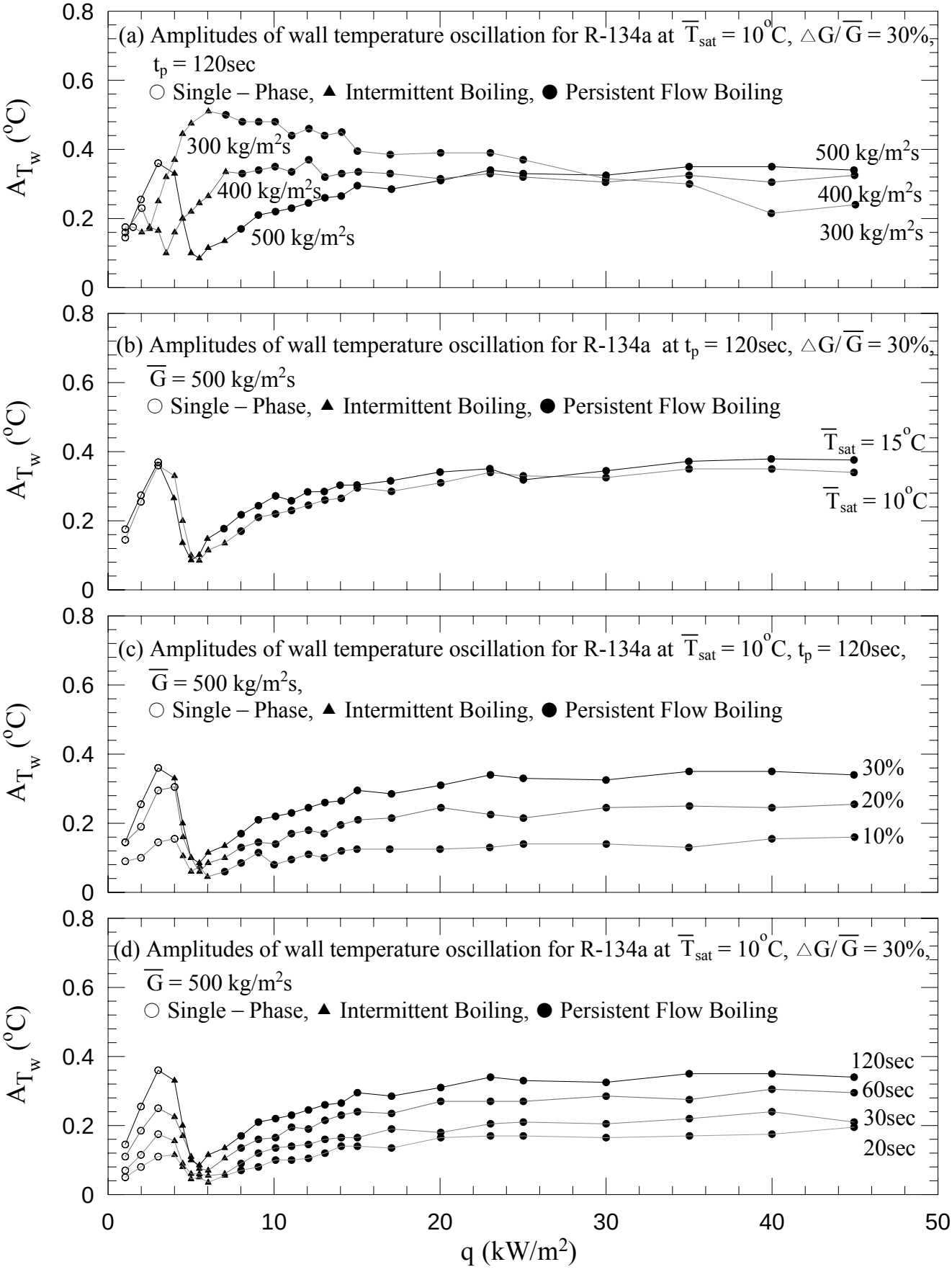


Fig. 4.9 Variations of amplitudes of heated wall temperature with imposed heat flux for various refrigerant mass fluxes (a), saturated temperatures (b), amplitudes of mass flux oscillation (c), periods of mass flux oscillation (d), and gap sizes (e).

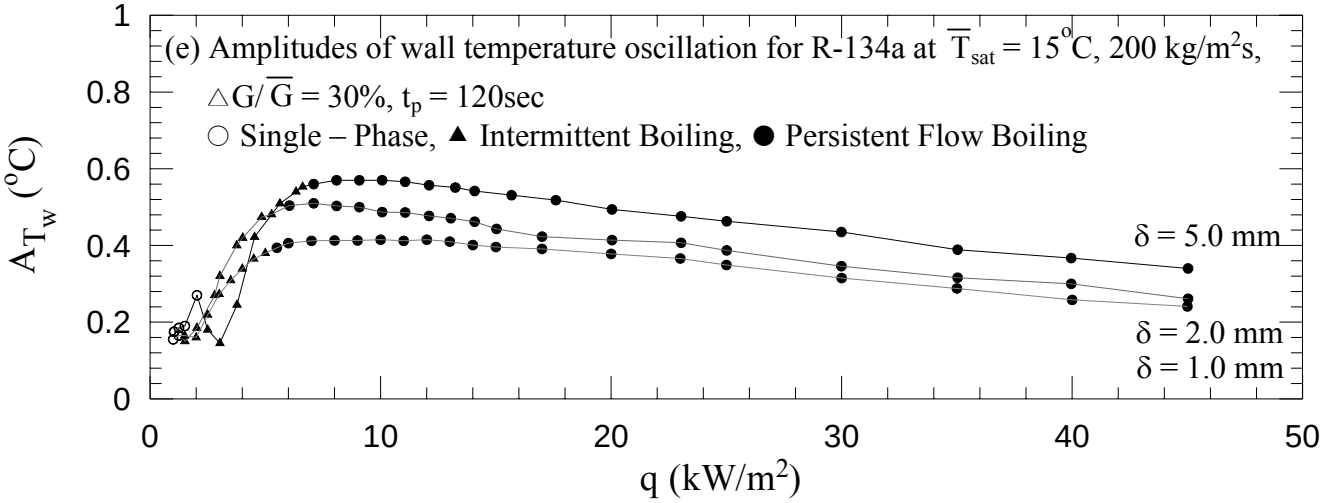


Fig. 4.9 Continued

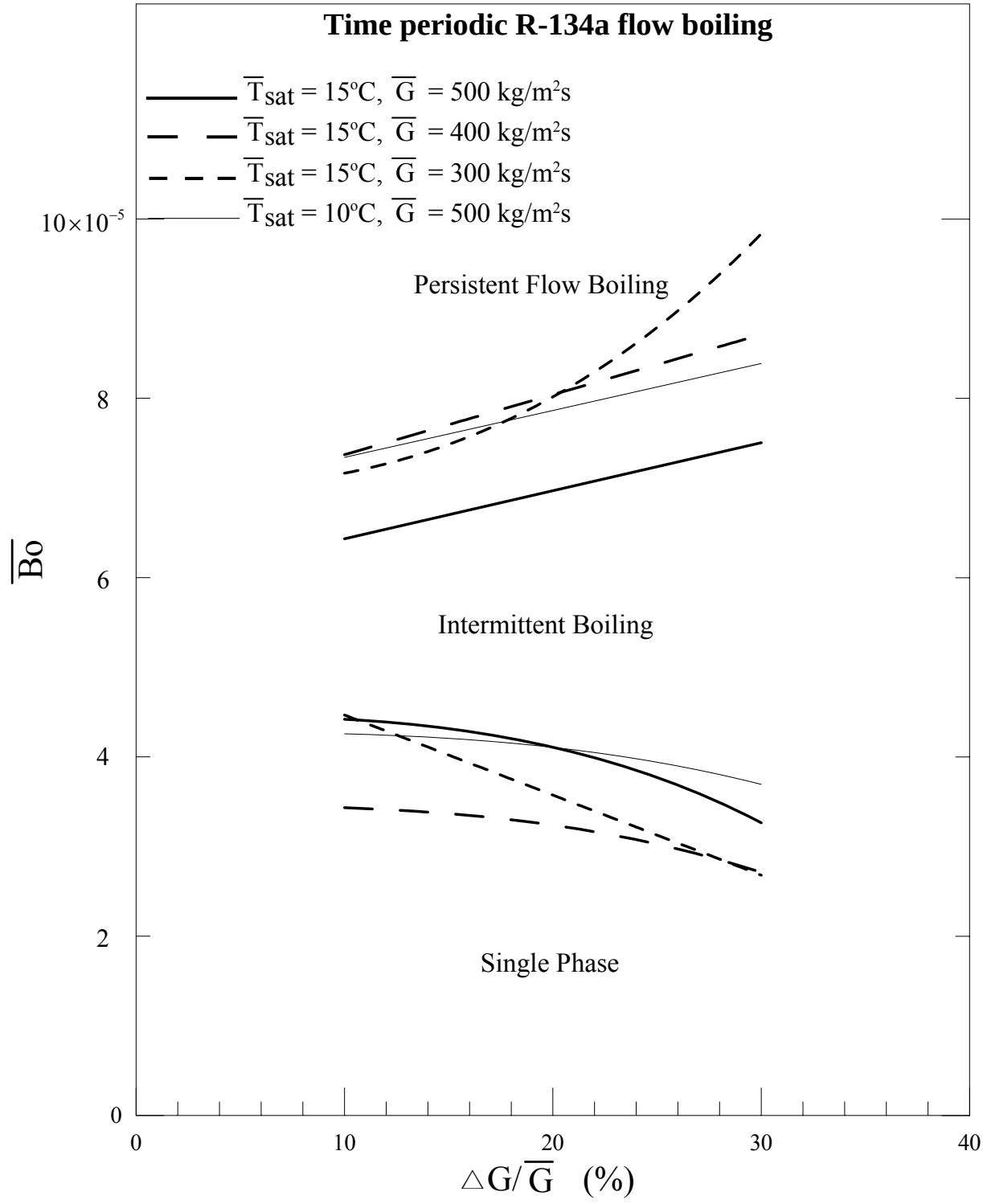


Fig. 4.10 Flow regime map for time periodic R-134a flow boiling in annular duct at δ = 2.0 mm.

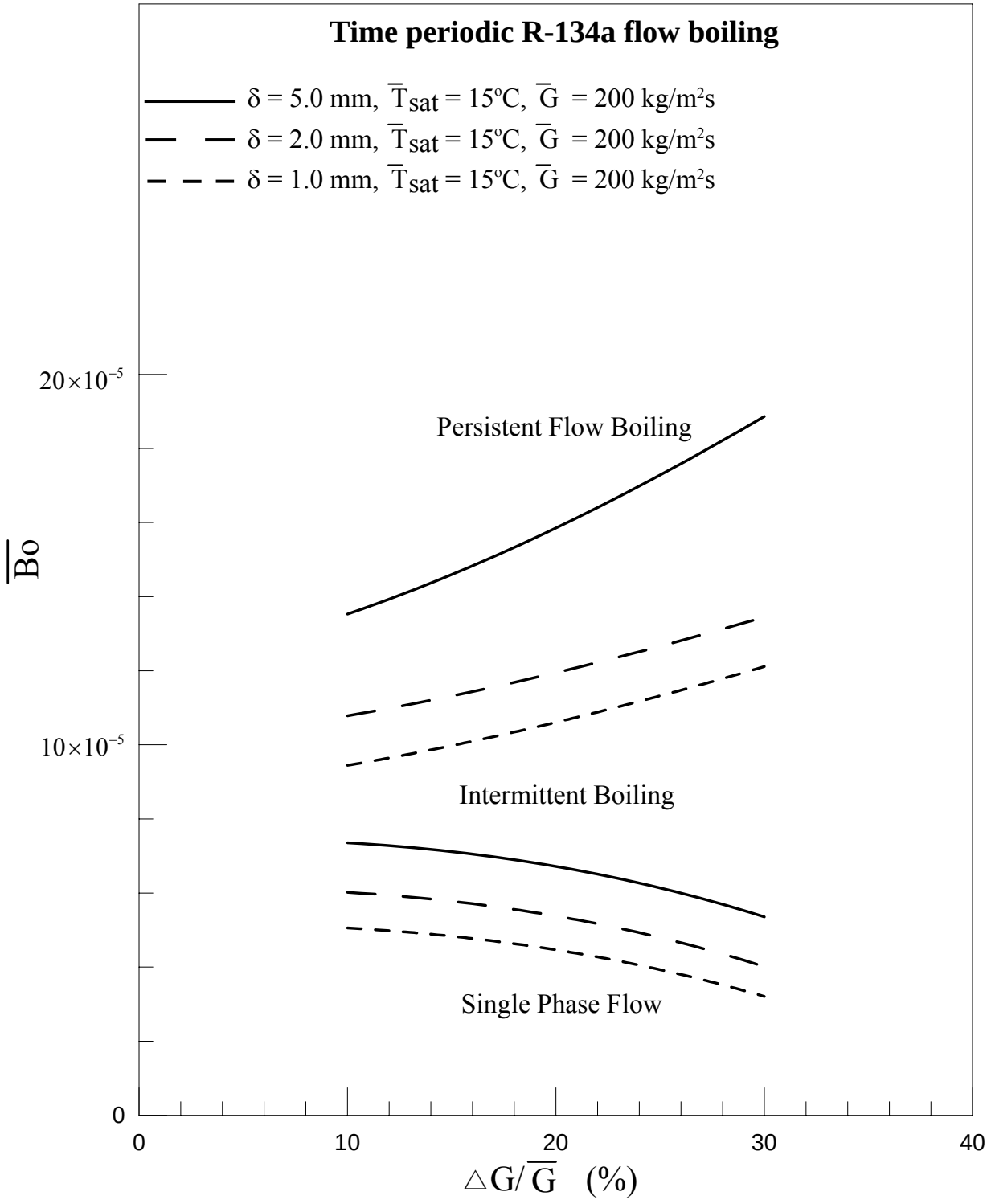


Fig. 4.11 Flow regime map of time periodic R-134a flow boiling in annular duct for various gap sizes.

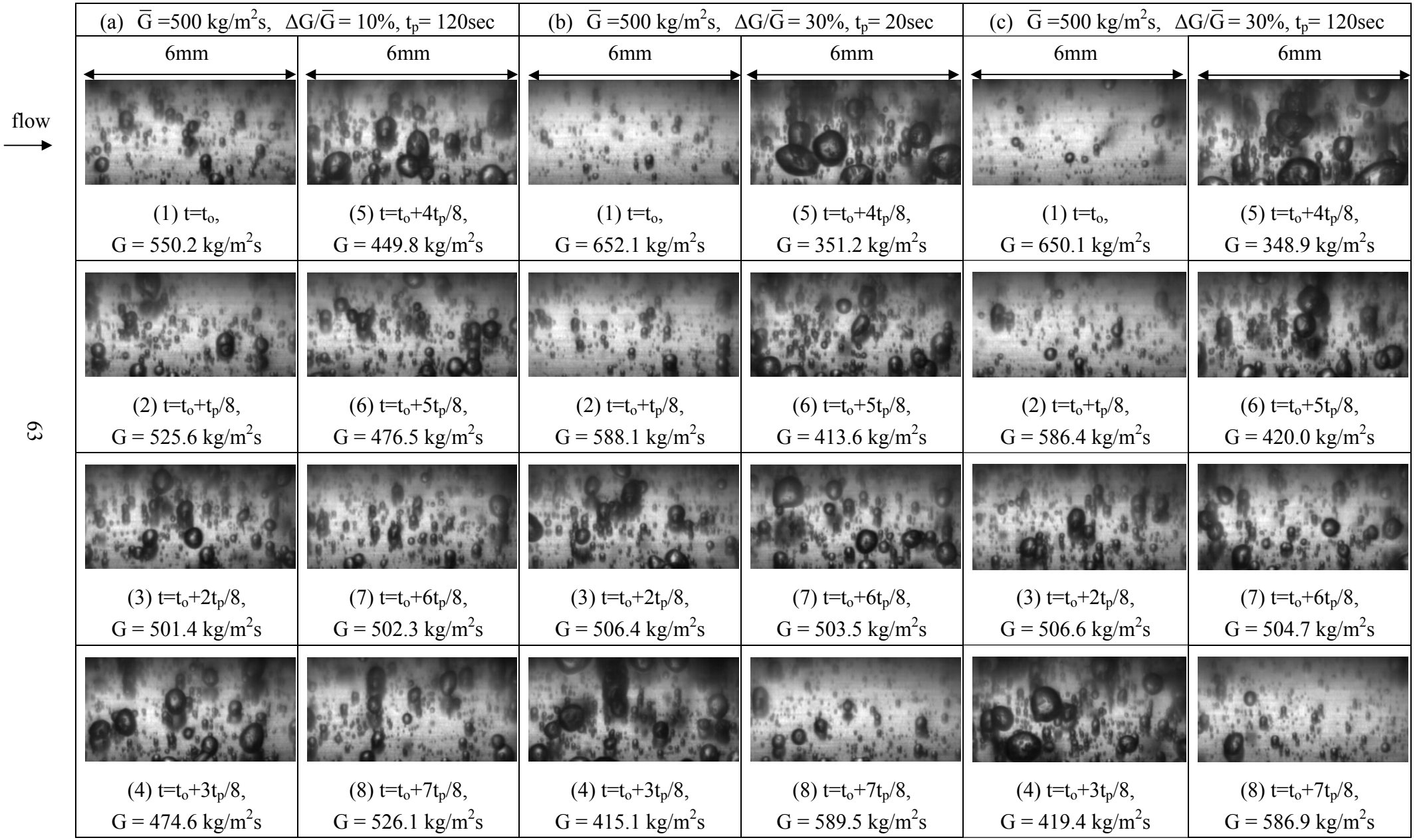


Fig. 4.12 Photos of bubbles in time periodic flow boiling of R-134a in a small region around the middle axial location at eight time instants in a typical periodic cycle at δ = 2.0 mm $\bar{T}_{sat}$ =15℃, q =15kW/m^2 and $\bar{G}$ =500 kg/m^{2}s for various $\Delta G/\bar{G}$ and t_p at δ = 2.0 mm.

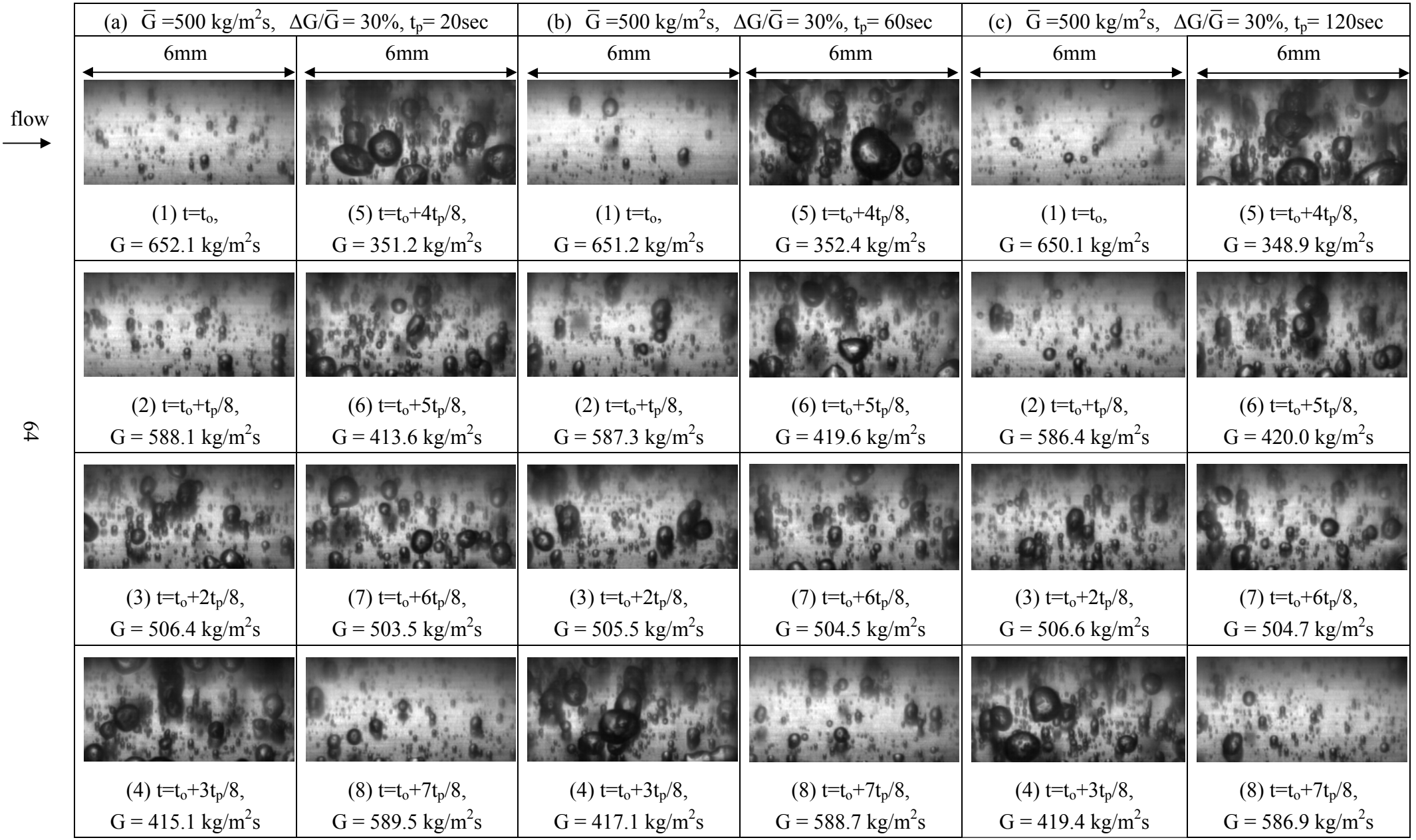


Fig. 4.13 Photos of bubbles in time periodic flow boiling of R-134a in a small region around the middle axial location at eight time instants in a typical periodic cycle at δ = 2.0 mm $\overline{T}_{sat}$ =15℃, q =15kW/m^2 and $\overline{G}$ =500 kg/m^{2}s for various t_p at δ = 2.0 mm.

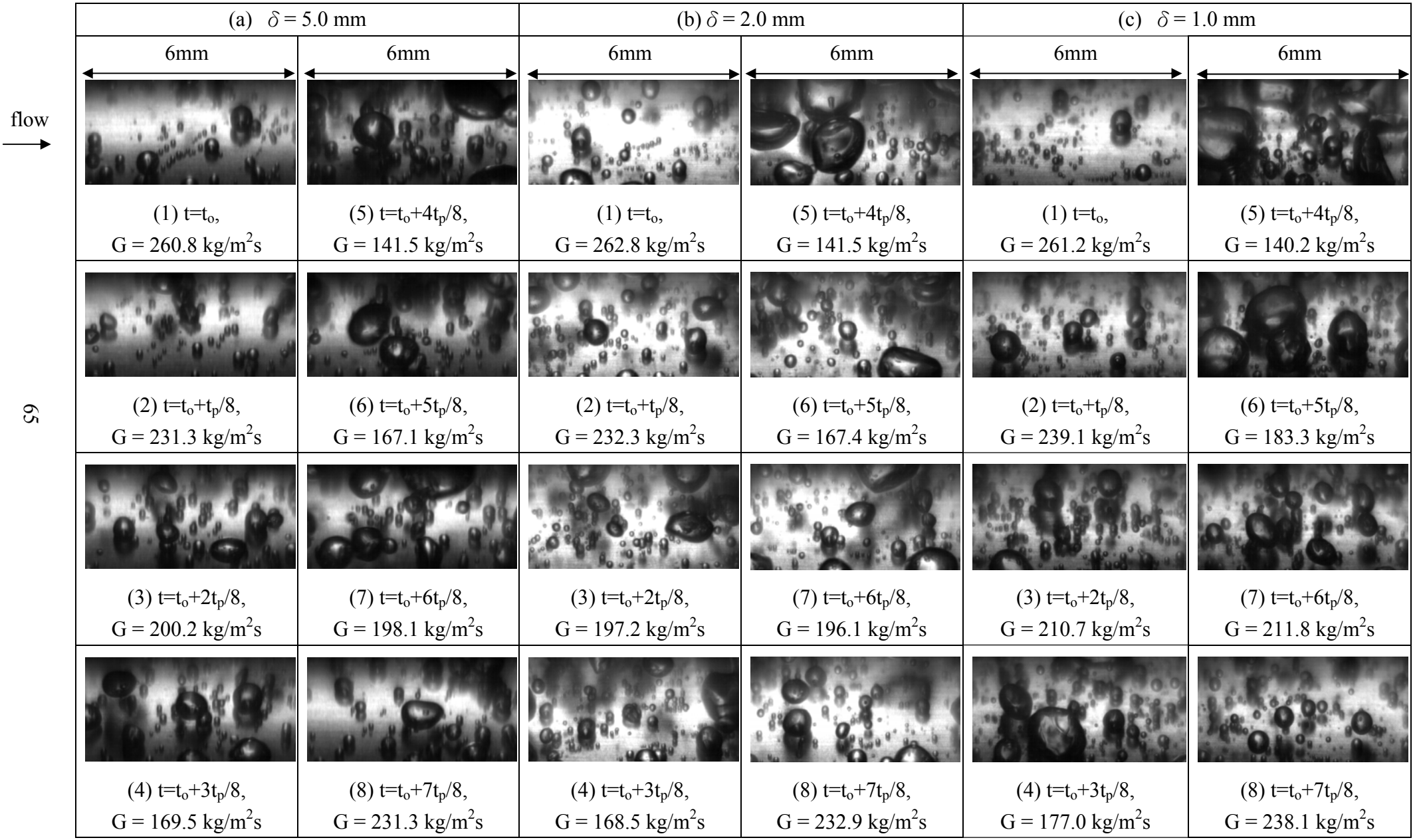


Fig. 4.14 Photos of bubbles in time periodic flow boiling of R-134a in a small region around the middle axial location at eight time instants in a typical periodic cycle at $\overline{T}_{sat}$ =15℃, q =10kW/m^2, $\overline{G}$ =200 kg/m^{2}s, $\Delta G/\overline{G}$ = 30% and t_p= 120sec for various gap sizes.

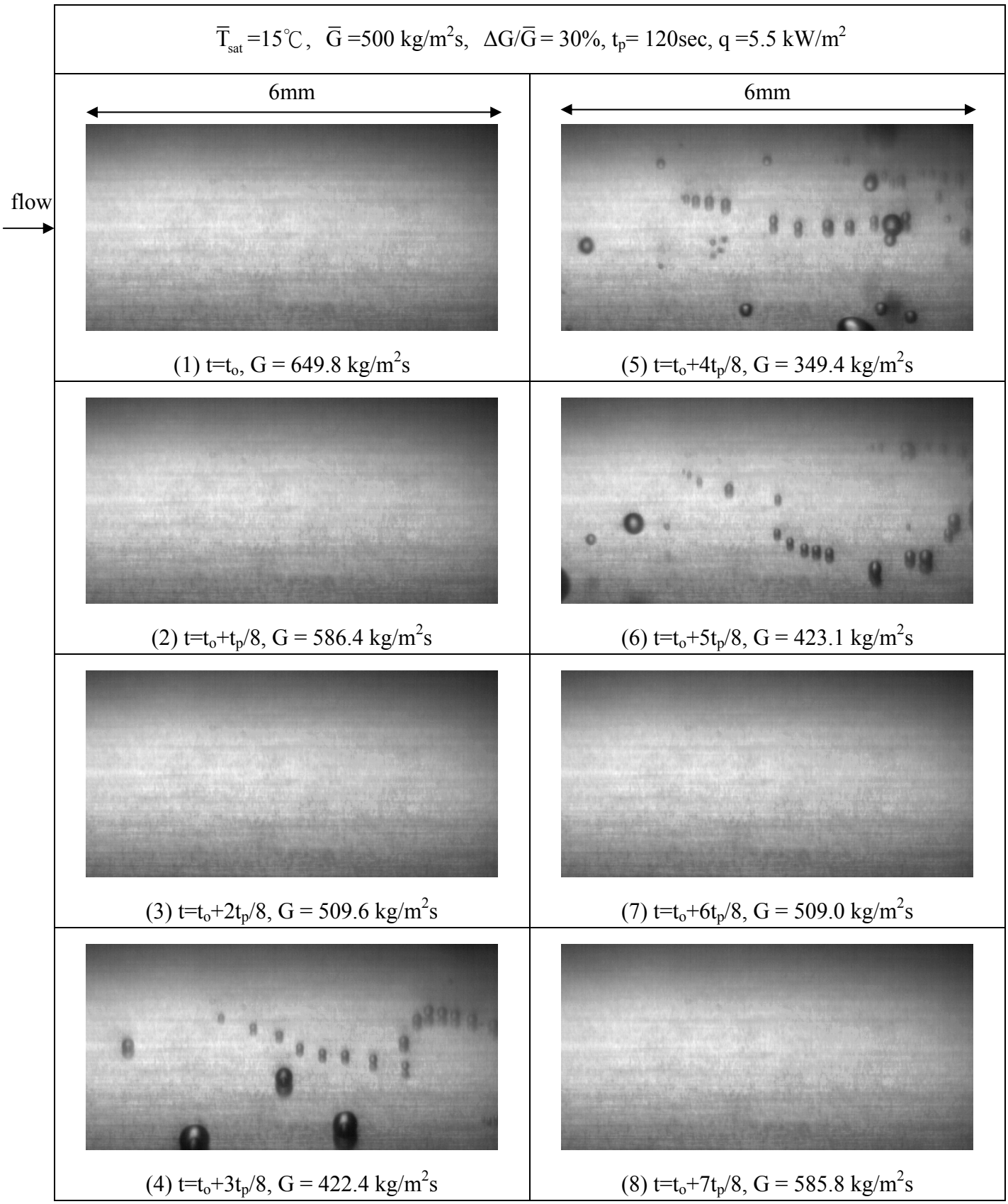


Fig. 4.15 Photos of bubbles in the time periodic intermittent flow boiling of R-134a in a small region around the middle axial location at eight time instants in a typical time periodic cycle for $\overline{T}_{sat}$ =15℃, $\overline{G}$ =500 kg/m²s, q =5.5 kW/m², ΔG/$\overline{G}$ = 30% and t_p= 120sec at δ = 2.0 mm.

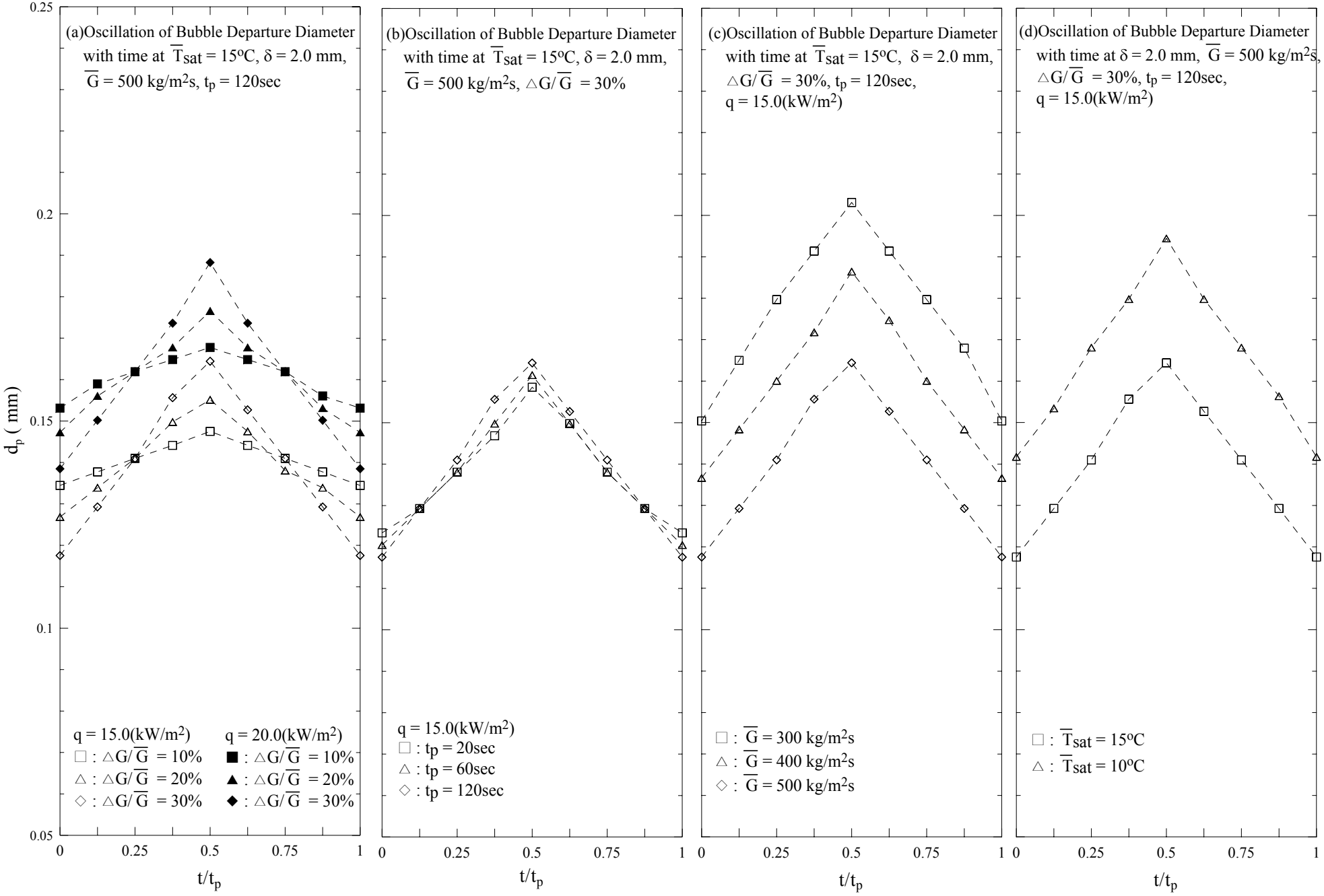


Fig.4.16 Mean bubble departure diameter variations with time in a typical periodic cycle for various $\Delta G/\overline{G}$ at q =15.0 & 20.0 kW/m²(a), t_p(b), $\overline{G}$ (c), and $\overline{T}_{sat}$ (d) at $\overline{G}$ =500 kg/m²s at δ = 2.0 mm.

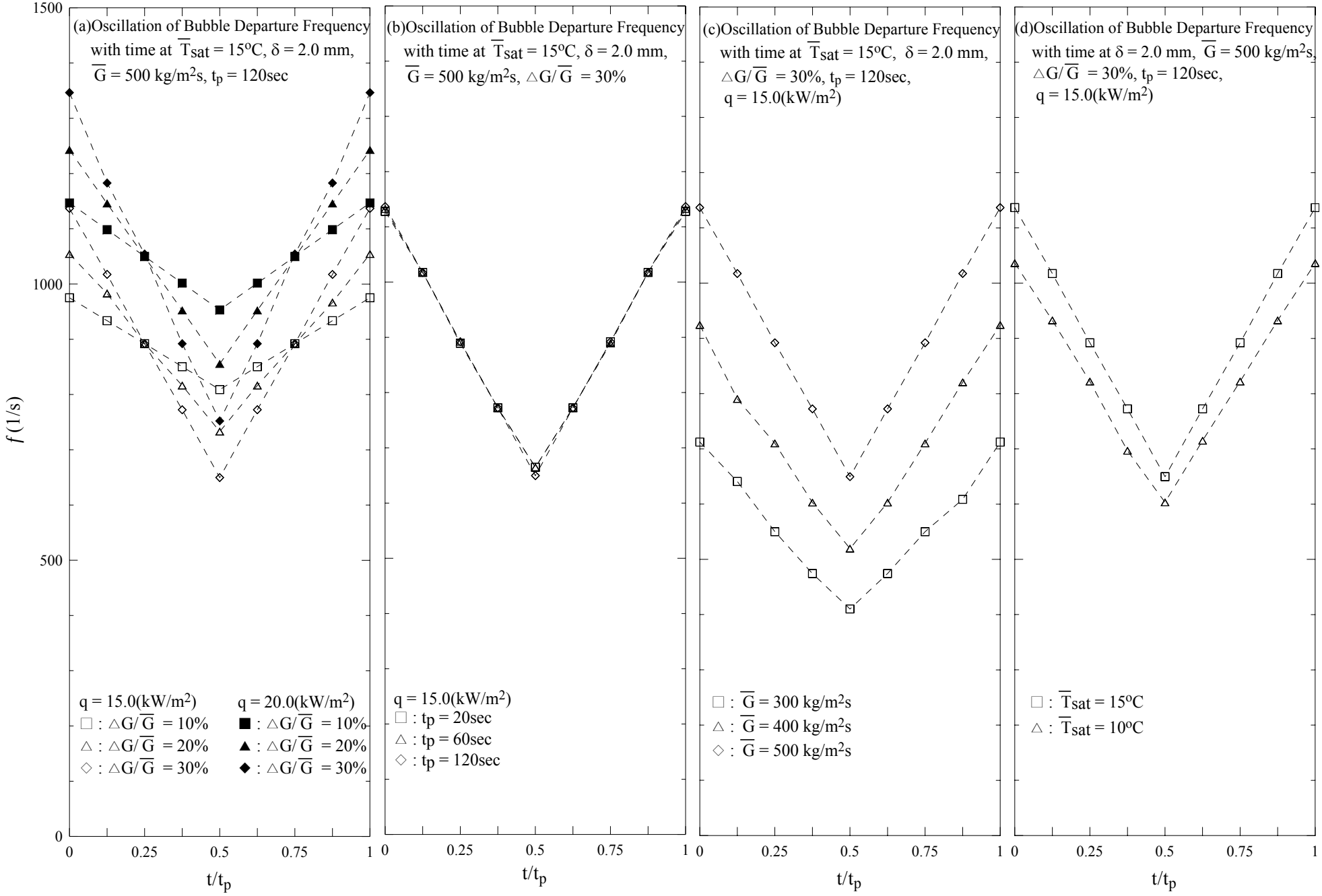


Fig. 4.17 Mean bubble departure frequency variations with time in a typical periodic cycle for various $\Delta G/\overline{G}$ at q =15.0 & 20.0 kW/m²(a), t_p(b), $\overline{G}$ (c), and $\overline{T}_{sat}$ (d) at $\overline{G}$ =500 kg/m²s at δ = 2.0 mm.

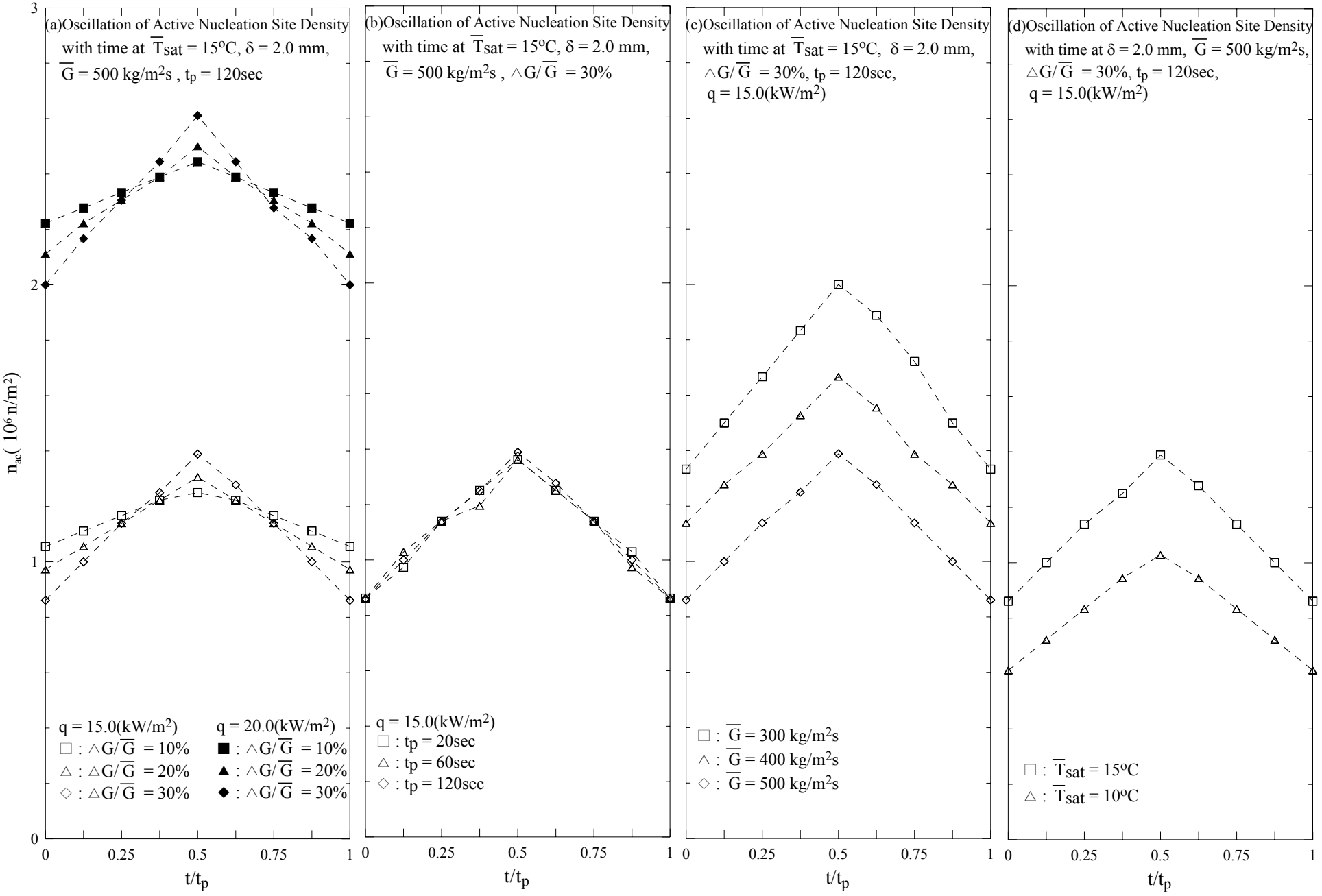


Fig. 4.18 Mean active nucleation site density variations with time in a typical periodic cycle for various $\Delta G/\overline{G}$ at q =15.0 & 20.0 kW/m²(a), t_p(b), $\overline{G}$ (c), and $\overline{T}_{sat}$ (d) at $\overline{G}$ =500 kg/m²s at δ = 2.0 mm.

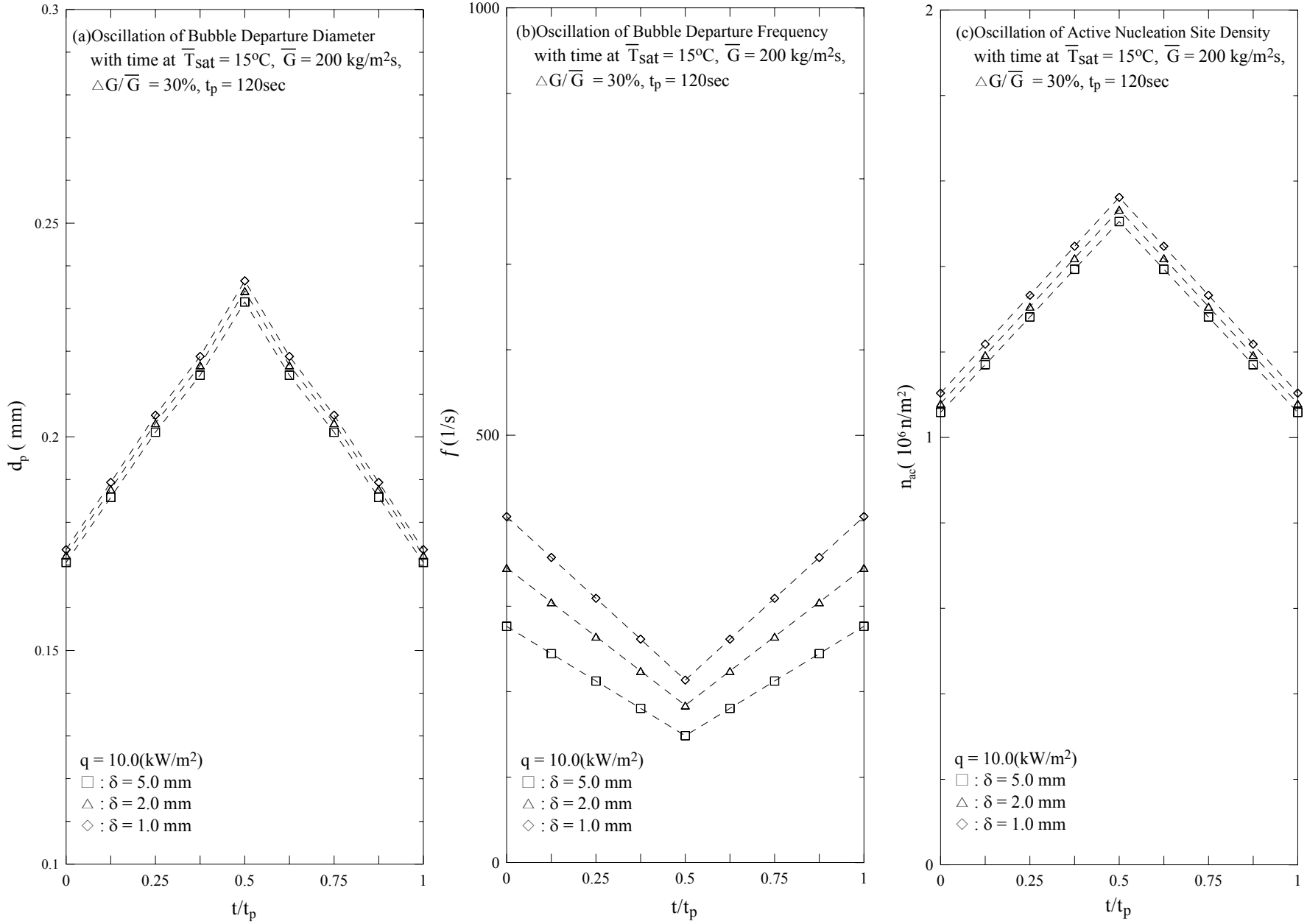


Fig. 4.19 Mean bubble departure diameter (a), bubble departure frequency (b), and active nucleation site density (c) variations with time in a typical periodic cycle at $\overline{T}_{sat}$ =15℃, q =10kW/m², $\overline{G}$ =200 kg/m²s, $\Delta G/\overline{G}$ = 30% and t_p= 120sec for various gap sizes.

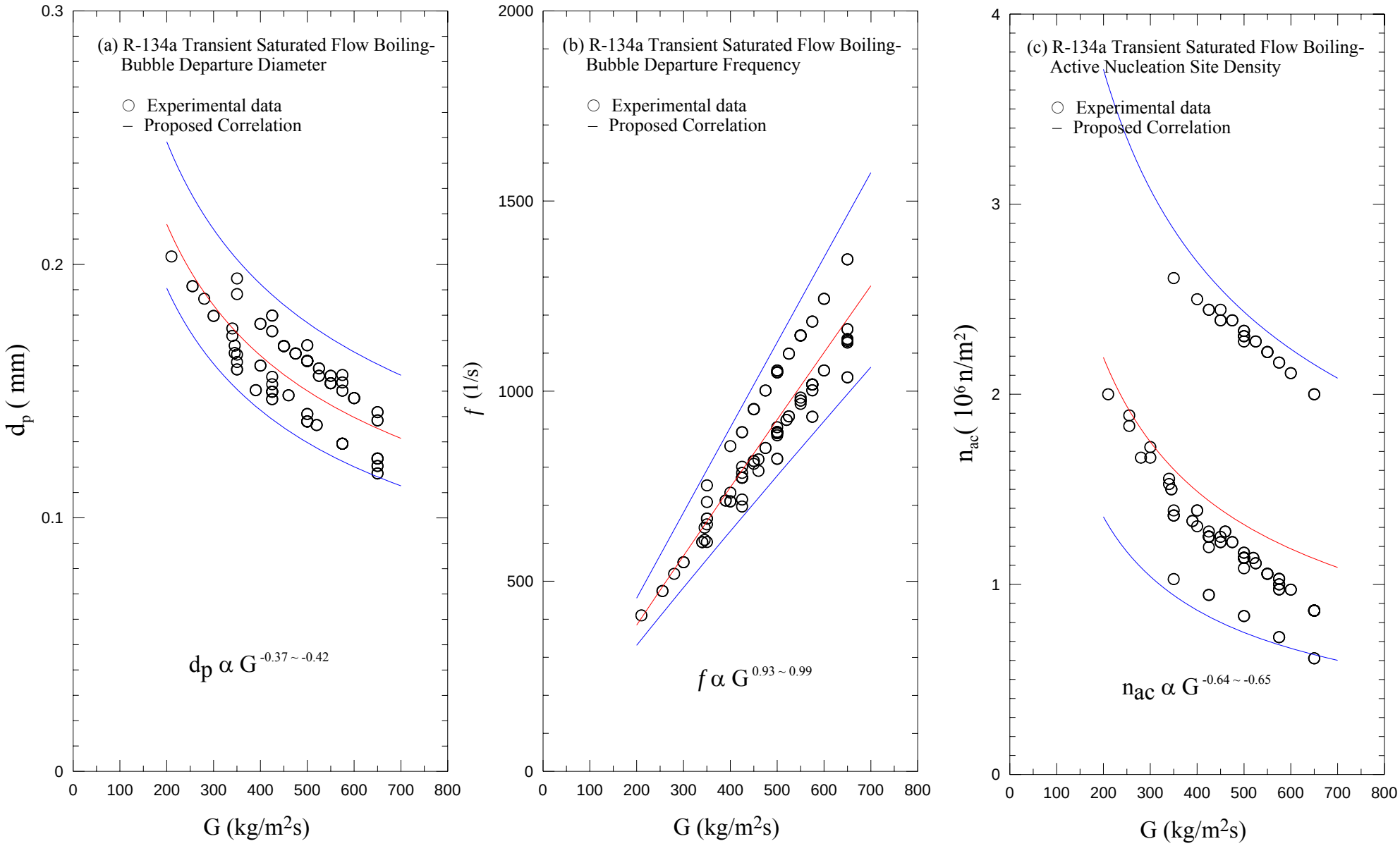


Fig. 4.20 Variations of bubble departure diameter (a), departure frequency (b), and active nucleation site (c) for time-periodic saturated flow boiling with mass flux of R-134a.

CHAPTER 5

Time Periodic Saturated Flow Boiling Heat Transfer of R-407C and Associated Bubble Characteristics in a Narrow Annular Duct due to Flow Rate Oscillation

In a flow with an imposed temporal mass flux oscillation the refrigerant pressure at the duct inlet also varies with time, so does the refrigerant saturated temperature. In the first part of the present study the inlet temperature of the refrigerant is controlled at the time-average value of the instantaneous saturated temperature of the refrigerant at the duct inlet. Besides, the refrigerant quality at the inlet is set at zero. This is designated as 〝saturated flow boiling〞 here. The mass flux oscillation is in the form of triangular waves. Results from the present measured heat transfer data and observed bubble characteristics for the saturated flow boiling of R-407C in the narrow annular duct affected by the imposed oscillating refrigerant mass flux, imposed heated flux, system pressure, and duct size are examined here. In this part of the experiment, results are obtained for the mean refrigerant mass flux $\overline{G}$ varied from 100 to 600 kg/m^{2}s and the amplitude of the mass flux oscillation $\Delta G/\overline{G}$ fixed at 10, 20, 30% of $\overline{G}$ with the period of the mass flux oscillation t_p fixed at 20, 60 and 120 seconds. The time-average refrigerant saturation temperature $\overline{T}_{sat}$ is set at 10 and 15℃ for the imposed heat flux varied from 0 to 45 kW/m^2. The gap between the inner and outer pipes δ is fixed at 1.0, 2.0 and 5.0 mm. The measured boiling heat transfer data are expressed in terms of the boiling curve and boiling heat transfer coefficient along with the time variations of the heated surface temperature. Besides, the close view flow photos taken at a small region around the middle axial station z =80 mm are presented to illustrate the bubble characteristics in the time periodic boiling flow. Then, comparison between the time periodic R-407C saturated flow boiling data due to the mass flux oscillation with that of stable boiling is conducted. Moreover, the quantitative bubble characteristics in the time periodic flow boiling will be examined.

5.1 Single-phase Heat Transfer

Before beginning the time periodic flow boiling experiments, the steady single-phase

convective heat transfer experiments are conducted for liquid R-407C. The measured single-phase convection heat transfer coefficients are compared with the correlations proposed by Dittus-Boelter [46] and Gnielinski [55]. In the steady single-phase heat transfer tests the refrigerant mass flux is varied from 200 to 1,050 kg/m^{2}s for the annular gap of the duct δ=1.0 mm, 2.0 mm and 5.0 mm (corresponding to the Reynolds number of the refrigerant flow varied from 3,459 to 14,640) for the refrigerant saturated temperature T_{sat}=15℃ and inlet liquid subcooling ΔT_{sub}=4℃. Selected data from these tests are plotted in Figure 5.1.

The Dittus-Boelter correlation is

$$Nu_l = 0.023 \cdot \mathrm{Re}^{0.8} \cdot \mathrm{Pr}^{0.4} \qquad \text{for } \mathrm{Re} > 10^4 \tag{4.1}$$

and the Gnielinski correlation is

$$Nu_l = \frac{(f_f/8)(\mathrm{Re}-1000)\,\mathrm{Pr}}{1+12.7\sqrt{f_f/8}\,(\mathrm{Pr}^{2/3}-1)} \qquad \text{for } 2{,}300 < \mathrm{Re} < 10^6 \tag{4.2}$$

where $f_f = (1.82 \times \log_{10} \mathrm{Re} - 1.64)^{-2}$ (4.3)

The results in Figure 5.1 manifest that the present data for h_l can be well correlated by the Gnielinski correlations with a mean absolute error of 3.9%.

5.2 Stable and Time-average Saturated Flow Boiling Curves and Heat Transfer Coefficients

To illustrate the effects of the mass flux oscillation on the flow boiling characteristics, data for the R-407C saturated flow boiling for a constant refrigerant mass flux, the so called 〝stable flow boiling〞, shown in Figs. 5.2-5.7 are first compared with the time-average data for the cases with the time periodic refrigerant mass flux oscillation. The results from this comparison are shown in Figs. 5.2-5.7 by presenting the boiling curves for various mean mass fluxes and amplitudes and periods of the mass flux oscillation and for various refrigerant saturated temperatures and duct gaps. Note that at a low q for each time-average boiling curve the temperature of the heated wall at the middle axial location

increases gradually with the imposed heat flux from the time-average saturated temperature of the refrigerant to a certain value just slightly higher than $\overline{T}_{sat}$ and no bubble nucleation is observed. The heat transfer in this region is completely due to the single-phase forced convection. With the continuing increase in the surface heat flux, bubbles begin to appear on the surface and the boiling curve is characterized by a sharp increase in the surface heat flux for a small rise in the temperature of the heated surface. We have onset of nucleate boiling (ONB) in the flow. The reason causing the sharp increase in the slope of the boiling curve is due to a significant increase in the surface heat transfer by the boiling processes when ONB occurs. For the cases with oscillating refrigerant mass fluxes the ONB locations marked in these plots are the time-average values. Note that beyond ONB the refrigerant mass flux has slight effects on the boiling curves, suggesting that the time-average surface heat transfer is mainly dominated by the fully developed nucleate boiling. Besides, at a higher G the required heat flux for ONB is higher and this implies that more energy is needed for the vapor to nucleate from the wall since the residence time of the refrigerant on the heated surface is shorter and the refrigerant is at a lower temperature. It can be concluded from the results in Figs. 5.2 - 5.7 that the time-average boiling curves are not affected by the mean level, amplitude and period of the refrigerant mass flux oscillation and by the time-average refrigerant saturated temperature to a significant degree.

We move further to explore how the sable and transient time-average saturated flow boiling heat transfer coefficients h_r are affected by the R-407C mass flux oscillation. The results for the variations of the time-average h_r with the imposed surface heat flux at the middle axial location presented in Figs. 5.8-5.13 reveal that the amplitudes and periods of the refrigerant mass flux oscillation have negligible influences on the time-average boiling heat transfer coefficients. However, for a given refrigerant mass flux the time-average boiling heat transfer coefficient increases substantially with the imposed heat flux.

5.3 Time Periodic Flow Boiling Heat Transfer Characteristics

The oscillatory saturated flow boiling heat transfer characteristics of R-407C in the annular duct resulting from the imposed temporal refrigerant mass flux oscillation are illustrated by presenting the time variations of the space-average heated surface temperature T_w and boiling heat transfer coefficient h_r at the middle axial location. For the

limiting case of stable flow boiling (ΔG=0) the measured heated surface temperature at z=80 mm for various q are essentially steady (Figs. 5.14 and 5.15). Data for various $\Delta G/\overline{G}$, $\overline{T}_{sat}$, δ and t_p are shown in Figs. 5.16-5.24 for various imposed heat fluxes and mean mass fluxes. The results indicate that at low imposed heat flux the single-phase liquid flow prevails in the duct and the heated surface temperature oscillates significantly with time for a large $\Delta G/\overline{G}$. At a high imposed heat flux intensive persistent boiling dominates. But, the heated surface temperature oscillation is milder. For the in-between intermediate imposed heat flux we observe boiling activity only in a certain fraction of the periodic cycle. Otherwise, the flow is in single-phase state. Thus at this intermediate heat flux we have intermittent boiling in the flow. The corresponding T_w oscillation is in an amplitude smaller than that for the single-phase flow and for the persistent boiling. A close inspection of these data reveals that in the single-phase flow the heated surface temperature increases with time as the imposed mass flux decreases with time. But an opposite trend is noted in the flow dominated by the persistent boiling in which the heated surface temperature decreases as the imposed mass flux is lowered. This phenomenon is somewhat unusual and will be examined in detail later when the quantitative data for the bubble characteristics are analyzed. Note that temporal oscillation of the heated surface temperature is also periodic in time and is at the same frequency as the mass flux oscillation. The saturation temperature of the refrigerant mass flux exhibits relatively weak effects on the T_w oscillation. Besides, the T_w oscillation amplitude varies nonmonotonically with an increase in the channel gap depending on the imposed heat flux level. Moveover, the T_w oscillation lags slightly behind the mass flux oscillation due to the thermal inertia of the heated pipe wall.

The appearance of the intermittent boiling in the flow needs to be examined closely. Based on the detailed flow observation, we note that at the imposed heat flux around that for the onset of stable flow boiling bubbles start to nucleate from the heated surface when the refrigerant mass flux is lowered to a certain level in the first half of the periodic cycle and more bubbles nucleate from the surface for a further reduction in the refrigerant mass flux. This trend is reversed when the mass flux increases in the second half of the periodic cycle. Specifically, at a certain high level of the mass flux the bubble nucleation stops and the flow is in single-phase state. Obviously, the single-phase flow prevails for a continuing rise in the mass flux. The above processes repeatedly occur forming the intermittent

boiling. For the imposed heat flux well below and well above the onset heat flux of stable flow boiling, apparently the flow is dominated respectively by the single-phase liquid and persistent boiling. The time instants for the start and stop of the bubble nucleation are marked on the curves for the cases with the intermittent boiling.

The appearance of heated surface temperature decreases with mass flux increases in the persistent flow boiling needs to be examined. Based on the detailed flow observation, we note that at the imposed heat flux around that for the onset of stable flow boiling bubbles start to nucleate from the heated surface when the refrigerant mass flux is lowered to a certain level in the first half of the periodic cycle and more bubbles nucleate from the surface for a further reduction in the refrigerant mass flux. The results that heated surface temperature became lower. This trend is reversed when the mass flux increases in the second half of the periodic cycle. Specifically, at a certain high level of the mass flux the bubble nucleation reduces. Obviously, when the bubble nucleation reduces, the heated surface temperature rises with the mass flux increase. The above processes repeatedly occur forming the persistent flow boiling.

The corresponding time variations of the space-average flow boiling heat transfer coefficient affected by the refrigerant mass flux oscillation are shown in Figs. 525 – 5.33. The results manifest that the flow boiling heat transfer coefficients also oscillate periodically in time and at the same frequency as the G oscillation. At a higher imposed heat flux and for a larger amplitude in the mass flux oscillation, the boiling heat transfer coefficients oscillate stronger. Besides in the first half of the periodic cycle at which the mass flux decreases with the time, the space-average heat transfer coefficient for the persistent boiling increases with time. The opposite processes occur in the second half of the periodic cycle. But for the cases with the single-phase flow h_r decreases with time in the first half of the cycle in which G decreases with time. And the opposite is the case in the second half of the cycle. Moreover, the oscillation in h_r also lags slightly behind the mass flux oscillation.

Finally, we move further to present the data in Figs. 5.34 and 5.35 to elucidate the effects of the experimental parameters on the amplitude of T_w oscillation over a wide range of the imposed heat flux covering the single-phase, intermittent and persistent boiling flow regimes. The results in Figs. 5.34(a) and (b) indicate that for all boiling flow regimes the T_w oscillation is stronger for a higher amplitude and a longer period of the mass flux

oscillation. The data shown in Figs 534(c) suggest that the saturation temperature of the refrigerant mass flux exhibits relatively weak effects on the T_w oscillation. Besides, the mean mass flux exhibits a nonmonotonic effect on the amplitude of the T_w oscillation, as evident from the data in Figs 5.35(a). Then, the data shown in Figs. 5.35(b) and (c) indicate that T_w oscillation increases noticeably with a increase in the channel gap in the persistent flow boiling for $q > 20 W/cm^2$. At the lower q the effects of duct gap on the amplitude of the Tw oscilation is milder. Moreover, for given $\overline{G}$, $\Delta G/\overline{G}$, $\overline{T}_{sat}$, t_p and δ the variation of the amplitude of the T_w oscillation with the imposed heat flux is also nonmonotonic.

5.4 Intermittent Boiling

It is of interest to note in the visualization of the boiling flow over the heated annular duct that for the imposed heat flux close to that needed for the ONB of the stable boiling, intermittent boiling appears. More specifically, in a typical periodic cycle for given heat flux and amplitude and period of the mass flux oscillation bubble nucleation in the heated annular duct is first seen at a certain time instant after the mass flux decrease to a certain low level. We have a start of boiling in the flow. Since then the boiling process continues. But after some period of time following the increase of the mass flux to a certain high level, bubble nucleation disappears and the boiling stops. The above process of intermittent boiling is repeatedly seen in the flow. To be more clear, we indicate the time instants at which boiling starts and stops in Figs. 5.16 – 5.33 for the cases with the presence of the intermittent boiling. Note that at a lower mean refrigerant mass flux and a higher imposed heat flux the onset of boiling is earlier and the termination of boiling is later. A flow regime map to delineate the boundaries separating different flow boiling regimes in terms of boiling number versus the relative amplitude of the mass flux oscillation is given in Fig. 5-36 for δ=2.0mm. The results show that the intermittent boiling prevails over a significantly wider range of the boiling number for a higher amplitude of the mass flux oscillation, a higher mean saturated temperature of the refrigerant, and the mean refrigerant flux lower from 400 to 300 kg/m^2s.

5.5 Time Periodic Bubble Characteristics in Saturated Flow Boiling

To elucidate the time-periodic saturated flow boiling heat transfer characteristics, the data for the bubble characteristics of R-407C flow boiling obtained from the present flow visualization are examined in the following. The side views of the boiling flow in a small

region around the middle axial location of the duct for various refrigerant mass fluxes and imposed heat fluxes are shown in Figs. 5.37-5.54 for the time periodic saturated flow boiling. At first, the bubble characteristics for the limiting cases of constant mass fluxes are illustrated by the photos in Fig. 5.37. It is noted from the flow visualization and the results in Fig. 5.37 that the vapor bubbles begin to appear as the heated surface temperature exceeds the boiling incipient superheat. In the beginning, tiny bubbles are observed in the active nucleation sites. The bubbles grow and then detach from the heated surface with certain mean bubble departure diameter. As the imposed heat flux increases, more bubbles are generated on more active nucleation sites and more bubbles detach from the heated surface. Besides, the detached bubbles tend to merge into larger bubbles. Note that the large bubbles become distorted and elongated as they slide on the heating surface. Moreover, at a higher mass flux the bubbles are smaller and the bubble coalescence is less significant. Next, the bubble characteristics in the time dependent flow boiling are illustrated by presenting the photos of the boiling flow at eight selected time instants in a typical periodic cycle in Figs. 5.38–5.54. In these figures the symbol " $t=t_o$ " signifies the time instant at which the instantaneous mass flux is at the highest level and starts to decrease with time. The results for the persistent flow boiling(Figs. 5.46-5.54)indicate that for a given imposed heat flux and fixed mean level, amplitude and period of the mass flux oscillation the bubbles get smaller and become more dispersed in the period of the time in which the instantaneous mass flux increases. The opposite processes take place when the instantaneous mass flux decreases with time. These changes of the bubble characteristics with the instantaneous mass flux become more significant for an increase in the amplitude of the mass flux oscillation.

Then, the bubble behavior in the intermittent flow boiling for the intermediate imposed heat fluxes is shown in Figs. 5.38 – 5.45. The results clearly indicate that initially at small t the instantaneous mass flux decreases with time but is still well above $\overline{G}$ no bubble nucleates from the heated surface. The flow is in single-phase state. Note that for the case shown in Fig. 5.38 the bubbles start to nucleate from the heated surface at a certain instant after $t_0+t_p/8$ at which the instantaneous mass flux already decreases a certain level. Note that the number and size of the bubbles increase noticeably with time in second quarter of the periodic cycle for the continuing decrease of the mass flux. Then in the third quarter of the periodic cycle the number and size of the bubbles diminish noticeably with time due to the increase of the mass flux with time. The bubbles cease to nucleate from the

heated surface at a certain time instant after $t_0+6t_p/8$ when the mass flux slightly exceeds $\overline{G}$ and bubble nucleation stop completely. Single-phase flow again dominates. We have to wait until about the end of the first quarter of the next cycle to see the bubble nucleation appearing on the heated surface. The above processes repeat in each cycle. The precise time instants of the onset and termination of nucleate boiling vary with the flow condition.

To quantify the bubble characteristics, the measured data for the time variations of the space-average bubble departure diameter and frequency and active nucleation site density in a typical periodic cycle are given in Figs. 5.55 – 5.63 for various mean levels, fluxes, amplitudes and periods of the mass flux oscillations and for various imposed heat fluxes and other parameters. Now as the mass flux oscillation is at low amplitude of 10%, the bubble departure diameter varies slightly with time Fig. 5.55(a). More specifically, the size of the departing bubbles increases almost linearly in the first half of the periodic cycle in which the mass flux decreases with time. While in the second half of the cycle an opposite process is noted since the mass flux increases with time. Similar trend is noted in Fig. 5.55(a) for higher $\triangle G/\overline{G}$ of 20% and 30%. The results in Fig. 5.55(a) further manifest that at the larger amplitude of the mass flux oscillation the time variation of the bubble departure diameter is noticeably stronger. Moreover, an increase in the period of the mass flux oscillation causes a relatively slight variation of the bubble departure diameter with time (Fig. 5.55(b)). Furthermore, an increase in the mean refrigerant mass flux and duct gap cause larger time variations of d_p.

Next, the data for the time variations of the space-average bubble departure frequency for various cases are shown in Figs. 5.58 – 5.60. The increase of f with G is ascribed to the higher drag on the bubbles attaching to the heated surface by the liquid refrigerant moving at a higher speed for a higher G. This in turn, causes an earlier departure of the bubbles from the surface, resulting in a higher departure frequency. For a oscillation mass flux the bubbles depart from the heated surface at a decreasing rate in the first half of the periodic cycle in which the mass flux decreases with time. Apparently, in the second half of the cycle in which the mass flux increases with time the bubble departing rate increases. It should be pointed out that the time variations of the bubble departure frequency are stronger for the higher amplitude of the mass flux oscillation. But the effects of the period of the mass flux oscillation on the time variation of the bubble departure frequency are relatively milder. Obviously, reducing the duct gap causes a much larger variation of the

bubble departure frequency with time. But increasing G and $\overline{T}_{sat}$ mainly results in a higher mean level of the bubble departure frequency.

Finally, the time variation of the space-average active nucleation site density on the heated surface affected by the mass flux oscillation is illustrated in Figs. 5.61 – 5.63. Note that in the time periodic flow boiling the active nucleation site density increases with time in the first half of the periodic cycle in which the mss flux decreases with time. The reverse process appears in the second half of the cycle in which the mass flux increases with time. At the higher amplitude of the mass flux oscillation the time variation of n_{ac} is stronger. The effects of the period of the mass flux oscillation on the time variation of n_{ac} are relatively small. Besides, a lower mean refrigerant mass flux and a higher mean refrigerant saturation temperature mainly cause higher mean level of n_{ac}. It is due to the lower surface tension for R-407C at a higher saturated temperature which in turn facilitates the bubble nucleation. But reducing the duct gap from 2.0 to 1.0 mm results in a much weaker time variation of n_{ac} (Fig. 5.63(a)). For δ reduced from the 5.0 to 2.0 mm the mean level of n_{ac} becomes much lower (Fig. 5.63(b)).

Based on the present data, the dependence of the quantitative bubble characteristics on the mass flux oscillation can be approximately expressed as $d_p \alpha G^{-a}$, $f \alpha G^{b}$ and $n_{ac} \alpha G^{-c}$ in Figs. 5.63&5.64. Here the exponents a, b and c range respectively from 0.22 to 0.27, 0.355 to 0.41 and 0.84 to 0.96. Note that the latent heat transfer resulting from bubble nucleation in the persistent boiling q_b is proportional to d_p^3, f and n_{ac}, as discussed in the previous study [14]. Thus, $q_b \alpha G^{-d}$, here d varies from 1.145 to 1.36. This result clearly indicates that the flow boiling heat transfer gets better at decreasing refrigerant mass flux since q_b prevails in the boiling heat transfer. Besides, the dominated effect of the mass flux oscillation on the boiling heat transfer comes from the very significant influence of the mass flux on the active nucleation site density. Note that $q_s=h_l(T_w-T_{sat})$. Hence it can be expressed as $q_s \alpha G^{e}$ in Fig. 4.65, here e varies from 0.97 to 1.03. We calculate q_s and q_b for $q_t=15kW/m^2$ and find $q_s/(q_s+q_b)=0.39$. So q_b has a very significant influence on the total boiling heat transfer.

CHAPTER 7

TRANSIENT SATURATED FLOW BOILING OF FC-72 OVER A SMALL HEATED COPPER PLATE

The results obtained in the first part of the study are presented in this chapter to illustrate how the FC-72 mass flux oscillation affects the transient saturated flow boiling heat transfer of FC-72 over a small heated circular copper flat plate flush mounted on the bottom of a horizontal rectangular channel. The present experiments are carried out for the mean FC-72 mass flux fixed at 300 and 400 kg/m^2s for the imposed heat flux varying from 0.1 W/cm^2 to 10 W/cm^2. Besides, the amplitude of the coolant mass flux oscillation is set at 0%, 5% and 10% of the mean coolant mass flux. Moreover, the period of the mass flux oscillation is fixed at 10, 20 and 30 seconds. The coolant in the test section is at slightly subatmospheric pressure of 99 kPa with T_{sat} = 55°C for FC-72. In the following, the effects of the mean level, oscillation amplitude and period of the coolant mass flux, and the imposed heat flux on the transient FC-72 saturated flow boiling heat transfer performance are examined in detail. Note that for the limiting case of 0% mass flux oscillation for a given coolant mass flux we have saturated boiling of FC-72 at a coolant mass flux rate in the test section, which is designated as stable flow boiling. The heat transfer performance is presented mainly in terms of the transient variations of the average surface temperature of the copper plate and the boiling heat transfer coefficient.

7.1 Single-phase Liquid Convective Heat Transfer

Before beginning the two-phase flow boiling experiments, steady single-phase convective heat transfer experiments are conducted for liquid FC-72 flow in the

rectangular channel. The measured average heat transfer coefficients for single-phase convection from the heated copper surface to the coolant are compared with the correlation proposed by Gersey and Mudawar [8]. The correlation of Gersey and Mudawar [8] is

$$\overline{Nu}_L = 0.362 \cdot Re_L^{0.614} \cdot Pr^{1/3} \tag{7.1}$$

where

$$Re_L = \frac{G \cdot L}{\mu_l} \tag{7.2}$$

$$\bar{h}_{1\phi} = \frac{k_l}{L} \cdot \overline{Nu}_L \tag{7.3}$$

for the flow velocity ranging from 13 cm/s to 400 cm/s. Their correlation is based on the experimental data procured from the same liquid and same flow configuration as the present data and the comparison is shown in Fig. 7.1 for the dimensional and dimensionless heat transfer coefficients. The results indicate that our data are in good agreements with their correlation.

It should be mentioned that all of the working fluid properties used in reducing the data for Fig. 7.1 from Equations 7.1 - 7.3 are calculated at the coolant inlet temperature. The copper plate diameter is chosen as the characteristic length in defining the Reynolds number Re_L and average Nusselt number $\overline{Nu}_L$ because of its significant effect on the heat transfer performance [8].

7.2 Stable and Time-average Saturated Flow Boiling Curves and Heat Transfer Coefficient

To illustrate the effects of the mass flux oscillation on the boiling characteristics, data for the FC-72 saturated flow boiling for a constant coolant mass flux are first compared with the time-average data for a transient oscillatory coolant mass flux. The

results from this comparison are shown in Figures 7.2 and 7.3 by presenting the boiling curves for various mean mass fluxes and amplitudes and periods of the mass flux oscillation. Note that for each boiling curve at a given G the mean temperature of the copper plate increases gradually with the imposed heat flux at a low q from the saturated temperature of the coolant to a certain value just slightly higher than T_{sat} and no bubble nucleation is observed. The heat transfer in this region is completely due to the single-phase forced convection. With the continuing increase in the surface heat flux, bubbles begin to appear on the surface and the boiling curve is characterized by a sharp increase in the surface heat flux for a small rise in the temperature of copper surface. We have onset of nucleate boiling (ONB) in the flow. The reason causing the sharp increase in the slope of the boiling curve is due to a significant increase in the surface heat transfer by the boiling processes when ONB occurs. For the cases with oscillating coolant mass fluxes the ONB locations marked in these plots are the time-average values. Note that beyond ONB the coolant mass flux has slight effects on the boiling curves, suggesting that the surface heat transfer is mainly dominated by the fully developed nucleate boiling. Besides, at a higher G the required heat flux for ONB is higher and this implies that more energy is needed for the vapor to nucleate from the wall since the residence time of the coolant on the heated surface is shorter. It can be concluded from the results in Figures 7.2 and 7.3 that the time-average boiling curves are not affected by the amplitude and period of the coolant mass flux oscillation to a significant degree.

We move further to explore how the stable and transient time-average saturated flow boiling heat transfer coefficients $h_{2\phi,sat}$ are affected by the FC-72 coolant mass flux oscillation. The results for the variations of the time-average $h_{2\phi,sat}$ with the surface heat flux presented in Figures 7.4 and 7.5 reveal that the coolant mass flux

oscillation amplitude and period show negligible influences on the time-average flow boiling heat transfer coefficients. However, for a given coolant mass flux the boiling heat transfer coefficient increases substantially with the imposed heat flux. For example, at T_{sat} =55°C and $\bar{G}$ =400 kg/m^{2}s, the saturated boiling heat transfer coefficient for q =9.7 W/cm^2 is about 102% higher than that for q =3.2 W/cm^2 (Figure 7.4(a)).

7.3 Transient Flow Boiling Heat Transfer Characteristics

The transient boiling heat transfer characteristics for FC-72 flow over the heated copper plate resulting from the temporal coolant mass flux oscillation are illustrated by presenting the time variations of the space-average heated surface temperature T_w and heat transfer coefficient $h_{2\phi}$ for various imposed heat fluxes and mass fluxes. For comparison purpose the results for T_w for the limiting cases of constant coolant mass fluxes are shown in Figure 4.6. These data indicate that the fluctuations of the average heated surface temperature with time for various q and G are relatively small. The boiling can be regarded as at a statistically stable state.

Now when the coolant mass flux oscillates periodically in time in a form of nearly a triangular wave, significant temporal oscillations in the space average heated surface temperature occur for the imposed heat flux slightly higher than that for the time average ONB, as evident from the data shown in Figures 7.7 – 7.18 for the oscillation amplitude being 5% and 10% of the mean mass flux. Note that the temporal oscillation of the heated surface temperature is also periodic in time and is at the same frequency as the mass flux. Besides, the T_w oscillation gets stronger for higher imposed heat flux and higher amplitude of the mass flux oscillation. However, the period of the mass flux oscillation only slightly affects the T_w oscillation. It is of

interest to note that at a higher amplitude of the mass flux oscillation with $\triangle G$ being 10% of $\overline{G}$, even in the single-phase forced convection the space average heated surface temperature also oscillates noticeably with time at a relatively low imposed heat flux with $q < \overline{q}_{ONB}$ (Figures 7.13 – 7.18). Here $\overline{q}_{ONB}$ is the time-average heat flux for ONB for the cases with the oscillating mass flux. But for the imposed heat flux around $\overline{q}_{ONB}$ the T_w oscillation is small for most cases except for $\overline{G}$ =300 kg/m^{2}s with an intermediate period of the G oscillation at 20 seconds (Figure 7.15). A close inspection of the data given in Figures 7.7 – 7.18 further reveals that the T_w oscillation slightly lags the mass flux oscillation. Moreover for q substantially above $\overline{q}_{ONB}$ and in the period of time at which the instantaneous mass flux is higher than the average level, the space average heated surface temperature is higher than the corresponding time-average level, suggesting that the flow boiling heat transfer over the heated surface is poorer at a higher instantaneous G. But in the single-phase region the opposite is the case (Figures 7.13 - 7.15 and 7.17 – 7.18). The trend for the single-phase flow is apparently due to the better convection heat transfer for a higher mass flux. This somewhat unusual trend for the boiling flow requires more investigation into the bubble characteristics which will be examined later.

The corresponding time variations of the space-average flow boiling heat transfer coefficient affected by the coolant mass flux oscillation are shown in Figures 7.19 – 7.30. The results manifest that the flow boiling heat transfer coefficients also oscillate periodically in time and at the same frequency as the G oscillation. At a higher imposed heat flux and for the larger amplitude in the mass flux oscillation, the boiling heat transfer coefficients oscillate stronger. Besides in the period of time at which the mass flux is higher than the mean level, the space average boiling heat transfer coefficient is below the corresponding time-average level. Moreover, the oscillation in

$h_{2\phi}$ also lags slightly behind the mass flux oscillation.

In this transient oscillatory boiling flow the time variation of the coolant pressure at the inlet of the test section is also of interest in thermal-fluid design. These data are shown in Figures 7.31 – 7.42 for various cases. The results indicate that the inlet coolant pressure oscillates nearly in phase with the mass flux oscillation. Note that the inlet coolant pressure oscillation becomes somewhat irregular for the larger amplitude of the mass flux oscillation and a higher average mass flux (Figures 7.36, 7.38, 7.40 and 7.42). Finally, the quantitative data evaluated from the above results are summarized in Table 7.1 for the relative oscillation amplitudes of the space average heated surface temperature and boiling heat transfer coefficient $A_{T_w}/\Delta\bar{T}_{sat}$ and $A_{h2\varphi}/\bar{h}_{2\varphi}$ at various imposed heat fluxes and the amplitude and period of the coolant mass flux oscillation.

7.4 Transient Bubble Characteristics in Saturated Flow Boiling

To elucidate the transient saturated flow boiling heat transfer characteristics, the data for the bubble characteristics of FC-72 obtained from the present flow visualization are examined in the following. The top views of the boiling flow in a small region around the geometric center of the heated surface for various coolant mass fluxes and imposed heat fluxes are shown in Figs. 7.43 - 7.67 for the transient saturated flow boiling. At first, the bubble characteristics for the limiting cases of constant mass fluxes are illustrated by the photos in Figure 7.43. It is noted in the flow visualization and the results in Figure 7.43 that the vapor bubbles begin to appear as the heated surface temperature exceeds the boiling incipient superheat. In the beginning, tiny bubbles are observed in the active nucleation sites. The bubbles grow and then detach from the heated surface with certain mean bubble departure diameters.

As the imposed heat flux increases, more bubbles are generated on more active nucleation sites and more bubbles detach from the heated surface. Besides, the detached bubbles tend to merge into larger bubbles. Note that the large bubbles become distorted and elongated as they slide on the heating surface. Moreover, at a higher mass flux the bubbles are smaller and the bubble coalescence is less significant.

Next, the bubble characteristics in the transient flow boiling are illustrated by presenting the photos of the boiling flow at eight selected time instants in a typical periodic cycle in Figures 7.44 – 7.67. In these figures the symbol " $t=t_o$ " signifies the time instant at which the instantaneous mass flux is at the mean level and starts to increase with time. The results indicate that for a given imposed heat flux and fixed mean level, amplitude and period of the mass flux oscillation the bubbles get smaller and become more dispersed in the period the instantaneous mass flux increases. The opposite processes take place when the instantaneous mass flux decreases with time. These changes of the bubble characteristics with the instantaneous mass flux become more significant for an increase in the amplitude of the mass flux oscillation (Figures 7.44 and 7.56 and Figures 7.46 and 7.58). It is of interest to note that the mean level of the mass flux oscillation exhibits significant influences on the bubble characteristics in the transient flow boiling, as evident from comparing the results in Figures 4.44 and 4.46. Besides, the bubble characteristics are only affected slightly by the period of the mass flux oscillation for the small mass flux oscillation amplitude of 5%. But for the large amplitude of the mass flux oscillation of 10% the bubbles are larger for the cases with longer period of the mass flux oscillation (Figures 4.56 and 4.60).

To quantify the bubble characteristics, the measured data for the time variations of the space-average bubble departure diameter and frequency and active nucleation

site density in a typical periodic cycle are given in Figs. 4.68 – 4.94 for various mean coolant mass fluxes, amplitudes and periods of the coolant mass flux oscillations, and imposed heat fluxes.

The results in Fig. 4.68(a) indicate that the mean size of the bubbles departing from the copper plate is somewhat smaller for the mass flux raised from 300 to 400 kg/m^2s in the stable flow boiling. It reflects the fact that the coolant at a higher mass flux and hence at a higher speed tends to sweep the bubbles more quickly away from the heating surface. Now as the coolant mass flux oscillates, the bubble departure diameter varies significantly with time (Figures 4.68(b) - (c)). More specifically, the size of the departing bubbles decreases in the first and fourth quarters of the periodic cycle in which the instantaneous mass flux increases with time. While in the second and third quarters of the cycle an opposite process is noted since the instantaneous mass flux decreases with time. Besides, at a higher imposed heat flux the departing bubbles are larger. Similar trend is noted in Figures 4.69 – 4.71. Comparing the results in Figure 4.68 with Figure 4.69 and Figure 4.70 with Figure 4.71 indicates that at the larger amplitude of the mass flux oscillation the effects of the imposed heat flux on the bubble departure diameter are somewhat smaller. The results in Figures 4.72 – 4.75 indicate that the bubble departure diameters are only affected slightly by the period of the mass flux oscillation.

Next, the data for the variations of the space-average bubble departure frequency with time for various cases are shown in Figures 4.77 – 4.80. In the stable flow boiling the increase in the bubble departure frequency with the imposed heat flux and coolant mass flux is clearly seen. The increase of f with G is ascribed again to the higher drag on the bubbles still attaching to the heated surface by the liquid coolant moving at a higher speed for a higher G. This, in turn, causes an earlier departure of the bubbles from the surface, resulting in a higher departure frequency. For an

oscillation mass flux the bubbles depart from the heated surface at an increasing rate in the first and fourth quarters of the periodic cycle in which the coolant mass flux rises with time. Apparently, in the second and third quarters of the cycle in which G decreases the bubble departing rate reduces. It should be pointed out that the time variations of the bubble departure frequency are somewhat milder when compared with the bubble departure diameter. Figures 4.81 – 4.84 indicate that the bubble departure frequencies are only affected slightly by the period of the mass flux oscillation. The results shown in Figure 4.85 manifest that the mean level of the mass flux oscillation noticeably affects the bubble departure frequency.

Finally, the space-average active nucleation site density on the heated surface affected by the coolant mass flux oscillation is illustrated in Figures 4.86 – 4.89. The results in Figure 4.86(a) indicate that in stable flow boiling the active nucleation site density increases substantially with the imposed heat flux. But the increase is rather mild for the mass flux raised from 300 to 400 kg/m^{2}s. Note that in transient flow boiling the active nucleation site density decreases with time in the first and fourth quarters of the periodic cycle in which G increases. The reverse process appears in the second and third quarters of the cycle in which the coolant flow slows down. At the higher amplitude of the mass flux oscillation and at higher imposed heat flux the temporal variations of N_{ac} is stronger (Figures 4.88 and 4.89). The effects of the period of the mass flux oscillation on the time variations of N_{ac} are rather weak (Figures 4.90 – 4.93). The amplitude of the N_{ac} oscillation is slighter higher for a larger amplitude of the mass flux oscillation (Figure 4.94).

7.5 Correlation Equations

According to the present experimental data, empirical correlations for the space-average bubble departure diameters in FC-72 stable and transient saturated flow boiling on the heated circular copper flat plate flush mounted on the bottom of the

rectangular channel estimated from the present flow visualization are proposed as

$$\frac{d_p}{\sqrt{\sigma/g\cdot\Delta\rho}} = \frac{0.2\cdot(\rho_l/\rho_v)^{0.48}\cdot\overline{Bo}^{0.21}}{\overline{Re_D}^{0.08}} \quad \text{for stable flow boiling} \tag{4.4}$$

where $\overline{Re_D}$ and $\overline{Bo}$ are the mean Reynolds and Boiling numbers respectively. They are defined as

$$\overline{Re_D} = \frac{\bar{G}\cdot D}{\mu_l} \tag{4.5}$$

$$\overline{Bo} = \frac{q''}{\bar{G}\cdot i_{lv}} \tag{4.6}$$

and

$$\frac{d_p}{\sqrt{\sigma/g\cdot\Delta\rho}} = \frac{0.2\cdot(\rho_l/\rho_v)^{0.48}\cdot Bo^{0.22}}{Re_D^{0.08}} \quad \text{for transient flow boiling} \tag{4.7}$$

where Re_D and Bo are respectively the instantaneous Reynolds and Boiling numbers. They are defined as

$$Re_D = \frac{G\cdot D}{\mu_l} \tag{4.8}$$

$$Bo = \frac{q''}{G\cdot i_{lv}} \tag{4.9}$$

where $G(=\bar{G}+\Delta G)$ is the instantaneous coolant mass flux, $\bar{G}$ is the average coolant mass flux, ΔG is the amplitude of the mass flux oscillation, ρ_l is the liquid density, and D is the copper plate diameter. Figures 4.95 and 4.96 show that the present experimental data fall within ± 20 % of the correlations given in Equations (4.4) and (4.7). In addition, empirical equations are provided to correlate the data for the space-average bubble departure frequency as

$$\frac{f\cdot d_p}{\mu_l/\rho_l\cdot D_h} = 0.5\overline{Re_D}^{1.3}\cdot Pr^{0.7}\cdot\overline{Bo}^{0.66} \quad \text{for stable flow boiling} \tag{4.10}$$

and

$$\frac{f\cdot d_p}{\mu_l/\rho_l\cdot D_h} = 0.5Re_D^{1.3}\cdot Pr^{0.7}\cdot Bo^{0.7} \quad \text{for transient flow boiling} \tag{4.11}$$

Figures 4.97 and 4.98 reveal that the present experimental data for $f\cdot d_p$ can be correlated with the deviation less than ± 20 % and ± 25 % by the above two equations. Moreover, empirical correlations for the space-average active nucleation site density in the FC-72 saturated flow boiling deduced from the present flow visualization are proposed as

$$N_{ac} \cdot d_p^{\,2} = -0.065+(85 \cdot \overline{Bo}^{0.83} \cdot \overline{Re_D}^{-0.15}) \quad \text{for stable flow boiling} \tag{4.12}$$

and

$$N_{ac} \cdot d_p^{\,2} = -0.03+(45 \cdot Bo^{0.85} \cdot Re_D^{-0.13}) \quad \text{for transient flow boiling} \tag{4.13}$$

The comparison in Figs. 4.99 and 4.100 shows that more than 85 % of the present experimental data fall within ± 30 % and ± 40 % of the correlation given in Equations (4.12) and (4.13). Finally, the total heat flux input to the stable boiling flow q_t is considered to be roughly composed of two parts: one resulting from the bubble nucleation q_b and another due to the single phase forced convection q_c. Thus

$$q_t = q_b + q_c \tag{4.14}$$

Here q_b and q_c can be individually calculated from the quantitative data for the bubble characteristics examined in section 5.3 and single phase liquid forced convection as

$$q_b = \rho_v \cdot V_v \cdot f \cdot N_{ac} \cdot i_{lv} \tag{4.15}$$

where ρ_v is the vapor density, V_v is the vapor volume of the mean departing bubble defined as $\frac{4\pi}{3}(\frac{d_p}{2})^3$, f is the space-average bubble departure frequency, N_{ac} is the space-average active nucleation site density, i_{lv} is the enthalpy of vaporization, and

$$q_c = E \cdot \bar{h}_{1\phi} \cdot \Delta T_{sat} \tag{4.16}$$

where E is an enhancement factor added to account for the agitating motion of the bubbles which can enhance the single phase liquid convection heat transfer. From the experimental data, E can be empirically correlated as

$$E = 4.5 \cdot N_{conf}^{\,0.5} \cdot \overline{Fr_l}^{0.15} \cdot (1+280 \cdot \overline{Bo})^{1.8} \quad \text{for stable flow boiling} \tag{4.17}$$

Here $\overline{Fr_l}$ is the Froude number and N_{conf} is the Confinement number. They are respectively defined as

$$N_{conf} = \frac{(\sigma/g \cdot \Delta\rho)^{0.5}}{D_h} \tag{4.18}$$

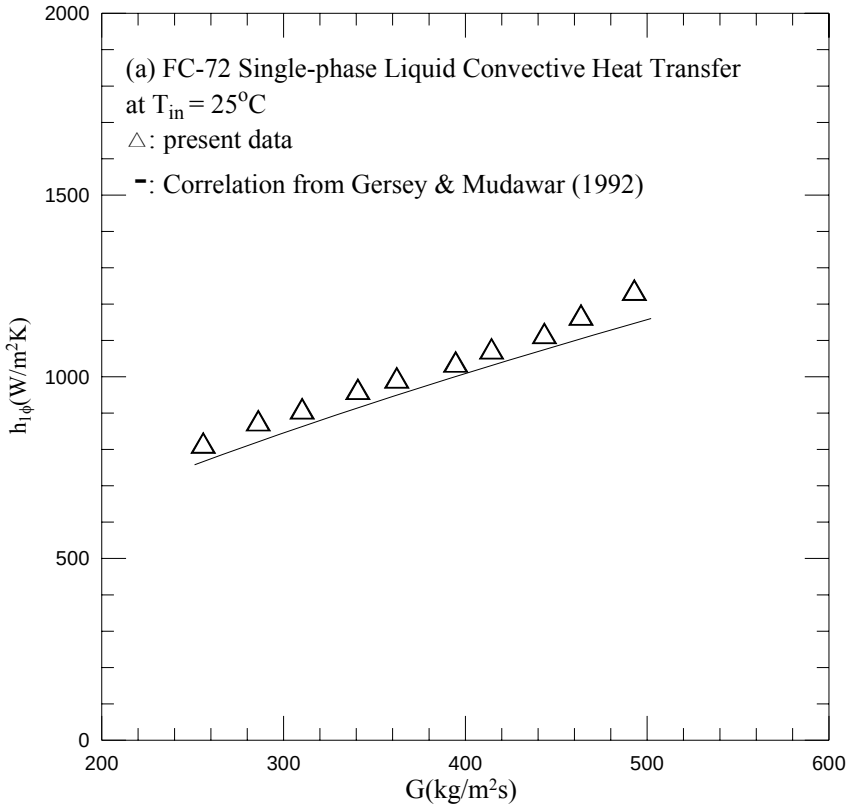
and

$$\overline{Fr_l} = \frac{\bar{G}^2}{\rho_l^2 \cdot g \cdot D_h} \tag{4.19}$$

where g is the acceleration due to gravity, D_h is the hydraulic diameter of the test section, and ΔT_{sat} (= T_w - T_{sat}) is the wall superheat. The results shown in Figure 4.101 indicate that the present data can be correlated with the deviation less than $\pm$ 25% by the empirical correlation given in Equations (4.14) - (4.19).

Table 7.1 Relative amplitudes of heated surface temperature and heat transfer coefficient oscillations in transient oscillatory saturated flow boiling for various imposed heat fluxes and the amplitudes and periods of the coolant mass flux oscillation.

$\Delta G/\bar{G}$	t_p (sec)	$\bar{G}$ =300 kg/m^{2}s			$\bar{G}$ =400 kg/m^{2}s		
		q(W/cm^2)	$A_{T_w}/\Delta\bar{T}_{sat}$	$A_{h_{2\varphi}}/\bar{h}_{2\varphi}$	q(W/cm^2)	$A_{T_w}/\Delta\bar{T}_{sat}$	$A_{h_{2\varphi}}/\bar{h}_{2\varphi}$
±5%	10	5.05	0.0097	0.0098	5.05	0.0099	0.0099
		6.23	0.0078	0.0078	6.24	0.0105	0.0105
		8.25	0.0095	0.0094	8.26	0.0096	0.0095
		9.74	0.0089	0.0088	9.74	0.0101	0.0100
	20	4.99	0.0098	0.0110	5.04	0.0179	0.0180
		6.18	0.0104	0.0128	6.18	0.0219	0.0221
		8.24	0.0083	0.0094	8.23	0.0153	0.0153
		9.75	0.0088	0.0087	9.76	0.0156	0.0156
	30	4.95	0.0084	0.0084	5.01	0.0182	0.0183
		6.15	0.0116	0.0116	6.16	0.0184	0.0184
		8.21	0.0094	0.0094	8.20	0.0141	0.0141
		9.70	0.0077	0.0077	9.72	0.0143	0.0144
±10%	10	5.04	0.0082	0.0082	5.03	0.0136	0.0136
		6.15	0.0153	0.0153	6.19	0.0178	0.0177
		8.17	0.0149	0.0149	8.20	0.0185	0.0185
		9.68	0.0151	0.0151	9.70	0.0185	0.0185
	20	4.95	0.0135	0.0135	4.99	0.0285	0.0285
		6.17	0.0177	0.0177	6.19	0.0280	0.0280
		8.21	0.0173	0.0173	8.22	0.0267	0.0267
		9.71	0.0185	0.0185	9.76	0.0230	0.0231
	30	4.94	0.0187	0.0188	5.02	0.0227	0.0227
		6.11	0.0189	0.0188	6.16	0.0226	0.0228
		8.18	0.0184	0.0184	8.20	0.0254	0.0256
		9.69	0.0184	0.0184	9.73	0.0252	0.0253



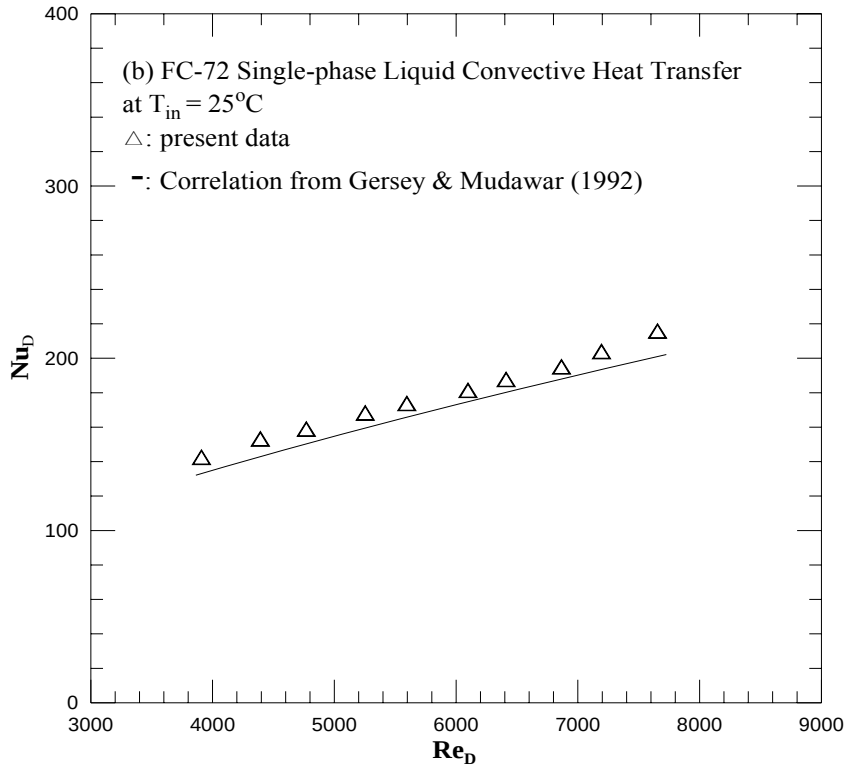


Fig. 7.1 Comparison of the present steady single-phase liquid convection heat transfer data with the correlation of Gersey and Mudawar (1992) for (a) $h_{1\phi}$ vs. G an (b) Nu_L vs. Re_L.

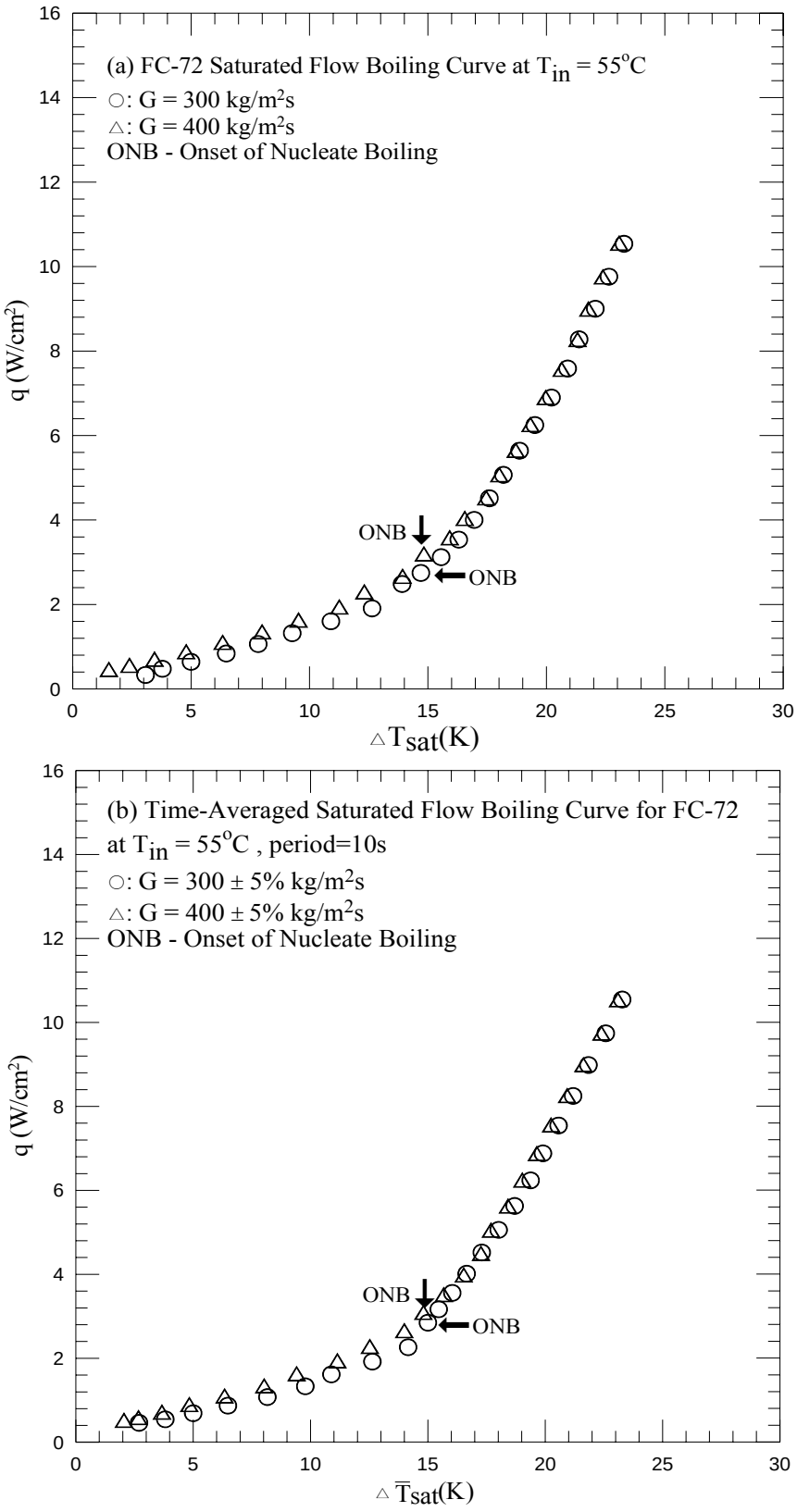


Fig. 7.2 Time-average flow boiling curves for various coolant mass fluxes for stable saturated flow boiling (a) and transient saturated flow boiling for t_p=10 sec (b), 20 sec (c) and 30 sec (d).

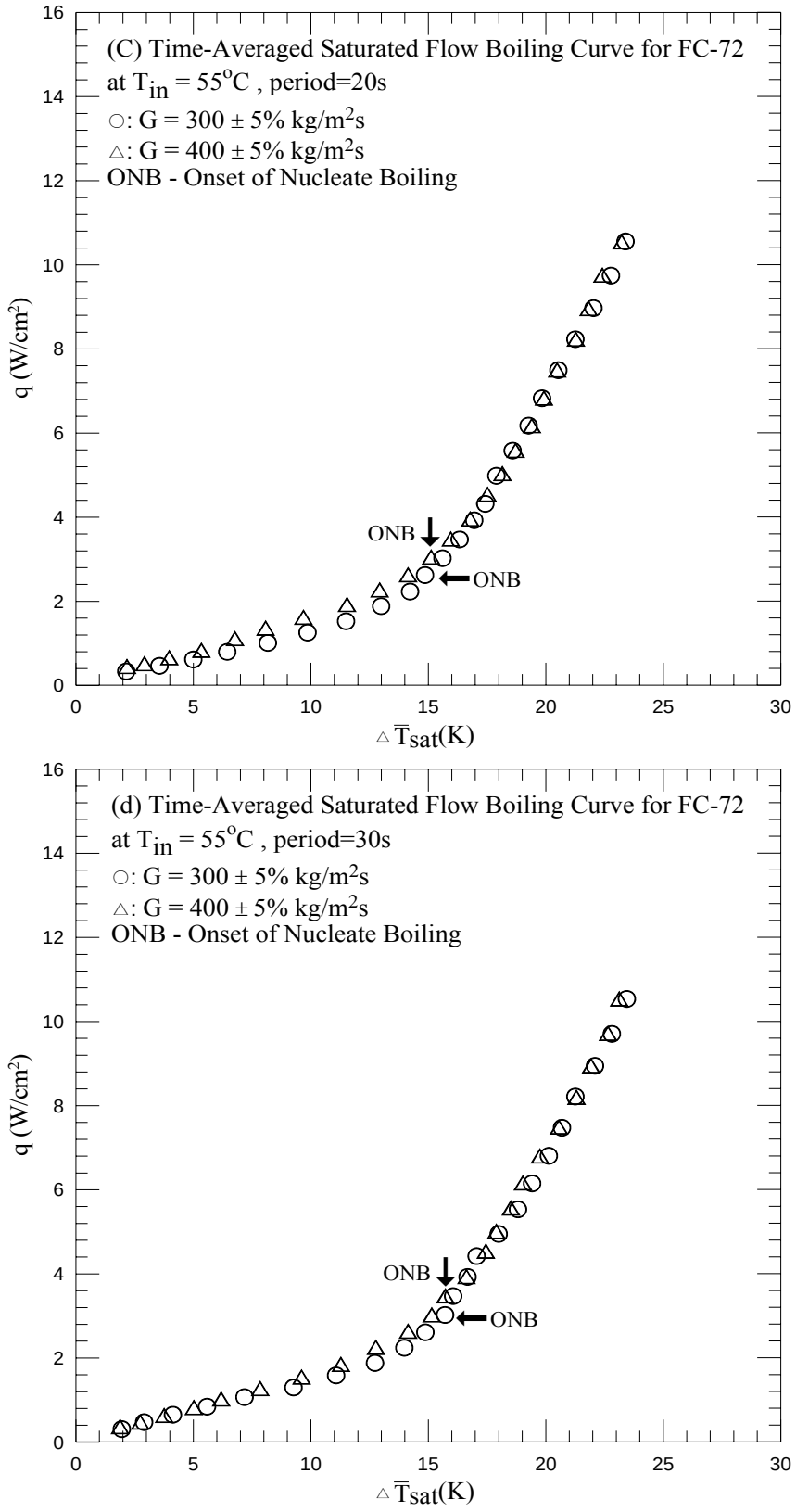


Fig. 7.2 Continued.

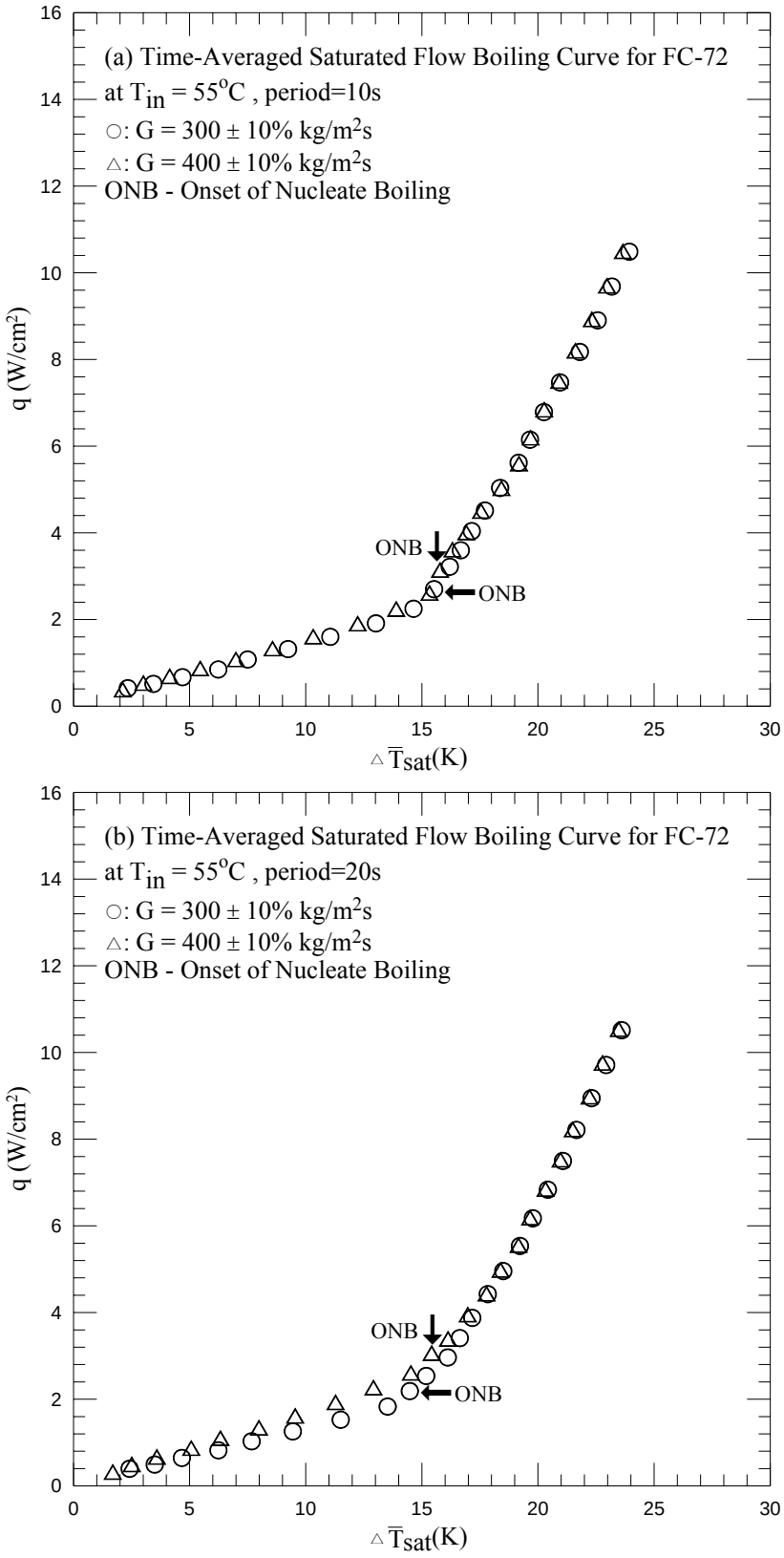


Fig. 7.3 Time-average flow boiling curves for various coolant mass fluxes for transient saturated flow boiling at t_p=10 sec (a), 20 sec (b) and 30 sec (c).

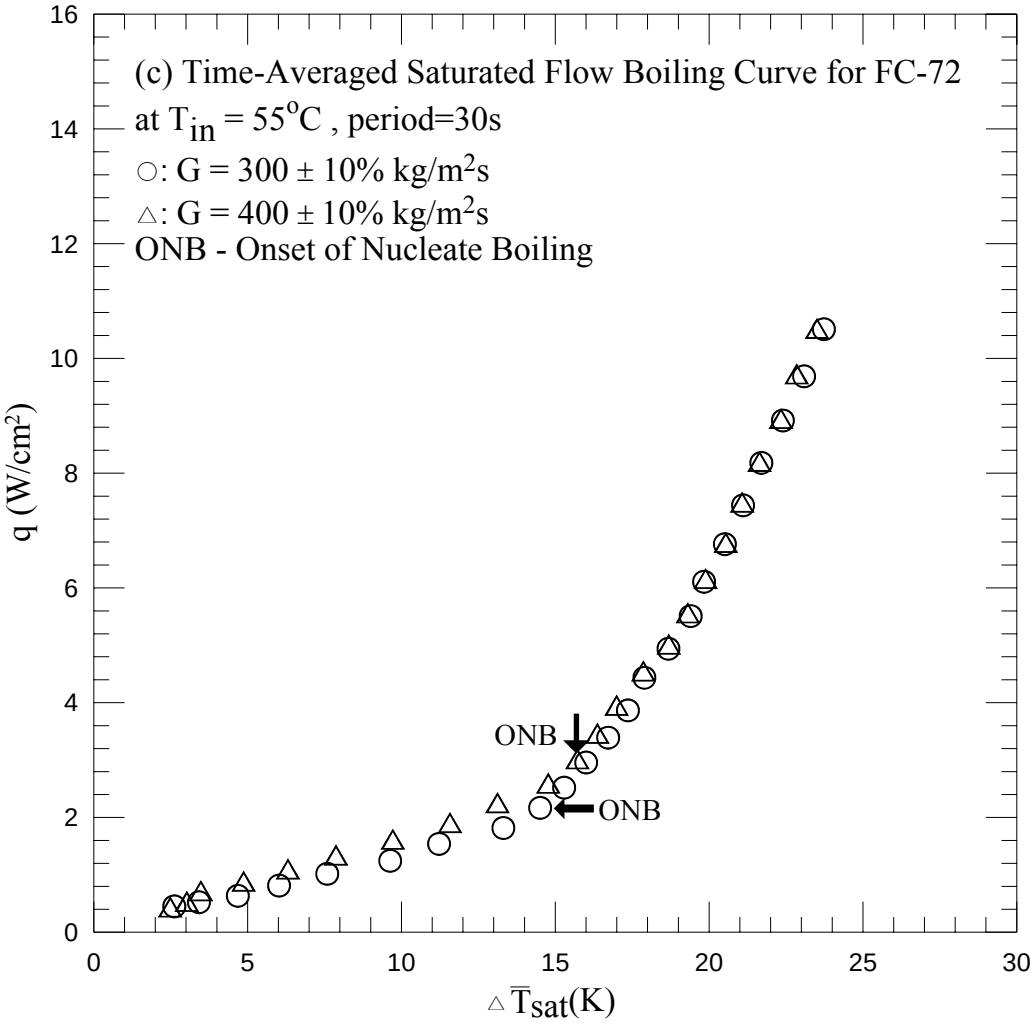


Fig. 7.3 Continued.

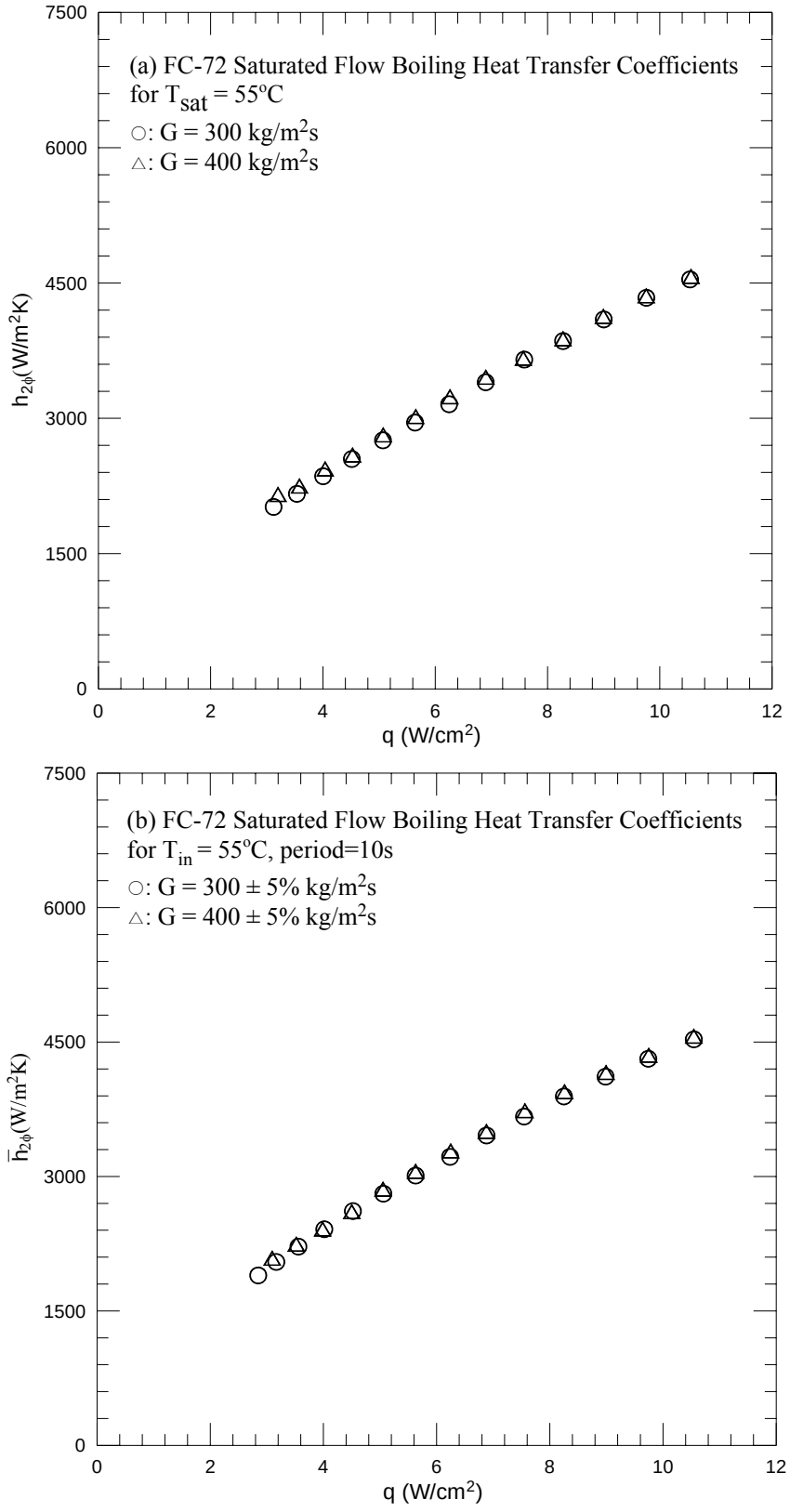
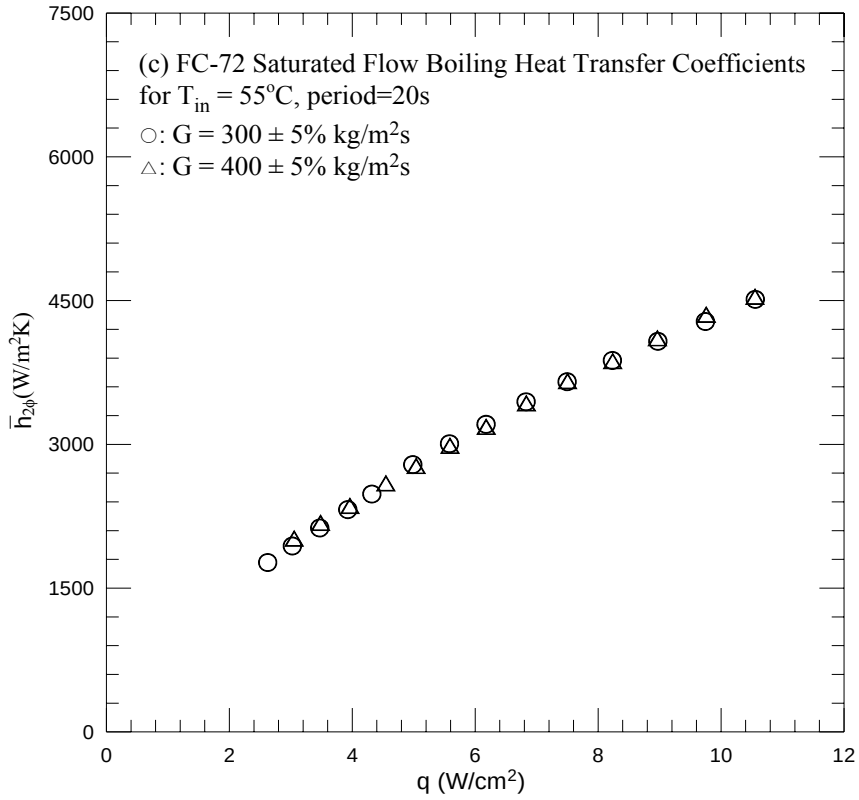


Fig. 7.4 Time-average flow boiling heat transfer coefficients for various coolant mass fluxes for stable saturated flow boiling (a) and transient saturated flow boiling at t_p=10 sec (b), 20 sec (c) and 30 sec (d).



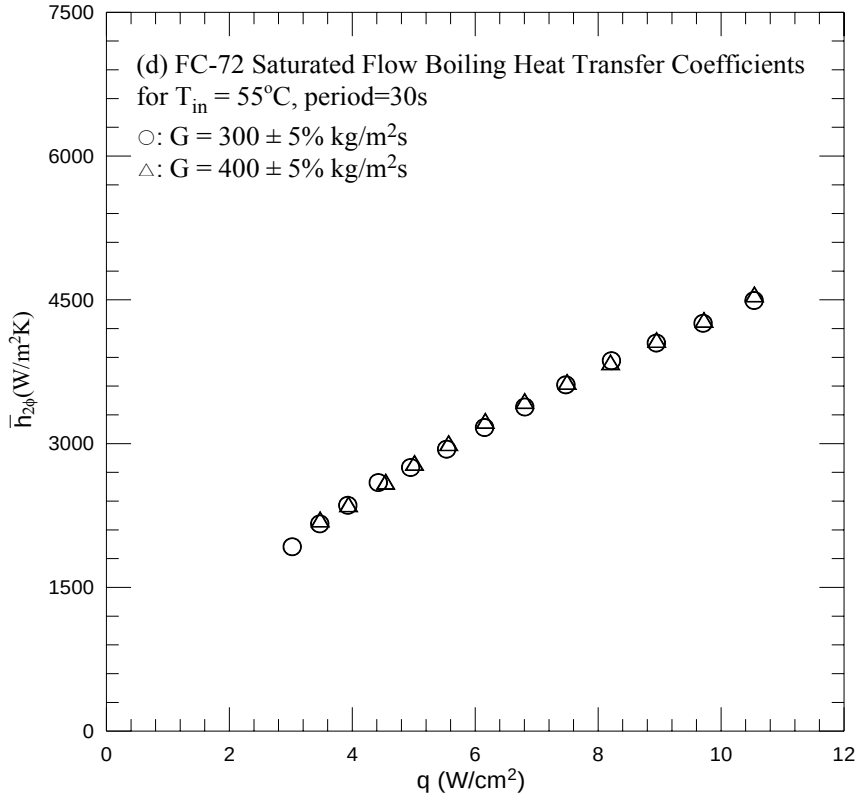
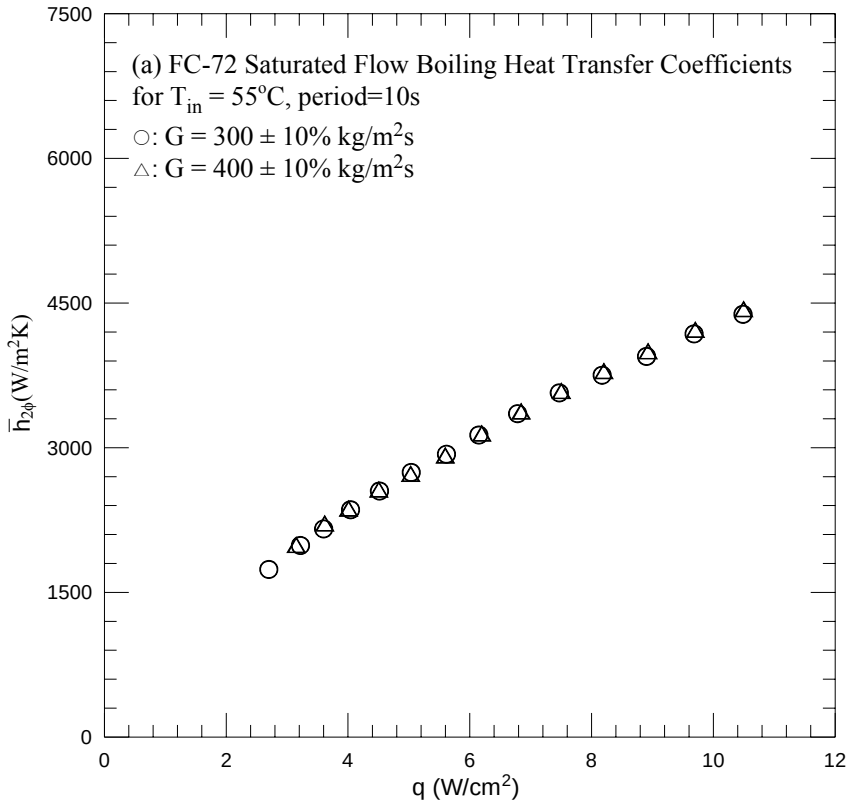


Fig. 7.4 Continued.



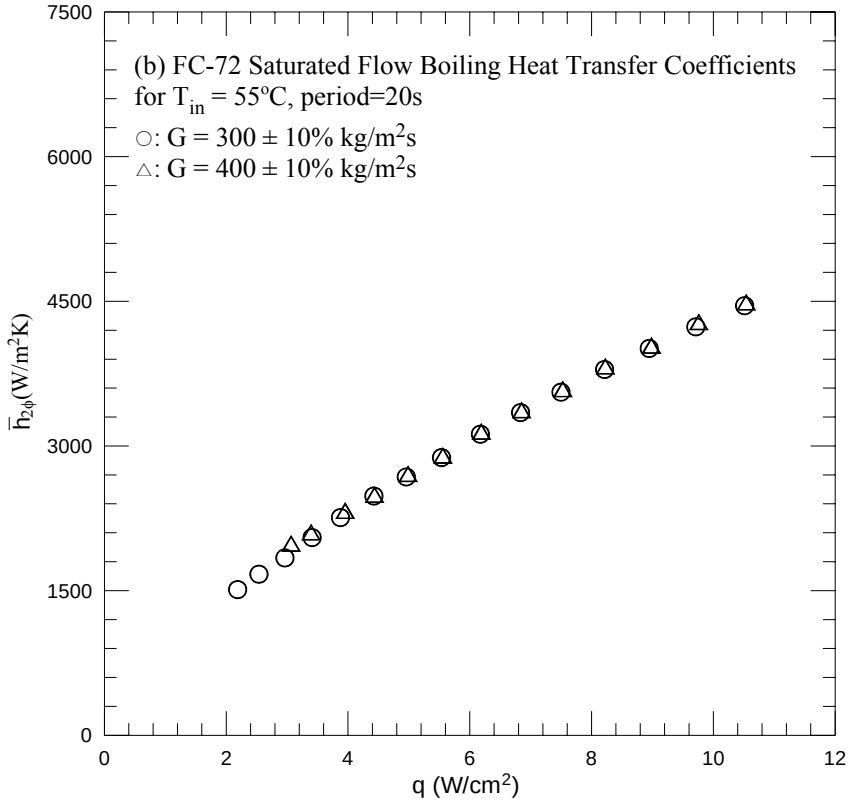


Fig. 7.5 Time-average flow boiling heat transfer coefficients for various coolant mass fluxes for transient saturated flow boiling at t_p=10 sec (a), 20 sec (b) and 30 sec (c).

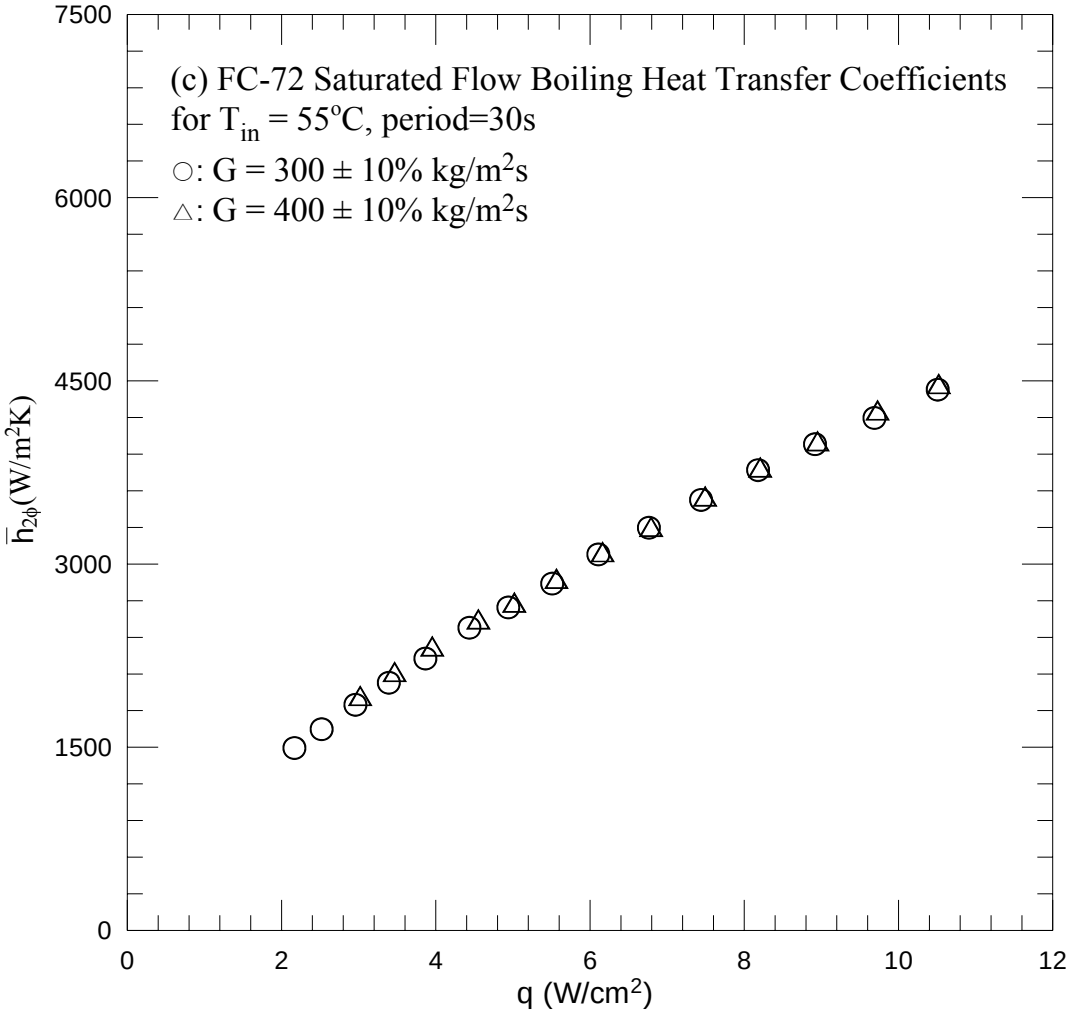


Fig. 7.5 Continued.

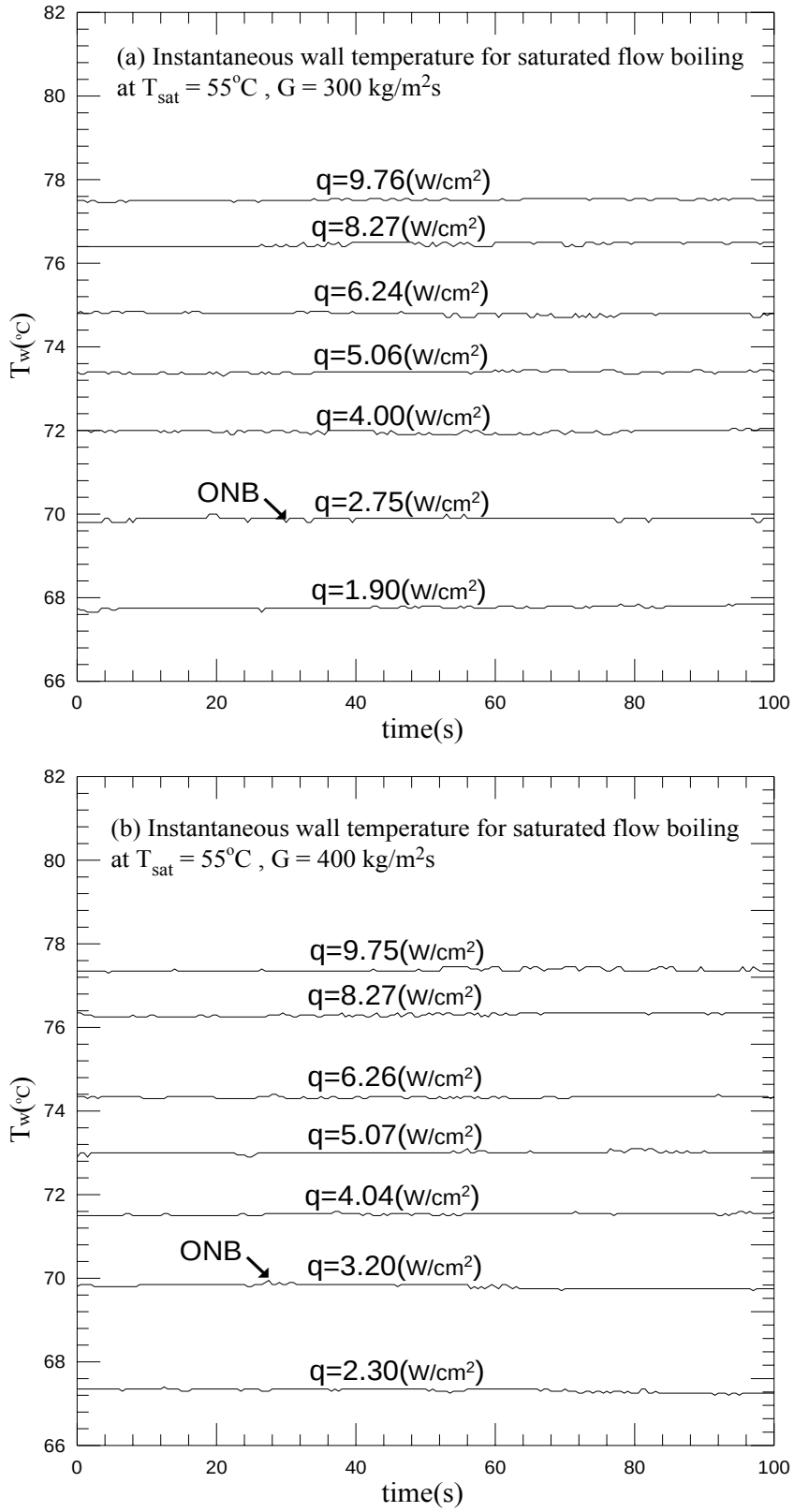


Fig. 7.6 Time variations of the copper plate temperature in stable saturated flow boiling for various imposed heat fluxes at (a) G=300 kg/m^{2}s and (b) G=400 kg/m^{2}s.

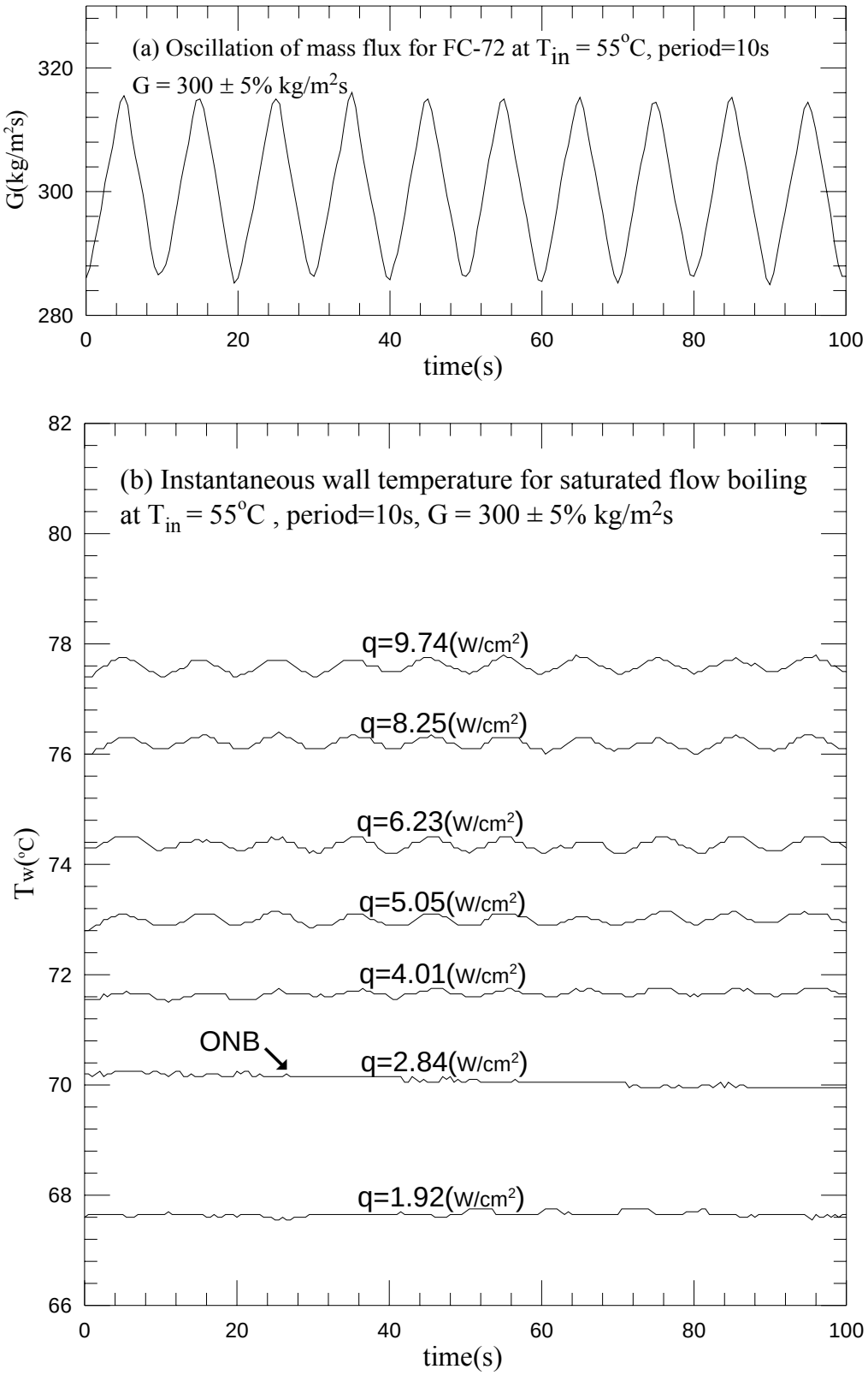


Fig. 7.7 Time variations of (a) imposed coolant mass flux and (b) copper plate temperature in transient oscillatory saturated flow boiling for various imposed heat fluxes for G=300±5% kg/m^{2}s with t_p=10 sec.($\overline{q}_{ONB}$ =2.84 w/cm^2 at G =300 kg/m^{2}s)

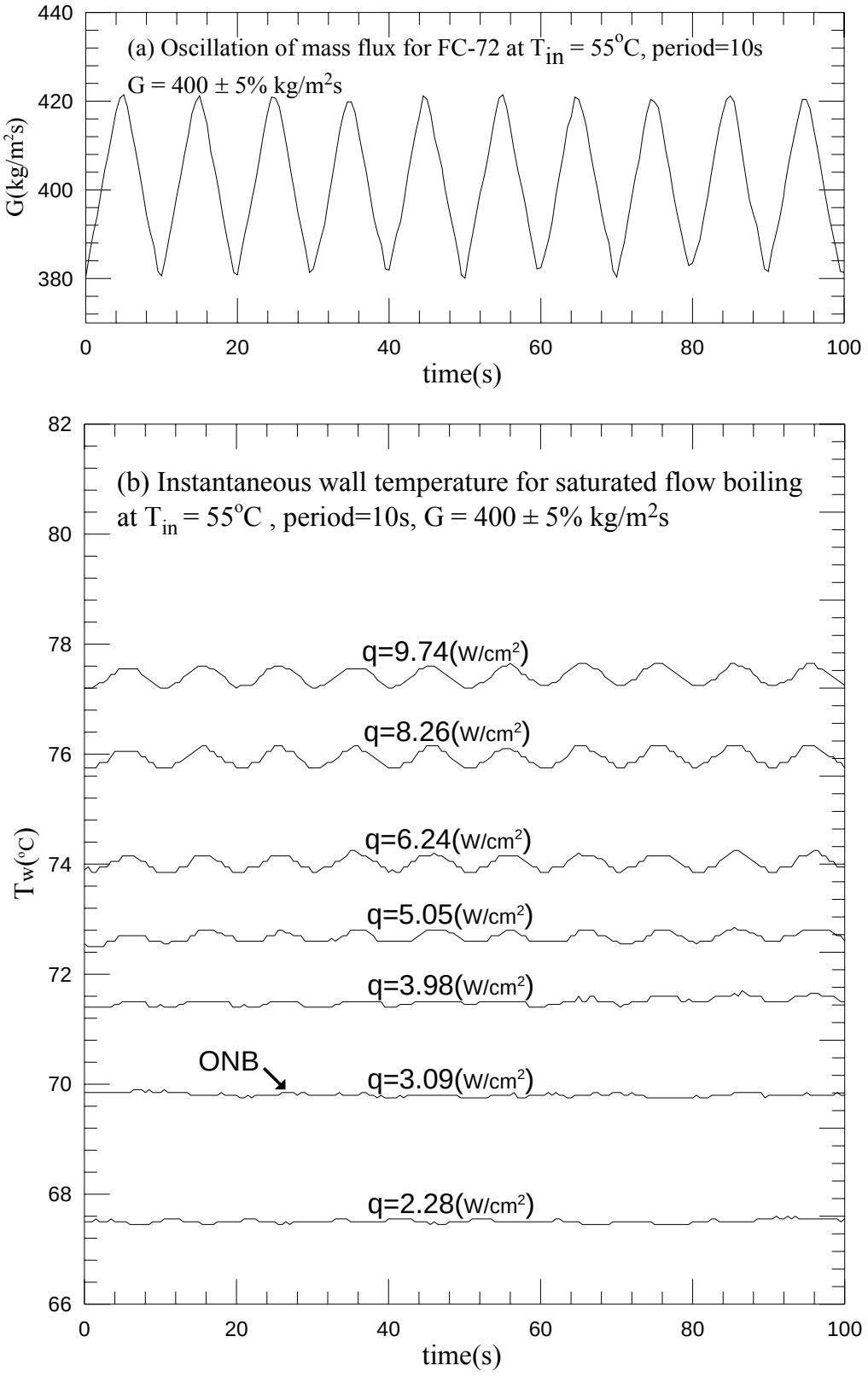


Fig. 7.8 Time variations of (a) imposed coolant mass flux and (b) copper plate temperature in transient oscillatory saturated flow boiling for various imposed heat fluxes for G=400±5% kg/m^{2}s with t_p=10 sec.($\bar{q}_{ONB}$ =3.09 w/cm^2 at G =400 kg/m^{2}S)

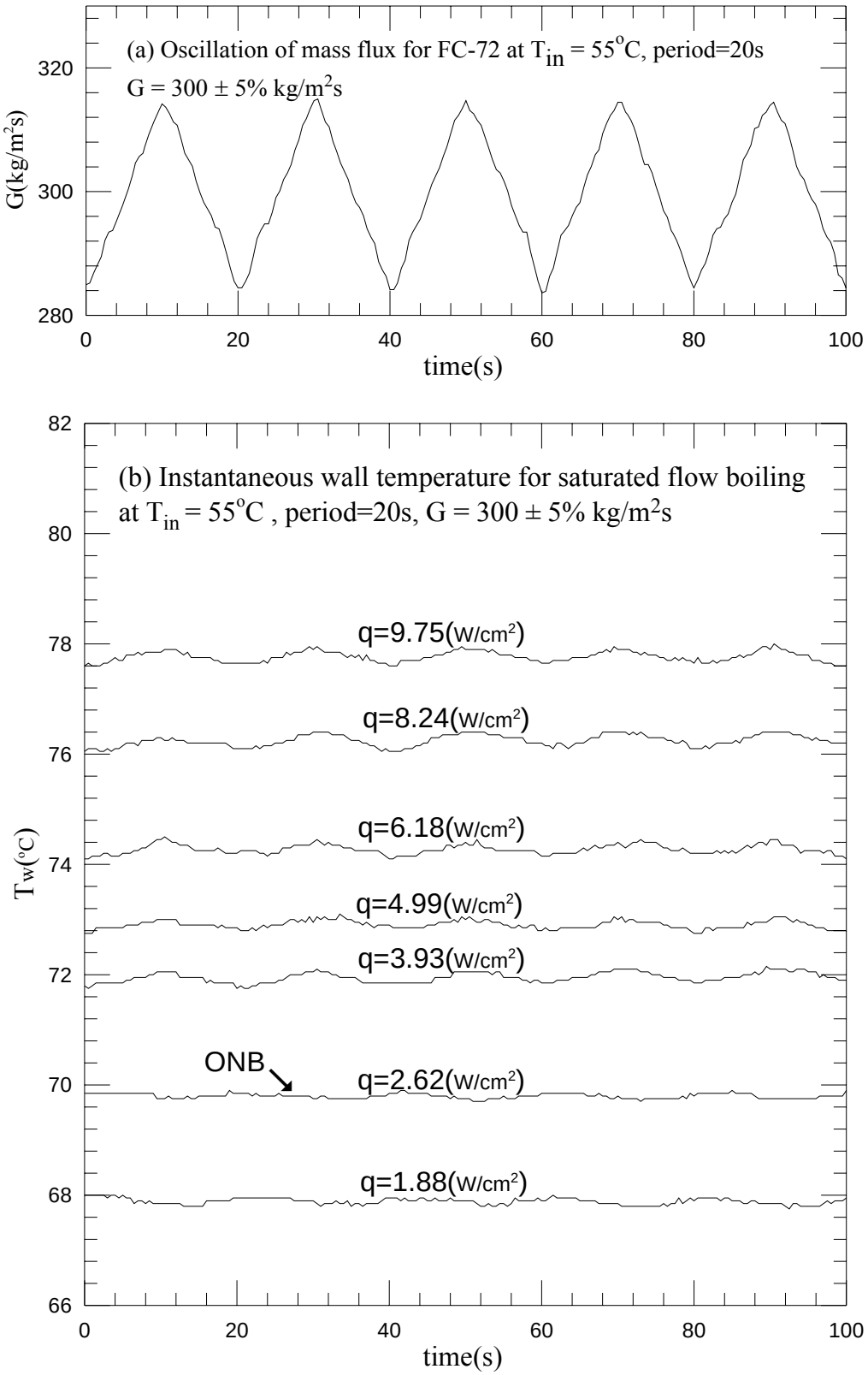


Fig. 7.9 Time variations of (a) imposed coolant mass flux and (b) copper plate temperature in transient oscillatory saturated flow boiling for various imposed heat fluxes for G=300±5% kg/m^{2}s with t_p =20 sec.($\bar{q}_{ONB}$ =2.62 w/cm^2 at G =300 kg/m^{2}s)

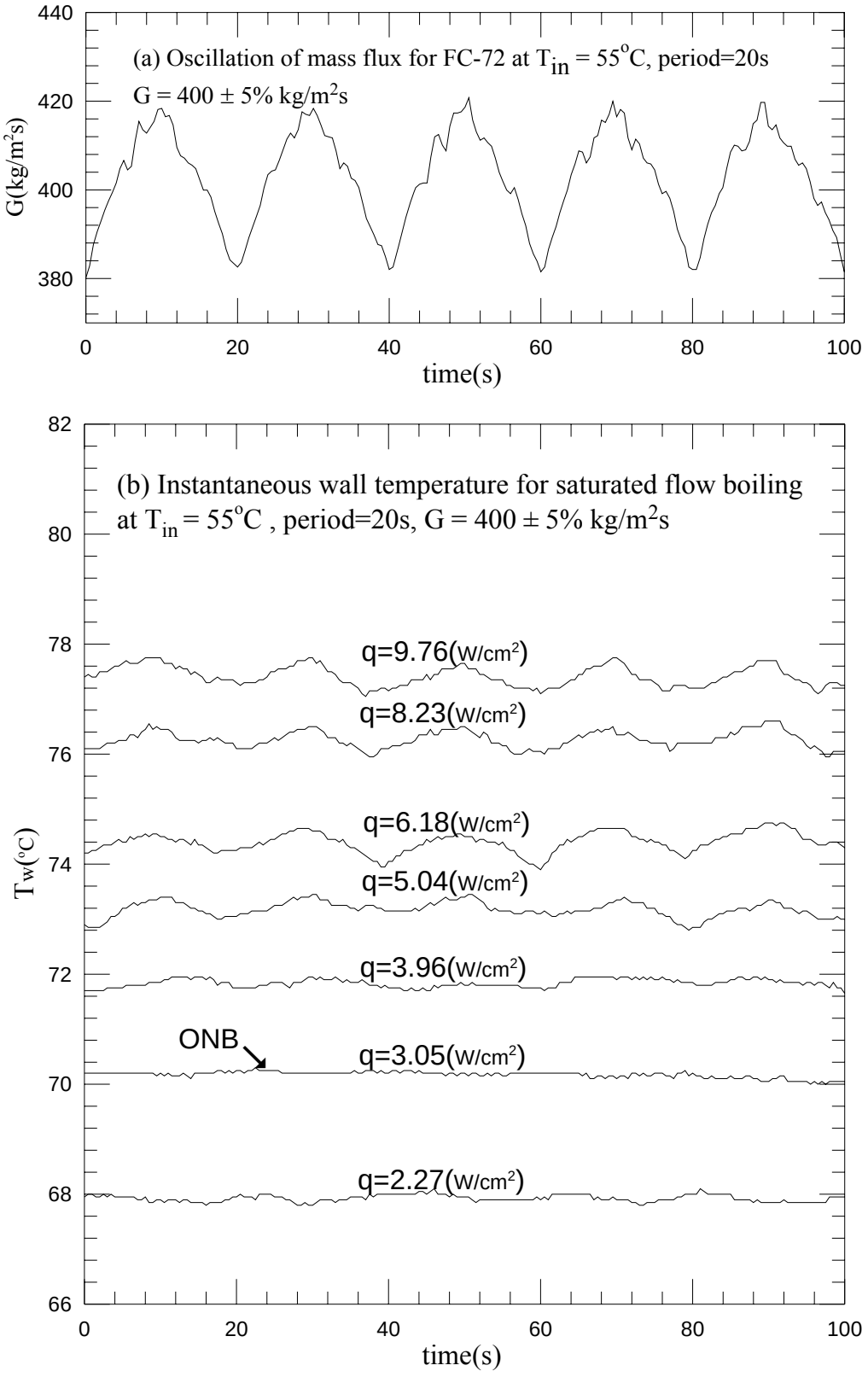


Fig. 7.10 Time variations of (a) imposed coolant mass flux and (b) copper plate temperature in transient oscillatory saturated flow boiling for various imposed heat fluxes for G=400±5% kg/m^{2}s with t_p =20 sec.($\bar{q}_{ONB}$ =3.05 w/cm^2 at G =400 kg/m^{2}S)

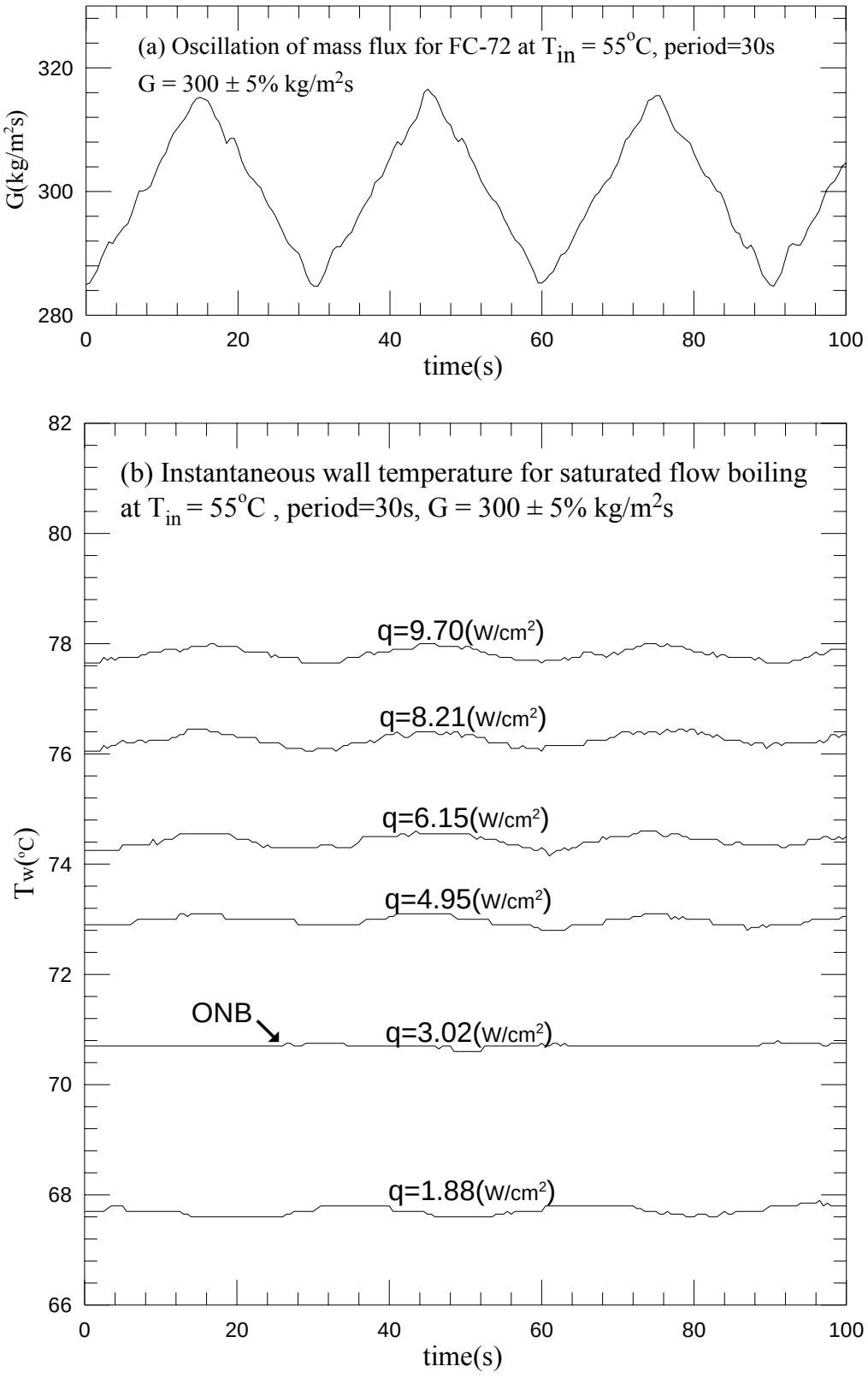


Fig. 7.11 Time variations of (a) imposed coolant mass flux and (b) copper plate temperature in transient oscillatory saturated flow boiling for various imposed heat fluxes for G=300±5% kg/m^{2}s with t_p =30 sec.($\bar{q}_{ONB}$ =3.02 w/cm^2 at G =300 kg/m^{2}S)

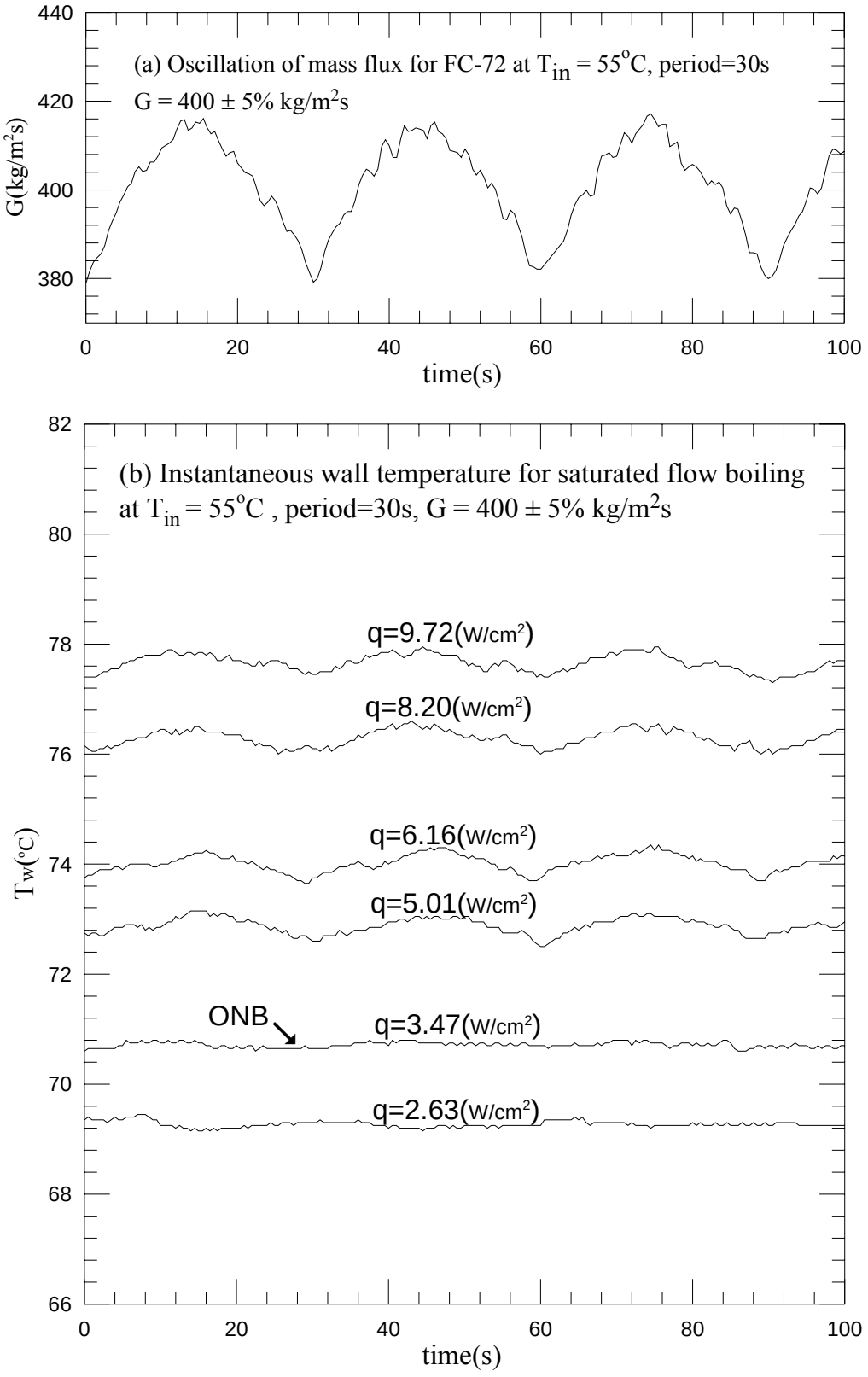


Fig. 7.12 Time variations of (a) imposed coolant mass flux and (b) copper plate temperature in transient oscillatory saturated flow boiling for various imposed heat fluxes for G=400±5% kg/m^{2}s with t_p =30 sec.($\bar{q}_{ONB}$ =3.47 w/cm^2 at G =400 kg/m^{2}S)

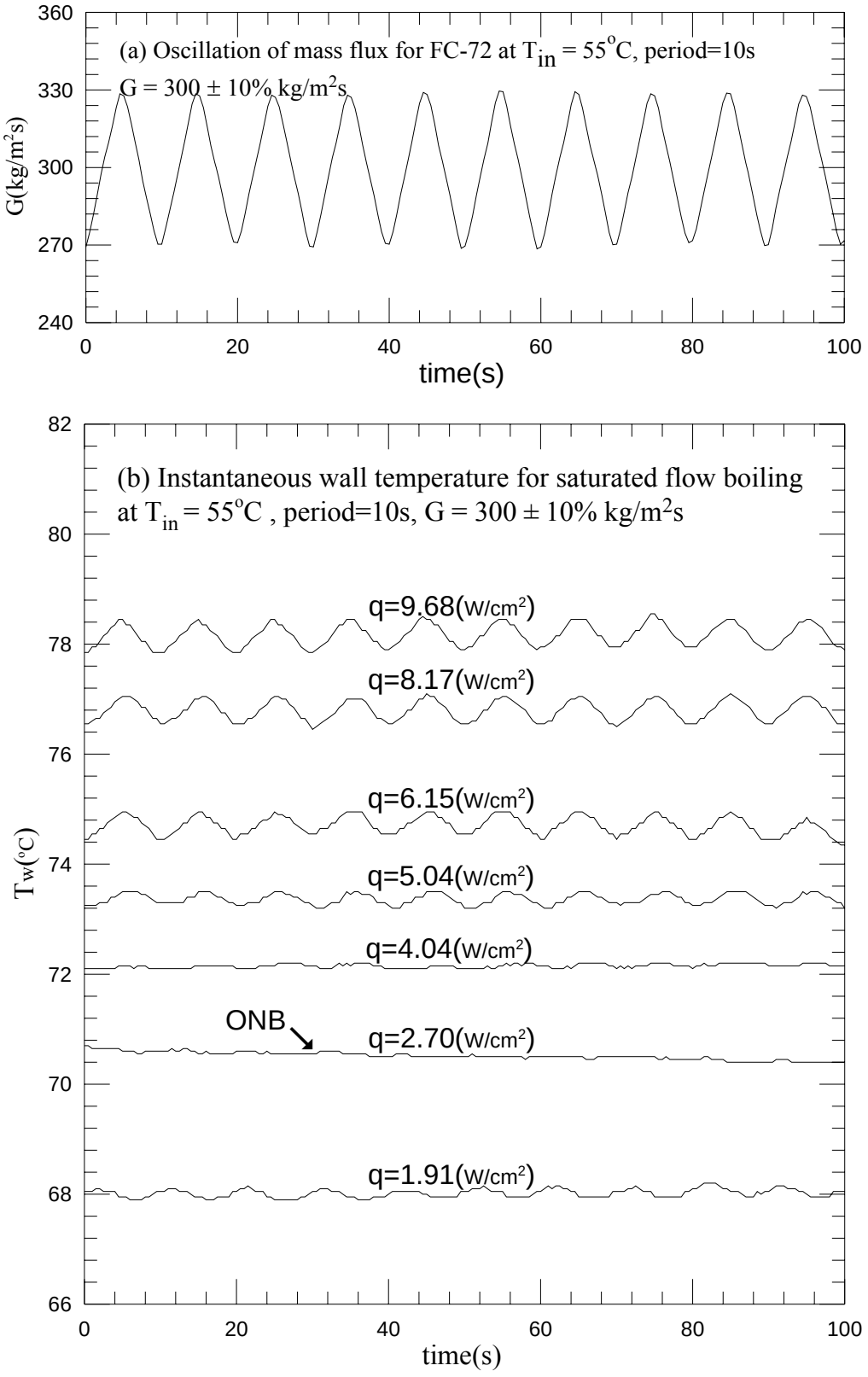


Fig. 7.13 Time variations of (a) imposed coolant mass flux and (b) copper plate temperature in transient oscillatory saturated flow boiling for various imposed heat fluxes for G=300±10% kg/m^{2}s with t_p =10 sec.($\bar{q}_{ONB}$ =2.70 w/cm^2 at G =300 kg/m^{2}s)

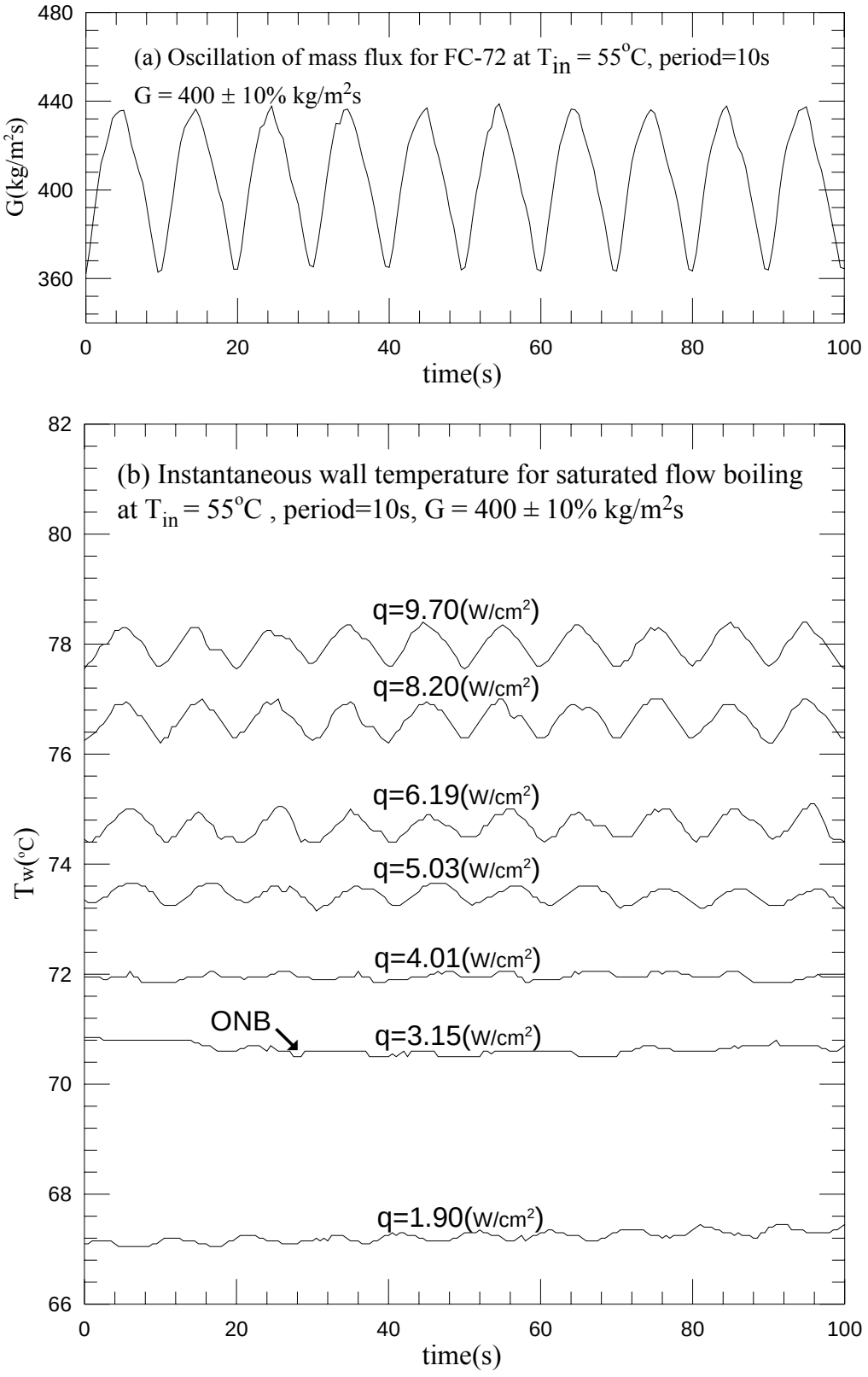


Fig. 7.14 Time variations of (a) imposed coolant mass flux and (b) copper plate temperature in transient oscillatory saturated flow boiling for various imposed heat fluxes for G=400±10% kg/m^{2}s with t_p =10 sec.($\bar{q}_{ONB}$ =3.15 w/cm^2 at G =400 kg/m^{2}s)

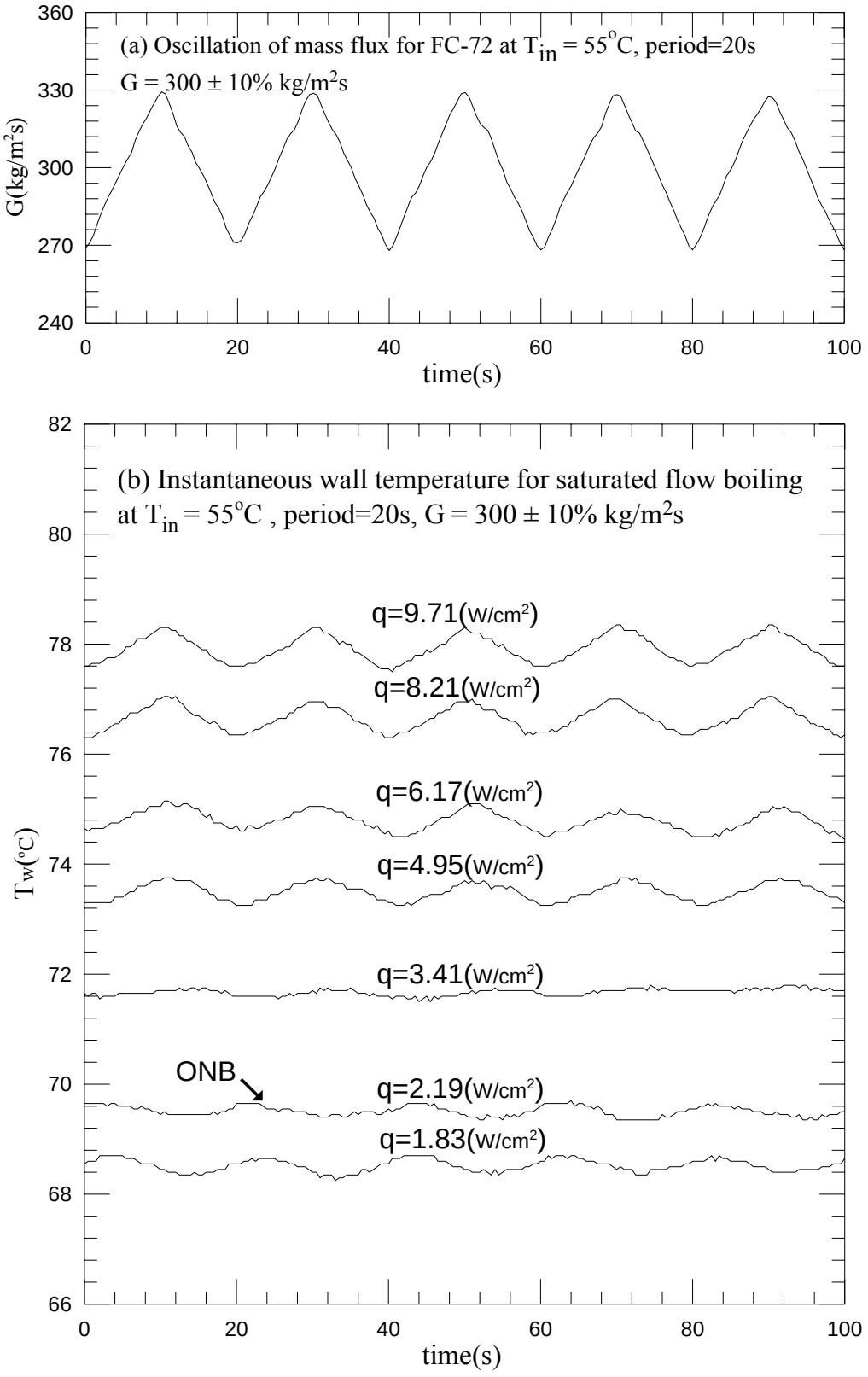


Fig. 7.15 Time variations of (a) imposed coolant mass flux and (b) copper plate temperature in transient oscillatory saturated flow boiling for various imposed heat fluxes for G=300±10% kg/m^{2}s with t_p =20 sec.($\bar{q}_{ONB}$ =2.19 w/cm^2 at G =300 kg/m^{2}S)

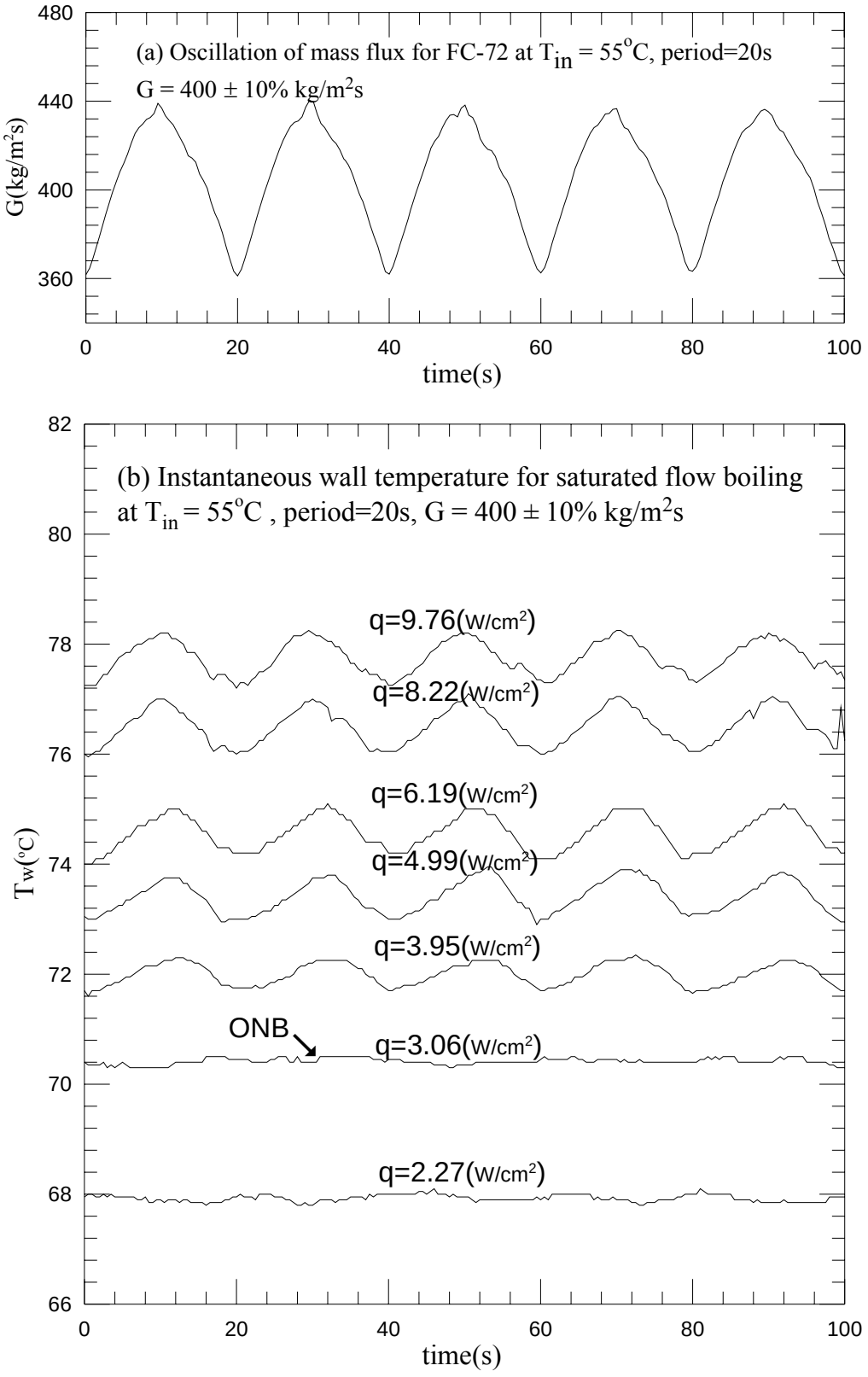


Fig. 7.16 Time variations of (a) imposed coolant mass flux and (b) copper plate temperature in transient oscillatory saturated flow boiling for various imposed heat fluxes for G=400±10% kg/m^{2}s with t_p =20 sec.($\bar{q}_{ONB}$ =3.06 w/cm^2 at G =400 kg/m^{2}s)

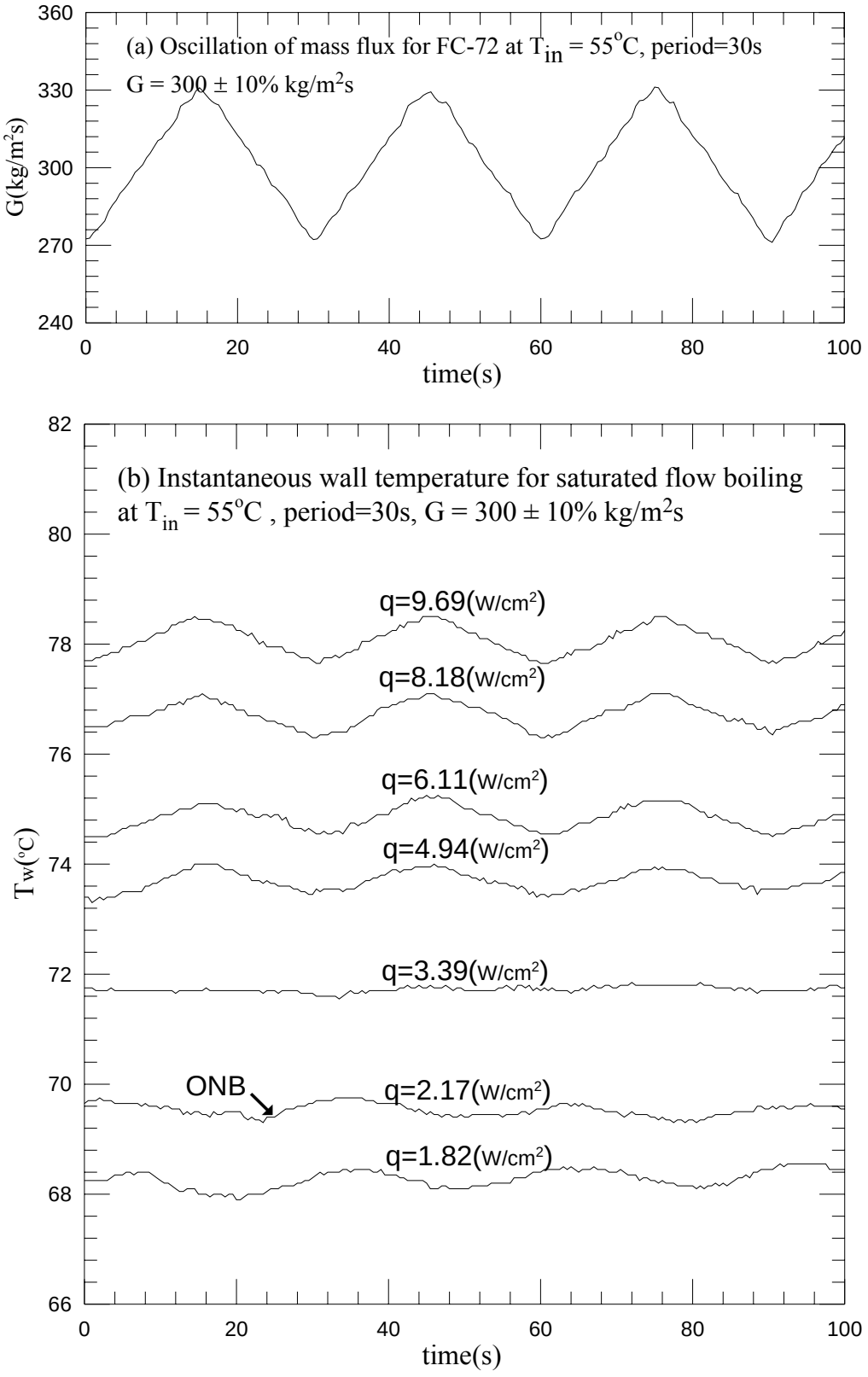


Fig. 7.17 Time variations of (a) imposed coolant mass flux and (b) copper plate temperature in transient oscillatory saturated flow boiling for various imposed heat fluxes for G=300±10% kg/m^{2}s with t_p =30 sec.($\bar{q}_{ONB}$ =2.17 w/cm^2 at G =300 kg/m^{2}s)

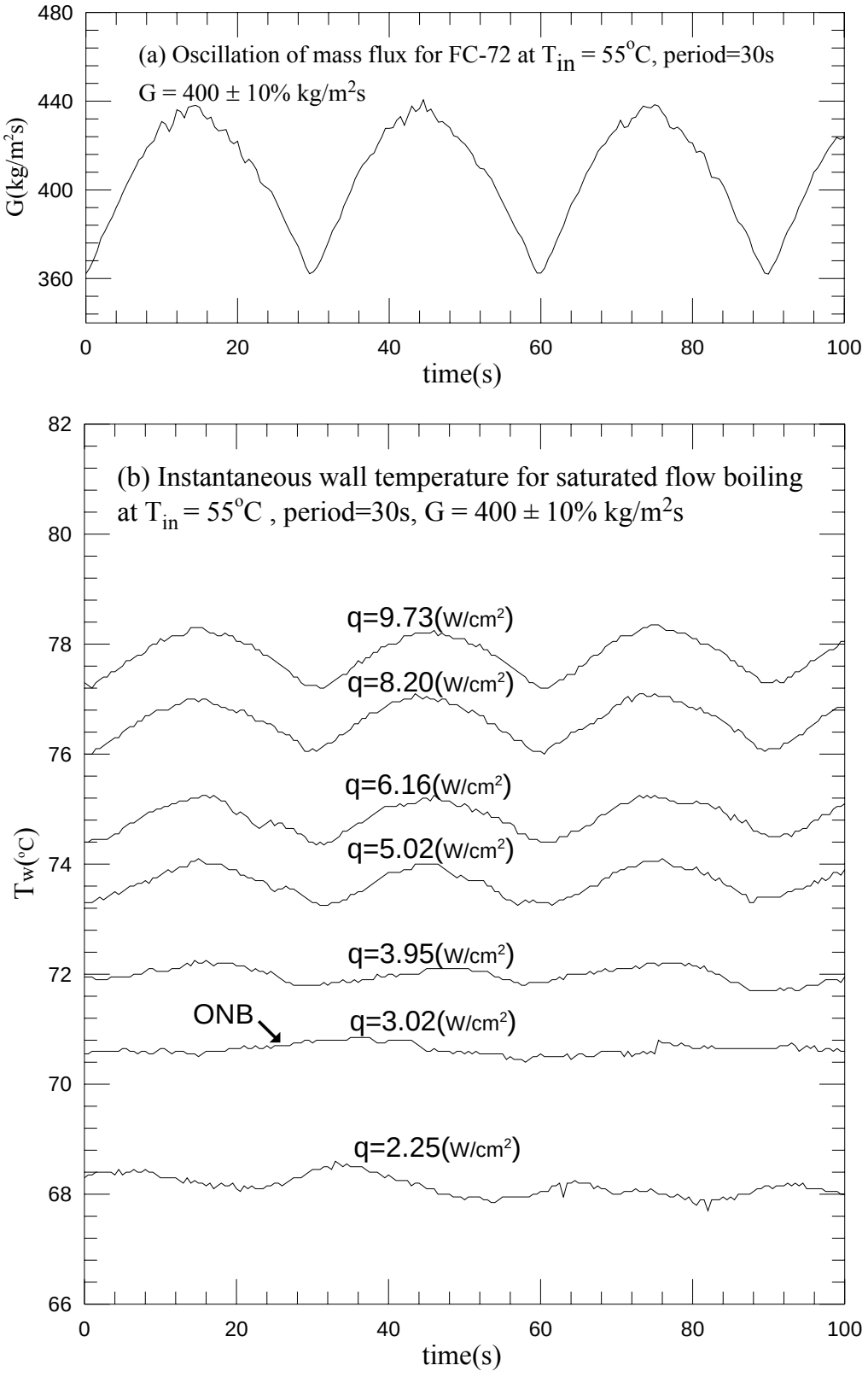


Fig. 7.18 Time variations of (a) imposed coolant mass flux and (b) copper plate temperature in transient oscillatory saturated flow boiling for various imposed heat fluxes for G=400±10% kg/m^{2}s with t_p =30 sec.($\bar{q}_{ONB}$ =3.02 w/cm^2 at G =400 kg/m^{2}s)

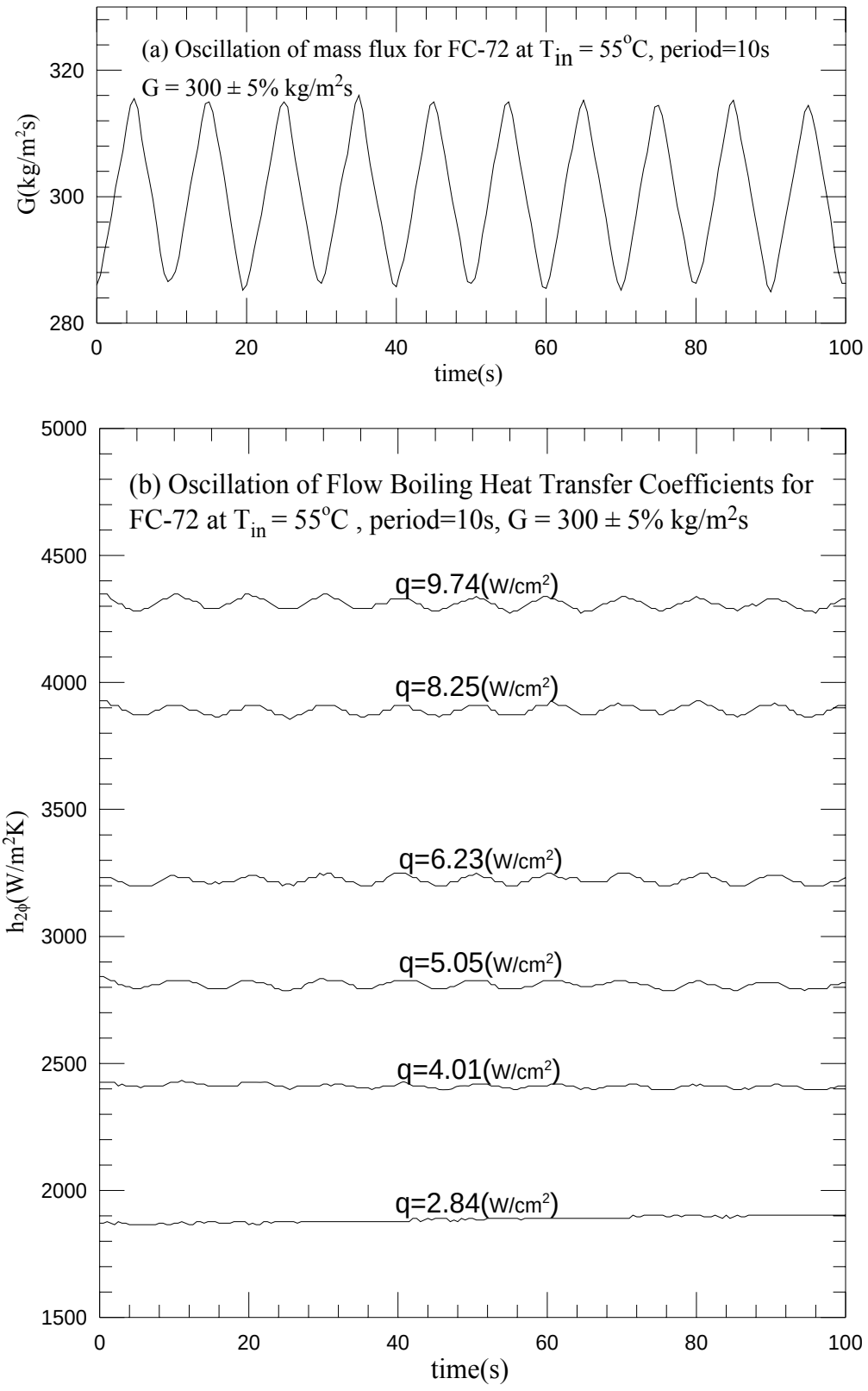


Fig. 7.19 Time variations of (a) imposed coolant mass flux and (b) flow boiling heat transfer coefficients in transient oscillatory saturated flow boiling for various imposed heat fluxes for G=300± 5% kg/m^{2}s with t_p =10 sec.

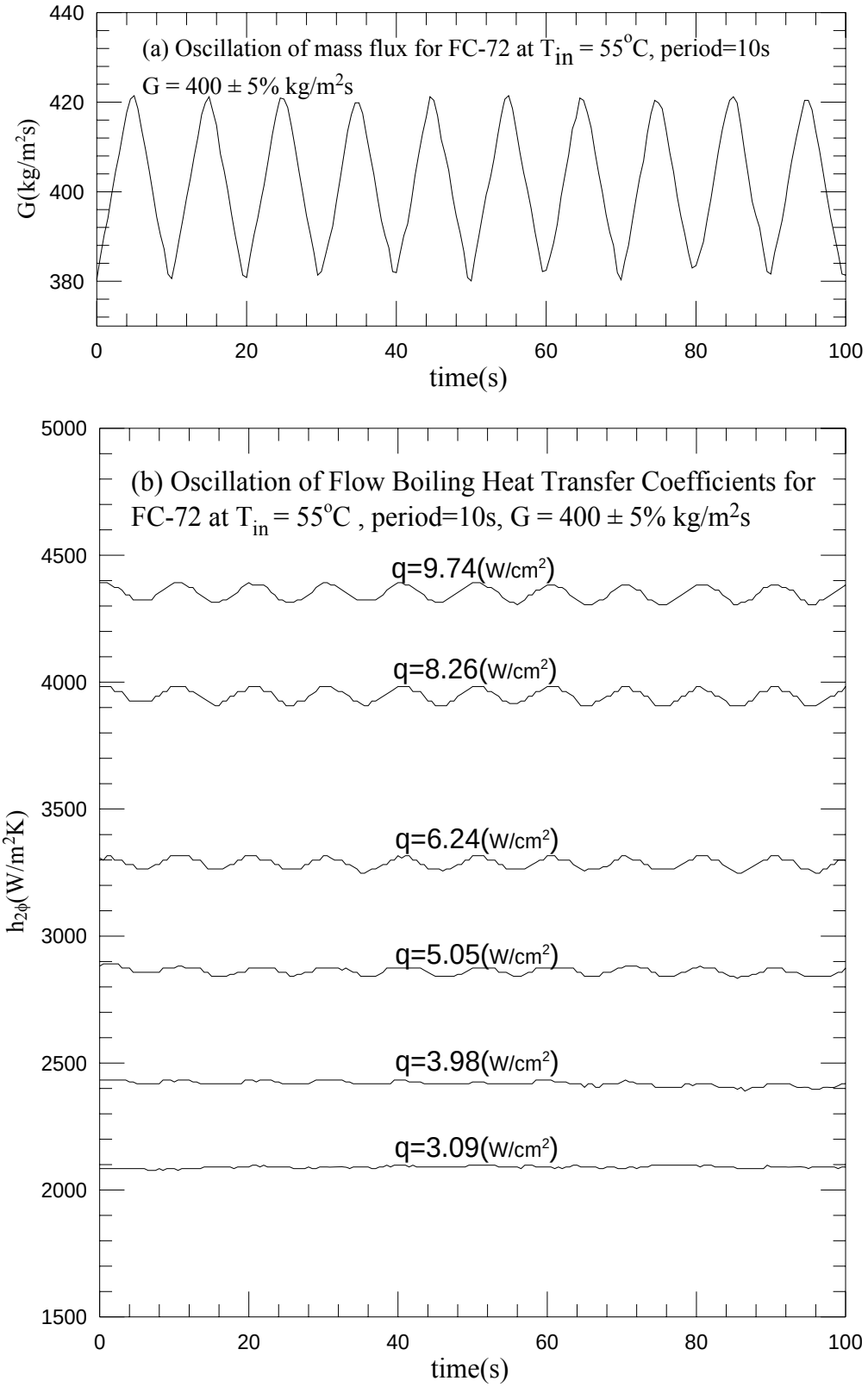


Fig. 7.20 Time variations of (a) imposed coolant mass flux and (b) flow boiling heat transfer coefficients in transient oscillatory saturated flow boiling for various imposed heat fluxes for G=400± 5% kg/m^{2}s with t_p =10 sec.

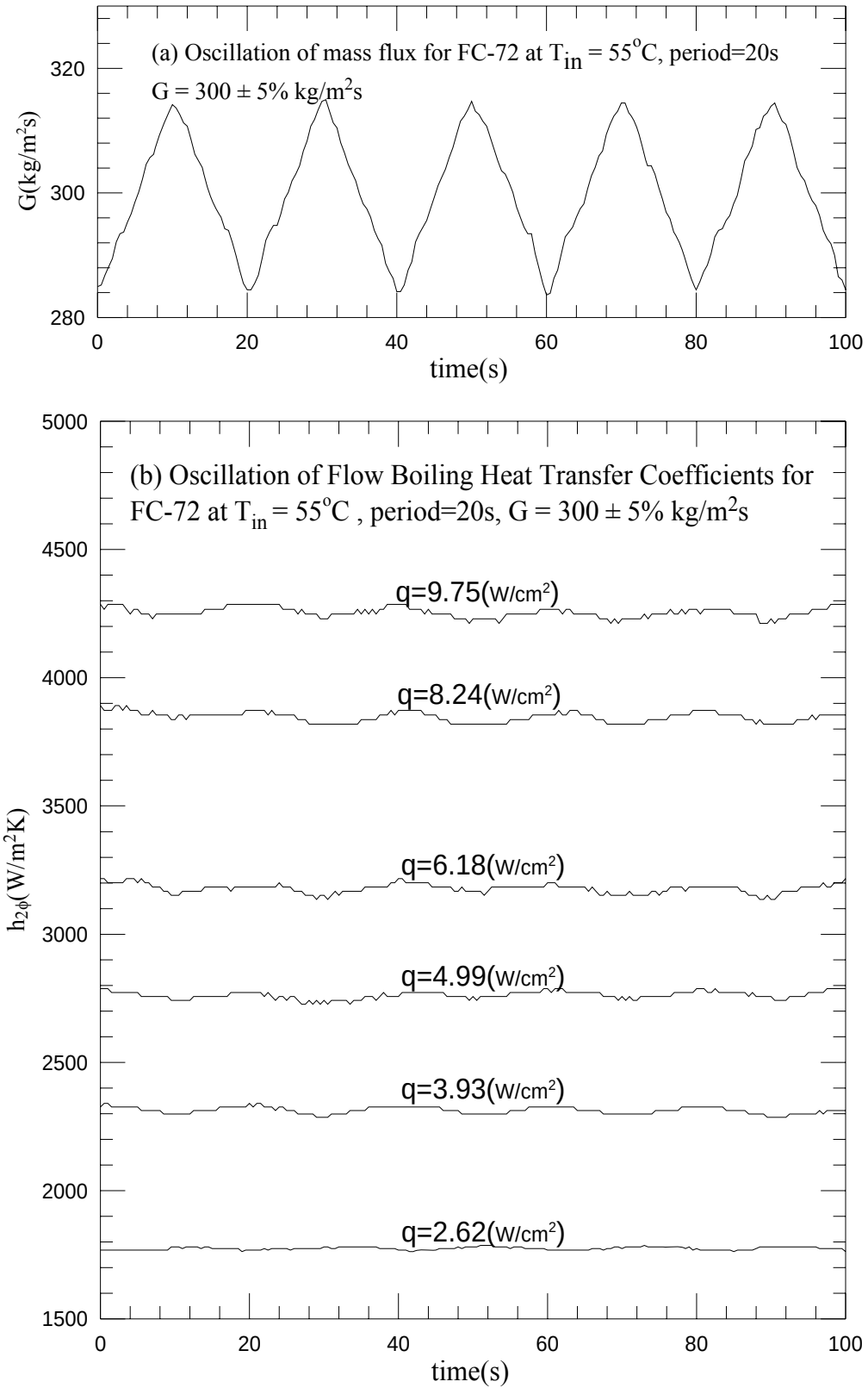


Fig. 7.21 Time variations of (a) imposed coolant mass flux and (b) flow boiling heat transfer coefficients in transient oscillatory saturated flow boiling for various imposed heat fluxes for G=300± 5% kg/m^{2}s with t_p =20 sec.

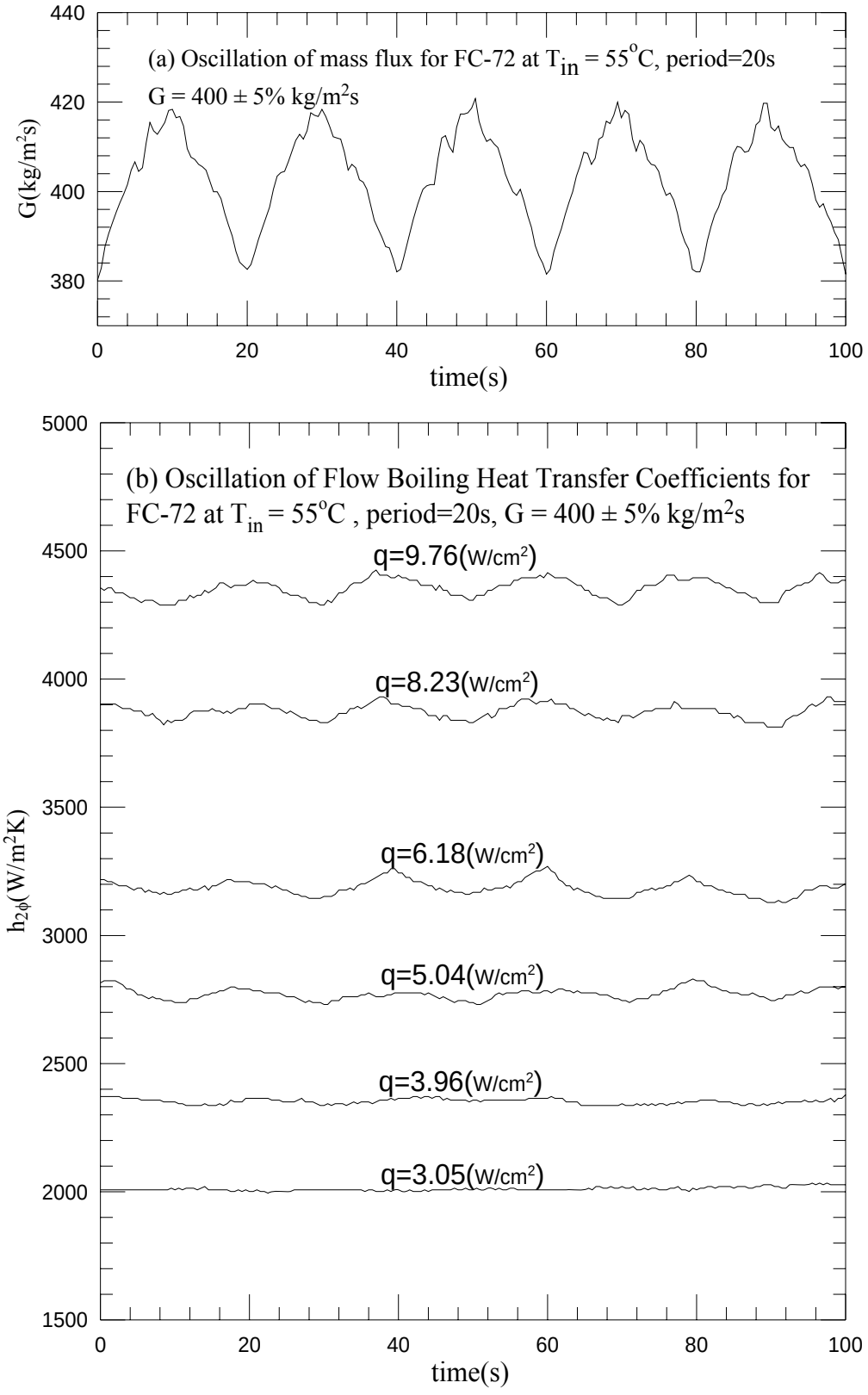


Fig. 7.22 Time variations of (a) imposed coolant mass flux and (b) flow boiling heat transfer coefficients in transient oscillatory saturated flow boiling for various imposed heat fluxes for G=400± 5% kg/m^{2}s with t_p =20 sec.

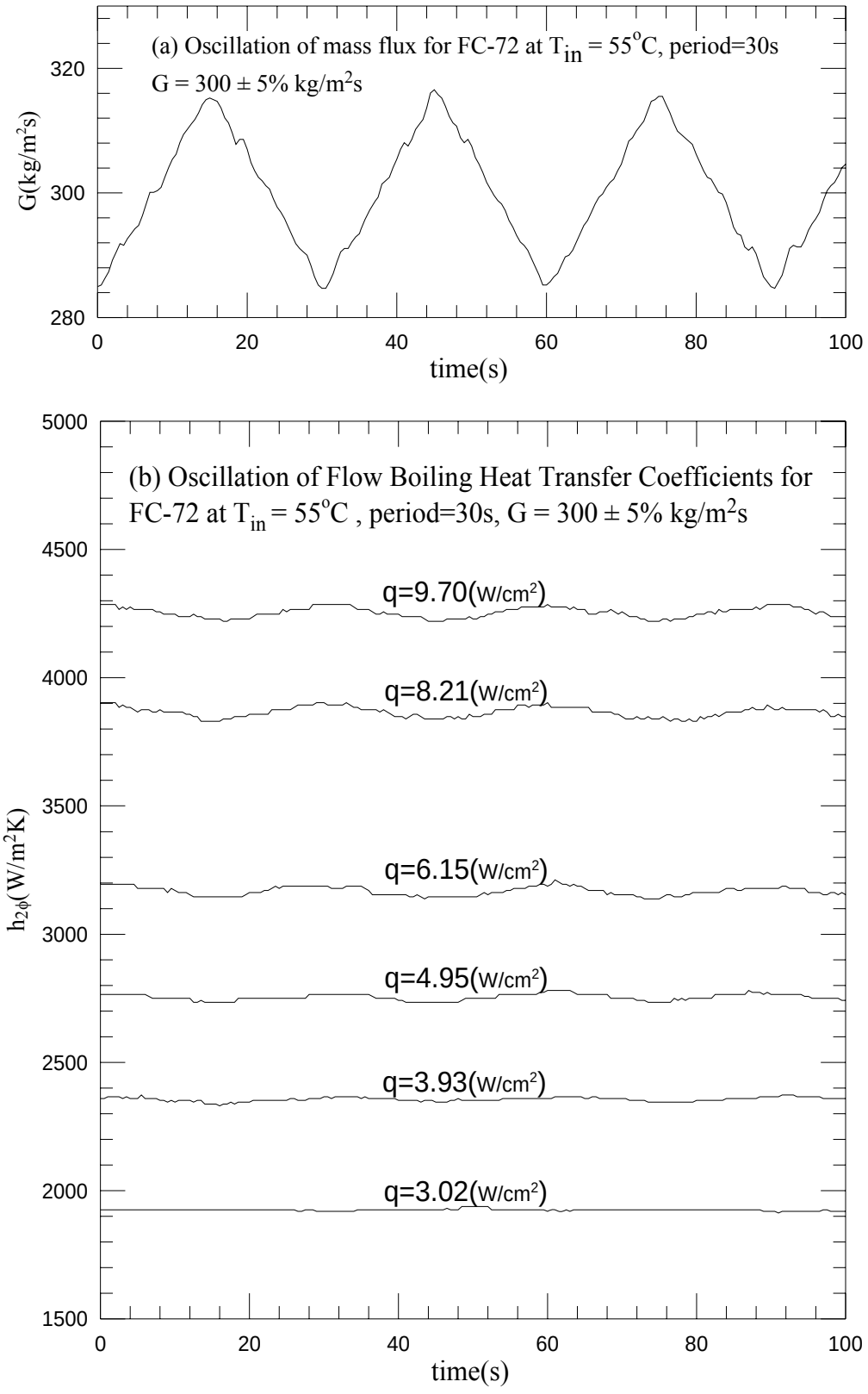


Fig. 7.23 Time variations of (a) imposed coolant mass flux and (b) flow boiling heat transfer coefficients in transient oscillatory saturated flow boiling for various imposed heat fluxes for G=300± 5% kg/m^{2}s with t_p =30 sec.

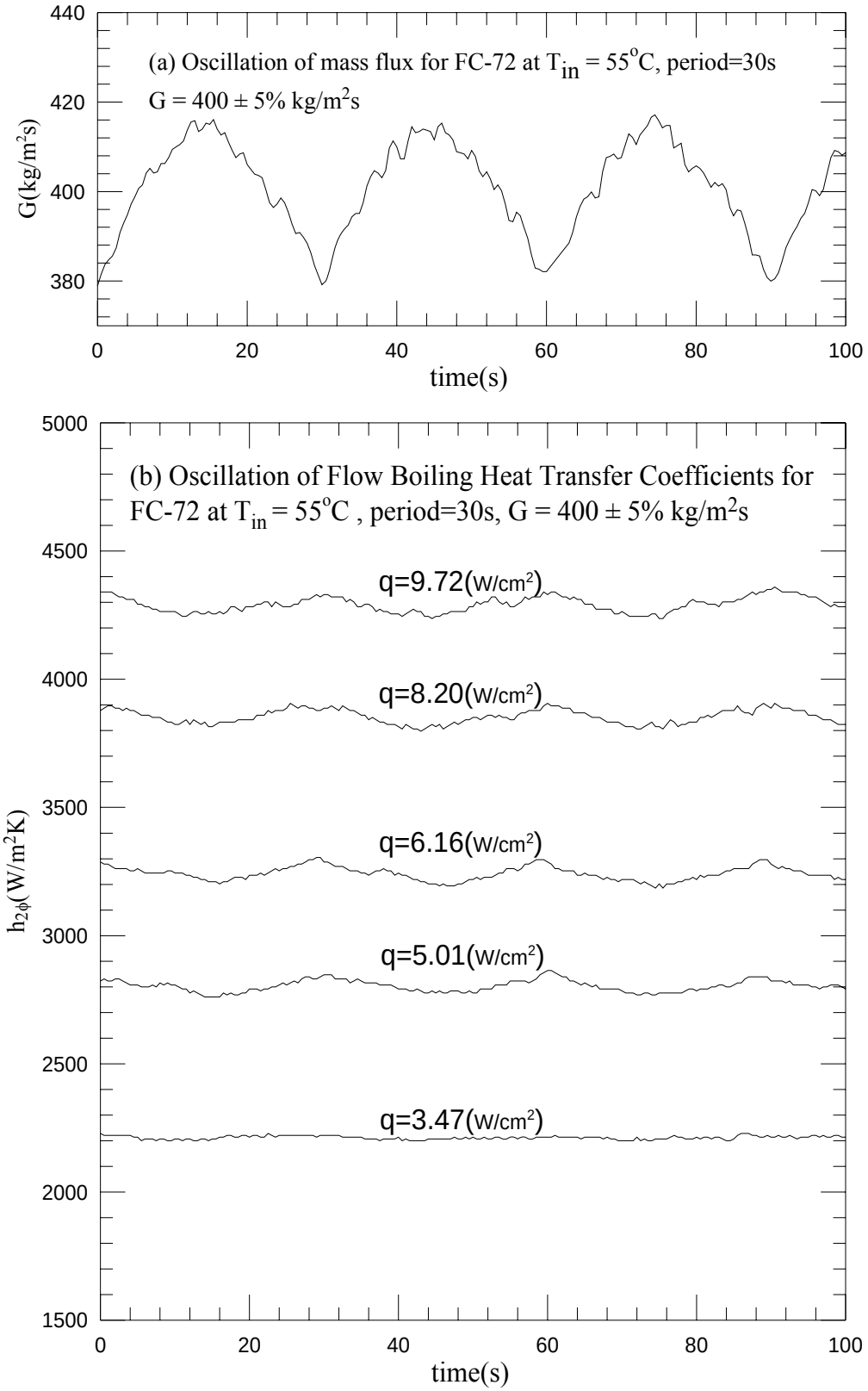


Fig. 7.24 Time variations of (a) imposed coolant mass flux and (b) flow boiling heat transfer coefficients in transient oscillatory saturated flow boiling for various imposed heat fluxes for G=400± 5% kg/m^{2}s with t_p =30 sec.

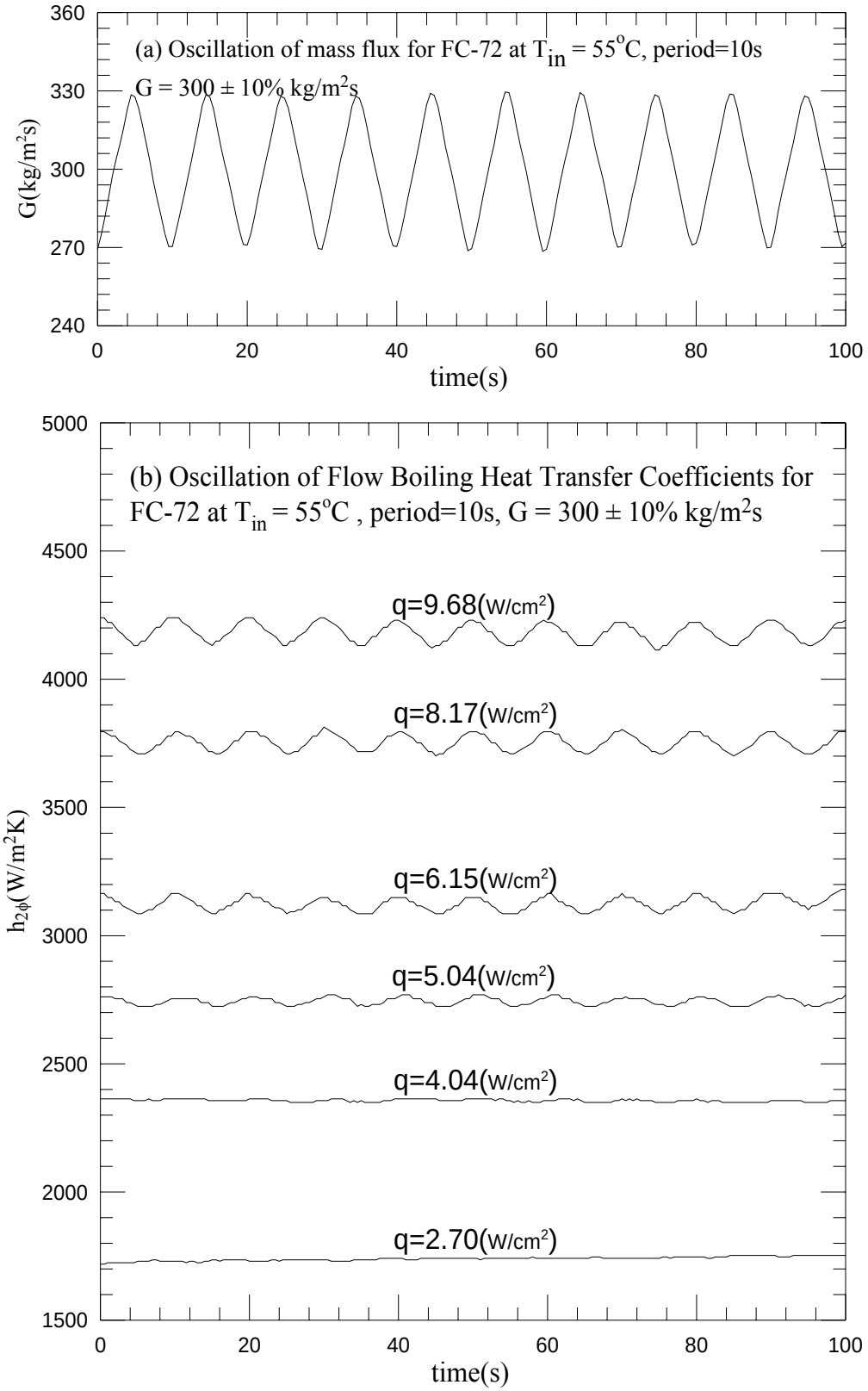


Fig. 7.25 Time variations of (a) imposed coolant mass flux and (b) flow boiling heat transfer coefficients in transient oscillatory saturated flow boiling for various imposed heat fluxes for G=300± 10% kg/m^{2}s with t_p =10 sec.

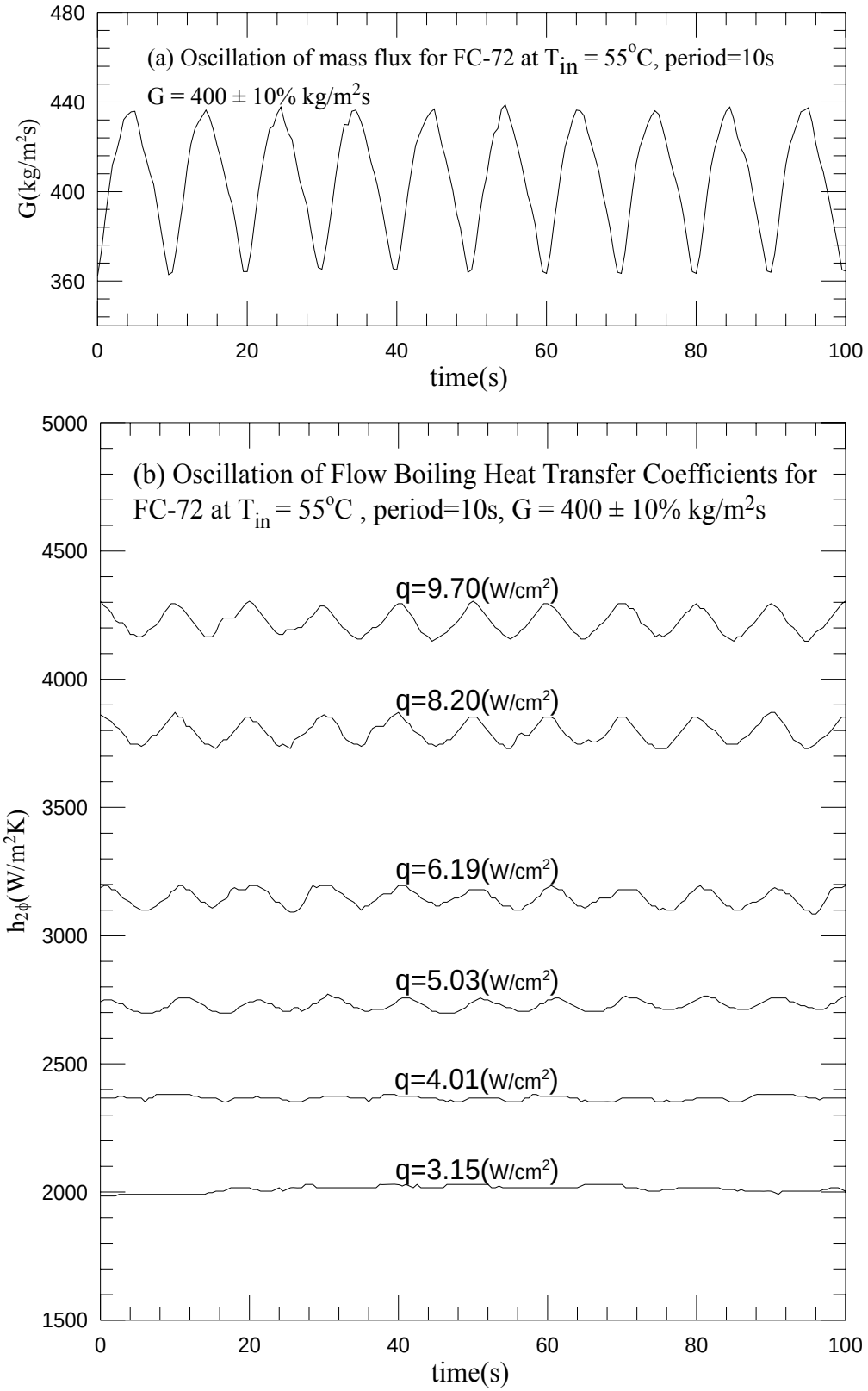


Fig. 7.26 Time variations of (a) imposed coolant mass flux and (b) flow boiling heat transfer coefficients in transient oscillatory saturated flow boiling for various imposed heat fluxes for G=400± 10% kg/m^{2}s with t_p =10 sec.

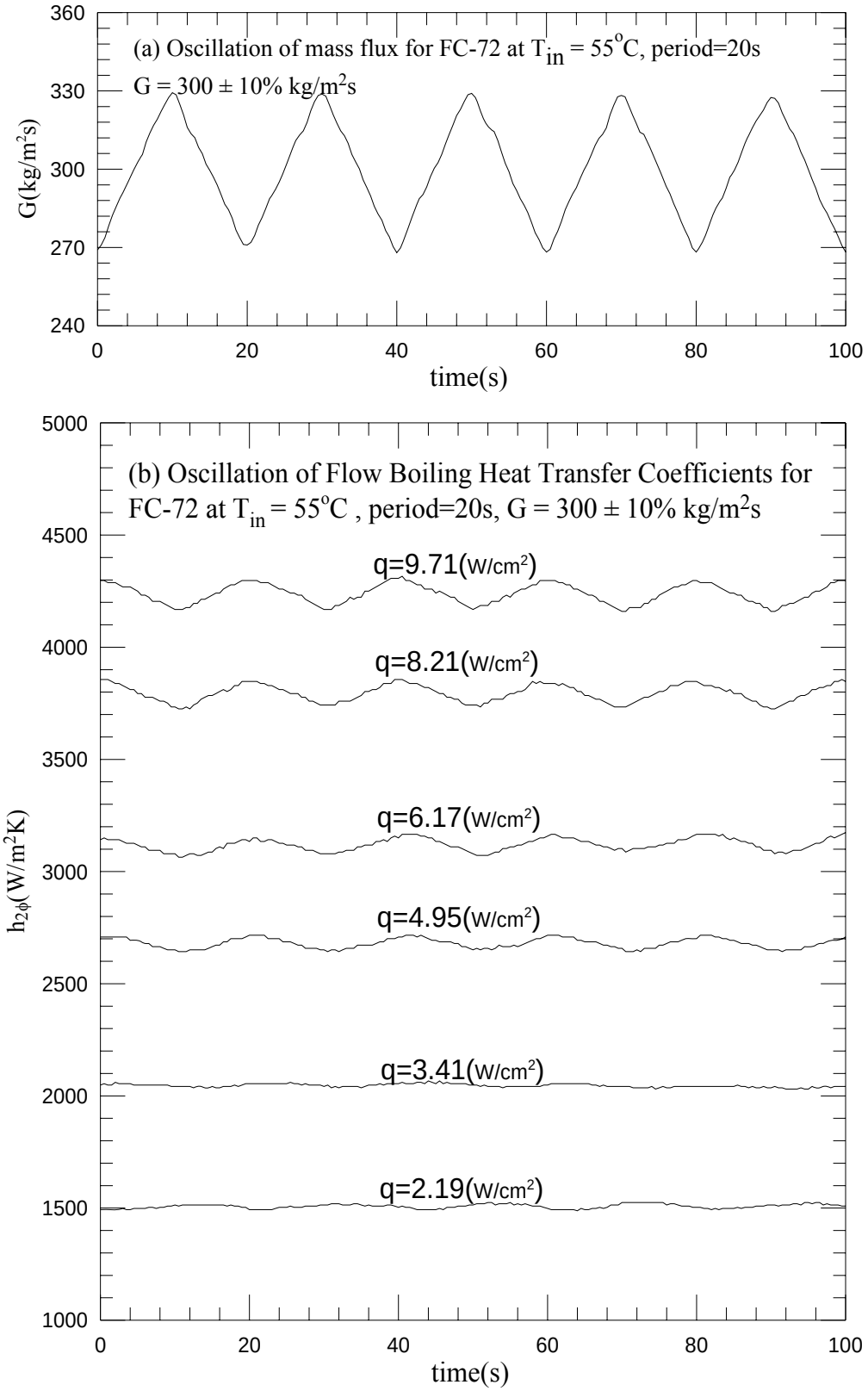


Fig. 7.27 Time variations of (a) imposed coolant mass flux and (b) flow boiling heat transfer coefficients in transient oscillatory saturated flow boiling for various imposed heat fluxes for G=300± 10% kg/m^{2}s with t_p =20 sec.

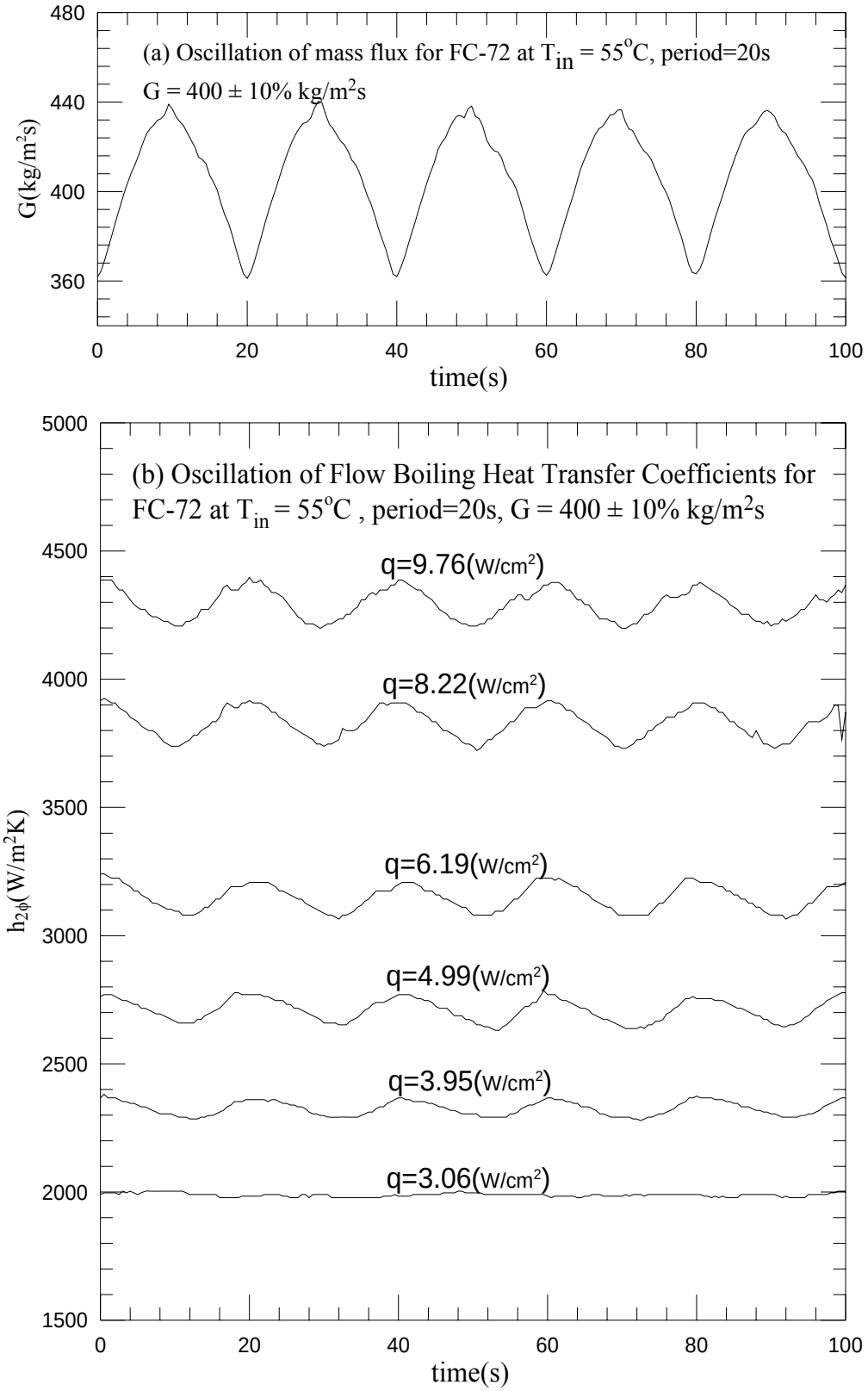


Fig. 7.28 Time variations of (a) imposed coolant mass flux and (b) flow boiling heat transfer coefficients in transient oscillatory saturated flow boiling for various imposed heat fluxes for G=400± 10% kg/m^{2}s with t_p =20 sec.

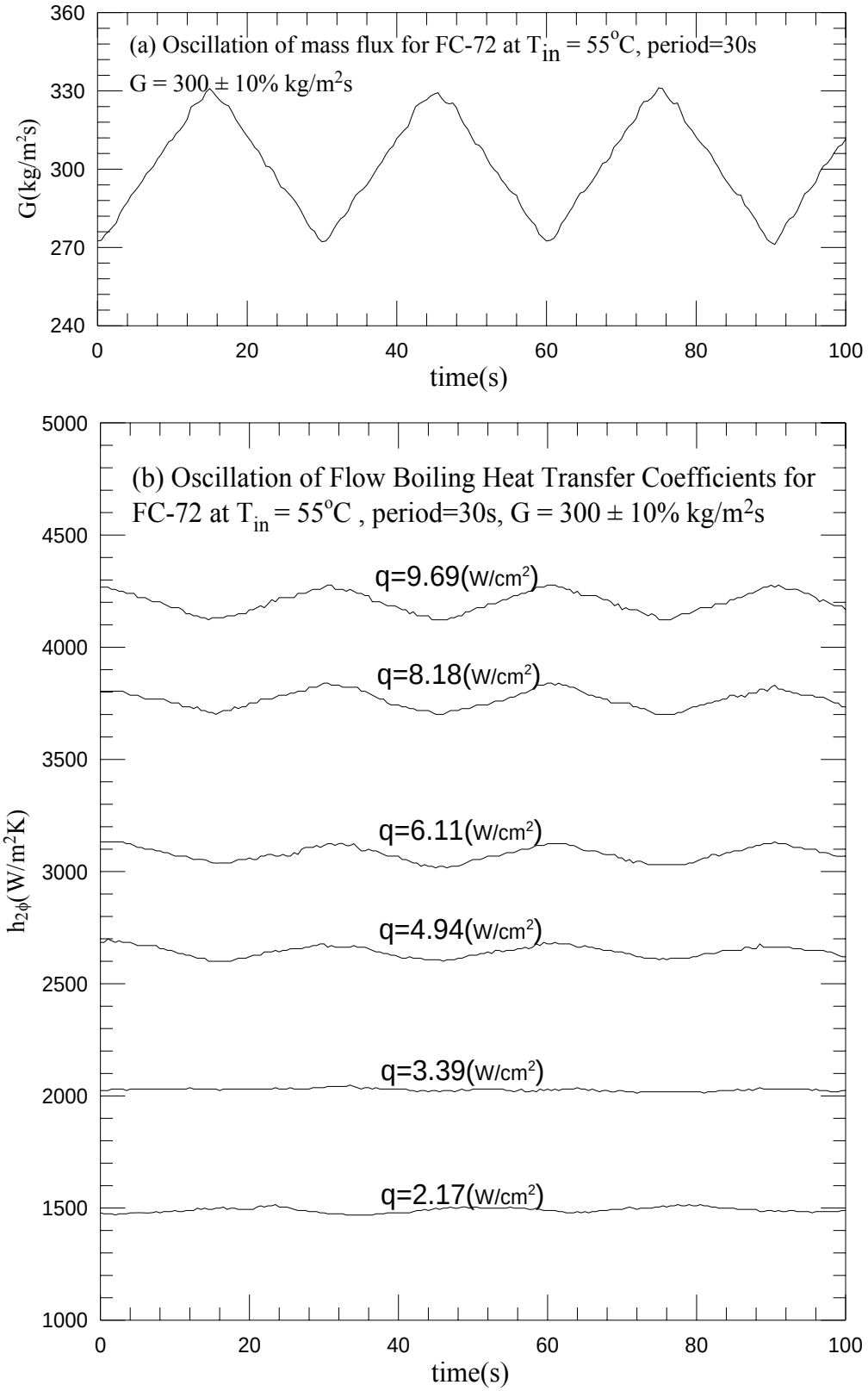


Fig. 7.29 Time variations of (a) imposed coolant mass flux and (b) flow boiling heat transfer coefficients in transient oscillatory saturated flow boiling for various imposed heat fluxes for G=300± 10% kg/m^{2}s with t_p =30 sec.

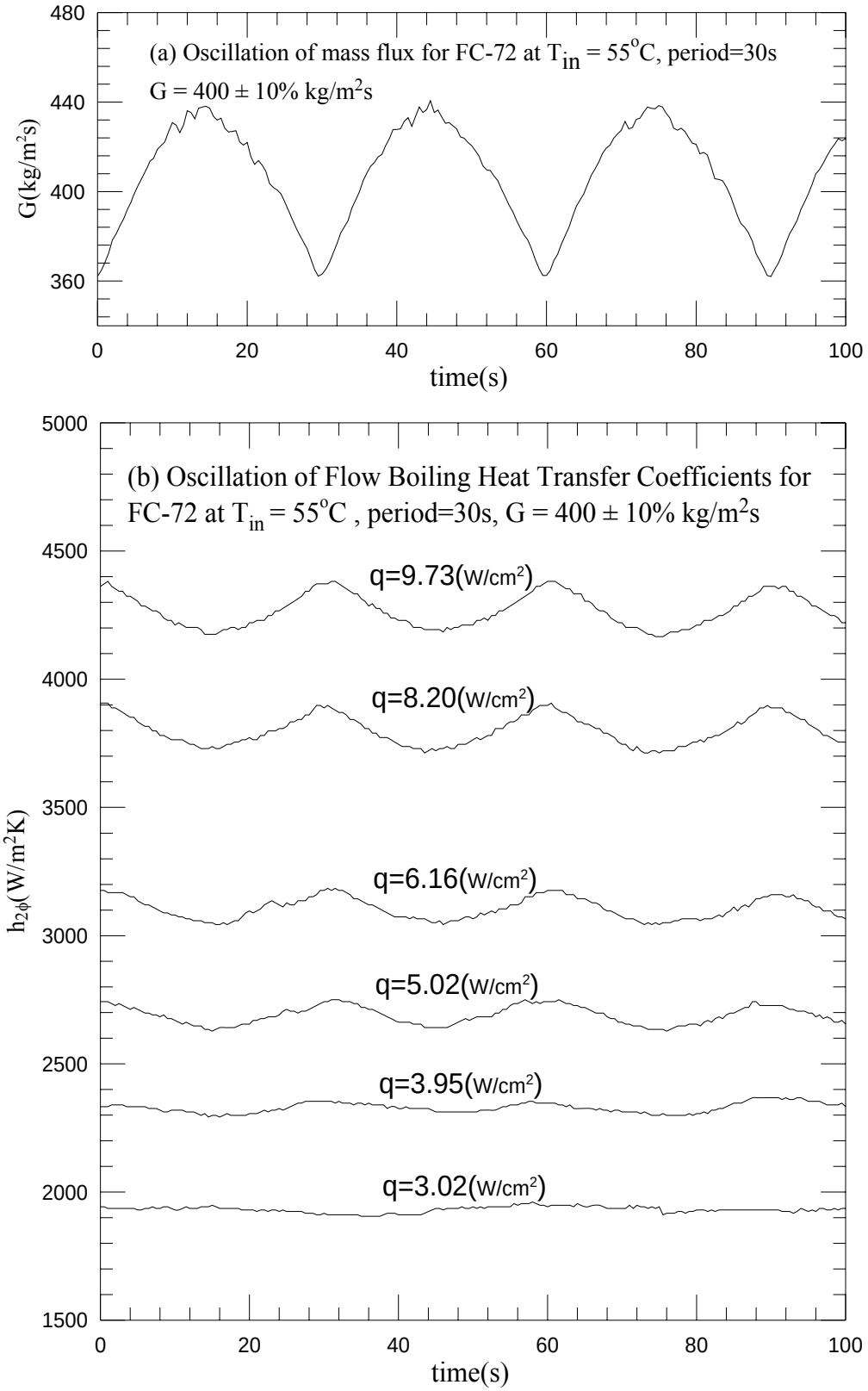


Fig. 7.30 Time variations of (a) imposed coolant mass flux and (b) flow boiling heat transfer coefficients in transient oscillatory saturated flow boiling for various imposed heat fluxes for G=400± 10% kg/m^{2}s with t_p =30 sec.

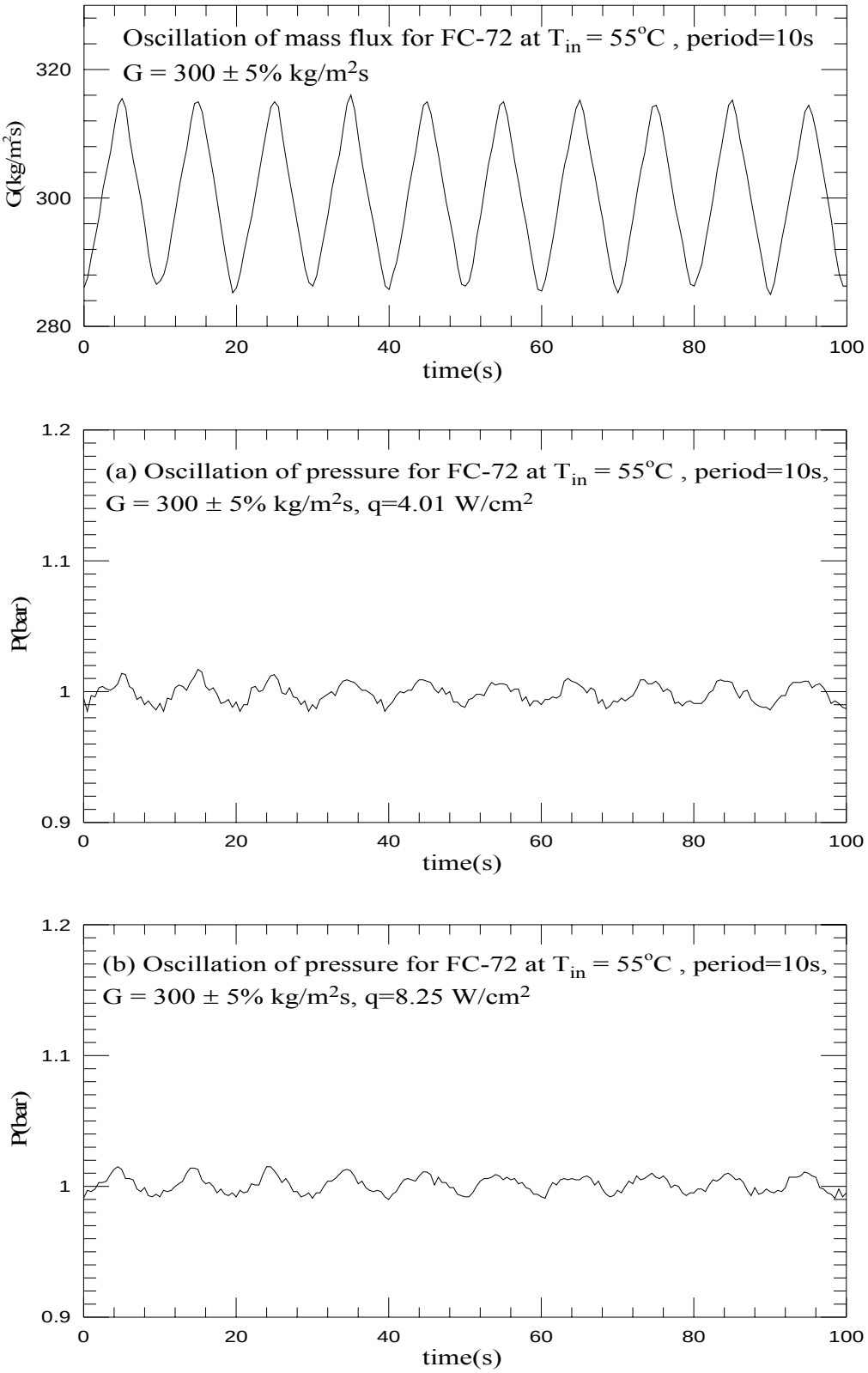


Fig.7.31 Time variations of coolant mass flux and inlet pressure in transient oscillatory saturated flow boiling for various imposed heat fluxes at (a) q=4.01 W/cm^2 and (b) q=8.25 W/cm^2 for G=300±5% kg/m^{2}S with t_p=10 sec.

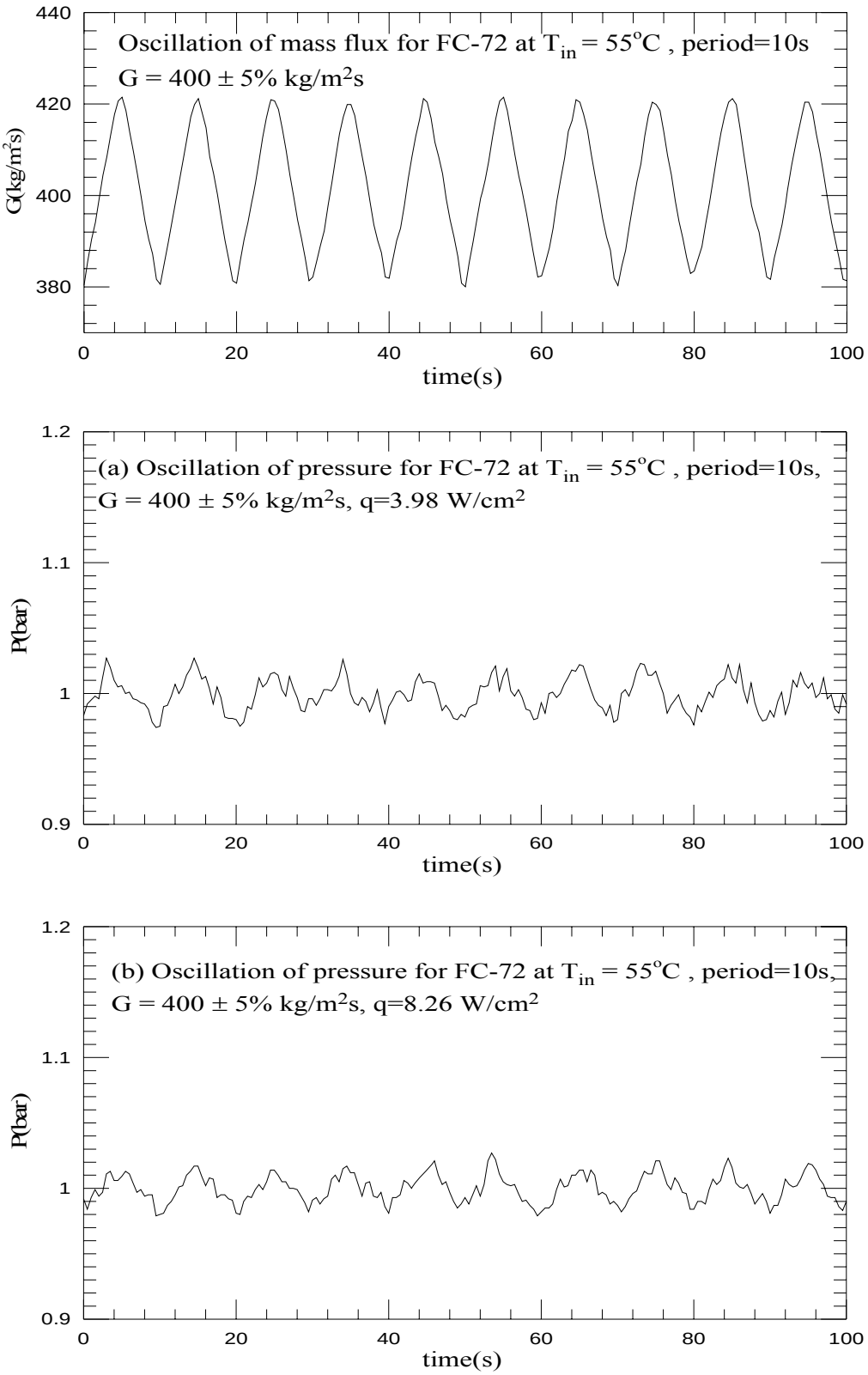


Fig.7.32 Time variations of coolant mass flux and inlet pressure in transient oscillatory saturated flow boiling for various imposed heat fluxes at (a) q=3.98 W/cm^2 and (b) q=8.26 W/cm^2 for G=400±5% kg/m^{2}S with t_p=10 sec.

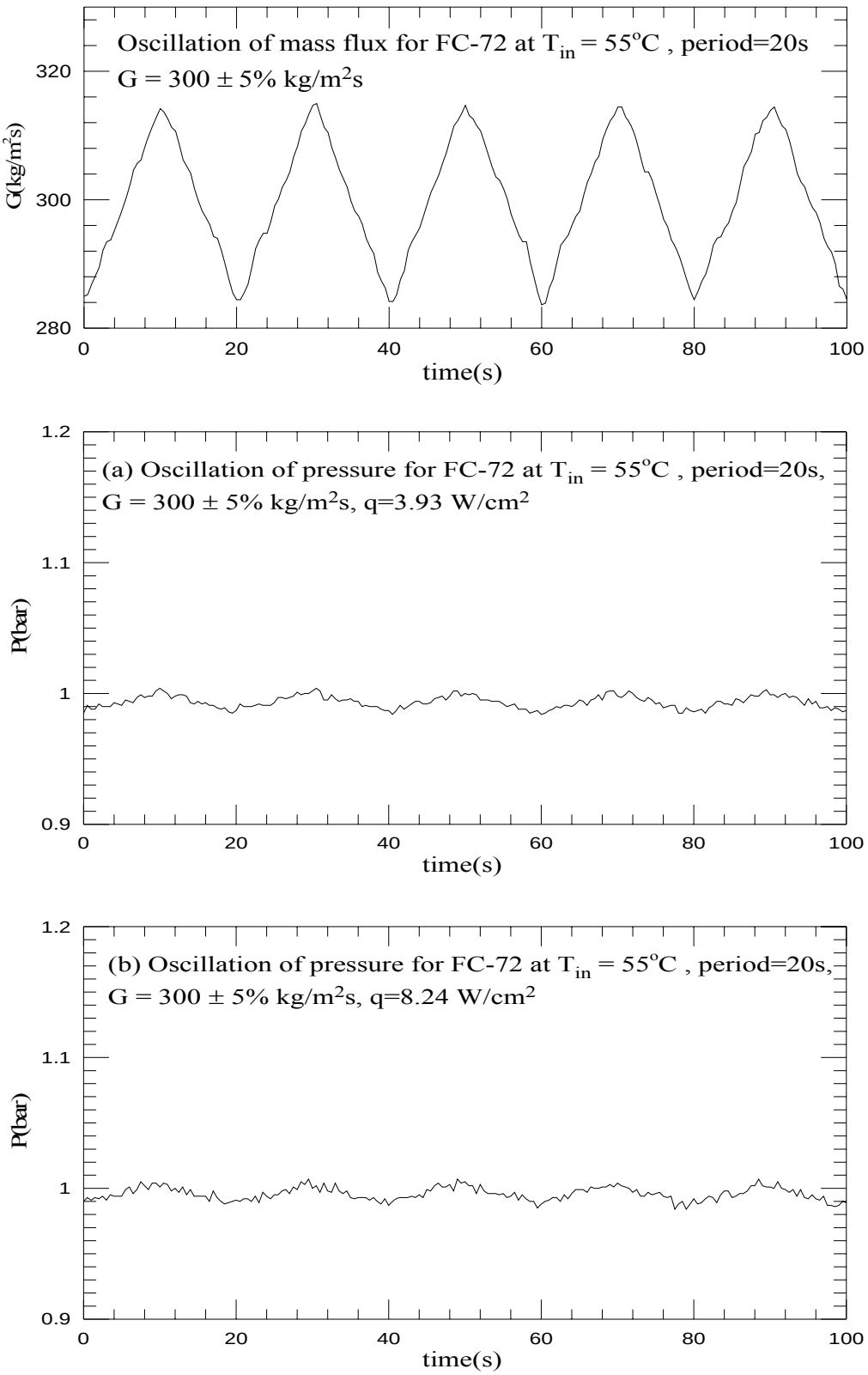


Fig.7.33 Time variations of coolant mass flux and inlet pressure in transient oscillatory saturated flow boiling for various imposed heat fluxes at (a) q=3.93 W/cm^2 and (b) q=8.24 W/cm^2 for G=300±5% kg/m^{2}S with t_p =20 sec.

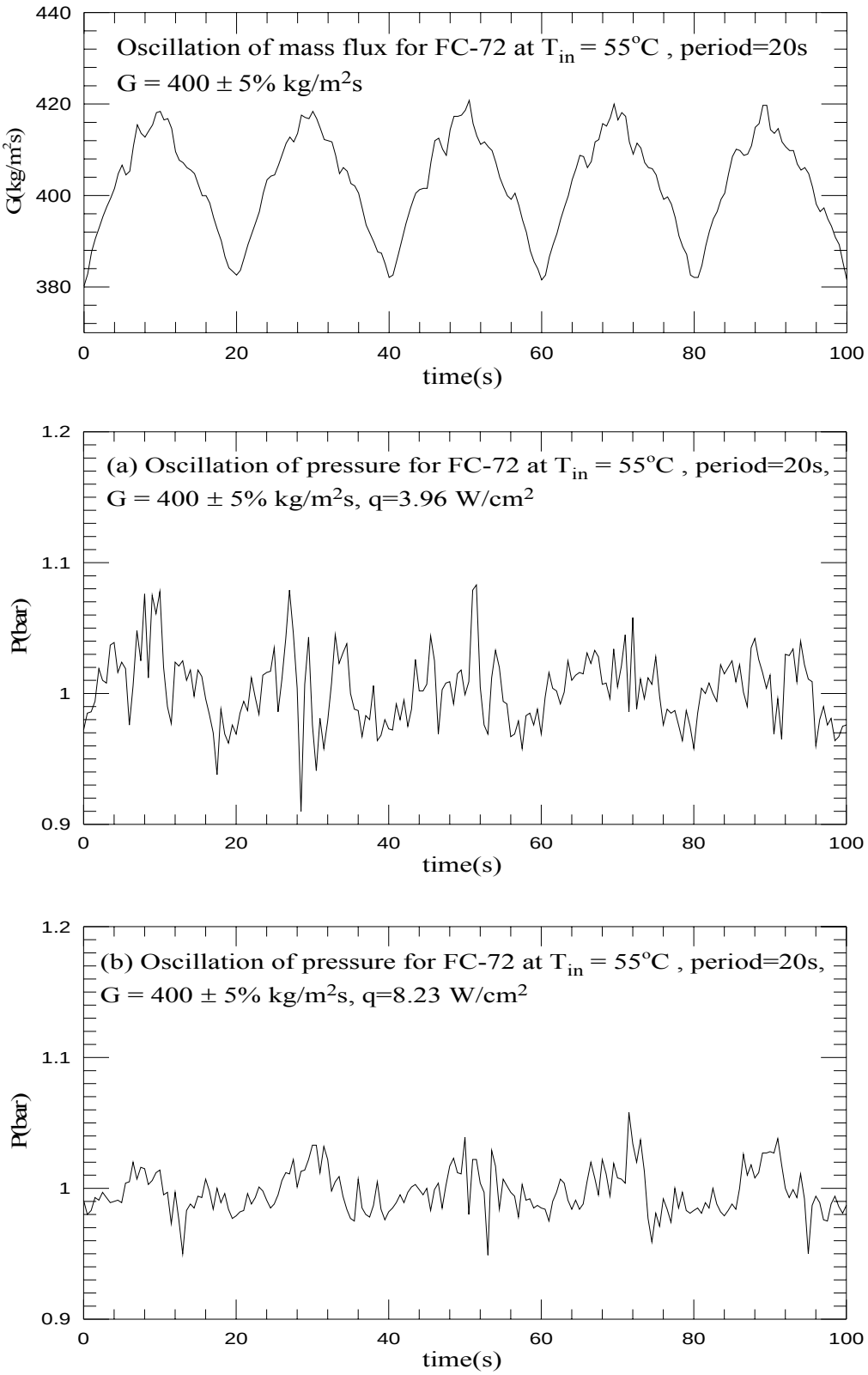


Fig.7.34 Time variations of coolant mass flux and inlet pressure in transient oscillatory saturated flow boiling for various imposed heat fluxes at (a) q=3.96 W/cm^2 and (b) q=8.23 W/cm^2 for G=400±5% kg/m^{2}S with t_p =20 sec.

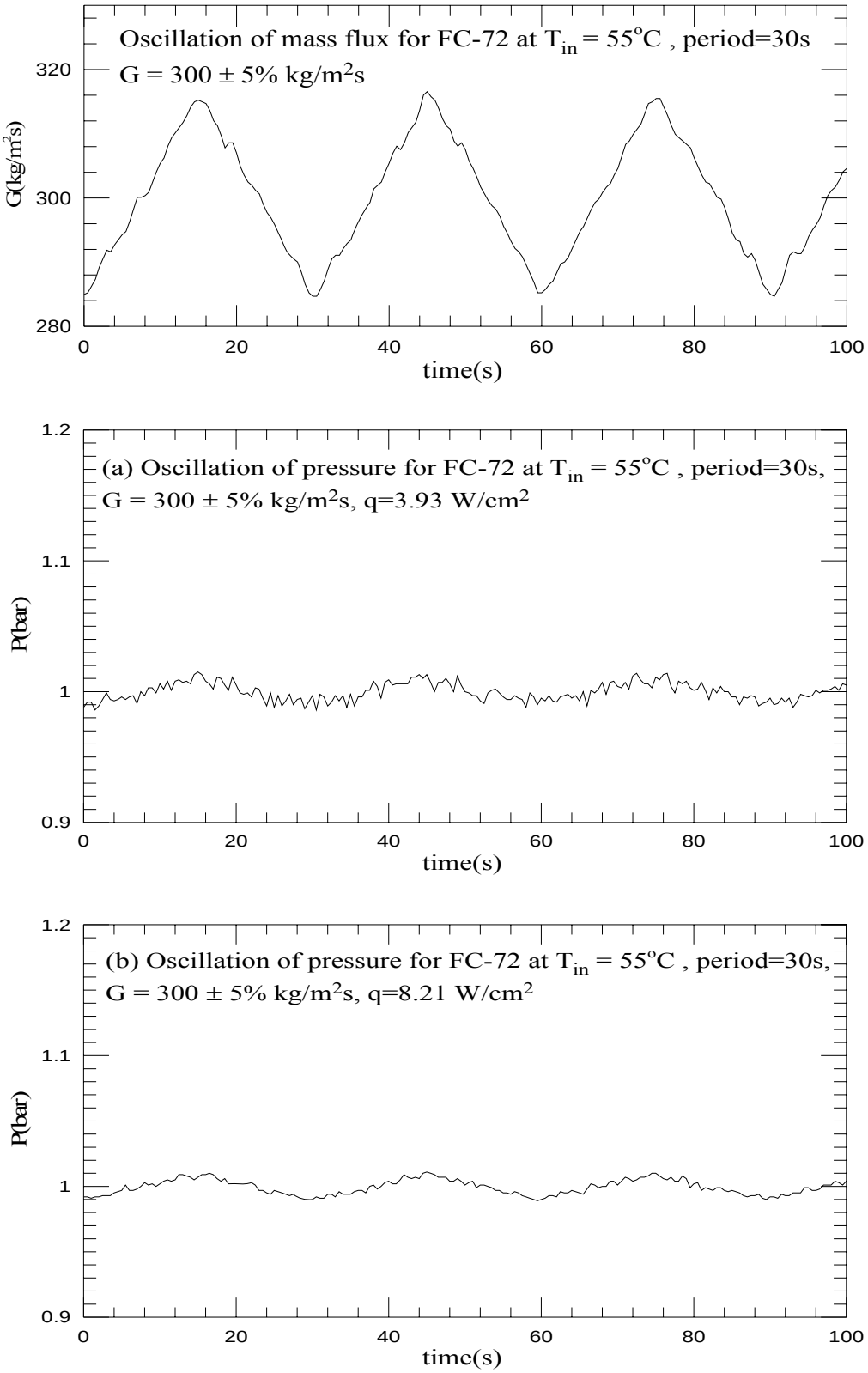


Fig.7.35 Time variations of coolant mass flux and inlet pressure in transient oscillatory saturated flow boiling for various imposed heat fluxes at (a) q=3.93 W/cm^2 and (b) q=8.21 W/cm^2 for G=300±5% kg/m^{2}S with t_p =30 sec.

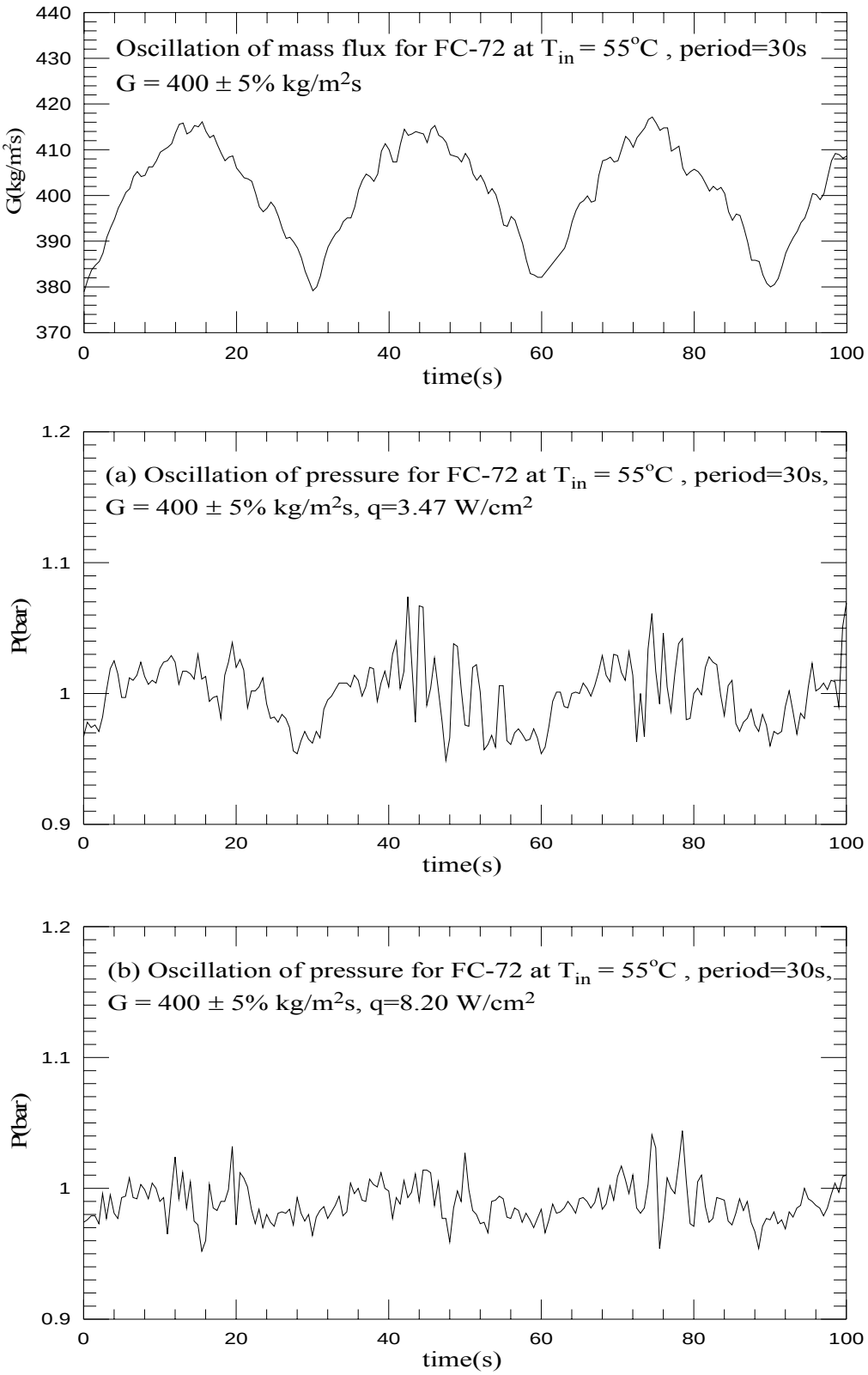


Fig.7.36 Time variations of coolant mass flux and inlet pressure in transient oscillatory saturated flow boiling for various imposed heat fluxes at (a) q=3.47 W/cm^2 and (b) q=8.20 W/cm^2 for G=400±5% kg/m^{2}S with t_p =30 sec.

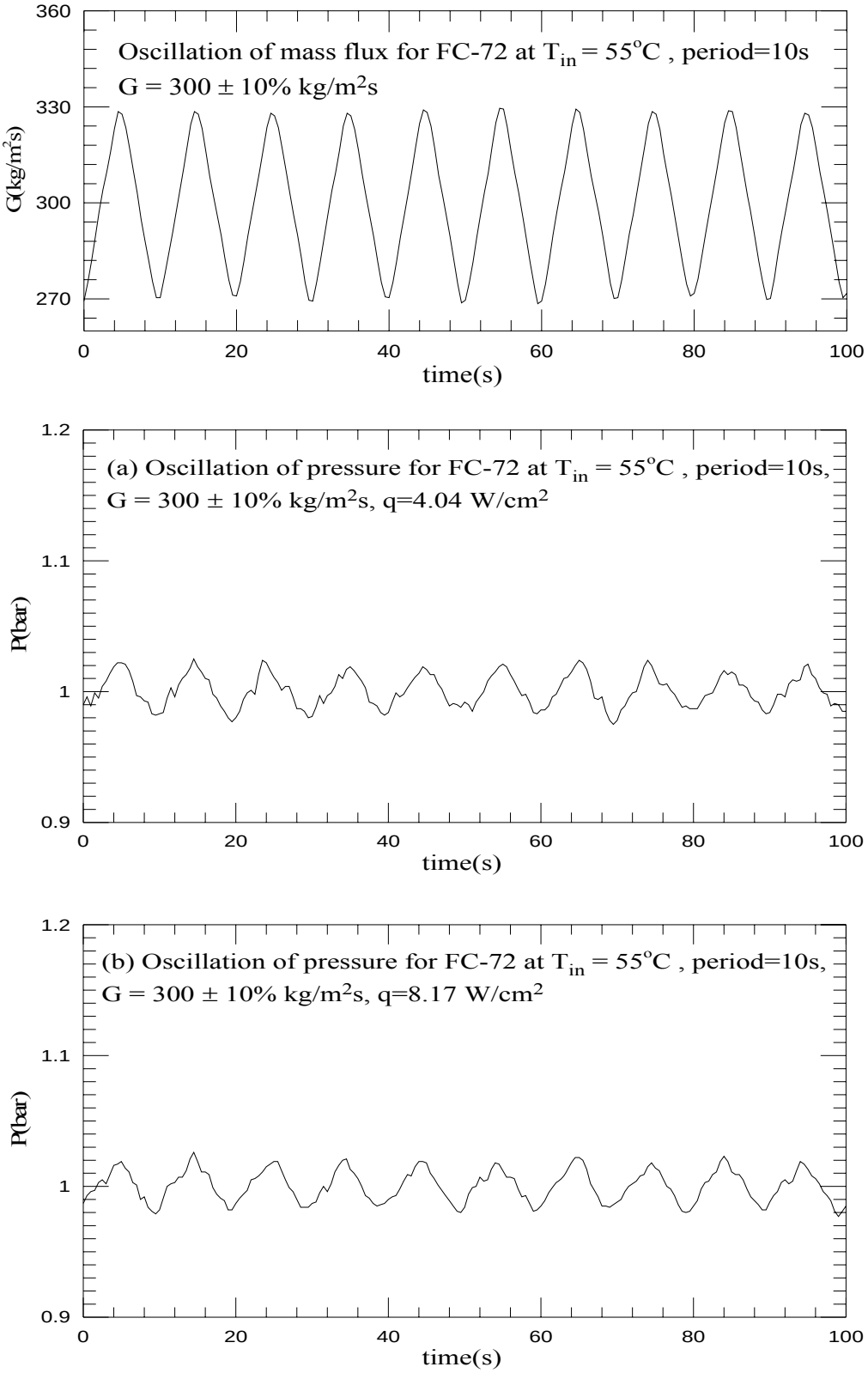


Fig.7.37 Time variations of coolant mass flux and inlet pressure in transient oscillatory saturated flow boiling for various imposed heat fluxes at (a) q=4.04 W/cm^2 and (b) q=8.17 W/cm^2 for G=300±10% kg/m^{2}S with t_p=10 sec.

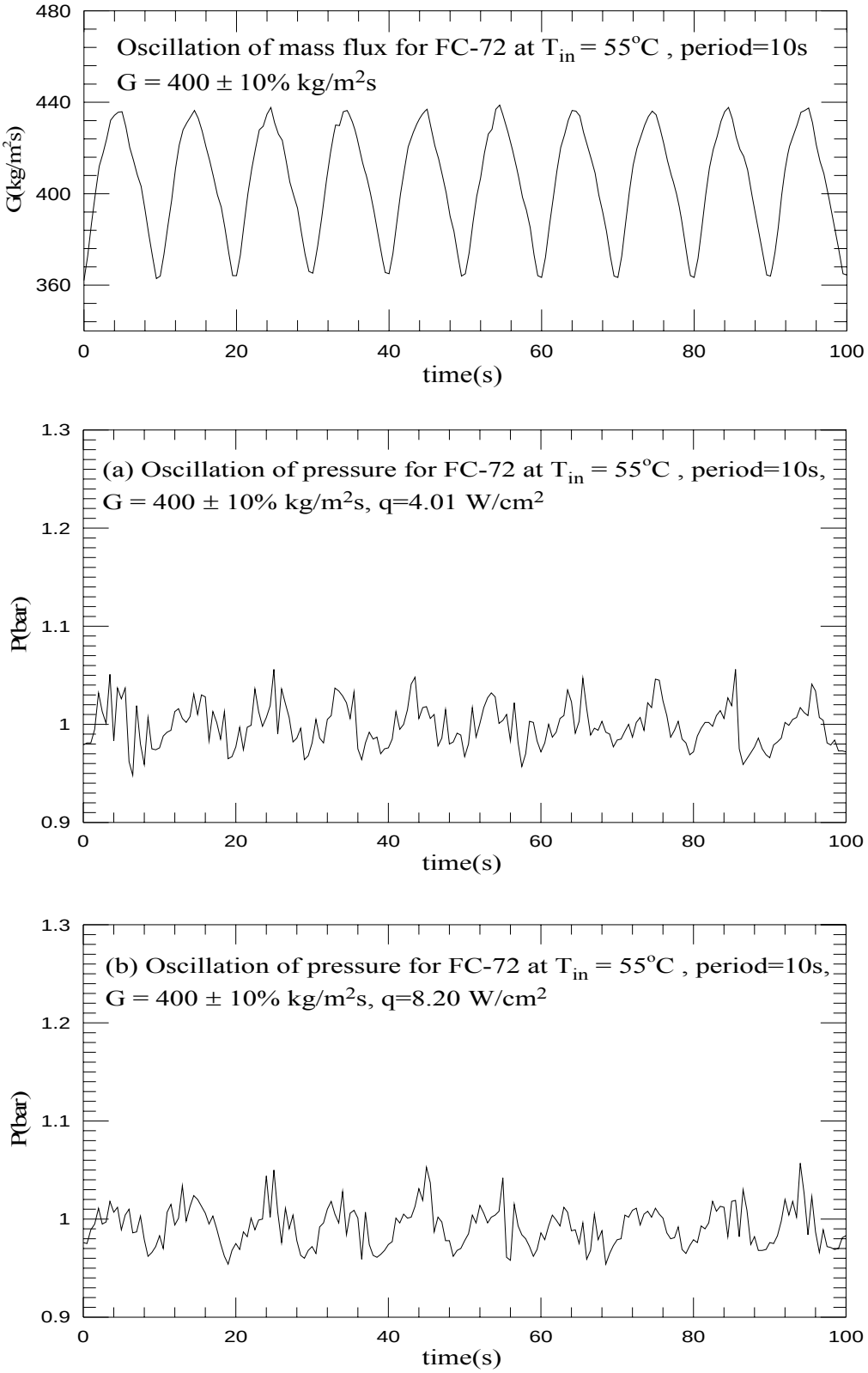


Fig.7.38 Time variations of coolant mass flux and inlet pressure in transient oscillatory saturated flow boiling for various imposed heat fluxes at (a) q=4.01 W/cm^2 and (b) q=8.20 W/cm^2 for G=400±10% kg/m^{2}S with t_p=10 sec.

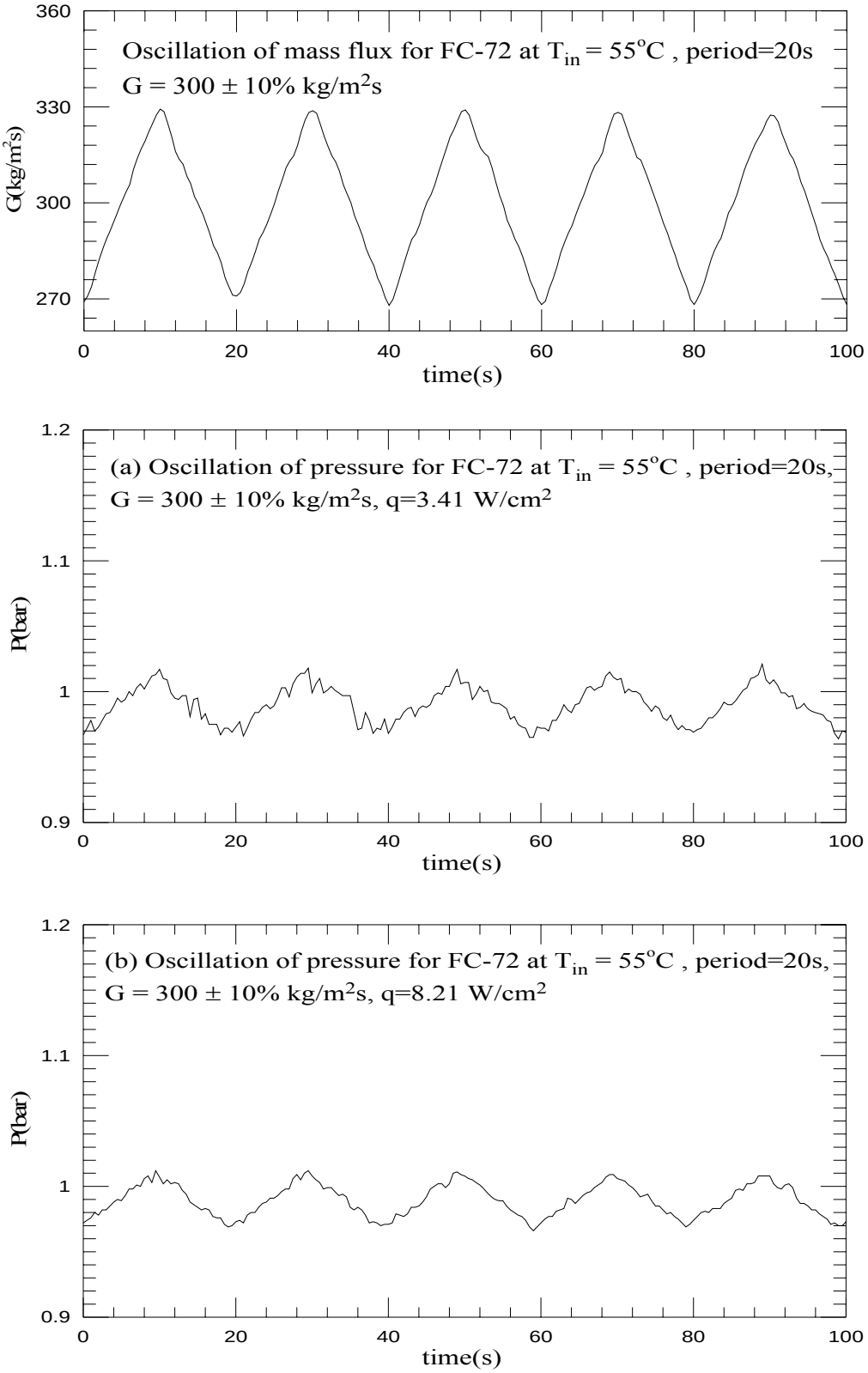


Fig.7.39 Time variations of coolant mass flux and inlet pressure in transient oscillatory saturated flow boiling for various imposed heat fluxes at (a) q=3.41 W/cm^2 and (b) q=8.21 W/cm^2 for G=300±10% kg/m^{2}S with t_p=20 sec.

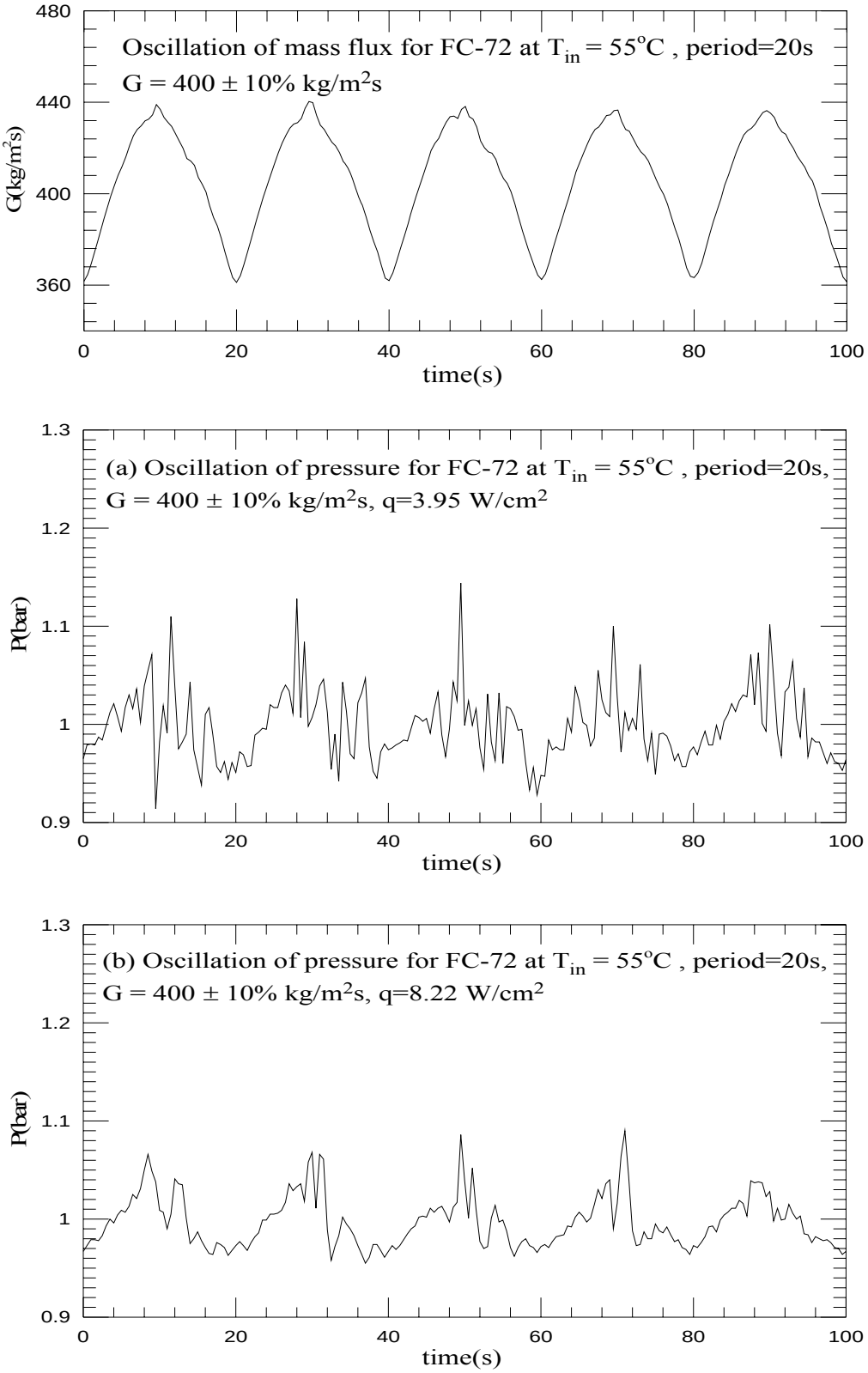


Fig.7.40 Time variations of coolant mass flux and inlet pressure in transient oscillatory saturated flow boiling for various imposed heat fluxes at (a) q=3.95 W/cm^2 and (b) q=8.22 W/cm^2 for G=400±10% kg/m^{2}S with t_p=20 sec.

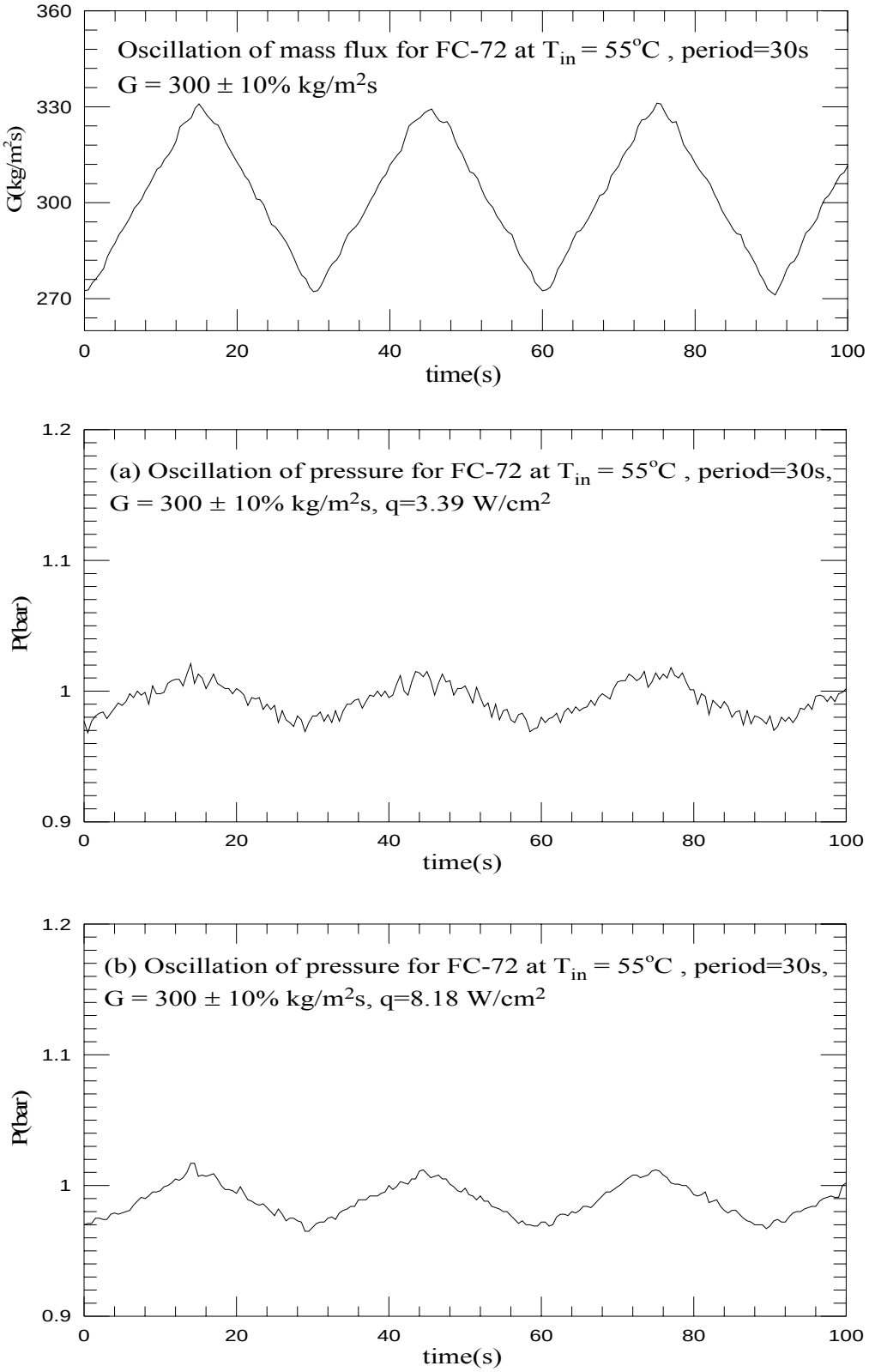


Fig.7.41 Time variations of coolant mass flux and inlet pressure in transient oscillatory saturated flow boiling for various imposed heat fluxes at (a) q=3.39 W/cm^2 and (b) q=8.18 W/cm^2 for G=300±10% kg/m^{2}S with t_p=30 sec.

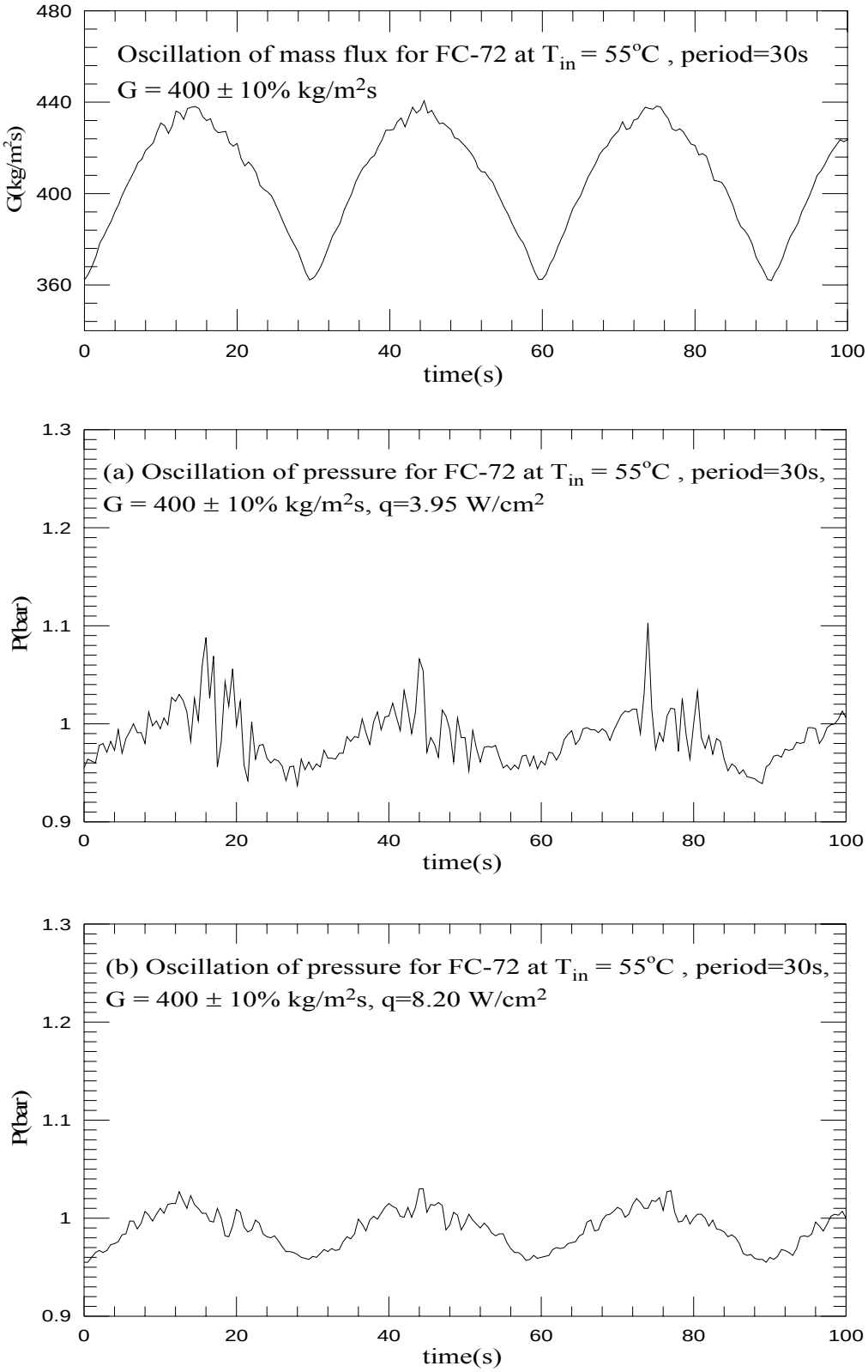


Fig.7.42 Time variations of coolant mass flux and inlet pressure in transient oscillatory saturated flow boiling for various imposed heat fluxes at (a) q=3.95 W/cm^2 and (b) q=8.20 W/cm^2 for G=400±10% kg/m^{2}S with t_p=30 sec.

CHAPTER 8

Time Periodic Saturated Flow Boiling Heat Transfer of R-134a and Associated Bubble Characteristics in a Narrow Annular Duct due to Heat Flux Oscillation

The results obtained for the R-134a saturated flow boiling resulting from the imposed heat flux oscillation only are presented in this chapter. The present time periodic R-134a saturated flow boiling experiment is performed for the refrigerant mass flux G varying from 100 to 600 kg/m^{2}s, mean imposed heat flux $\bar{q}$ from 0 to 45 kW/m^2, and system pressure P set at 414.6 kPa and 488.6 kPa (corresponding to the R-134a saturation temperature T_{sat}=10℃ and 15℃) for the gap of the duct δ = 1.0, 2.0 and 5.0 mm. Besides, the amplitude of the imposed heat flux oscillation Δq is set at 0, 10, 30 and 50% of $\bar{q}$. Moreover, the period of the heat flux oscillation t_p is fixed at 20, 30, 60 and 120 seconds. The ranges of the parameters chosen above are in accordance with some air-conditioning applications. Several time scales associated with the present saturated flow boiling over the heated inner pipe surface are given in Table 6.1. Specifically, there are four relevant time scales in the experiment. The conduction time scale t_1 is estimated by considering a copper slab of the characteristic length L_c (thickness) subject to a step heat input at one of its surface at certain time instant and t_1 is the duration for the other surface to begin to feel the heat input [86]. According the thermal diffusion speed, $t_1 \approx L_c^2/\alpha_w$. The convection time scale t_2 can be estimated by the equation $t_2=L/(G/\rho_l)$ [87]. The time scale for the bubble growth or departure t_3 is approximated by the empirical expression $t_3=\dfrac{d_p}{2000(\mu_l/(\rho_l D_h))}$ [88]. Finally, the time constant of the present flow boiling on the heated copper duct surface t_c is obtained by meauring T_w subject to a step input in the imposed heat flux for both single-phase and boiling conditions. The results in Tables 6.1-6.3 clearly indicate that the time constants associated with the single-phase liquid flow and flow boiling over the heat surface are much larger than the other time constants and hence dominate the time response of the duct wall to the heat flux oscillation. Besides, the time lag of the heated surface temperature behind the imposed heat flux oscillation is expected to be significant. In the following, attention will be mainly paid to examining the effects of the amplitude and period of the heat flux oscillation on the time periodic R-134a saturated flow boiling heat transfer

performance. Note that for the limiting case of $\Delta q / \overline{q} = 0\%$ we have saturated flow boiling of R-134a at a constant refrigerant mass flow rate in the test section, which is designated as 〝stable flow boiling〞 and has been investigated by Lie and Lin [21]. The measured boiling heat transfer data are expressed in terms of the boiling curve and boiling heat transfer coefficient. The thermal characteristics of the time periodic flow boiling is illustrated by the time variations of the instantaneous heated pipe wall temperature and boiling heat transfer coefficient. Moreover, selected flow photos and data deduced from the images of the time periodic boiling processes are presented to show the temporal bubble characteristics in the boiling flow.

8.1 Time-Average Boiling Curve and Heat Transfer Coefficient

At first, the time-average boiling curves and heat transfer coefficients measured at the middle axial location (z =80 mm) of the narrow annular duct for various amplitudes and periods of the heat flux oscillation are shown in Fig. 8.1 for $T_{sat} = 15℃$ and G= 500 kg/m^{2}s. The results in Fig. 8.1 clearly indicate that the time-average boiling curves and heat transfer coefficients are not affected by the amplitude and period of the heat flux oscillation to a significant degree. In fact, they are nearly the same as that for the stable boiling.

Then, the effects of the duct size on the time-average boiling curves are shown in Fig. 8.2(a). It is noted that the boiling curve shifts significantly to the left as the gap in the duct is reduced, indicating that the boiling heat transfer in the smaller duct is substantially better. It is also evident from the data that lower imposed heat flux and wall superheat are needed to initiate boiling on the heated surface for the smaller duct. This mainly results from the fact that for given $\overline{G}$, q and $\overline{T}_{sat}$ the mass flow rate through the duct is lower for a smaller gap. For the lower refrigerant mass flow rate the axial temperature rise of the refrigerant flow is faster, which, in turn, causes earlier bubble nucleation for a smaller gap. Then, the data shown in Fig. 8.2(b) indicate that the saturated boiling heat transfer increases noticeably with a decrease in the channel gap. Since the shear stress of the flow acting on the heated surface in a smaller channel is higher, the bubbles on the heating surface can be more easily swept away from the heated surface. Moreover, the flow pattern change from the bubbly flow to the slug flow for $\delta = 1.0$ mm occurs at a lower imposed heat flux than that for $\delta = 2.0$ mm. These effects are thought to be the main reasons for the enhancement of flow boiling heat transfer when the channel size is reduced.

8.2 Time Dependent Flow Boiling Heat Transfer Characteristics

The time periodic flow boiling heat transfer characteristics for R-134a flow in the annular duct resulting from the imposed periodic heat flux oscillation are illustrated in Figs. 8.3 - 8.6 by presenting the time variations of the heated wall temperature and boiling heat transfer coefficients at the middle axial location in the statistical state for various G, T_{sat}, $\Delta q/\overline{q}$, t_p and

$\bar{q}$. For clear illustration, the measured data for the time variations of the actual imposed heat flux are also given here. The results manifest that when q oscillates periodically in time nearly like a triangular wave, significant temporal oscillations in T_w and h_r nearly in the form of sinusoidal waves can occur. Note that the T_w and h_r oscillations are also periodic in time and are at the same frequency as the heat flux. Besides, the T_w and h_r oscillations get stronger for a higher amplitude and a longer period of the imposed heat flux oscillation. Moreover, the T_w oscillation is stronger for a higher mean imposed heat flux. Note that single-phase forced convection prevails in the duct at a relatively low imposed heat flux. The data given in Figs. 8.3 - 8.6 further reveals that the T_w oscillation significantly lags the heat flux oscillation for both single-phase and boiling flows. This time lag apparently results from the thermal inertia of the heated pipe wall. Note that for given G, T_{sat}, and $\Delta q/\bar{q}$ the duration of the time lag relative to the oscillation period t_l/t_p is slightly longer at a lower time-average imposed heat flux and a shorter period of the imposed heat oscillation. Furthermore, for the single-phase convection at low q and in the first half of the periodic cycle in which the heat flux decreases with time, after the time lag the wall temperature is found to decrease with time. The opposite process occurs in the second half of the cycle. It is further noted in the experiment that at a low $\bar{q}$ the temperature of the heating surface is lower than that required for the onset of nucleate boiling and no bubble nucleates from the heating surface in the whole periodic cycle. Hence heat transfer in the flow results completely from the single-phase forced convection. As the mean imposed wall heat flux is raised gradually, the heated surface temperature increases correspondingly. The corresponding T_w oscillation amplitude can be significant even when the single-phase flow prevails in the duct (Fig. 8.3(c)). At a certain higher wall temperature for a small increase in $\bar{q}$ bubbles start to nucleate from the heated surface at certain instant of time but bubble nucleation is not seen in the whole cycle. Thus, we have intermittent boiling in the flow in which nucleate boiling only exists in a partial duration of the periodic cycle. The time instants for the start and termination of the nucleate boiling are marked on the curves for T_w for the cases with the presence of the intermittent boiling. For some increase in the mean imposed heat flux nucleate boiling persists over the entire period of the cycle and we have persistent flow boiling in the duct. The results in Figs. 8.3 - 8.6 also show that after the time lag T_w and h_r both decrease with time in the first half of the periodic cycle in which the imposed heat flux decreases with time. While in the second half of the cycle the opposite process occurs. Then, the data shown in Fig. 8.5 indicate that the T_w oscillation amplitude increases noticeably with an increase in the channel gap in the persistent flow boiling.

8.3 Intermittent Flow Boiling

It is of interest to note in the visualization of the boiling flow in the annular duct that over a certain intermediate range of the mean imposed heat flux the intermittent boiling appears. More

specifically, in a typical periodic cycle of the imposed heat flux oscillation at a certain time instant in the first half of the cycle as the imposed heat flux decreases to a certain low level and the heated pipe wall temperature decreases to the level below that required for the onset of nucleate boiling, bubble nucleation on the heated inner pipe disappears and boiling stops. Single-phase flow prevails in the duct. At a certain later time instant in the second half of the cycle in which the imposed heat flux increases and T_w rises to exceed the wall superheat required for the onset of nucleate boiling, bubble nucleation is seen on the heated surface and boiling appears. The boiling process continues for some time interval. The above processes of the intermittent flow boiling are repeatedly seen on the heated surface. To be more clear, we mark the time instants at which boiling starts and stops in Fig. 8.3 on the curves for T_w for the cases with the presence of the intermittent boiling. Note that at a higher imposed heat flux the onset of boiling is earlier and the termination of boiling is later. Besides, the instants for the boiling inception and termination are affected by the amplitude and period of the heat flux oscillation to a noticeable degree (Fig. 8.3). Flow regime maps to delineate the boundaries separating different flow boiling regimes in terms of the Boiling number versus the relative amplitude of the imposed heat flux oscillation are given in Figs. 8.7 and 8.8. The results show that the intermittent boiling prevails over a significantly wider range of the Boiling number for a higher amplitude and a longer period of the imposed heat flux oscillation and for a lower refrigerant mass flux. Moreover, the intermittent boiling appears over a wider range of the Boiling number for a larger duct gap (Fig. 8.8). Furthermore, the onsets of nucleate boiling and persistent boiling take place at higher $\overline{\mathrm{Bo}}$ for a larger δ. Based on the present data for $\delta = 2.0$ mm, the conditions leading to the appearance of the intermittent boiling can be empirically correlated as

$$(5.96\times10^{-7} + 4.44\times10^{-10}\overline{\mathrm{Re}}^{0.5}) \le \overline{\mathrm{Bo}}^{1.2}\cdot(\Delta q/\overline{q})^{1.2}\cdot(t_p/t_c)^{1.2} \le (1.02\times10^{-4} - 4.31\times10^{-7}\overline{\mathrm{Re}}^{0.5}) \quad (8.1)$$

More than 97 % of the present data falls within the above correlation.

8.4 Effect of Heat Flux Oscillation at Extremely Short and Long Periods

How the period of the heat flux oscillation affects the time periodic flow boiling is further investigated by comparing the data for relatively short and long t_p in Fig. 8.9. Now when the oscillatory period is set to be 2.0 seconds, the heated surface temperature stays at a nearly constant level, as evident from the data shown in Fig. 8.9(a) for the oscillation amplitude of q being 50% of the mean imposed heat flux. In fact, for this case the amplitude of T_w oscillation is smaller than 0.2℃ which is below the random thermal disturbances from the background and is close to that in the stable boiling. Due to its heat capacity, the heated copper duct is not able to quickly respond to the very rapid change in the imposed heat flux. This situation appears when the period of the imposed heat flux oscillation is significantly shorter than the dominated time

constant of the flow boiling system.

On the other hand, when the oscillatory period is relatively long at 120 and 600 seconds, the data given in Figs. 8.9(b) and (c) manifest that the amplitude of the T_w oscillation is very large. Note that the T_w oscillation is slightly stronger for t_p raised from 120 to 600 seconds. The stronger T_w oscillation at a longer t_p can be attributed to the longer period of time for the thermal energy storing in and releasing from the wall of the heated inner pipe. This in turn causes the heated pipe wall to accumulate thermal energy over a longer period of time and hence results in a larger amplitude of the T_w oscillation.

8.5 Effect of Heat Flux Oscillation Amplitude

Then the effect of the amplitude of the heat flux oscillation on the time periodic flow boiling is examined. The data presented in Fig. 8.10 for five different amplitudes of the imposed heat flux oscillation with $\Delta q/\overline{q}$ = 10, 30, 50, 80 and 100% at t_p =120 seconds show that the T_w oscillation is significantly stronger for a larger amplitude of the imposed heat flux oscillation. Note that the time lag in T_w oscillation increases substantially when the amplitude of the imposed heat flux oscillation is raised from 10% to 30%. But a further increase in the amplitude of the heat flux oscillation does not increase the time lag noticeably.

8.6 Bubble Characteristics in Time Periodic Flow Boiling

The bubble characteristics associated with the stable saturated flow boiling of R-134a in the present narrow annular duct have been examined in our recent study [21]. These characteristics indicate that for the constant imposed heat flux exceeding that for onset of nucleate boiling the duct is dominated by the persistent boiling and a number of discrete bubbles nucleate from the cavities and slide along the heating surface. At a higher q the active bubble nucleation density increases and a lot of coalescence bubbles appear. More coalescence bubbles are seen and they are confined by the duct walls to become slightly deformed for a further increase in q. At even higher q the duct is mainly filled with the coalescence bubbles. They also reported that at a higher refrigerant mass flux the bubble departure frequency was higher and the bubbles were smaller and in violent agitating motion. However, the active nucleation site density is lower at a higher mass flux. But at the lower mass flux the bubble coalescence is more important and a number of bigger bubbles form in the duct. Then, at a lower saturation temperature of the refrigerant the bubbles were found to grow bigger and depart at a lower rate, and the active nucleation site density is lower due to the higher surface tension and enthalpy of vaporization.

By and large, in the time periodic flow boiling investigated here the effects of the mean imposed heat flux and refrigerant mass flux and saturation temperature on the bubble behavior exhibit similar trends to that in the stable flow boiling. Hence, we first illustrate here how the

time periodic bubble characteristics are affected by the amplitude and period of the heat flux oscillation for the persistent boiling in Figs. 8.11 and 8.12 by presenting the photos of the boiling flow for the cases with the imposed heat flux well above that required for ONB in a small region around the middle axial location at eight selected time instants in a typical periodic cycle in the statistical state. In the figure the symbol " $t = t_o$ " signifies the time instant at which the instantaneous heat flux is at the highest level and starts to decrease. The results indicate that for given G, $\bar{q}$, $\Delta q/\bar{q}$ and t_p the departuring bubbles get smaller in the duct in the first half of the cycle in which the heat flux decreases. The opposite processes take place in the second half of the cycle in which the heat flux increases with time. These changes of the bubble characteristics with the instantaneous heat flux become more significant for an increase in the amplitude of the heat flux oscillation, as evident by comparing the results in Fig. 8.11(a) with Fig. 8.11(c). Besides, the bubble coalescence occurs more frequently and more large bubbles appear in the duct for the cases with a longer period of the heat flux oscillation (Figs. 8.11(b) and (c)). Then, the bubble behavior in the intermittent flow boiling for a case with a given intermediate imposed heat flux is manifested in Fig. 8.13. The results clearly indicate that initially in the beginning of the cycle the instantaneous heat flux decreases with time but is still well above $\bar{q}_{ONB}$, bubbles nucleation from the heated surface is clearly seen. Note that the number and size of the bubbles decrease noticeably with time in the first quarter of the periodic cycle for the continuing decrease of the heat flux. Then the bubbles nucleation gradually disappears and finally boiling stops at certain time instant slightly after $t_0+3t_p/8$ when the heat flux is slightly below $\bar{q}_{ONB}$ and bubble nucleation stops completely. The flow is then in single-phase state over some period of time. But after a certain time instant slightly after $t_0+6t_p/8$ at which the imposed heat flux is raised to a certain high level, bubble nucleation on the heated surface is first seen and then more bubbles nucleate on the heated surface. Two-phase boiling flow again dominates in the duct. We have to wait until the end of the first quarter of the next cycle to see the bubble nucleation gradually disappears on the heated surface. The above processes repeat in each cycle. The precise instants of time at which the onset and termination of nucleate boiling take place vary with the flow conditions.

To be more quantitative on the bubble characteristics in the time periodic flow boiling due to the heat flux oscillation, we estimate the bubble departure diameter and frequency and the number density of the active nucleation sites on the heating surface in a typical periodic cycle at the middle axial location for the persistent flow boiling from the images of the boiling flow stored in the video tapes. Selected results from this estimation are manifested in Figs. 8.14-8.17 by presenting the effects of the amplitude and period of the imposed heat flux oscillation on the time dependent bubble characteristics. In these plots time "t = 0" denotes the instant of time the

imposed heat flux is at the highest level and starts to decrease in a typical periodic cycle. The data in Fig. 8.14 indicate that as the imposed heat flux oscillates time periodically, the bubble departure diameter also varies time periodically and to some degree like a triangular wave as the imposed heat flux oscillation. Note that the effect of the time lag in T_w oscillation is clearly seen. More specifically, the size of the departing bubbles does not decrease immediately with time in the first half of the periodic cycle in which the heat flux decreases with time. In fact, the bubble size increases in the initial transient for $t<t_1$ and then for t exceeding the time lag the departing bubbles decrease in size. While in the second half of the cycle an opposite process is noted when the heat flux increases with time. The above time variation of the bubble departure diameter resmbles the T_w oscillation presented in Fig. 8.3. Besides, the results in Fig. 8.14(a) show that at the larger amplitude of the heat flux oscillation the time variation of the bubble departure diameter is somewhat stronger. Moreover, the results in Fig. 8.14(b) indicate that to some degree the bubble departure diameter varies stronger with time for a longer period of the heat flux oscillation. Furthermore, increases in the refrigerant mass flux, saturation temperature and duct gap and a decrease in the mean imposed heat flux cause the departing bubbles to become smaller but do not change the wave form of the d_p variation with time (Figs. 8.14(a), (c), (d) and 8.17(a)). It is worth mentioning that in the present study even the size of the largest departing bubble is below 0.25 mm which is much smaller than the diameter of the outer glass pipe in the test section (D_p= 20.0 mm). Thus the observation of the bubble size through the curved surface of the glass pipe is not expected to produce significant error.

How the temporal variation of the bubble departure frequency is affected by the heat flux oscillation is shown in Fig. 8.15. Note that the bubble departure frequency also varies like a triangular wave. Besides, for an oscillation heat flux after the time lag for $t>t_1$ the bubbles depart from the heated surface at a decreasing rate in the first half of the periodic cycle in which the heat flux and heated surface temperature decrease with time (Fig. 8.15(a)). Note that in the initial stage for $t<t_1$ the bubble departure frequency increases with time as T_w. Apparently, in the second half of the cycle in which the heat flux increases the opposite process takes place. Moreover, the results in Fig. 8.15(a) indicate that at the larger amplitude of the heat flux oscillation the bubble departure frequency exhibits a stronger variation with time. Then, the results in Fig. 8.15(b) indicate that the bubble departure frequency oscillates in a larger amplitude at a longer period of the heat flux oscillation. Obviously, reducing the duct gap causes a larger variation of the bubble departure frequency with time (Fig. 8.17(b)). Finally, at higher $\bar{q}$, G and T_{sat} and at a smaller δ the bubble departure frequency is higher (Figs. 8.15(a), (c) and (d) and 8.17(b)).

The time variations of the associated number density of the active nucleation sites on the heating surface affected by the heat flux oscillation presented in Fig. 8.16 clearly show that in the time periodic flow boiling the active nucleation site density also varies like a triangular wave. Besides, n_{ac} decreases substantially with time after the time lag for $t>t_l$ in the first half of the periodic cycle in which the heat flux and heated wall temperature decrease with time. The reverse process appears in the second half of the cycle in which the heat flux rises. At a higher amplitude of the heat flux oscillation the temporal variation of n_{ac} is also stronger (Fig. 8.16(a)). Besides, for a longer period of the heat flux oscillation the time variation of n_{ac} is also stronger (Fig. 8.16(b)). But reducing the duct gap from 5.0 to 1.0 mm results in a slightly larger time variation of n_{ac} (Fig. 8.17(c)). Finally, n_{ac} is significantly higher at a lower G and higher $\overline{q}$ & T_{sat} (Figs. 8.16(a), (c) and (d)).

It is worth mentioning that the time instants at which d_p, f and n_{ac} attain their maximums and minimums are not exactly at the instants the imposed heat flux is at its highest and lowest levels respectively at t = 0 and t = t_p/2. This is a direct consequence of the significant time lag in the time response of the heated surface temperature in the present time periodic flow boiling subject to the imposed heat flux oscillation.

Based on the data in Figs. 8.14-8.16 for δ = 2.0 mm, in the persistent boiling at a high q the dependence of the quantitative bubble characteristics on the R-134a heat flux oscillation can be approximately expressed as $d_p \propto q^a$, $f \propto q^b$ and $n_{ac} \propto q^c$ when the time lag in the T_w oscillation is neglected. Here the exponents a, b and c range respectively from 0.15 to 0.26 , 0.35 to 0.56 , and 1.18 to 1.62, as shown in Fig. 8.18. Note that the latent heat transfer resulting from bubble nucleation in the persistent boiling q_b is proportional to d_p^3, f and n_{ac}, as discussed in the previous study [21]. Thus, $q_b \propto q^d$, here d varies from 1.98 to 2.96. This result clearly indicates that the flow boiling heat transfer gets better at increasing heat flux since q_b prevails in the boiling heat transfer. This in turn causes the heated wall temperature to decrease at decreasing heat flux and vice versa in the time periodic flow boiling, as already seen from Fig. 8.2. Besides, the dominant effect of the heat flux oscillation on the boiling heat transfer comes from the very strong influence of the heat flux on the active nucleation site density.

8.7. Concluding Remarks

The heat transfer data for the time periodic flow boiling of R-134a resulting from the imposed heat flux oscillation in the narrow annular duct have been presented here along with the bubble behavior. Effects of the mean level and oscillation amplitude and period of the heat flux oscillation on the time periodic R-134a flow boiling have been examined in detail. The major

results obtained here can be summarized in the following.

(1) The time-average boiling curves and heat transfer coefficients for the time periodic flow boiling of R-134a are not affected to a noticeable degree by the amplitude and period of the imposed heat flux oscillation.

(2) The heated pipe wall temperature, bubble departure diameter and frequency, and active nucleation site density also oscillate periodically in time and at the same frequency as the heat flux oscillation. Experiments also show that the resulting oscillation amplitudes of the heated surface temperature, heat transfer coefficient and bubble parameters, such as d_p, f and n_{ac}, get larger for a longer period and a larger amplitude of the imposed heat flux oscillation and for a higher mean imposed heat flux. Moreover, a significant time lag in the heated surface temperature oscillation is also noted, which apparently results from the thermal inertia of the copper inner pipe. The nondimensional time lag, defined as the ratio of the time lag to the period of the imposed heat flux oscillation, is longer at a lower mean imposed heat flux and a shorter period and for a larger amplitude of the imposed heat flux oscillation when the amplitude is below 30%. Furthermore, the bubbles become smaller and more dispersed after the time lag when the imposed heat flux decreases with time. The opposite processes take place at increasing heat flux. Finally, reductions in the size of the departing bubbles, the bubble departure frequency and active nucleation site density with time result in the time duration in which the heat flux is sinking. When the heat flux is rising the opposite processes occur.

(3) The effects of heat flux oscillation at extremely short and long periods have been explored. Due to the existence of the thermal inertia of the heated copper duct, the resulting heated surface temperature does not oscillate with time at an extremely short period of the imposed heat flux oscillation. But the oscillation amplitude of the heated surface temperature gets noticeably stronger for an extremely long period of the imposed heat flux oscillation.

(4) When the imposed heat flux over the heated surface is close to the heat flux corresponding to that for the onset of stable flow boiling, intermittent flow boiling appears. A flow regime map and an empirical correlation are given to delineate the boundaries separating different boiling flow regimes in the annular duct.

Table 8.1 Time scales for transient R-134a saturated flow boiling (δ = 1 mm)

Time scales		(sec)
Conduction time scale $t_1=L_c^2/\alpha_w$		0.346452
Convection time scale $t_2=L\Big/(\frac{G}{\rho_l})$	T_{sat} = 15℃, G = 600 kg/m^{2}s	0.331528
	T_{sat} = 15℃, G = 500 kg/m^{2}s	0.397833
	T_{sat} = 15℃, G = 400 kg/m^{2}s	0.497292
	T_{sat} = 15℃, G = 300 kg/m^{2}s	0.663056
	T_{sat} = 10℃, G = 600 kg/m^{2}s	0.336239
Time scale of saturated flow boiling $t_3=\frac{d_p}{2000(\mu_l/(\rho_l D_h))}$		0.0008875
Time constant $t_4=t_c$	T_{sat} = 15℃, G = 600 kg/m^{2}s	60.2 (Single-phase)
		43.3 (Saturated flow boiling)
	T_{sat} = 15℃, G = 500 kg/m^{2}s	61.6 (Single-phase)
		44.4 (Saturated flow boiling)
	T_{sat} = 15℃, G = 400 kg/m^{2}s	65.9 (Single-phase)
		46.2 (Saturated flow boiling)
	T_{sat} = 15℃, G = 300 kg/m^{2}s	67.65 (Single-phase)
		48.9 (Saturated flow boiling)
	T_{sat} = 10℃, G = 600 kg/m^{2}s	61.6 (Single-phase)
		45.2 (Saturated flow boiling)

Table 8.2 Time scales for transient R-134a saturated flow boiling (δ = 2 mm)

Time scales		(sec)
Conduction time scale $t_1=L_c^2/\alpha_w$		0.124723
Convection time scale $t_2=L\Big/(\frac{G}{\rho_l})$	T_{sat} = 15℃, G = 500 kg/m^{2}s	0.397833
	T_{sat} = 15℃, G = 400 kg/m^{2}s	0.497292
	T_{sat} = 15℃, G = 300 kg/m^{2}s	0.663056
	T_{sat} = 10℃, G = 500 kg/m^{2}s	0.403487
Time scale for the bubble growth in saturated flow boiling $t_3=\frac{d_p}{2000(\mu_l/(\rho_l D_h))}$		0.001775
Time constants for flow boiling on heated surface $t_4=t_c$	T_{sat} = 15℃, G = 500 kg/m^{2}s	27.7 (Single-phase)
		24.0 (Saturated flow boiling)
	T_{sat} = 15℃, G = 400 kg/m^{2}s	30.1 (Single-phase)
		25.5 (Saturated flow boiling)
	T_{sat} = 15℃, G = 300 kg/m^{2}s	31.1 (Single-phase)
		26.3 (Saturated flow boiling)
	T_{sat} = 10℃, G = 500 kg/m^{2}s	29.0 (Single-phase)
		25.1 (Saturated flow boiling)

Table 8.3 Time scales for transient R-134a saturated flow boiling (δ = 5 mm)

Time scales		(sec)
Conduction time scale $t_1=L_c^2/\alpha_w$		0.055432
Convection time scale $t_2=L\Big/(\frac{G}{\rho_l})$	T_{sat} = 15℃, G = 300 kg/m^{2}s	0.663056
	T_{sat} = 15℃, G = 200 kg/m^{2}s	0.994584
	T_{sat} = 15℃, G = 100 kg/m^{2}s	1.989167
	T_{sat} = 10℃, G = 300 kg/m^{2}s	0.672479
Time scale of saturated flow boiling $t_3=\frac{d_p}{2000(\mu_l/(\rho_l D_h))}$		0.0044375
Time constant $t_4=t_c$	T_{sat} = 15℃, G = 300 kg/m^{2}s	32.7 (Single-phase)
		26.9 (Saturated flow boiling)
	T_{sat} = 15℃, G = 200 kg/m^{2}s	33.6 (Single-phase)
		28.2 (Saturated flow boiling)
	T_{sat} = 15℃, G = 100 kg/m^{2}s	37.8 (Single-phase)
		30.1 (Saturated flow boiling)
	T_{sat} = 10℃, G = 300 kg/m^{2}s	33.9 (Single-phase)
		28.3 (Saturated flow boiling)

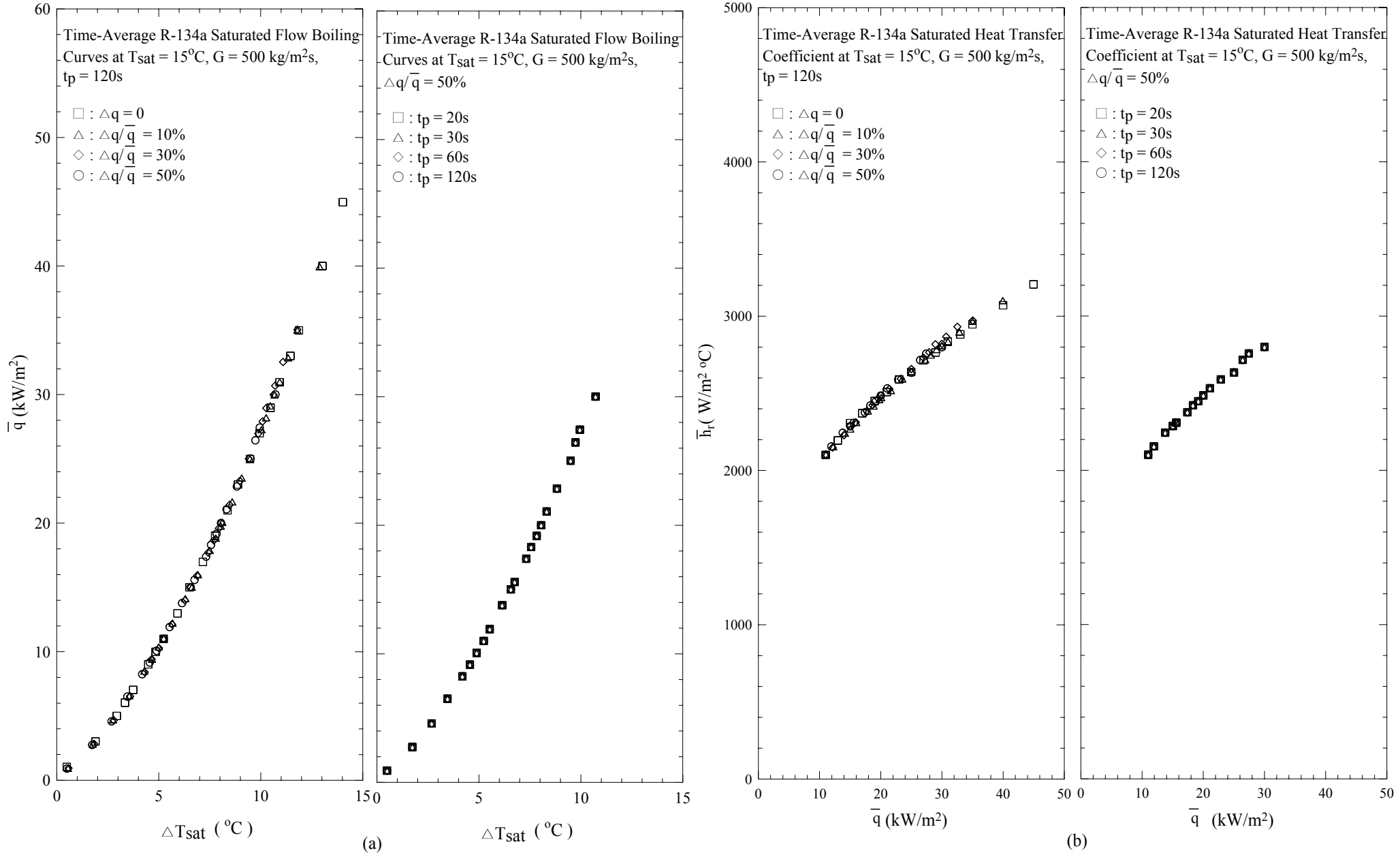


Fig. 8.1 Time-average R-134a saturated flow boiling curves (a) and saturated flow boiling heat transfer coefficients (b) for various $\Delta q/\overline{q}$ and t_p at $\delta = 2.0$ mm.

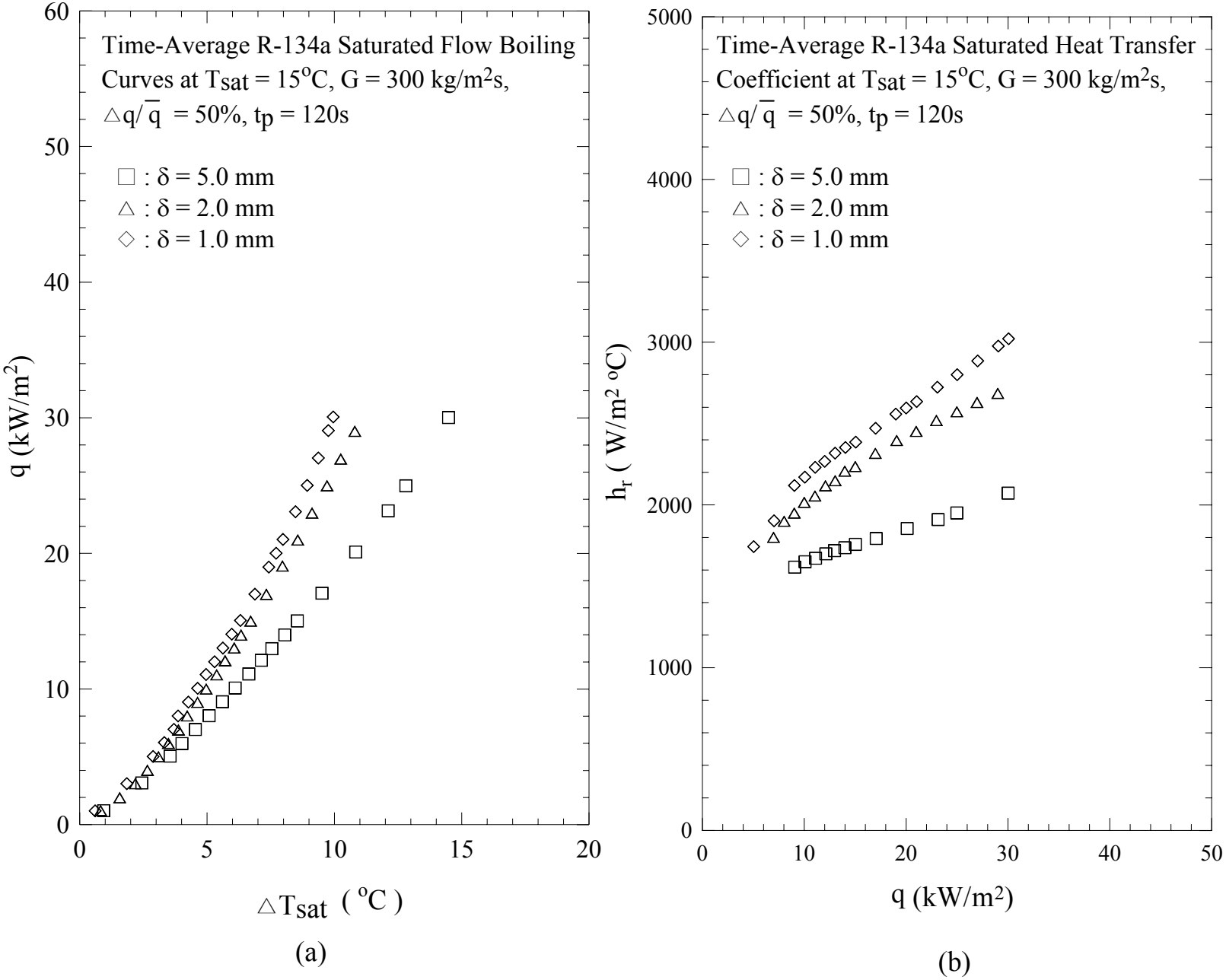


Fig. 8.2 Time-average R-134a flow boiling curves (a) and flow boiling heat transfer coefficients (b) for various gap sizes.

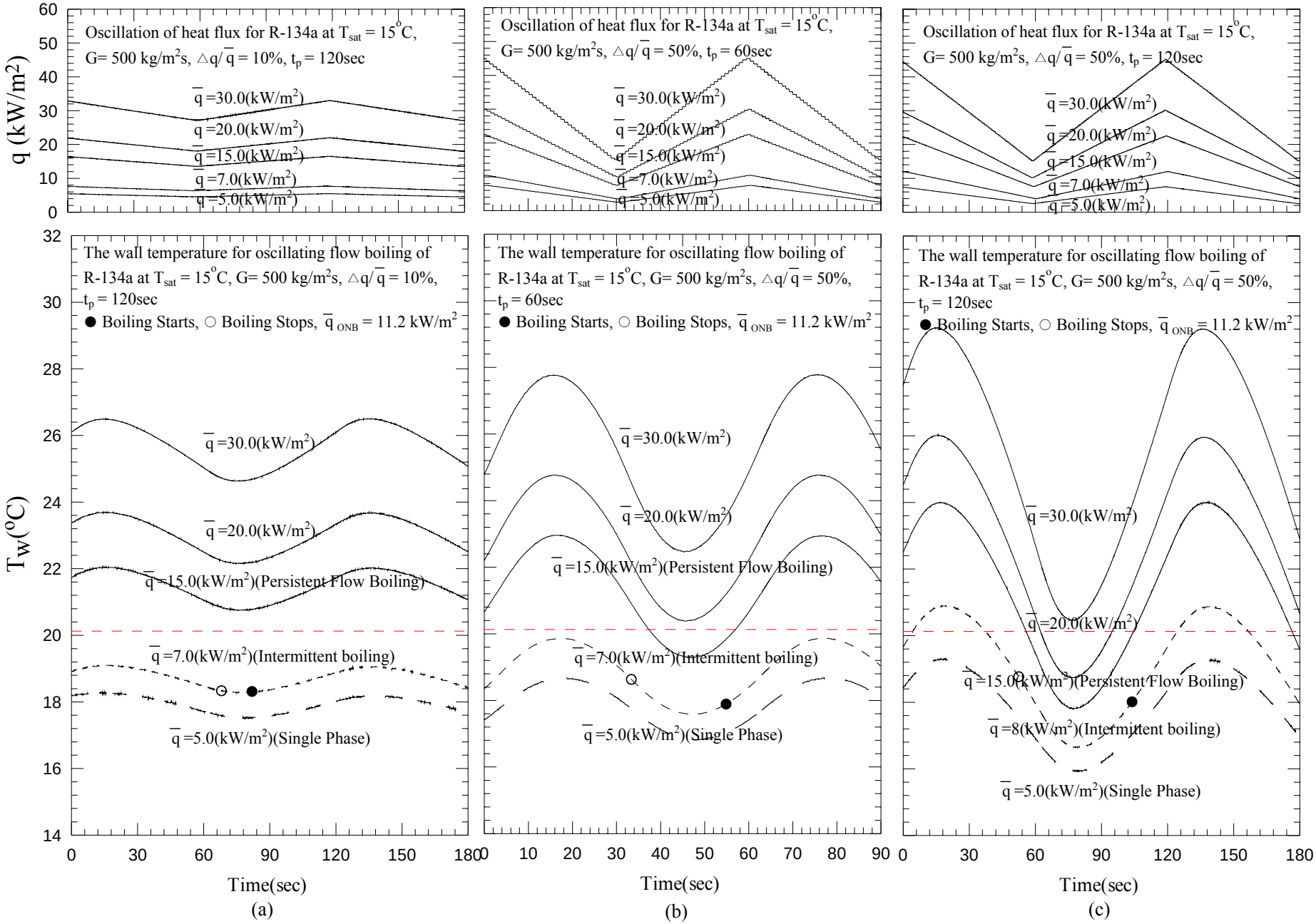


Fig. 8.3 Time variations of imposed heat flux and wall temperature at z = 80 mm for various $\bar{q}$, $\Delta q/\bar{q}$ and t_p at δ = 2.0 mm.

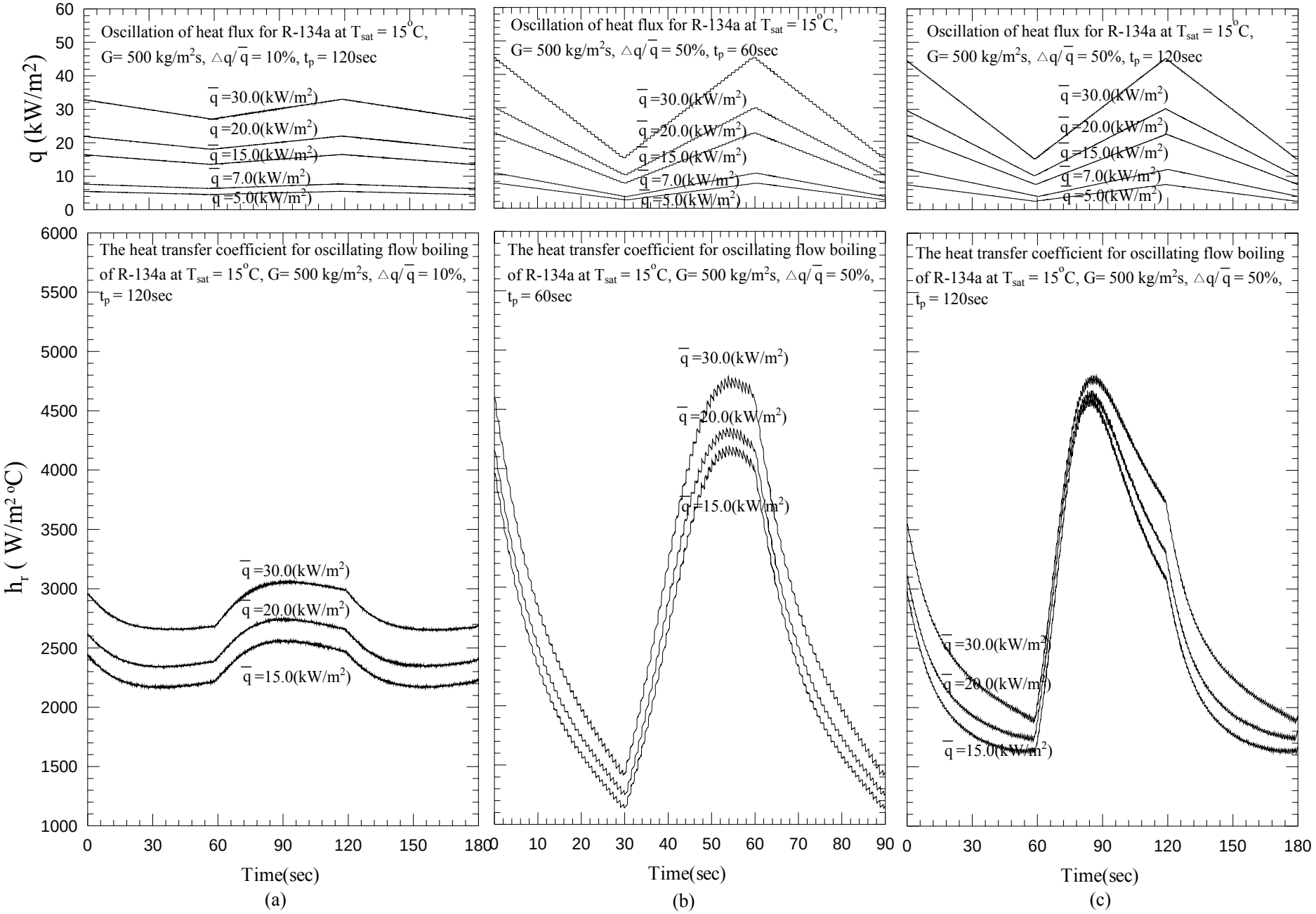


Fig. 8.4 Time variations of imposed heat flux and heat transfer coefficient at z = 80 mm in persistent boiling for various $\bar{q}$, $\Delta q/\bar{q}$ and t_p at δ = 2.0 mm.

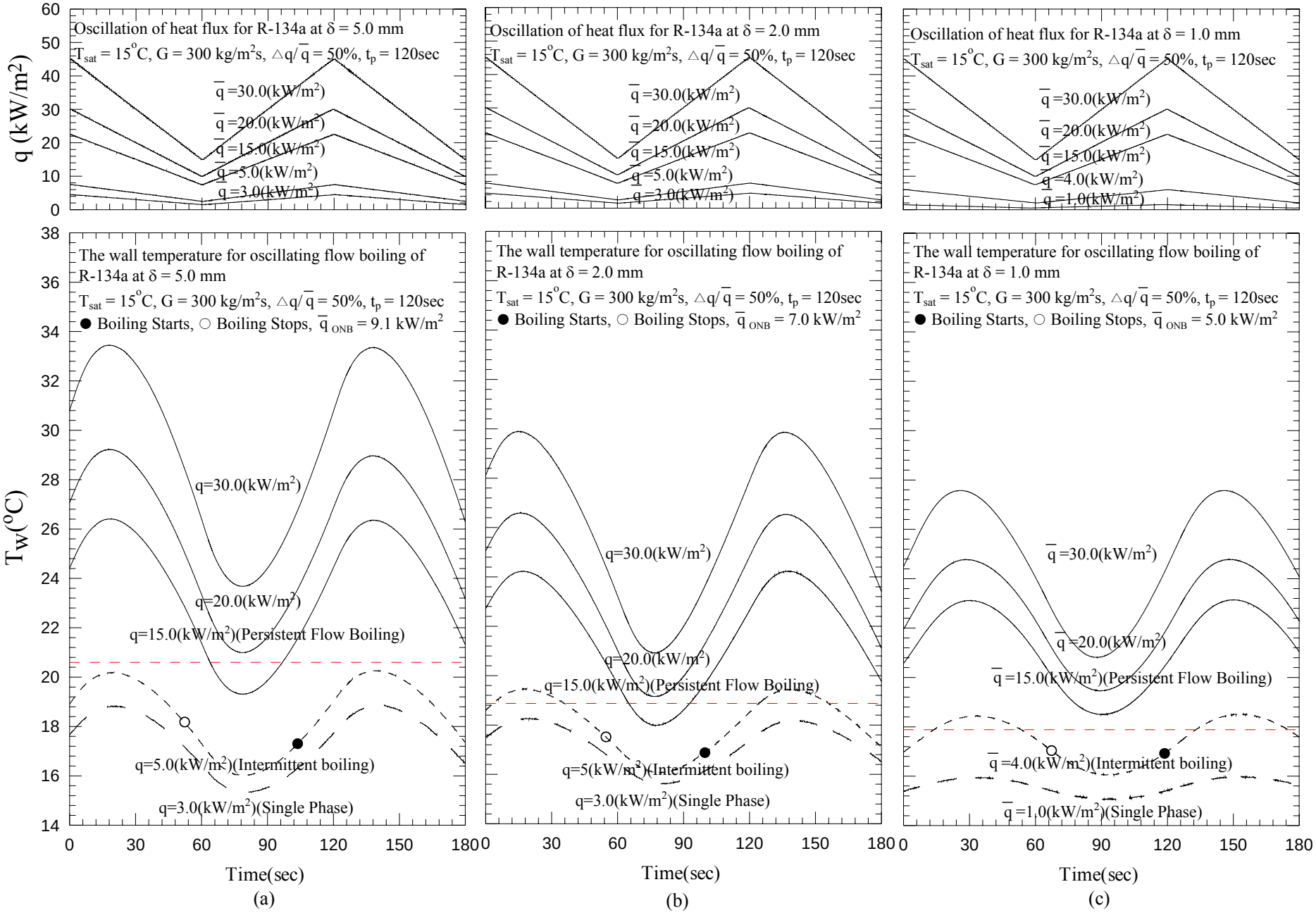


Fig. 8.5 Time variations of imposed mass flux, inlet pressure, and wall temperature at z = 80 mm for various gap sizes.

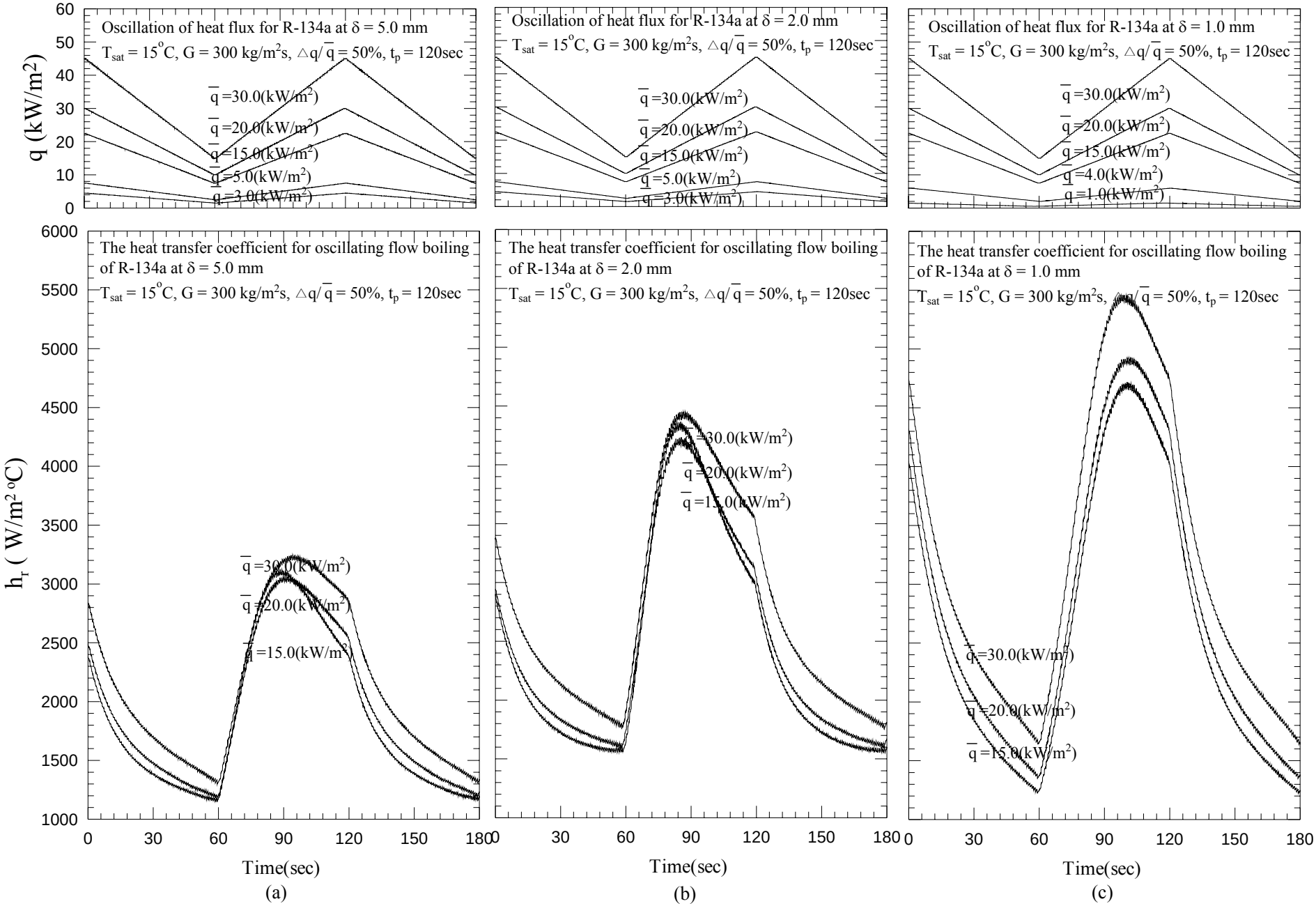


Fig. 8.6 Time variations of imposed mass flux, inlet pressure, and heat transfer coefficient at z = 80 mm in persistent boiling for various gap sizes.

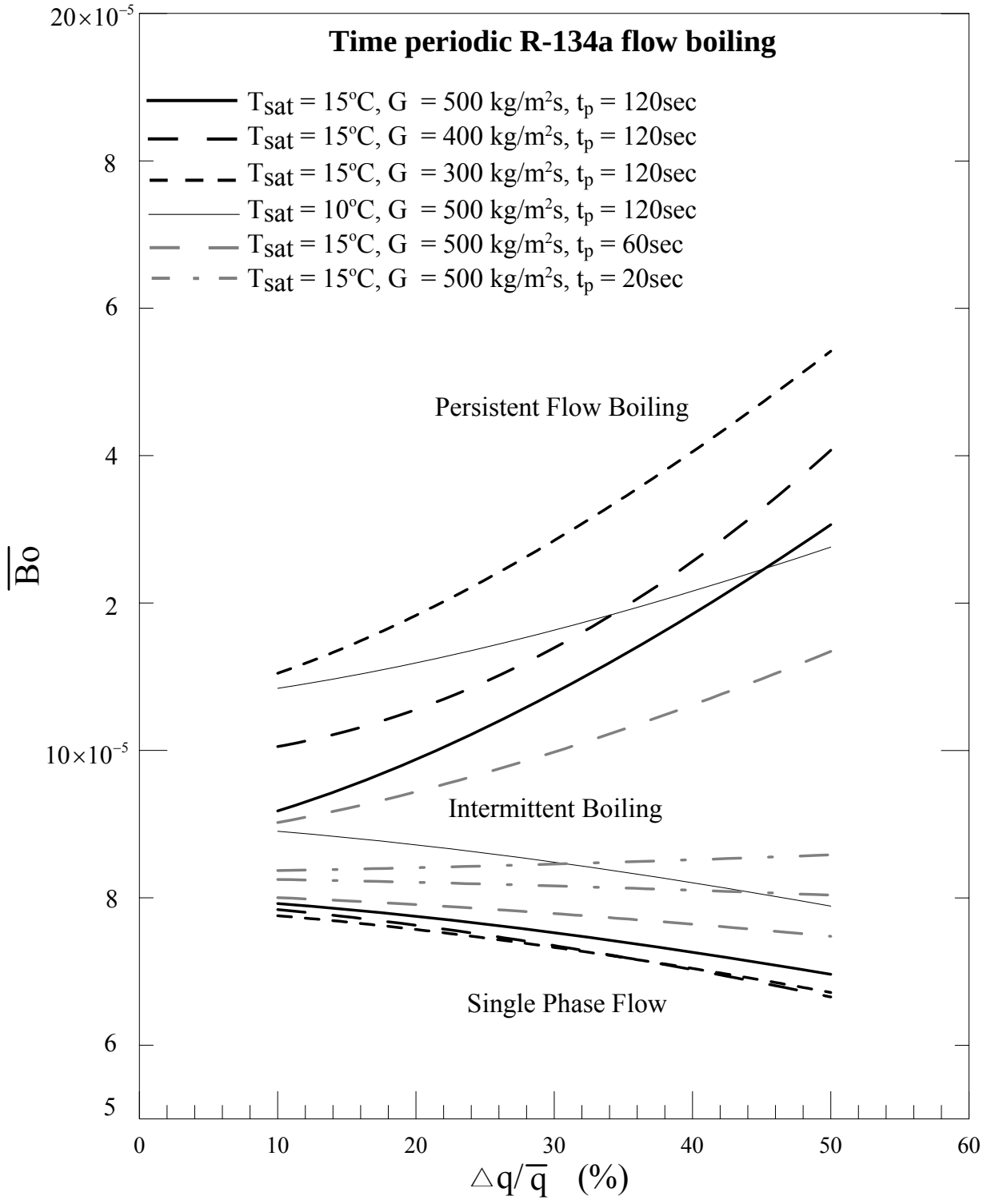


Fig. 8.7 Flow regime map for time periodic R-134a saturated flow boiling in annular duct at $\delta = 2.0$ mm.

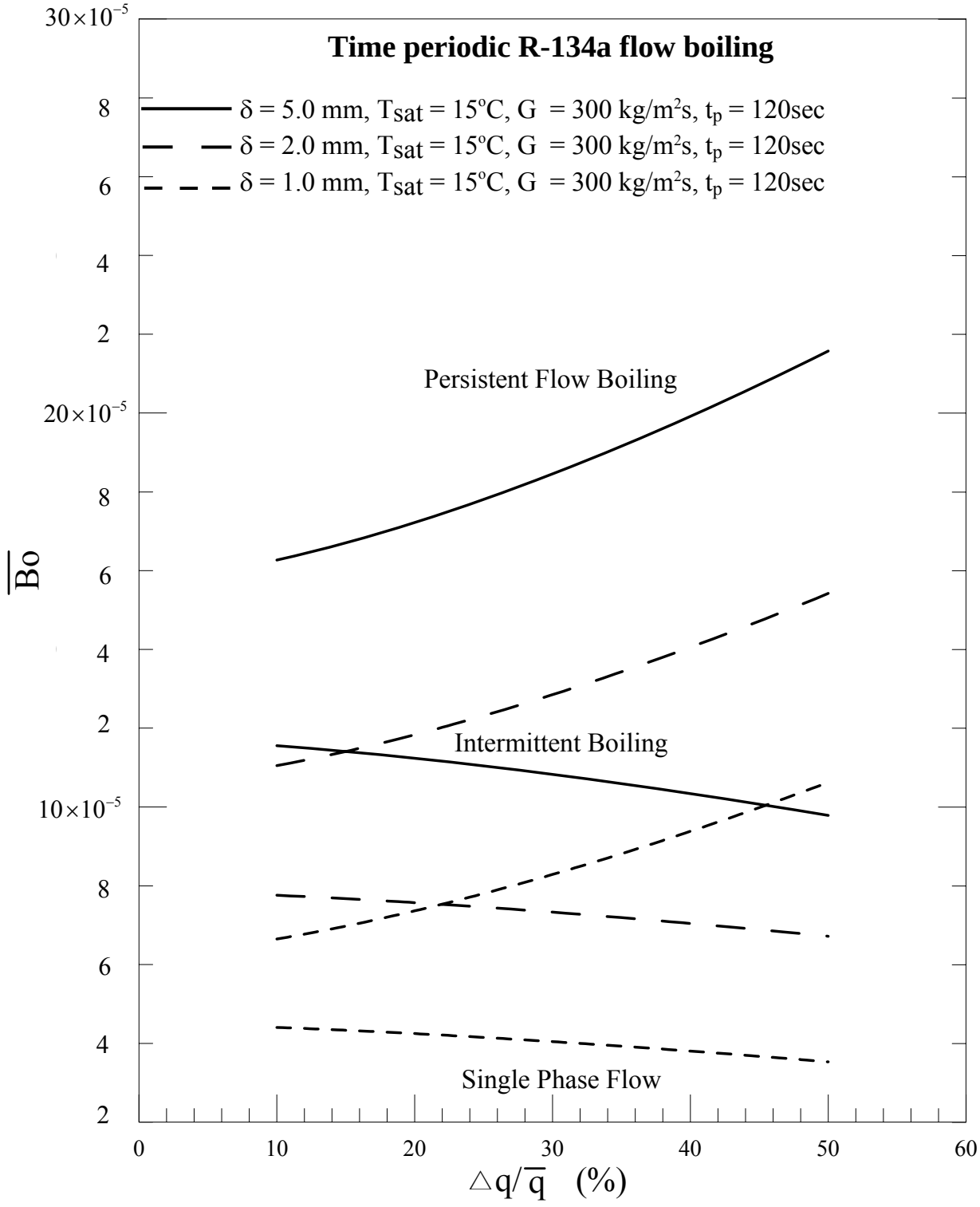


Fig. 8.8 Flow regime map of time periodic R-134a flow boiling in annular duct for various gap sizes.

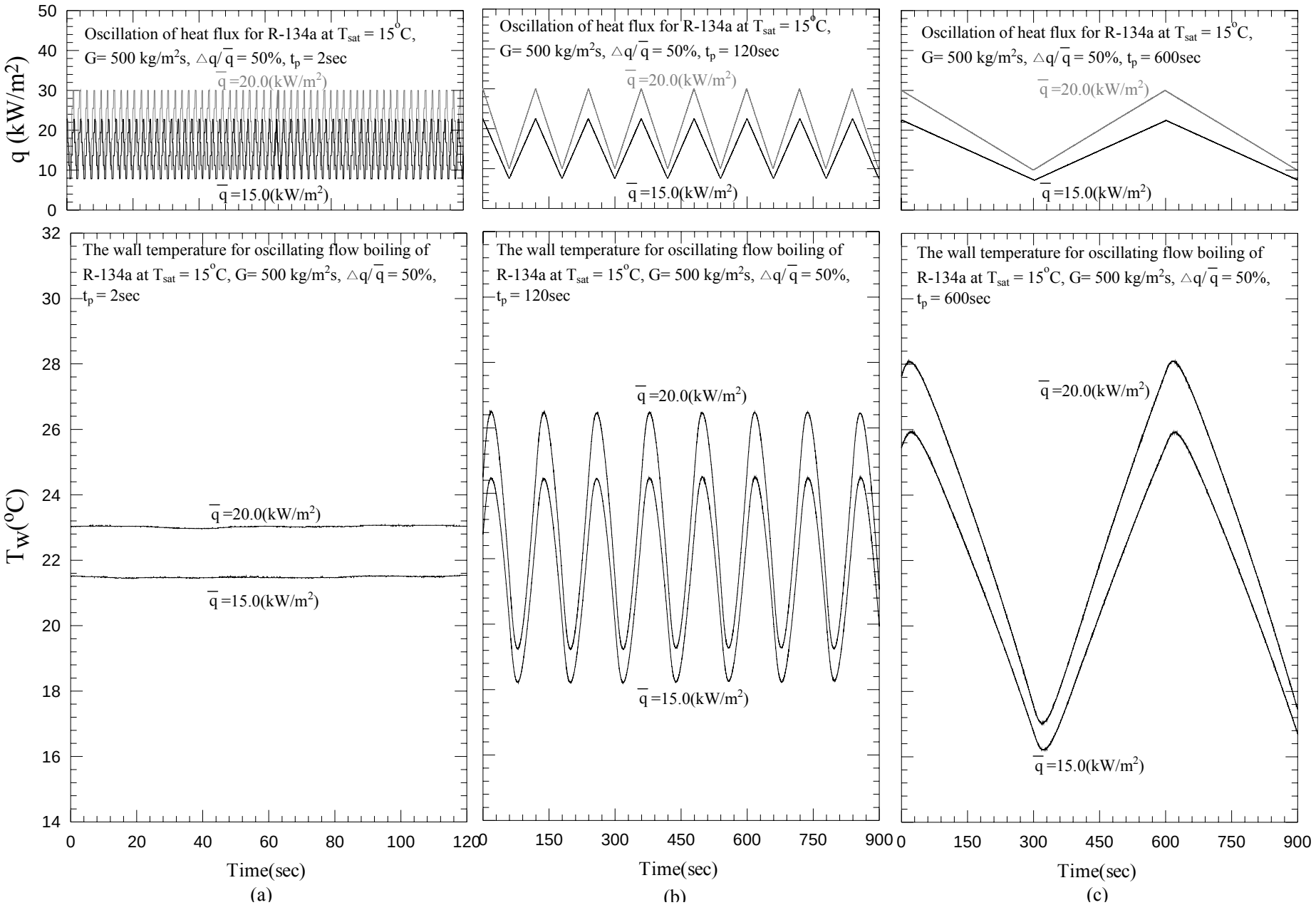


Fig. 8.9 Time variations of imposed heat flux and wall temperature at z = 80 mm for various t_p at δ = 2.0 mm.

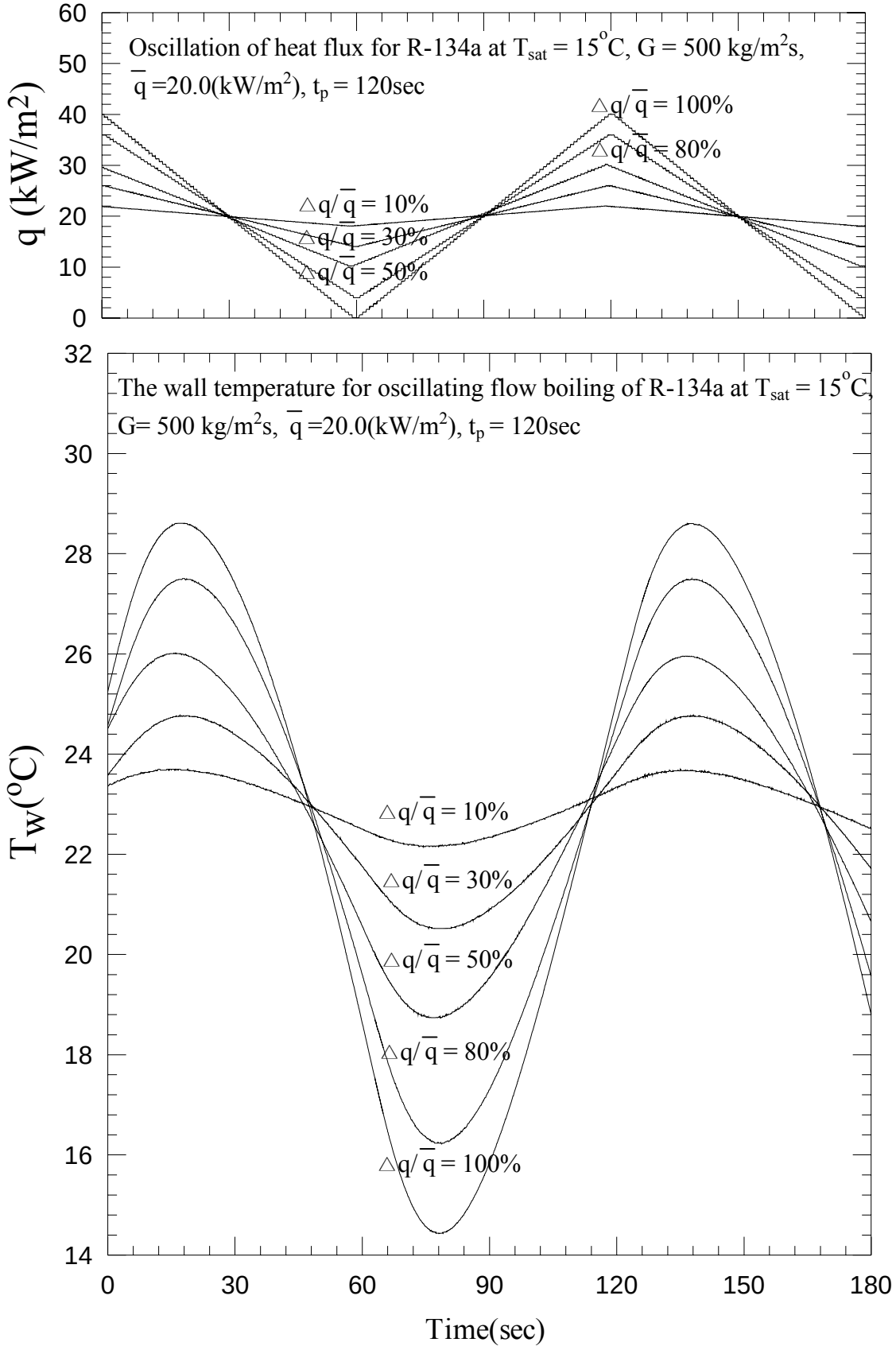


Fig. 8.10 Time variations of imposed heat flux and wall temperature at z = 80 mm for various $\Delta q/\bar{q}$ at δ = 2.0 mm.

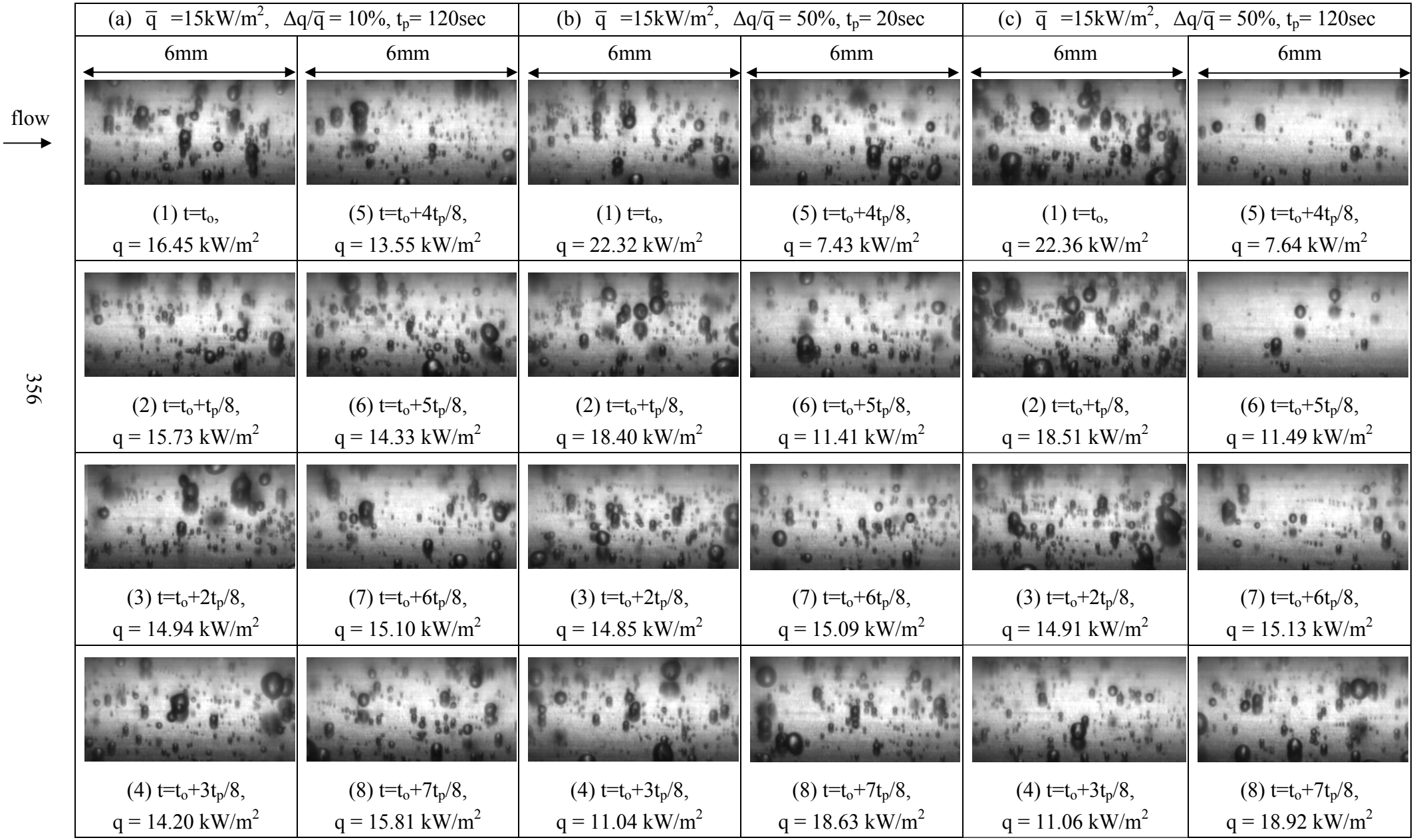


Fig. 8.11 Photos of bubbles in time periodic flow boiling of R-134a in a small region around the middle axial location at eight time instants in a typical periodic cycle at T_{sat} =15℃, G =500 kg/m^{2}s and $\bar{q}$ =15kW/m^2 for various $\Delta q/\bar{q}$ and t_p at δ = 2.0 mm.



Fig. 8.12 Photos of bubbles in time periodic flow boiling of R-134a in a small region around the middle axial location at eight time instants in a typical periodic cycle at T_{sat} =15℃, G =300 kg/m^{2}s, $\bar{q}$ =15kW/m^2, $\Delta q/\bar{q}$ = 50% and t_p= 120sec for various gap sizes.

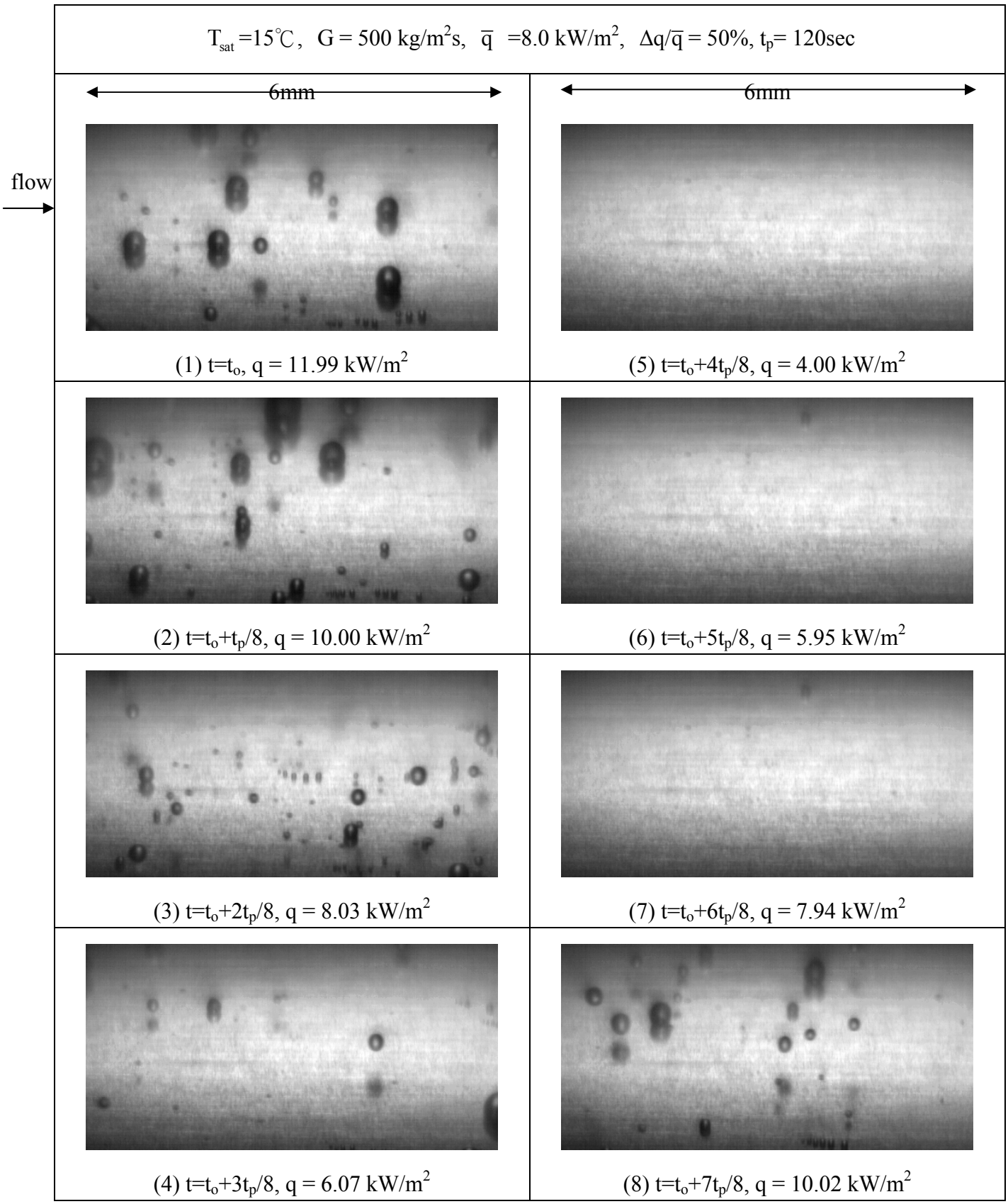


Fig. 8.13 Photos of bubbles in the time periodic intermittent flow boiling of R-134a in a small region around the middle axial location at eight time instants in a typical time periodic cycle for T_{sat} =15℃, G=500 kg/m^{2}s, $\bar{q}$ =8.0 kW/m^2, $\Delta q/\bar{q}$ = 50% and t_p= 120sec at δ = 2.0 mm.

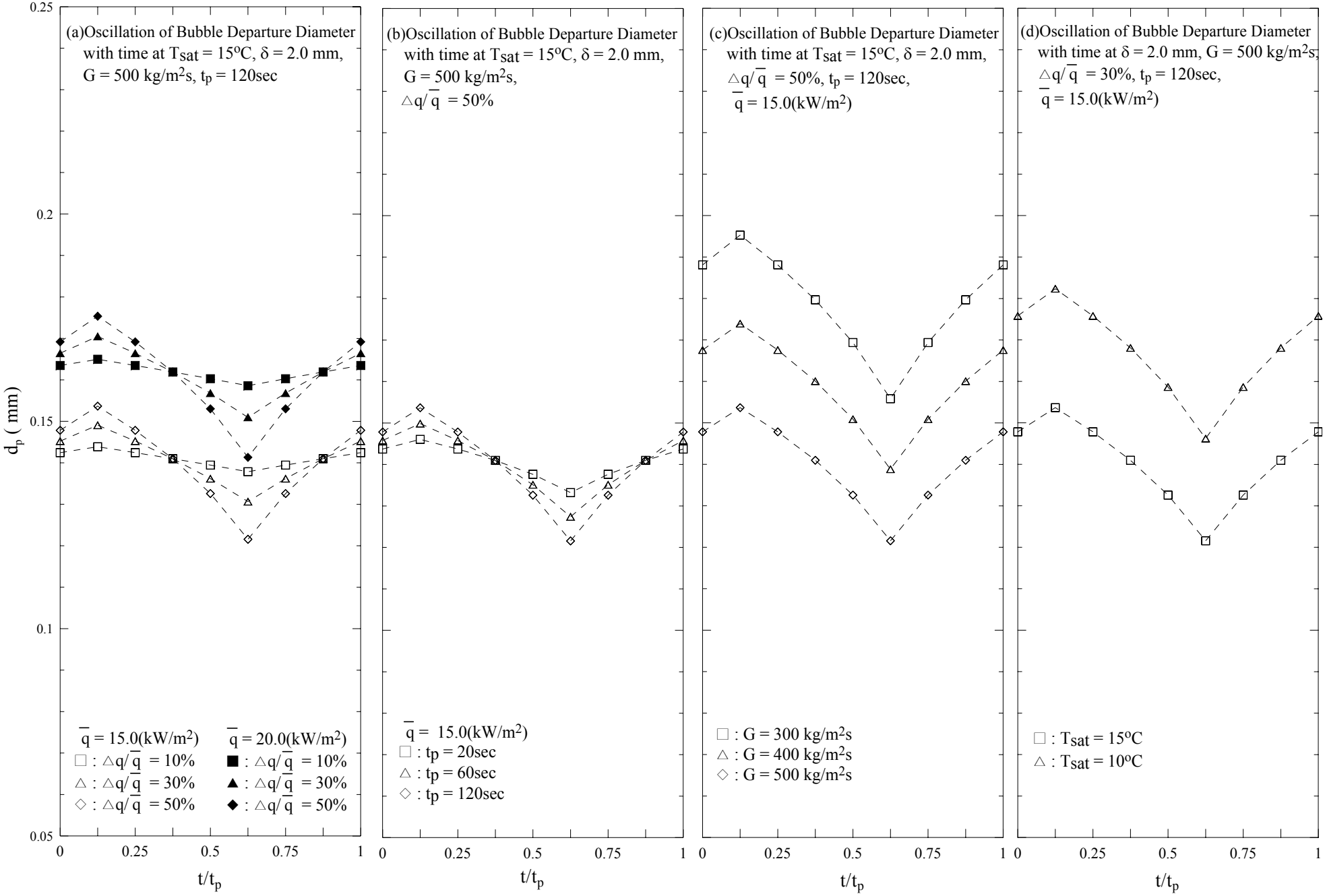


Fig.8.14 Mean bubble departure diameter variations with time in a typical periodic cycle for various $\Delta q/\bar{q}$ at q =15.0 & 20.0 kW/m^2(a), t_p(b), G(c), and T_{sat} (d) at G =500 kg/m^{2}s at δ = 2.0 mm.

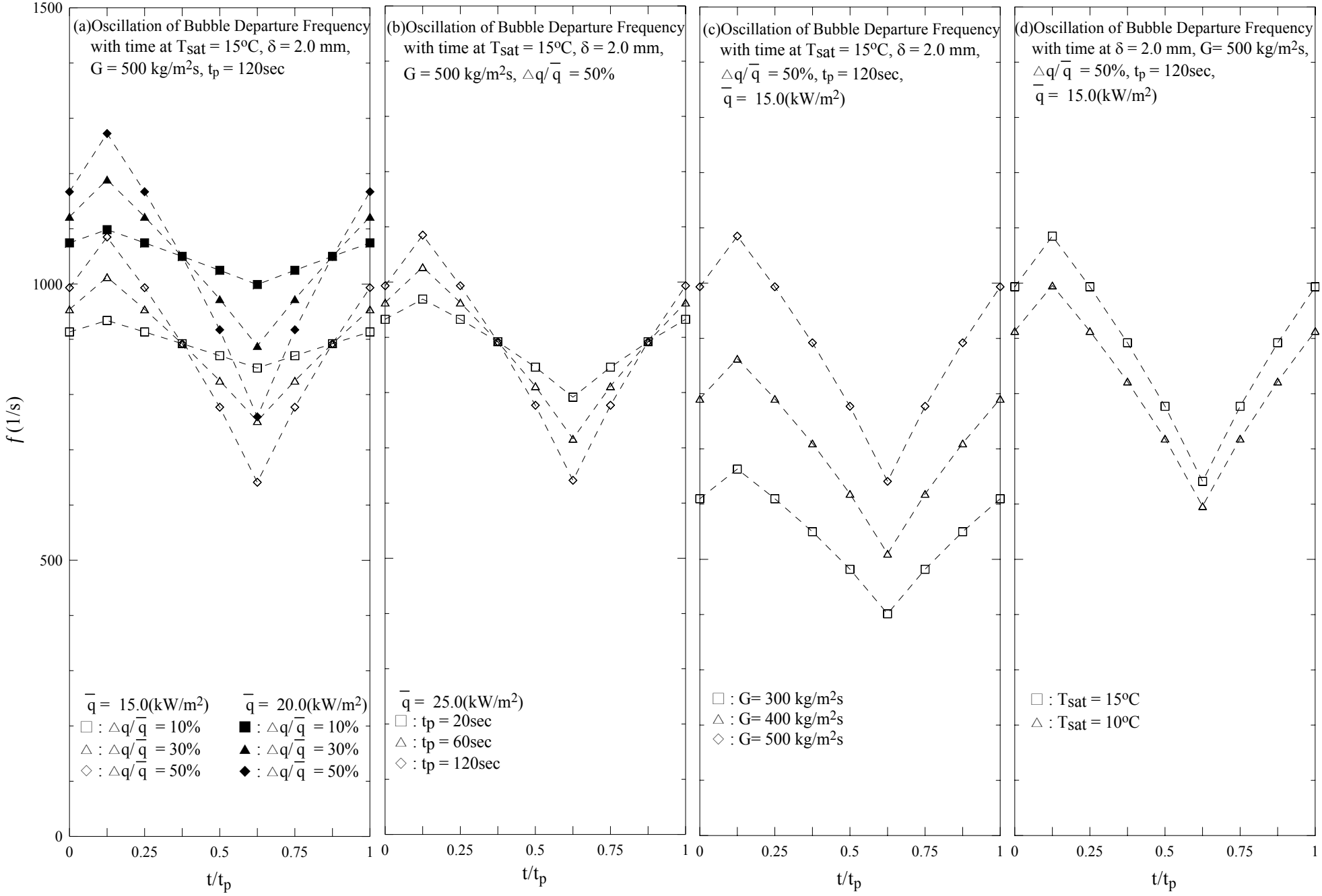


Fig.8.15 Mean bubble departure frequency variations with time in a typical periodic cycle for various $\Delta q/\bar{q}$ at q =15.0 & 20.0 kW/m^2(a), t_p(b), G(c), and T_{sat} (d) at G =500 kg/m^{2}s at δ = 2.0 mm.

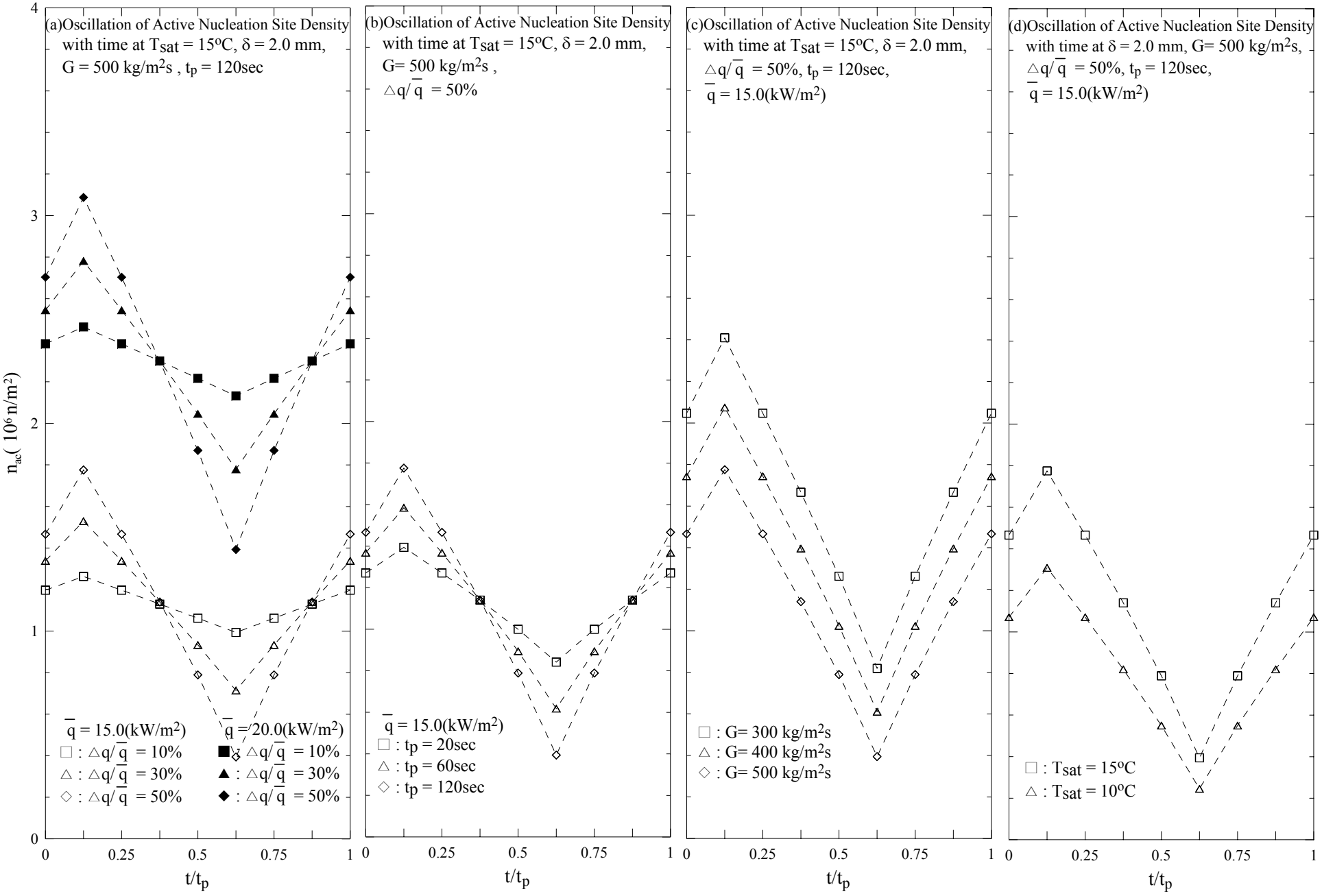


Fig.8.16 Mean active nucleation site density variations with time in a typical periodic cycle for various $\Delta q/\bar{q}$ at q =15.0 & 20.0 kW/m^2(a), t_p(b), G(c), and T_{sat} (d) at G =500 kg/m^{2}s at δ = 2.0 mm.

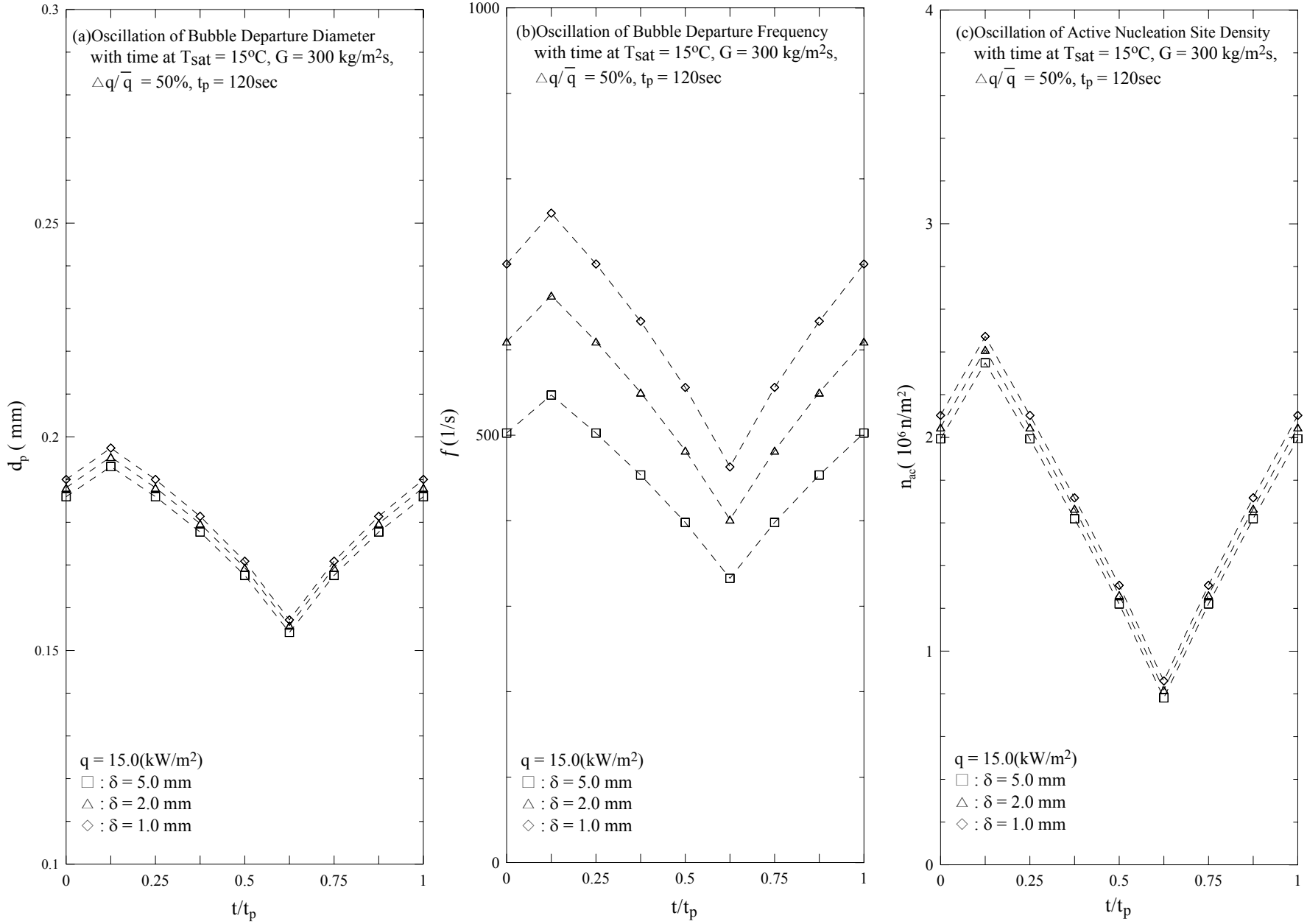


Fig. 8.17 Mean bubble departure diameter (a), bubble departure frequency (b), and active nucleation site density (c) variations with time in a typical periodic cycle at T_{sat} =15℃, G=300 kg/m^{2}s, $\bar{q}$ =15.0 kW/m^2, $\Delta q/\bar{q}$ = 50% and t_p= 120sec for various gap sizes.

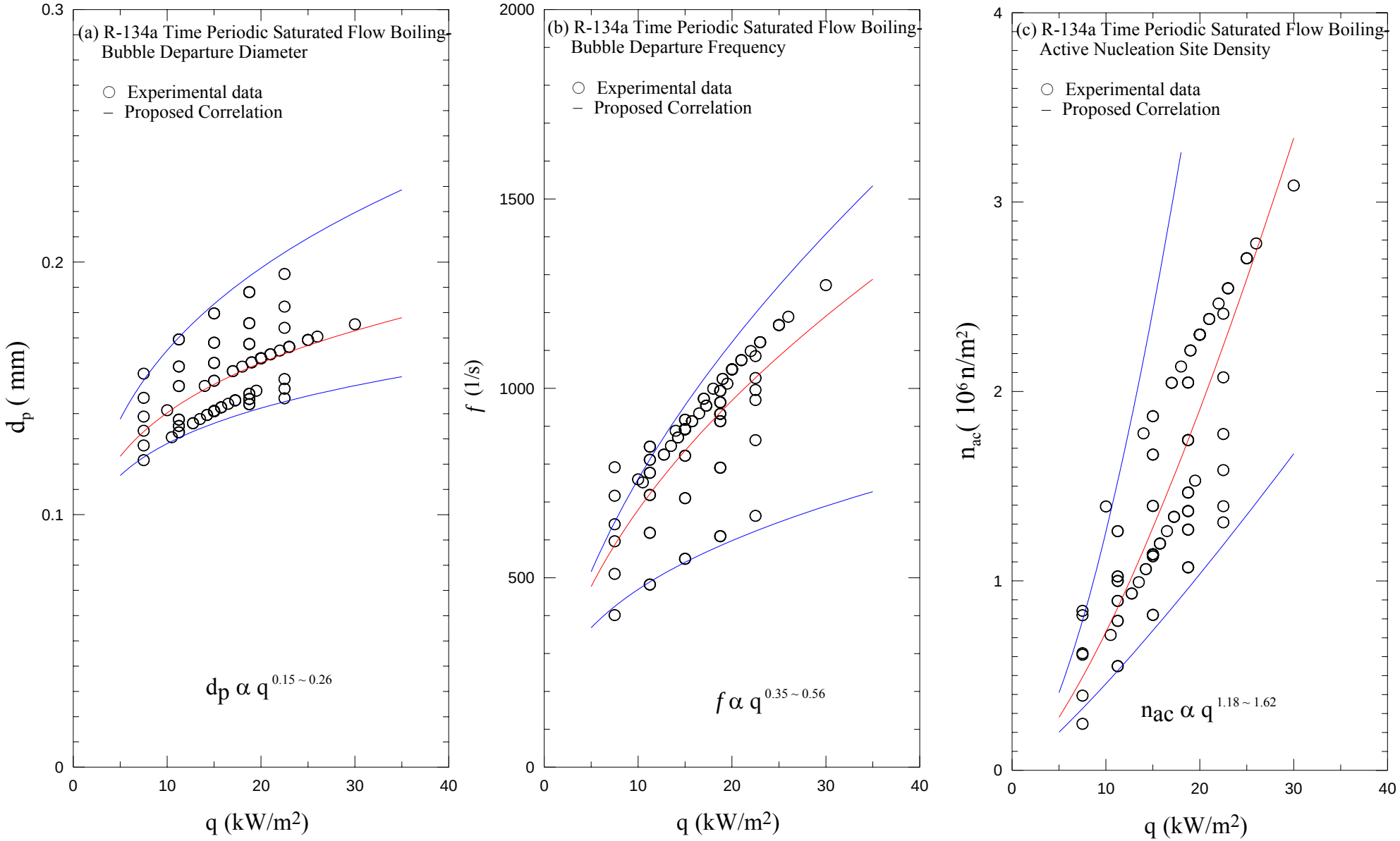


Fig. 8.18 Variations of bubble departure diameter (a), departure frequency (b), and active nucleation site (c) for time-periodic saturated flow boiling with heat flux for R-134a.

CHAPTER 9

TIME PERIODIC SATURATED FLOW BOILING OF R-410A IN A NARROW ANNULAR DUCT DUE TO HEAT FLUX OSCILLATION

The results obtained in the second part of the present study for the time periodic saturated flow boiling of R-410A in the duct due to the imposed heat flux oscillation are examined in this chapter. The present experiments are conducted for the refrigerant mass flux G varied from 300 to 500 kg/m^{2}s, mean imposed heat flux $\bar{q}$ from 0 to 45 kW/m^2, and the amplitude of the heat flux oscillation $\Delta q/\bar{q}$ fixed at 10, 30, 50% of $\bar{q}$ with the period of the heat flux oscillation t_p fixed at 20, 60 and 120 seconds. The refrigerant saturation temperature T_{sat} is set at 5, 10 and 15℃. The gap between the inner and outer pipes δ is fixed at 2.0 mm. Several time scales associated with the present saturated flow boiling over the heated inner pipe surface are given in Table 5.1. Specifically, there are four relevant time scales in the experiment. The conduction time scale t_1 is estimated by considering a copper slab of the characteristic length L_c (thickness) subject to a step heat input at one of its surface at certain time instant and t_1 is the duration for the other surface to begin to feel the heat input. According the thermal diffusion speed, $t_1 \approx L_c^2/\alpha_w$. The convection time scale t_2 can be estimated by the equation $t_2 = L/(G/\rho_1)$. The time scale for the bubble growth or departure t_3 is approximated by the empirical expression $t_3 = \frac{d_b}{2003\{\mu_1/(\rho_1 D_h)\}}$. Finally, the time constant of the present flow boiling on the heated copper duct surface t_c is obtained by measuring T_w subject to a step input in the imposed heat flux for both single-phase and boiling conditions. The results in Table 5.1 for various time constants for selected cases clearly indicate that the values of t_c associated with the single-phase liquid flow and flow boiling over the heated surface are much larger than the other time constants and dominate the time response of the duct wall to the heat flux oscillation. Besides, the time lag of the heated surface temperature behind the imposed heat flux oscillation is expected to be significant. In the following, attention will be mainly paid to examining the effects of the amplitude and period of the heat flux oscillation on the time periodic R-410A saturated flow boiling heat transfer performance. Note that for the

limiting case of $\Delta q/\bar{q} = 0\%$ we have saturated flow boiling of R-410A at constant refrigerant mass flow rate and imposed heat flux in the test section, which is designated as 〝stable flow boiling〞 here. The measured boiling heat transfer data are expressed in terms of the boiling curves and boiling heat transfer coefficients along with the time variations of the heated surface temperature. Besides, selected flow photos and data deduced from the images of the time periodic boiling processes are presented to show the temporal bubble characteristic in the boiling flow.

9.1 Time-average Saturated Flow Boiling Curves and Heat Transfer Coefficients

At first, Figs. 9.1 & 9.2 show the time-average boiling curves and heat transfer coefficients $\bar{h}_r$ measured at the middle axial location (z =80 mm) of the narrow annular duct for various amplitudes and periods of the heat flux oscillation. The results in Figs. 9.1 & 9.2 reveal that the amplitudes and periods of the refrigerant mass flux oscillation have negligible influences on the time-average boiling curves and heat transfer coefficients. In fact, they are nearly the same as that for the stable flow boiling.

9.2 Time Periodic Flow Boiling Heat Transfer Characteristics

The time periodic saturated flow boiling heat transfer characteristics of R-410A in the annular duct resulting from the imposed heat flux oscillation are illustrated by presenting the time variations of the space-average heated surface temperature T_w and boiling heat transfer coefficient h_r at the middle axial location in the saturated state for various G, T_{sat}, $\Delta q/\bar{q}$, t_p and q are shown in Figs. 9.3-9.20. For clarity, the measured data for the time variations of the actual imposed heat flux are also given here. The results manifest that when q oscillates periodically in time nearly like a triangular wave, significant temporal oscillations in T_w and h_r occur and they are also periodic in time and are at the same frequency as the heat flux. The results indicate that T_w and h_r oscillations get stronger for a higher amplitude and a longer period of the imposed heat flux oscillation, and T_w also oscillates stronger for a higher mean imposed heat flux. Note that single-phase forced convection prevails in the duct at a relatively low imposed heat flux. The data given in Figs. 9.3-9.20 further reveals that the T_w oscillation significantly lags the heat flux oscillation for

both single-phase and boiling flows. The time lag apparently results from the thermal inertia of the heated pipe wall. Note that for given G, T_{sat}, and $\Delta q/\bar{q}$ the duration of time lag relative to the oscillation period t_l/t_p is slightly longer at a lower time-average imposed heat flux and a shorter period of the imposed heat flux. Furthermore, the heat flux decreases with time in the first half of the periodic cycle for the single-phase convection, after the time lag the heating wall temperature is found to decrease with time. The opposite process occurs in the second half of the cycle. It is noted that at low mean imposed heat flux no bubble nucleates from the heating surface in the whole periodic cycle. Hence heat transfer in the flow results completely from the single-phase forced convection. As the mean imposed wall heat flux is raised gradually, the heating surface temperature increases correspondingly and the corresponding T_w oscillation amplitude can be significant. At a certain higher $\bar{q}$ bubbles start to nucleate from the heating surface at certain instant of time but bubble nucleation is not seen in the whole cycle. Thus, we have intermittent boiling in the flow in which nucleate boiling only exists in a partial duration of the periodic cycle. The time instants for the start and termination of the nucleate boiling are marked on the curves for T_w for the cases with the presence of the intermittent boiling. Moreover, for a much higher $\bar{q}$ nucleate boiling persists over the entire period of the cycle and we have persistent flow boiling in the duct. Note that after the time lag, T_w and h_r both decrease with time in the first half of the periodic cycle in which the imposed heat flux decreases with time for the single-phase flow, intermittent flow boiling and persistent flow boiling. The results in Figs. 9.10 and 9.11 also show that at a higher refrigerant saturated temperature, the amplitude of the T_w oscillation is larger in persistent flow boiling. This is because of the surface tension of R-410A is smaller at higher refrigerant saturated temperature, so more bubbles nucleate at the heating surface.

9.3 Intermittent Boiling

It is of interest to note in the visualization of the boiling flow over the heated inner pipe in the annular duct that over a certain intermediate range of the mean imposed heat flux the intermittent boiling appears, as already mentioned earlier. More specifically, in a typical periodic cycle of the imposed heat flux oscillation bubble nucleation in the heated annular duct disappears at a certain time instant after the heat flux decreases to a certain low level and the pipe wall temperature decreases to the level below that required for the

onset of nucleate boiling. Single-phase flow prevails in the duct. At a certain later time instant in the second half of the cycle in which the imposed heat flux increases and T_w rises to exceed the wall superheat required for the onset of nucleate boiling, bubble nucleation is seen on the heated surface and boiling appears. The above process of intermittent boiling is repeatedly seen on the heated surface. To be more clearer, we indicate the time instants at which boiling starts and stops in Figs. 9.3 – 9.11 for the cases with the presence of the intermittent boiling. Note that at a higher imposed heat flux the onset of boiling is earlier and the termination of boiling is later. A flow regime map to delineate the boundaries separating different flow boiling regimes in terms of the Boiling number versus the relative amplitude of the heat flux oscillation is given in Fig. 9.21. The results show that the intermittent boiling prevails over a significantly wider range of the boiling number for a higher amplitude of the imposed heat flux oscillation and a lower refrigerant mass flux. However, the effects of refrigerant saturated temperature are small. Based on the present data, the conditions leading to the appearance of the intermittent boiling can be empirically correlated as

$$\left(2.16\times10^{-7}+3.47\times10^{-9}\overline{\mathrm{Re}}^{0.5}\right)\le\overline{\mathrm{Bo}}^{1.2}\cdot\left(\Delta q/\bar{q}\right)^{1.2}\cdot\left(t_p/t_c\right)^{1.2}\le\left(2.21\times10^{-5}-4.12\times10^{-8}\overline{\mathrm{Re}}^{0.5}\right) \quad (9.1)$$

More than 97% of the present data falls within the above correlation.

9.4 Effect of Heat Flux Oscillation at Extremely Short and Long Periods

How the period of the heat flux oscillation affects the time periodic flow boiling is further investigated by comparing the data for relatively short and long t_p in Figs. 9.22 – 9.24. Now when the oscillatory period is set to be much shorter than the time constant t_c at 2.0 seconds (Fig. 9.22), the heated surface temperature stays at a nearly constant level even for the case with the oscillation amplitude Δq being 50% of the mean imposed heat flux. In fact, for this case the amplitude of T_w oscillation is smaller than 0.1℃ which is below the random thermal disturbances from the background and is close to that in the stable boiling. At this short t_p the heated copper duct is not able to quickly respond to the very rapid change in the imposed heat flux because of its heat capacity. This situation appears when the period of the imposed heat flux oscillation is significantly shorter than the dominated time constant of the flow boiling system.

On the other hand, when the oscillatory period is relatively long at 120 and 600

seconds, the data given in Figs. 9.23 & 9.24 manifest that the amplitude of the T_w oscillation is very large. Note that the T_w oscillation is slightly stronger for t_p raised from 120 to 600 seconds. The stronger T_w oscillation at a longer t_p can be attributed to the longer period of time for the thermal energy storing in and releasing from the wall of the heated inner pipe. This in turn causes the heat pipe wall to accumulate and release thermal energy over a longer period of time and hence results in a larger amplitude of the T_w oscillation.

9.5 Effect of Heat Flux Oscillation Amplitude

The effect of the amplitude of the heat flux oscillation on the time periodic flow boiling of R-410A is examined further, too. The results in Fig. 9.25 for three different amplitudes of the imposed heat flux oscillation with $\Delta q/\bar{q}$ = 10, 30 and 50% at t_p = 60 seconds show that the T_w oscillation is significantly stronger for a larger amplitude of the imposed heat flux oscillation. Note that the time lag in T_w oscillation increases substantially when the amplitude of the imposed heat flux oscillation is raised from 10% to 30%. But a further increase in the amplitude of the heat flux oscillation does not increase the time lag noticeably.

9.6 Time Periodic Bubble Characteristics in Saturated Flow Boiling

To elucidate the time periodic saturated flow boiling heat transfer characteristics resulting from the imposed heat flux oscillation, the data for the bubble characteristics of R-410A flow boiling obtained from the present flow visualization are examined in the following. The side views of the boiling flow in a small region around the middle axial location of the duct for various imposed heat fluxes are shown in Figs. 9.26-9.43 for selected cases for the time periodic saturated flow boiling. In these figures the symbol " $t=t_o$ " signifies the time instant at which the instantaneous heat flux is at the highest level and starts to decrease with time. The bubble behavior in the intermittent flow boiling for the cases with given intermediate imposed heat fluxes is manifested in Figs. 9.26-9.34. The results clearly indicates that initially in the beginning of the cycle the instantaneous heat flux decreases with time but is still well above $\bar{q}_{ONB}$, bubbles nucleation from the heated surface is clearly seen. Note that the number and size of the bubbles decrease noticeably with time in the first quarter of the periodic cycle for the continuing decrease of

the heat flux. Then the bubble nucleation gradually disappears and finally boiling stops at certain time instant slightly after $t_0+3t_p/8$ when the heat flux is slightly below $\bar{q}_{ONB}$ and bubble nucleation stops completely. The flow is in single-phase state. But after a certain time instant slightly after $t_0+6t_p/8$ at which the imposed heat flux is raised to a certain high level, T_w rises to exceed the wall superheat required for the onset of nucleate boiling so that bubble nucleation on the heated surface is seen and more bubbles nucleate on the heated surface as time increases. Two-phase boiling flow again dominates in the duct. We have to wait until about the end of the first quarter of the next cycle to see the bubble nucleation gradually disappears on the heated surface. The above processes repeat in each cycle. The precise instants of time at which the onset and termination of nucleate boiling vary with the flow condition.

Then, we illustrate here how the time periodic bubble characteristics are affected by the amplitude and period of the heat flux oscillation for the persistent boiling in Figs. 9.35-9.43. The results indicate that for given G, $\bar{q}$, $\Delta q/\bar{q}$ and t_p the departure bubbles get smaller in the duct in the first half of the cycle in which the heat flux decreases. The opposite processes take place in the second half of the cycle in which the heat flux increases with time. These changes of the bubble characteristics with the instantaneous heat flux become more significant for an increase in the amplitude of the heat flux oscillation, as shown from the results in the Figs. 9.35~9.37. Besides, the bubble coalescence occurs more frequently and more large bubbles appear in the duct for the cases with a longer period of the heat flux oscillation (Figs. 9.38&9.39). The results given in Figs. 9.42&9.43 indicate that for a higher refrigerant saturated temperature, more large bubbles appear in the duct. This is due to lower surface tension of R-410A at higher refrigerant saturated temperature.

To be more quantitative on the bubble characteristics in the time periodic flow boiling due to the heat flux oscillation, we estimate the bubble departure diameter and frequency and the number density of the active nucleation sites on the heating surface in a typical periodic cycle at the middle axial location for the persistent flow boiling. The results in Figs. 9.44 – 9.49 show the effects of the experimental parameters on d_p, f and n_{ac}. In these plots time 〝t = 0〞 denotes the instant of time the imposed heat flux is at the highest level and starts to decrease in a typical periodic cycle. The results in Figs. 9.44 and 9.45 indicate that as the imposed heat flux oscillates time periodically, the bubble departure diameter

also varies time periodically and to some degree like a triangular wave as the imposed heat flux oscillation. Note that the effect of the time lag on the T_w oscillation is clearly seen. More specifically, the size of the departing bubbles does not decrease immediately with time in the first half of the periodic cycle in which the heat flux decreases with time. In fact, the bubble size increases in the initial transient for $t < t_l$ and then for $t > t_l$ the bubble departure diameter decreases. While in the second half of the cycle an opposite process is noted when heat flux increases with time. The results in Fig. 9.44(a) show that at the larger amplitude of the heat flux oscillation and mean imposed head flux the time variation of bubble departure diameter is somewhat stronger. Moreover, the results in Fig. 9.44(b) indicate that to some degree the bubble departure diameter varies stronger with time for a longer period of the heat flux oscillation. Furthermore, the results in Figs. 9.45(a) and (b) show that increases in the refrigerant mass flux and saturated temperature cause the departing bubbles to become smaller but do not change the wave form of the d_p variation with time.

How the temporal variation of the bubble departure frequency is affected by the heat flux oscillation is shown in Figs. 9.46 and 9.47. Note that the bubble frequency also varies like a triangular wave. At first, for $t < t_l$ the bubble departure frequency increases with time. Then, for an oscillation heat flux after the time lag for $t > t_l$ the bubbles depart from the heated surface at a decreasing rate in the first half of the periodic cycle in which the heat flux decreases with time (Fig. 9.46(a)). Apparently, in the second half of the cycle in which the heat flux increases the opposite process takes place. Moreover, the results in Fig. 9.46(a) indicate that at the larger amplitude of the heat flux oscillation and mean imposed heat flux the bubble departure frequency exhibits a stronger variation with time. Then, the results in Fig. 9.46(b) indicate that the bubble departure frequency oscillates in a larger amplitude at a longer period of the heat flux oscillation. Finally, at higher G and T_{sat} the bubble departure frequency is higher (Figs. 9.47(a) and (b)).

The data given in Figs 9.48 and 9.49 show the time variations of the associated number density of the active nucleation sites on the heating surface affected by the heat flux oscillation. The results clearly indicate that in the time periodic flow boiling the active nucleation site density also varies like a triangular wave. Besides, n_{ac} decreases substantially with time after the time lag for $t > t_l$ in the first half of the periodic cycle in which the heat flux decreases with time. The reverse process appears in the second half of

the cycle in which the heat flux rises. At higher amplitude of the heat flux oscillation and mean imposed heat flux the temporal variation of n_{ac} is also stronger (Fig. 9.48(a)). Moreover, for a longer period of the heat flux oscillation the time variation of n_{ac} is also stronger (Fig. 9.48(b)). Finally, n_{ac} is significantly higher at a lower G and higher T_{sat} (Figs. 9.49(a) and (b)).

It's worth mentioning that the time instants at which d_p, f and n_{ac} attain their maximums and minimums are not exactly at the instants the imposed heat flux is at its highest and lowest levels respectively at t = 0 and t = t_p/2. This is a direct consequence of the significant time lag in the time response of the heated surface temperature in the present time periodic flow boiling subject to the imposed heat flux oscillation.

Based on the data in Figs. 9.44 – 9.49, in the persistent boiling at a high q the dependence of the quantitative bubble characteristics on the R-410A heat flux oscillation can be approximately expressed as $d_p \alpha q^a$, $f \alpha q^b$, and $n_{ac} \alpha q^c$ when the time lag in the T_w oscillation is neglected. Here the exponents a, b and c range respectively from 0.02 to 0.13, 0.36 to 0.64 and 0.77 to 1.18, as shown in Fig. 5.50. Note that the latent heat transfer resulting from bubble nucleation in the persistent boiling q_b is proportional to d_p^3, f and n_{ac}, as discussed in the previous study [8]. Thus, $q_b \alpha q^d$, here d varies from 1.19 to 2.21. This result clearly indicates that flow boiling heat transfer gets better at increasing heat flux since q_b prevails in the boiling heat transfer. Besides, the dominant effect of the heat flux oscillation on the boiling heat transfer comes from the very strong influence of the heat flux on the active nucleation site density.

Table 9.1 Time scales for transient R-410A saturated flow boiling (δ=2mm)

Time scales		(sec)
Conduction time scale $t_1=L_c^2/\alpha_w$		1.247×10^{-11}
Convection time scale $t_2=L/(G/\rho_1)$	T_{sat} =10°C ,G = 300kw/m^{2}s	0.6016
	T_{sat} =10°C ,G = 400kw/m^{2}s	0.4512
	T_{sat} =10°C ,G = 500kw/m^{2}s	0.3610
	T_{sat} =15°C ,G = 400kw/m^{2}s	0.4436
Time scale of saturated flow boiling $t_3 = \frac{d_p}{2000(\mu_1/(\rho_1 D_h))}$		0.00109
Time constant $t_4 = t_c$	T_{sat} =10°C ,G = 300kw/m^{2}s	30 (Single-phase)
		24.4 (Saturated flow boiling)
	T_{sat} =10°C ,G = 400kw/m^{2}s	29.4 (Single-phase)
		23.5 (Saturated flow boiling)
	T_{sat} =10°C ,G = 500kw/m^{2}s	28.5(Single-phase)
		22.7(Saturated flow boiling)
	T_{sat} =15°C ,G = 400kw/m^{2}s	27.9 (Single-phase)
		23.4(Saturated flow boiling)

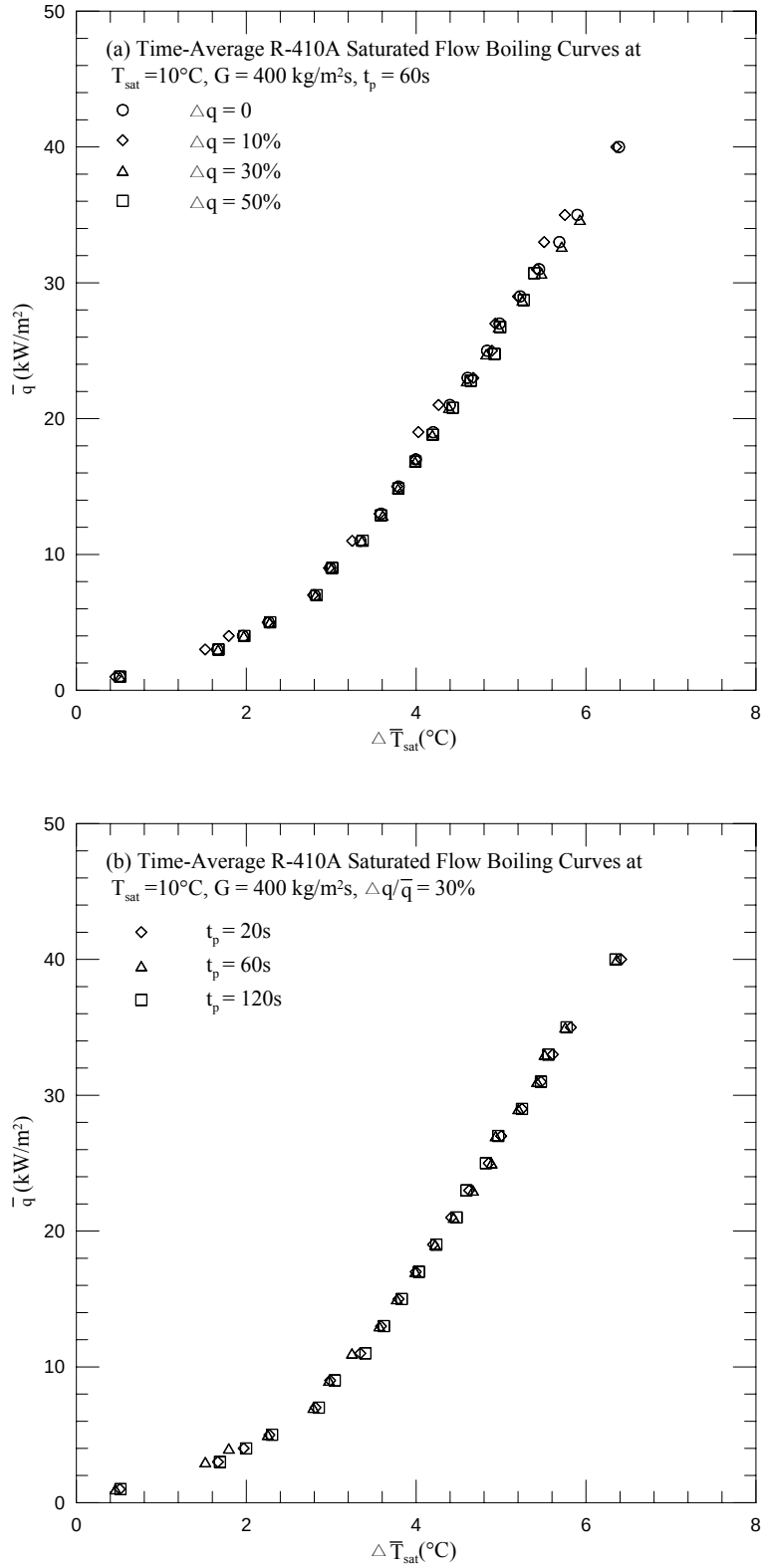


Fig. 9.1 Time-average flow boiling curves for R-410A for (a) various amplitudes of imposed heat flux oscillation at T_{sat} = 10℃, δ =2.0 mm, G=400kg/m^2 and t_p = 60 sec. and (b) various periods of heat flux oscillation at T_{sat} = 10℃, δ = 2.0 mm, G=400kg/m^2 and $\Delta q/\overline{q}$=30%.

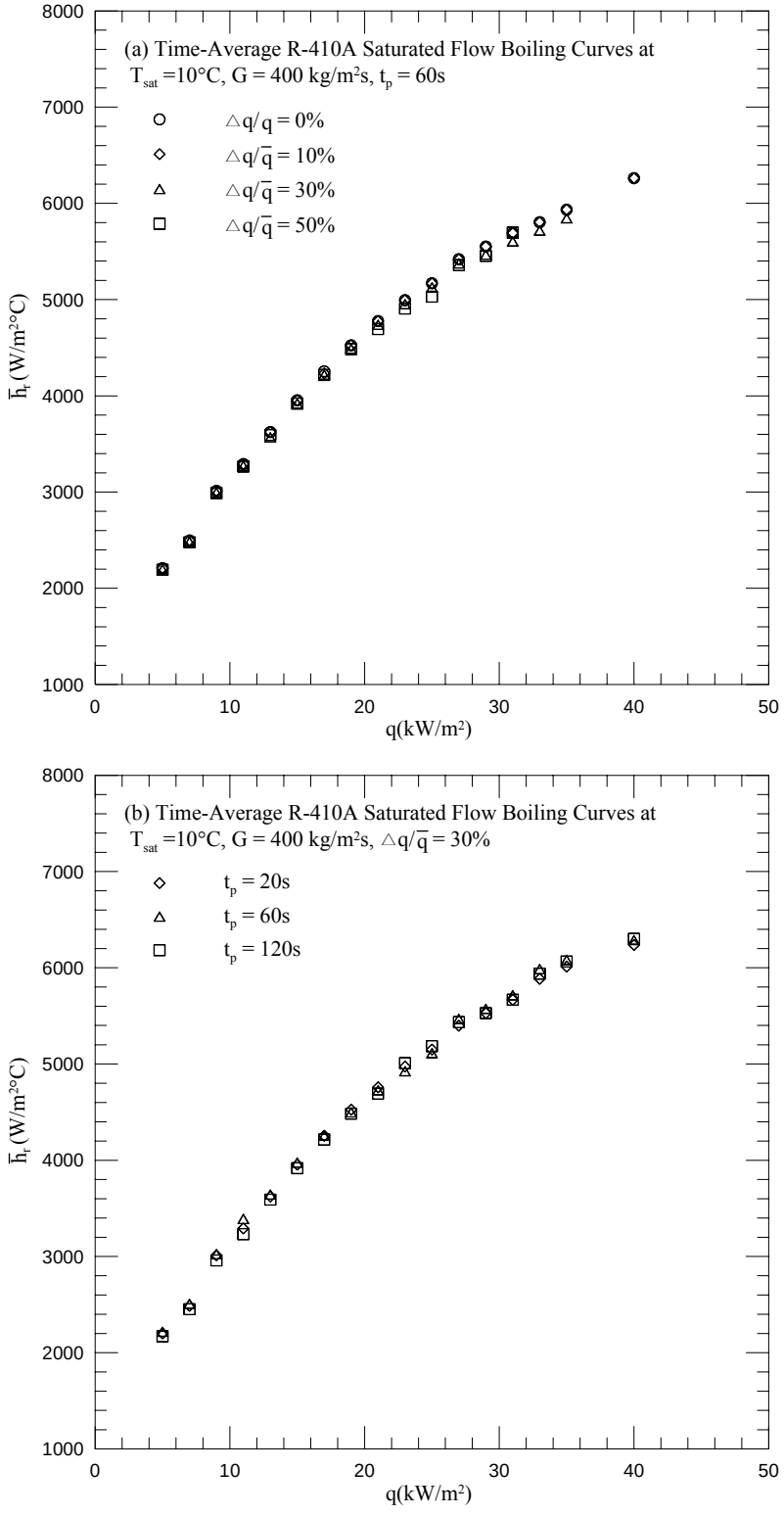


Fig. 9.2 Time-average flow boiling heat transfer coefficients for R-410A for (a) various amplitudes of imposed heat flux oscillation at T_{sat} = 10℃, δ =2.0 mm, G=400kg/m^2 and t_p = 60 sec. and (b) various periods of heat flux oscillation at T_{sat} = 10℃, δ = 2.0 mm, G=400kg/m^2 and $\Delta q/\bar{q}$=30%.

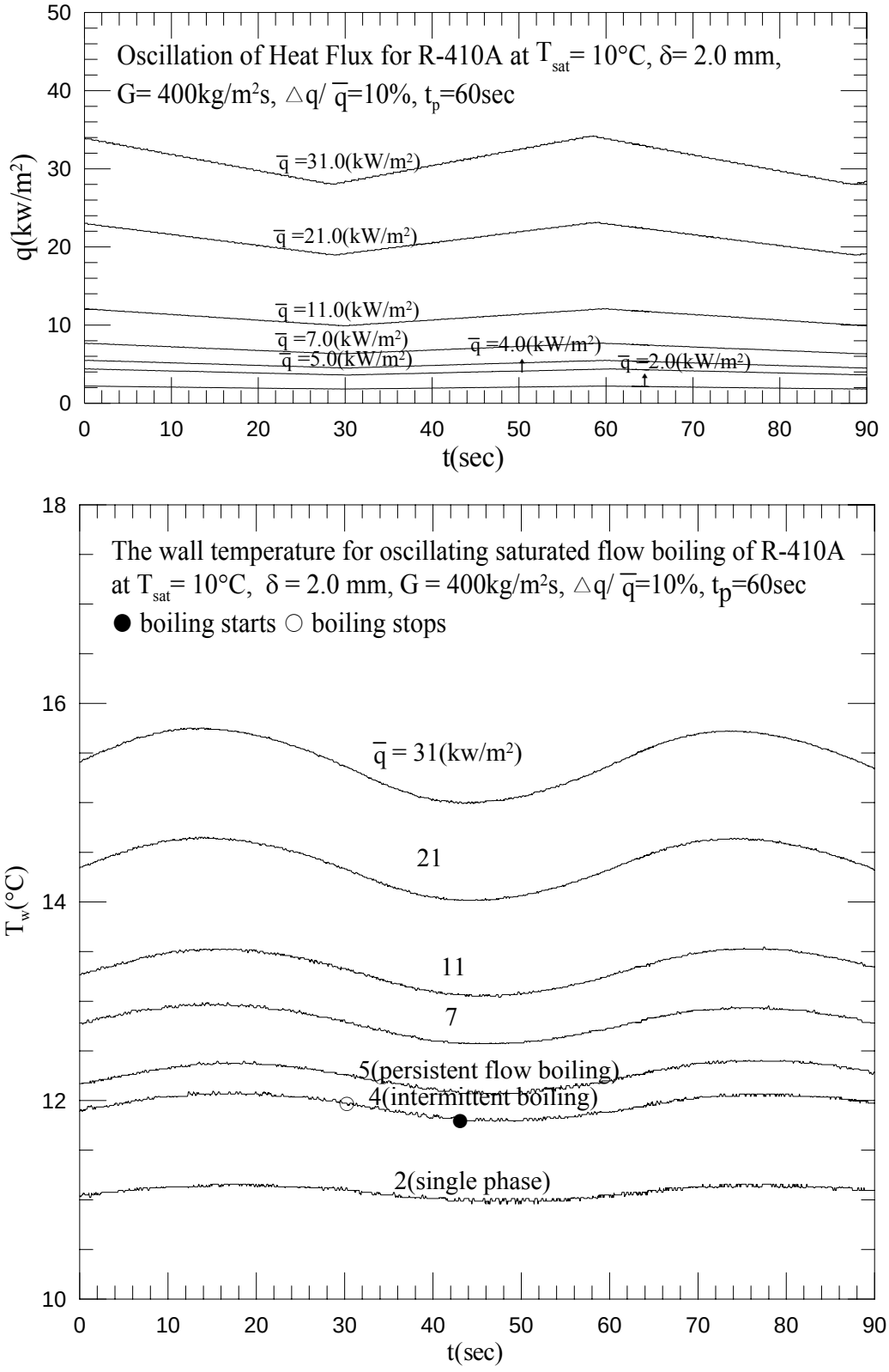


Fig. 9.3 Time variations of imposed heat flux and measured wall temperature in time periodic saturated flow boiling of R-410A at T_{sat} = 10℃, δ = 2.0mm, t_p = 60 sec and G =400kg/m²s with $\Delta q/\bar{q} = 10\%$.

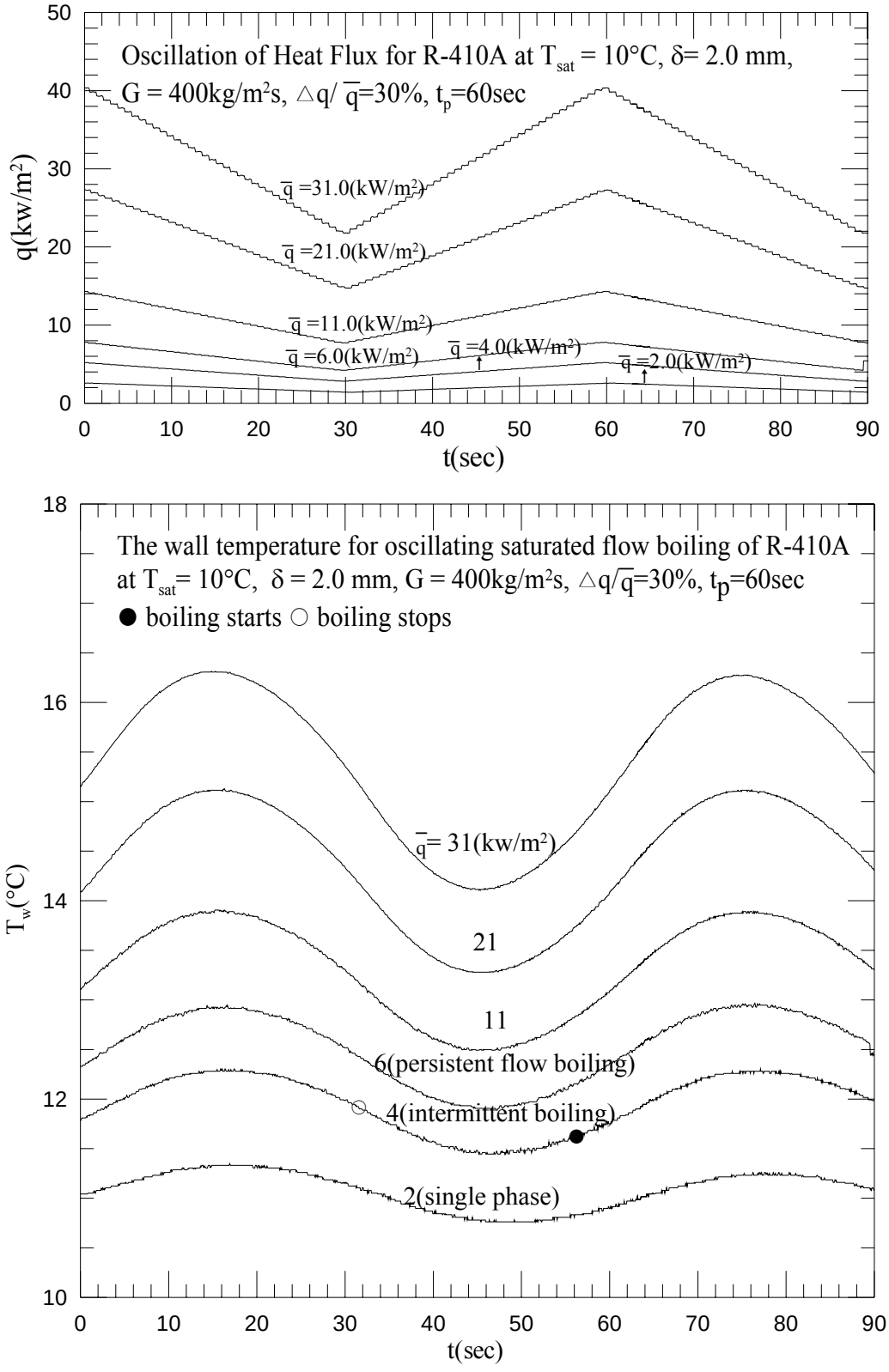


Fig. 9.4 Time variations of imposed heat flux and measured wall temperature in time periodic saturated flow boiling of R-410A at T_{sat} = 10℃, δ = 2.0mm, t_p = 60 sec and G =400kg/m²s with $\Delta q/\bar{q} = 30\%$.

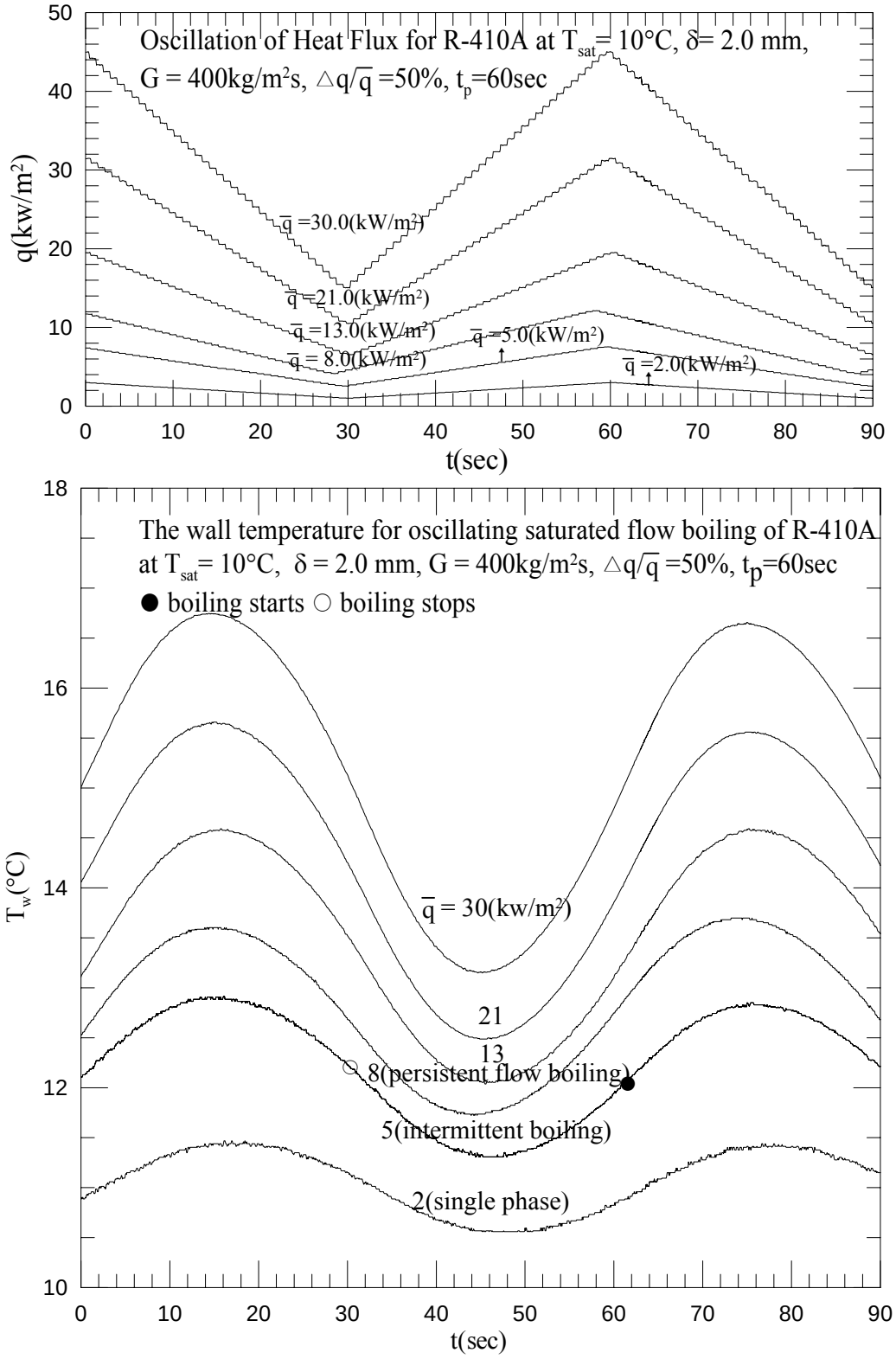


Fig. 9.5 Time variations of imposed heat flux and measured wall temperature in time periodic saturated flow boiling of R-410A at T_{sat} = 10℃, δ = 2.0mm, t_p = 60 sec and G = 400kg/m²s with $\Delta q/\bar{q} = 50\%$.

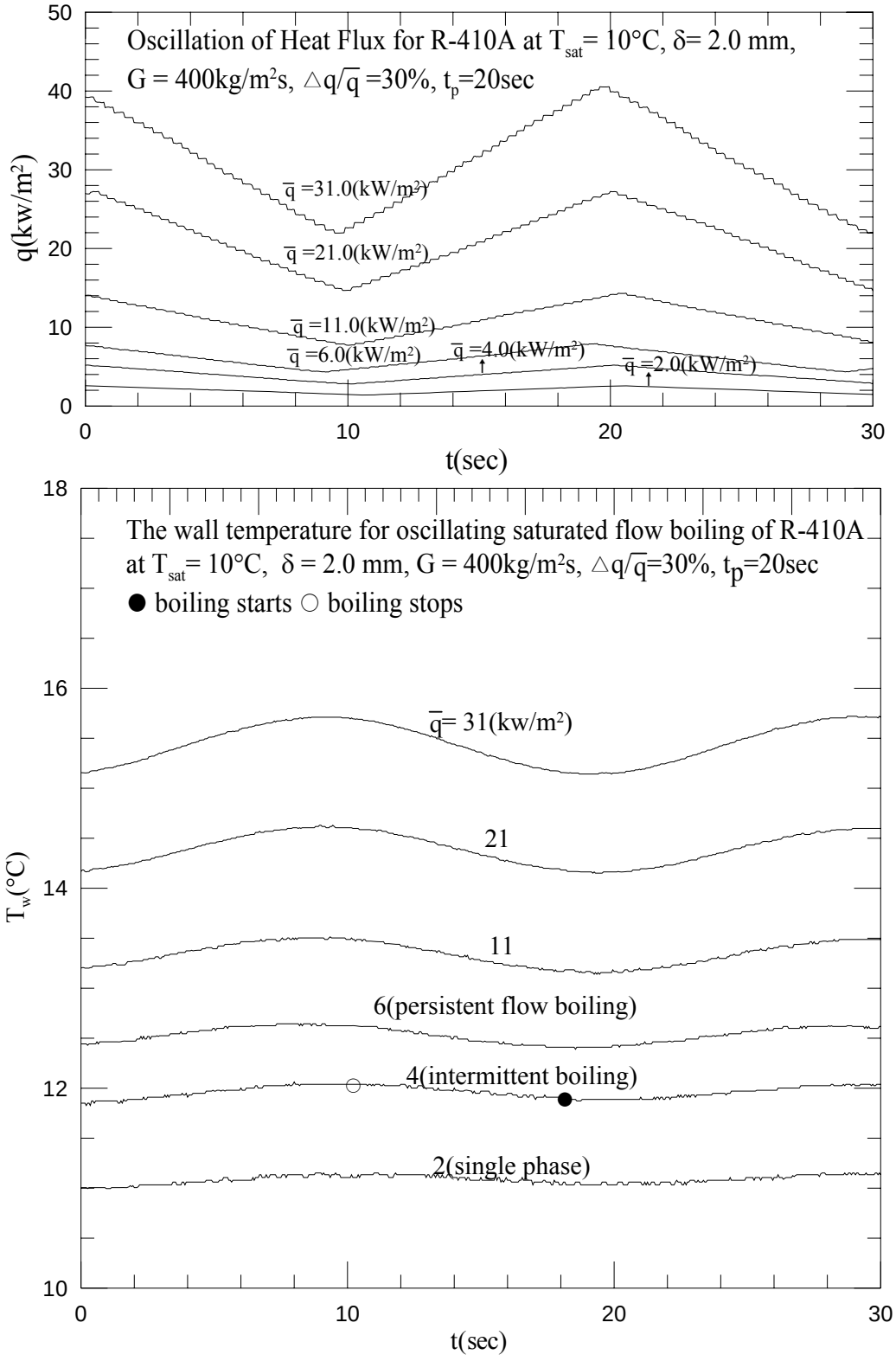


Fig. 9.6 Time variations of imposed heat flux and measured wall temperature in time periodic saturated flow boiling of R-410A at T_{sat} = 10℃, δ = 2.0mm, t_p = 20 sec and G = 400kg/m²s with $\Delta q/\bar{q} = 30\%$.

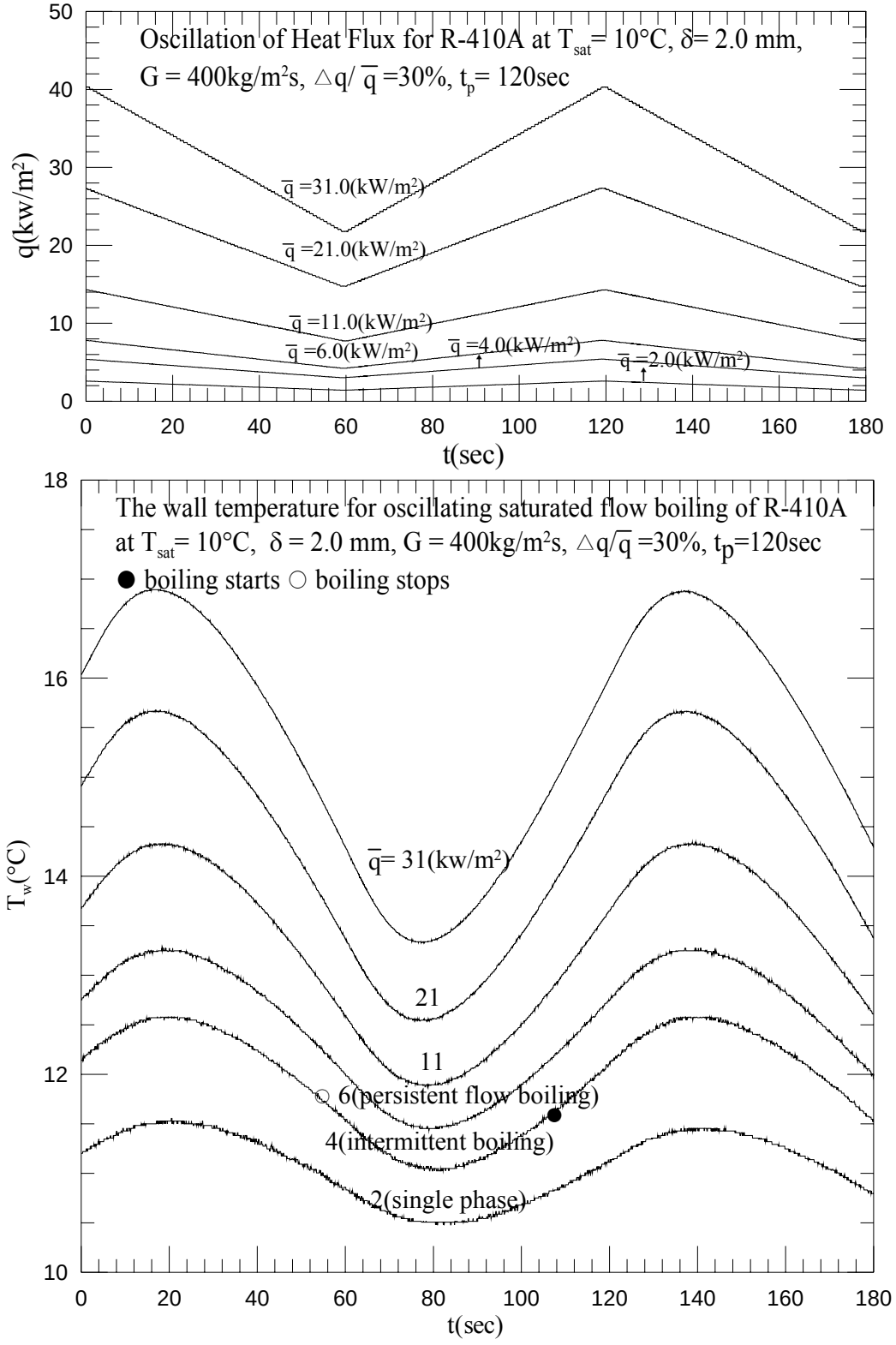


Fig. 9.7 Time variations of imposed heat flux and measured wall temperature in time periodic saturated flow boiling of R-410A at T_{sat} = 10℃, δ = 2.0mm, t_p = 120 sec and G = 400kg/m²s with $\Delta q/\bar{q} = 30\%$.

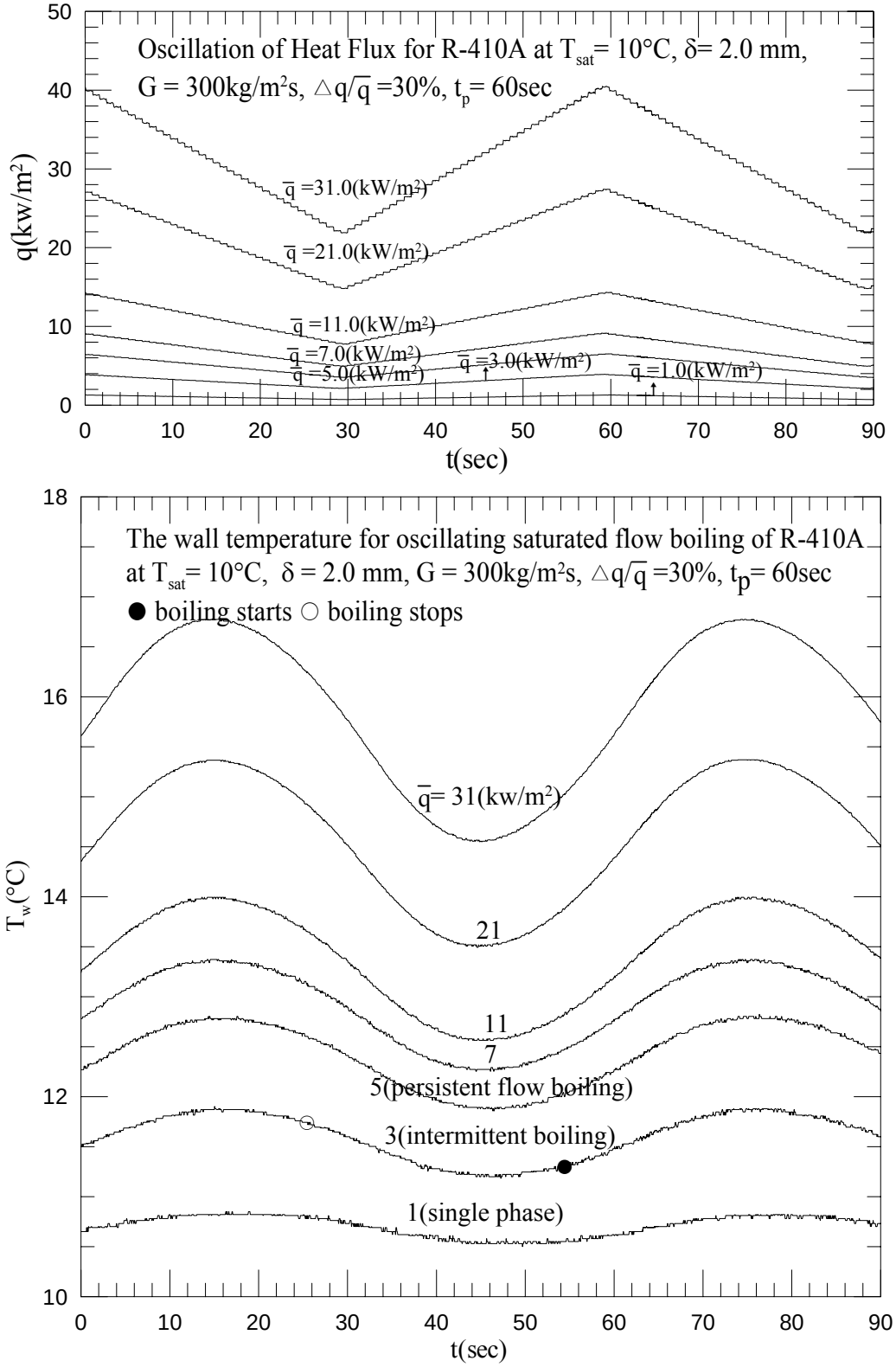


Fig. 9.8 Time variations of imposed heat flux and measured wall temperature in time periodic saturated flow boiling of R-410A at T_{sat} = 10℃, δ = 2.0mm, t_p = 60 sec and G =300kg/m²s with $\Delta q/\bar{q}$ = 30%.

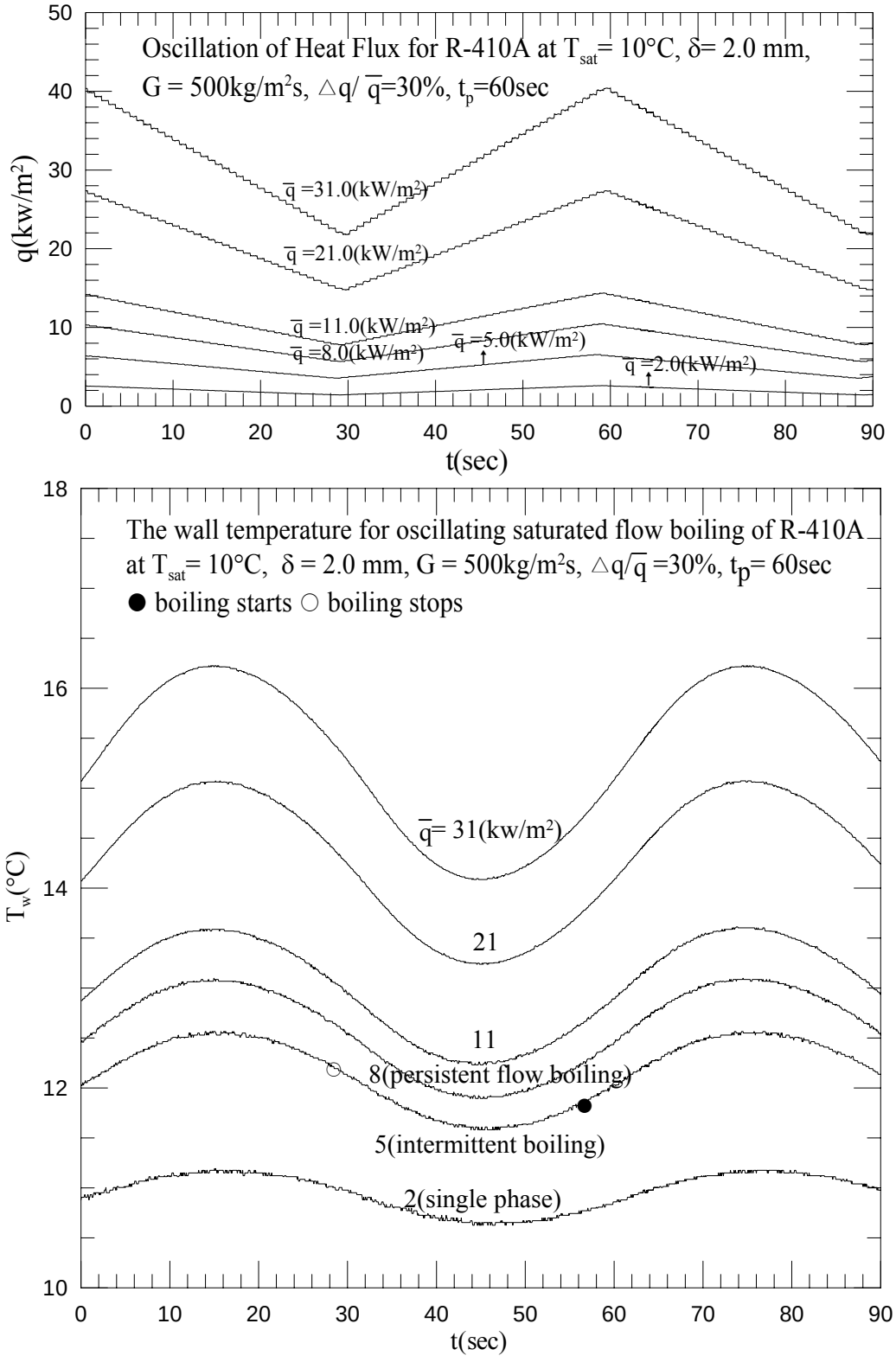


Fig. 9.9 Time variations of imposed heat flux and heat transfer coefficient in time periodic saturated flow boiling of R-410A at T_{sat} = 10℃, δ = 2.0mm, t_p = 60 sec and G = 500kg/m²s with $\Delta q/\bar{q} = 30\%$.

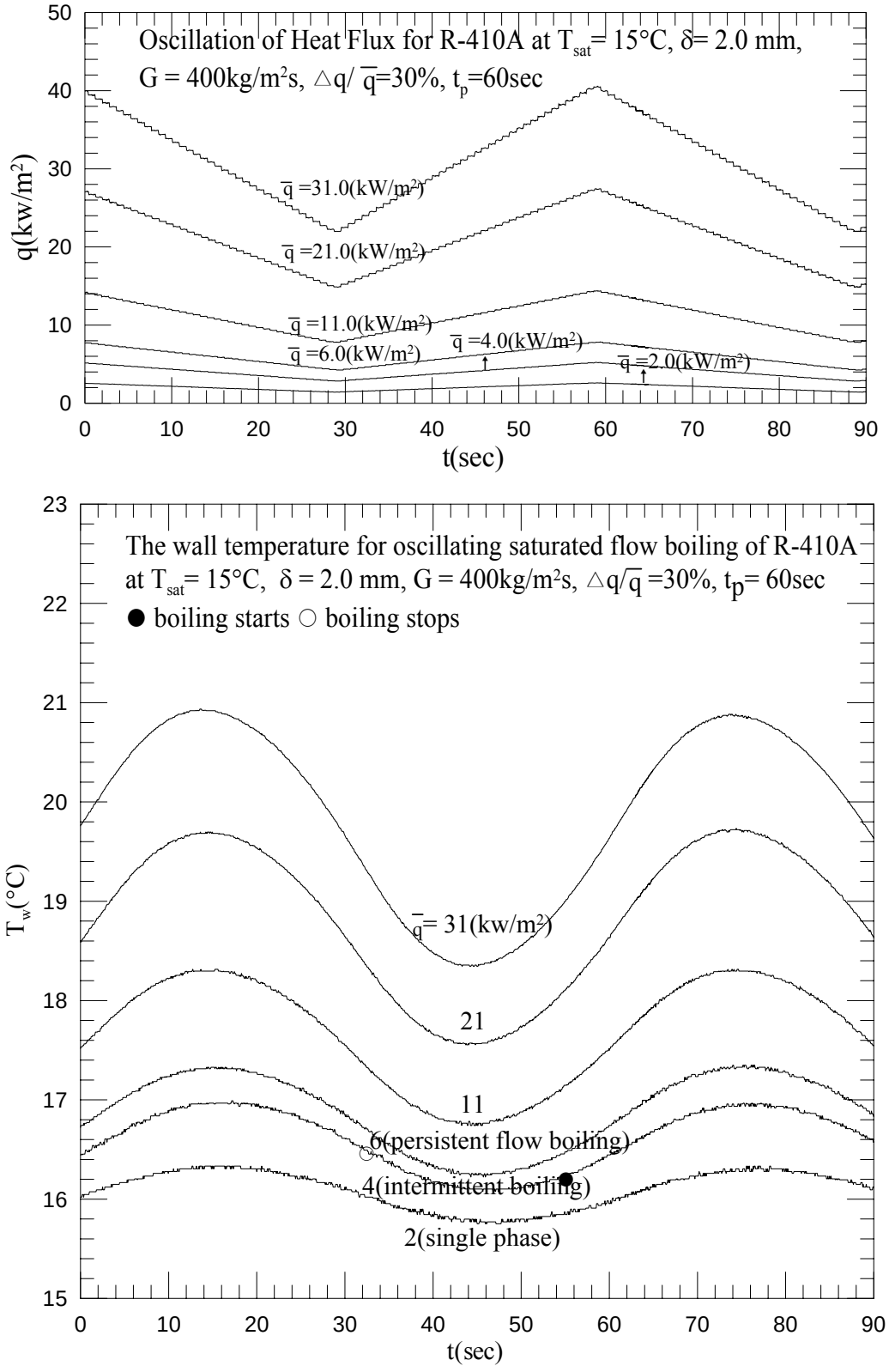


Fig. 9.10 Time variations of imposed heat flux and heat transfer coefficient in time periodic saturated flow boiling of R-410A at T_{sat} = 15℃, δ = 2.0mm, t_p = 60 sec and G = 400kg/m²s with $\Delta q/\bar{q} = 30\%$.

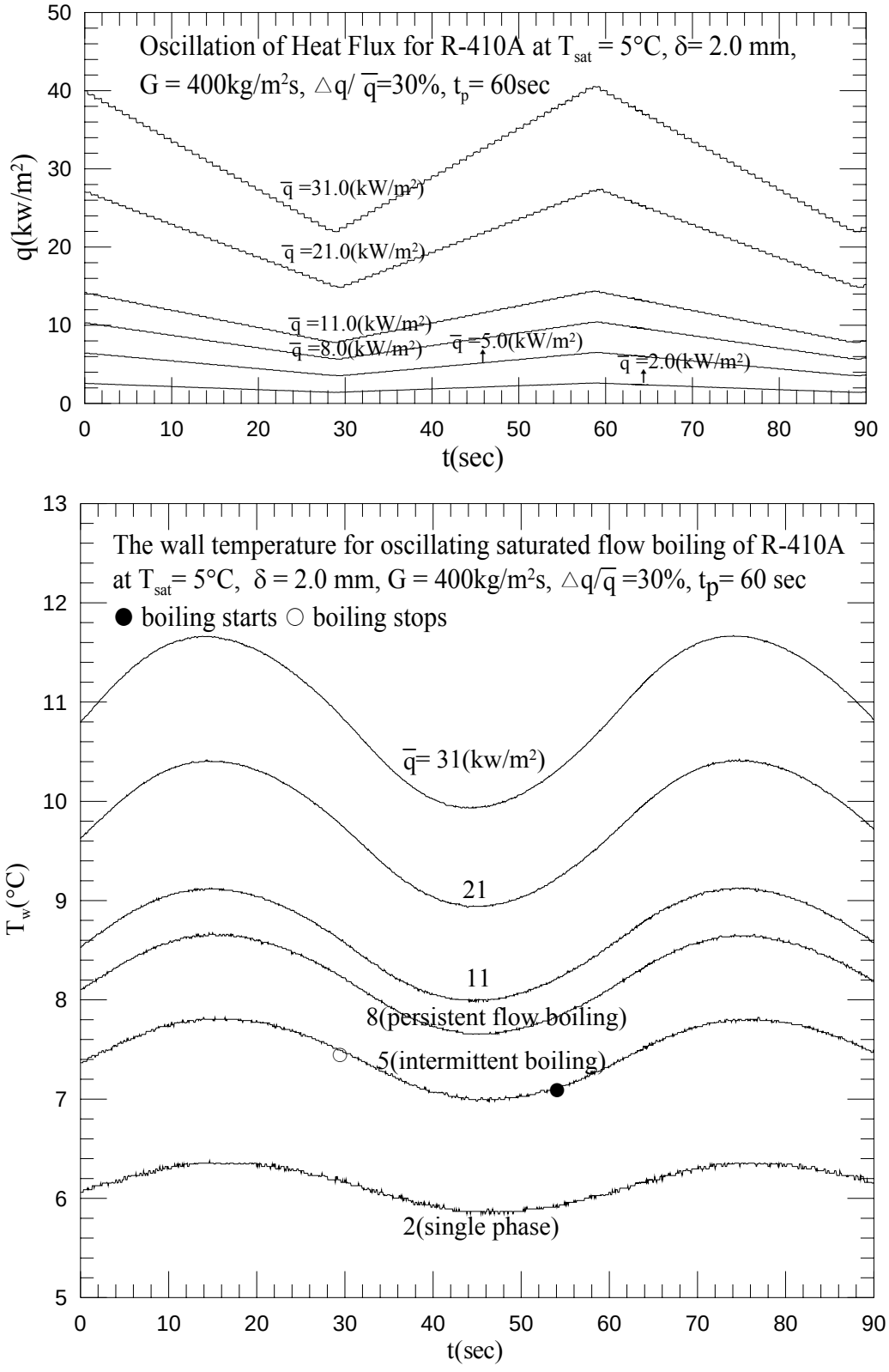


Fig. 9.11 Time variations of imposed heat flux and heat transfer coefficient in time periodic saturated flow boiling of R-410A at T_{sat} = 5℃, δ = 2.0mm, t_p = 60 sec and G = 400kg/m²s with $\Delta q/\bar{q} = 30\%$.

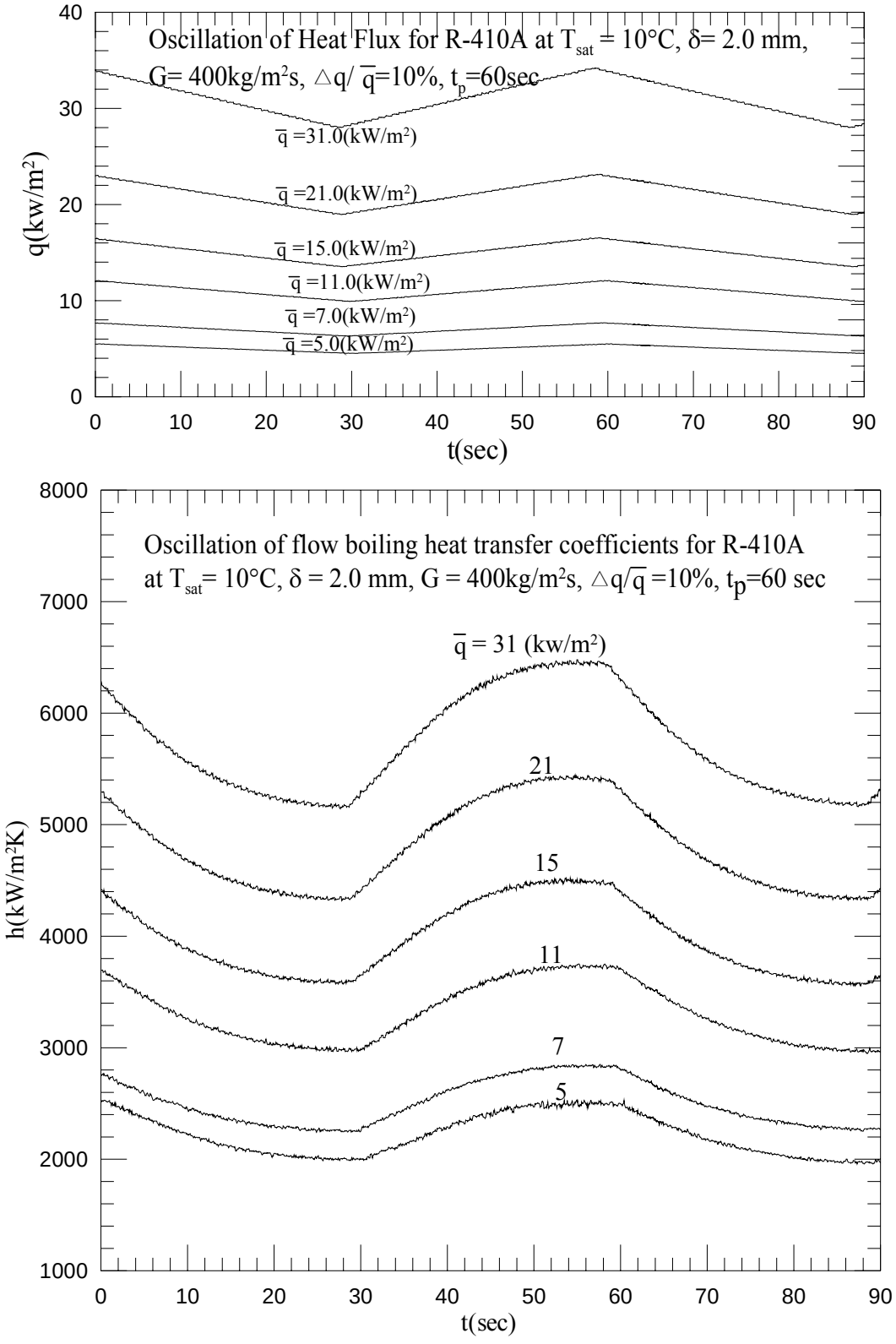


Fig. 9.12 Time variations of imposed heat flux and heat transfer coefficient in time periodic saturated flow boiling of R-410A at T_{sat} = 10℃, δ = 2.0mm, t_p = 60 sec and G =400kg/m²s with $\Delta q/\bar{q} = 10\%$.

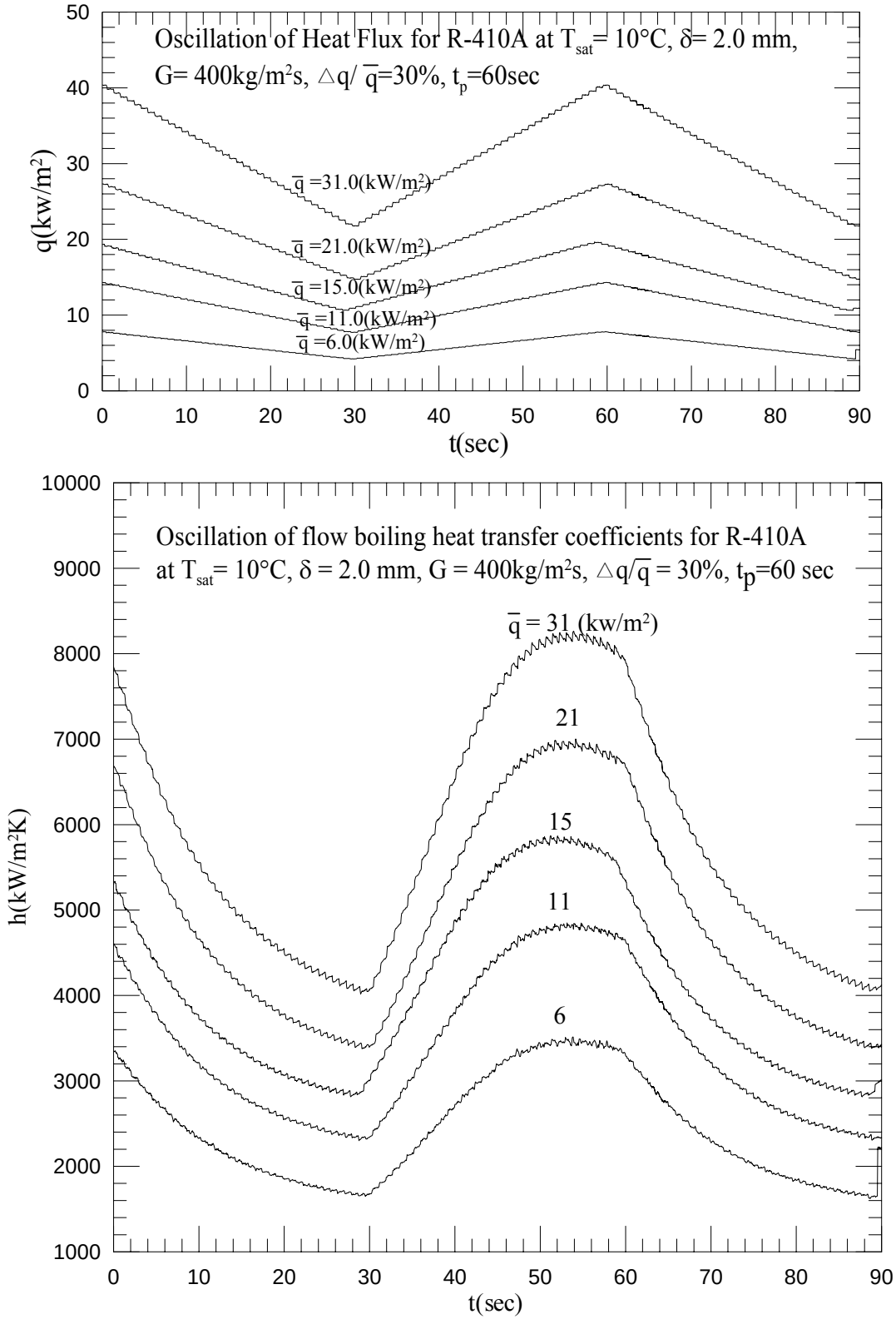


Fig. 9.13 Time variations of imposed heat flux and heat transfer coefficient in time periodic saturated flow boiling of R-410A at T_{sat} = 10℃, δ = 2.0mm, t_p = 60 sec and G = 400kg/m²s with $\Delta q/\bar{q} = 30\%$.

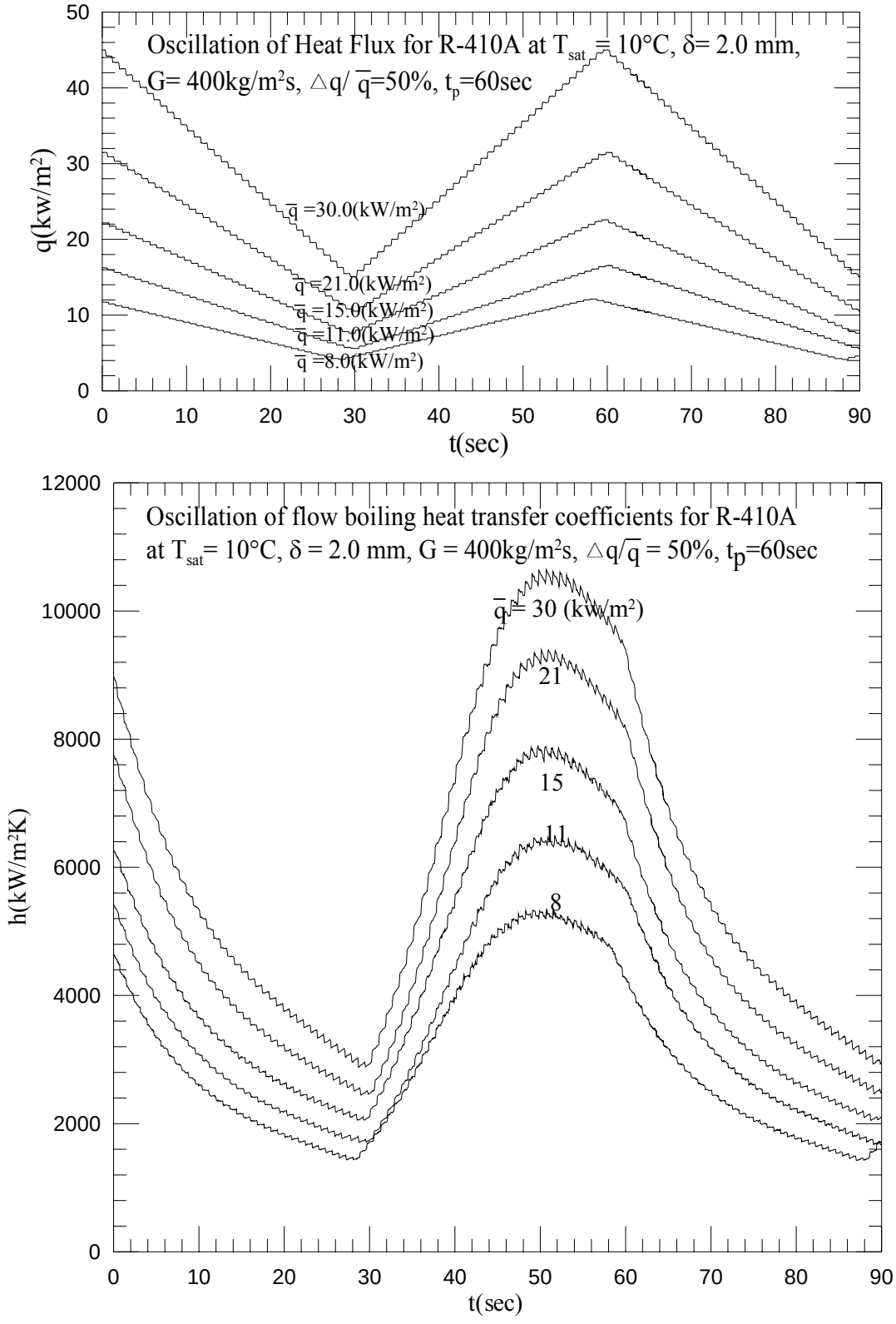


Fig. 9.14 Time variations of imposed heat flux and heat transfer coefficient in time periodic saturated flow boiling of R-410A at T_{sat} = 10℃, δ = 2.0mm, t_p = 60 sec and G = 400kg/m²s with $\Delta q/\bar{q} = 50\%$.

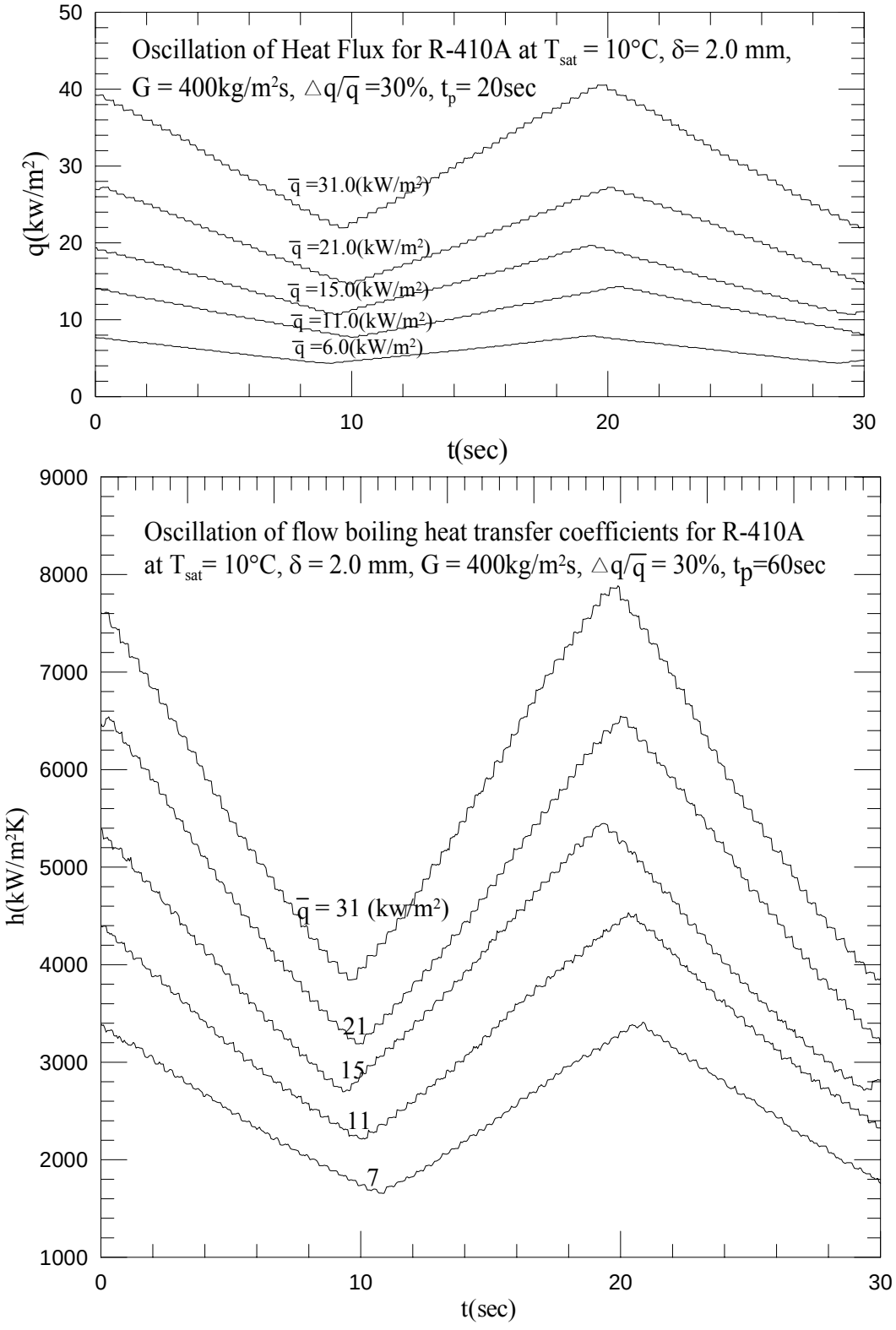


Fig. 9.15 Time variations of imposed heat flux and heat transfer coefficient in time periodic saturated flow boiling of R-410A at T_{sat} = 10℃, δ = 2.0mm, t_p = 20 sec and G = 400kg/m^{2}s with $\Delta q/\bar{q} = 30\%$.

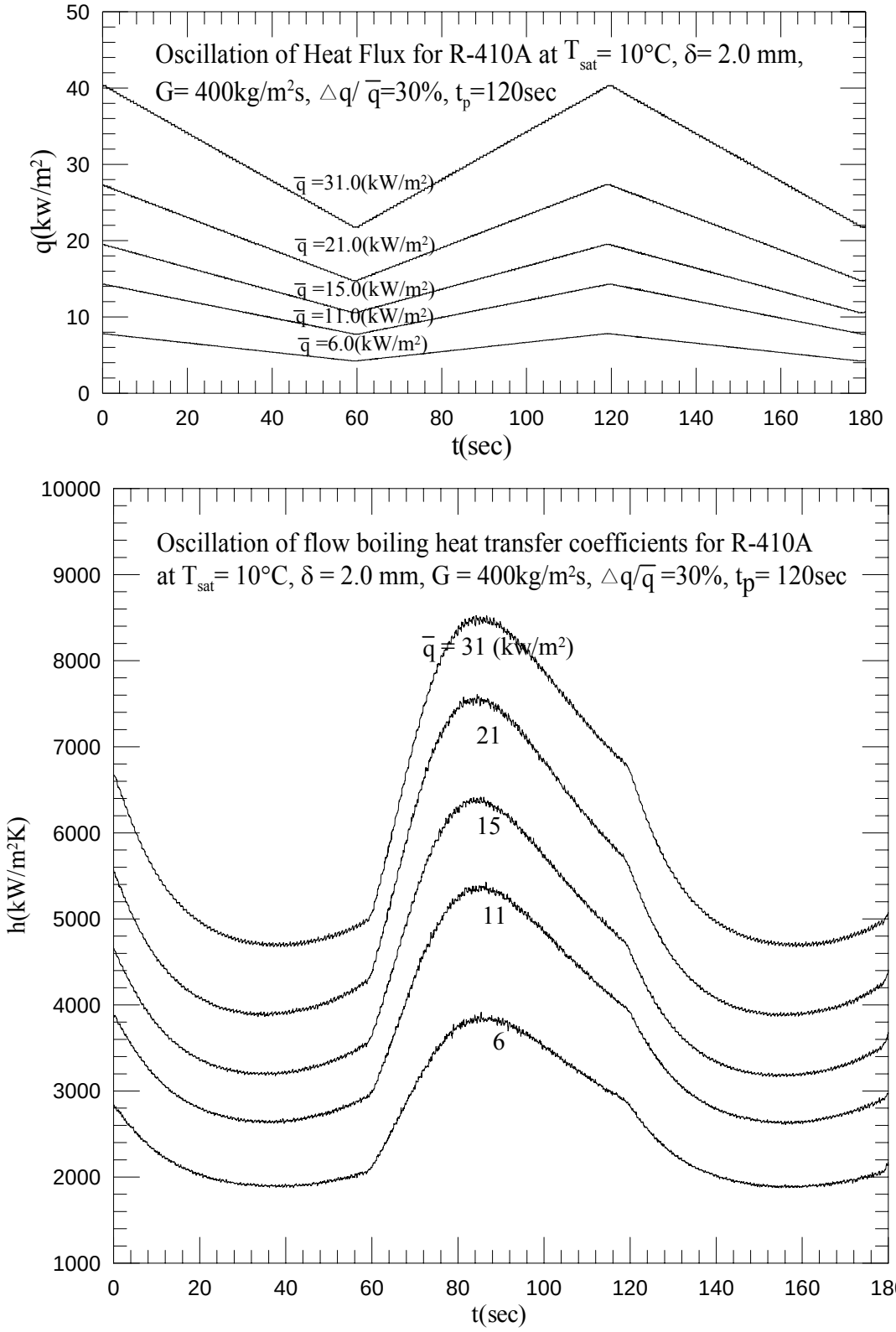


Fig. 9.16 Time variations of imposed heat flux and heat transfer coefficient in time periodic saturated flow boiling of R-410A at T_{sat} = 10℃, δ = 2.0mm, t_p = 120 sec and G = 400kg/m^{2}s with $\Delta q/\bar{q}$ = 30%.

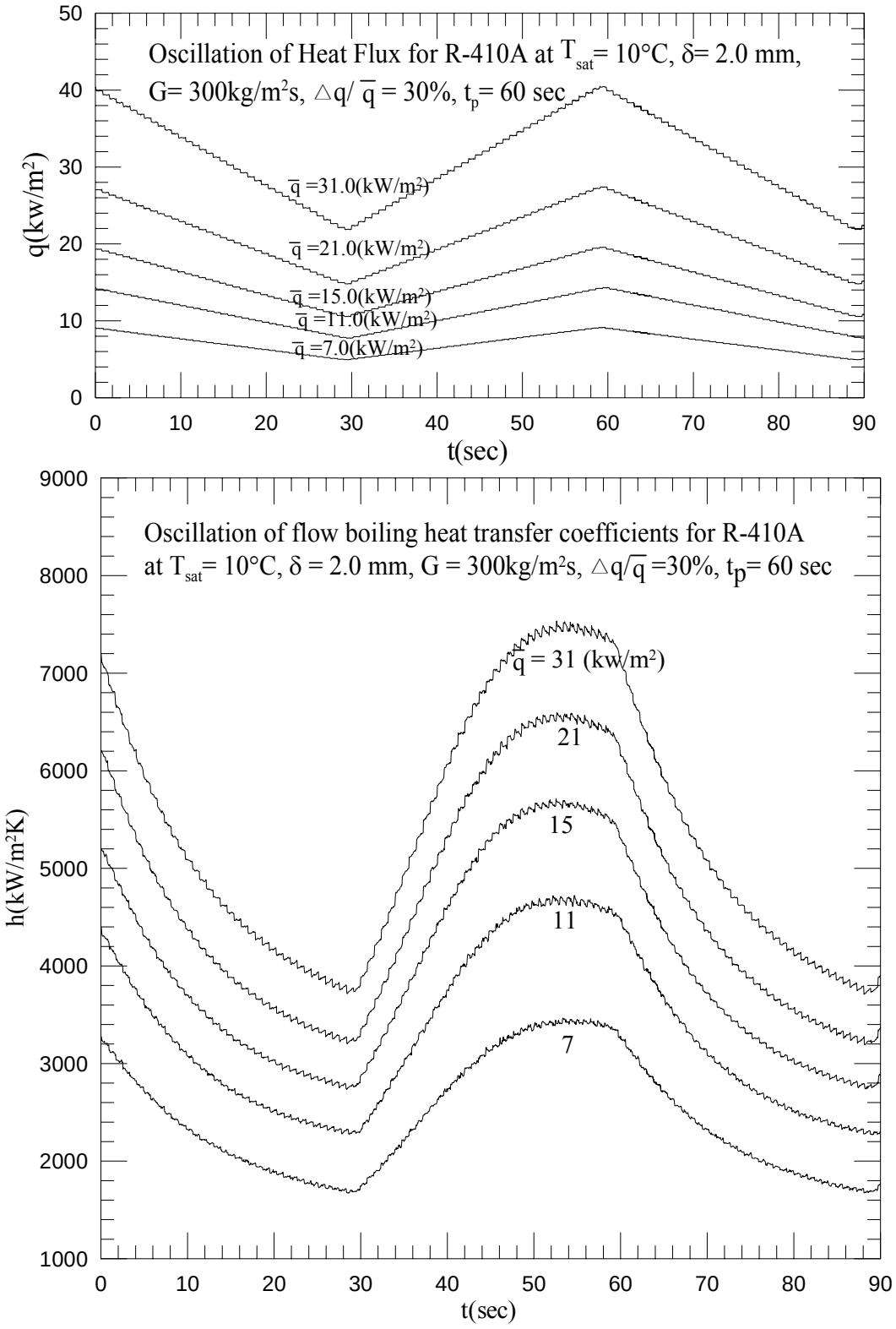


Fig. 9.17 Time variations of imposed heat flux and heat transfer coefficient in time periodic saturated flow boiling of R-410A at T_{sat} = 10℃, δ = 2.0mm, t_p = 60 sec and G = 300kg/m²s with $\Delta q/\bar{q} = 30\%$.

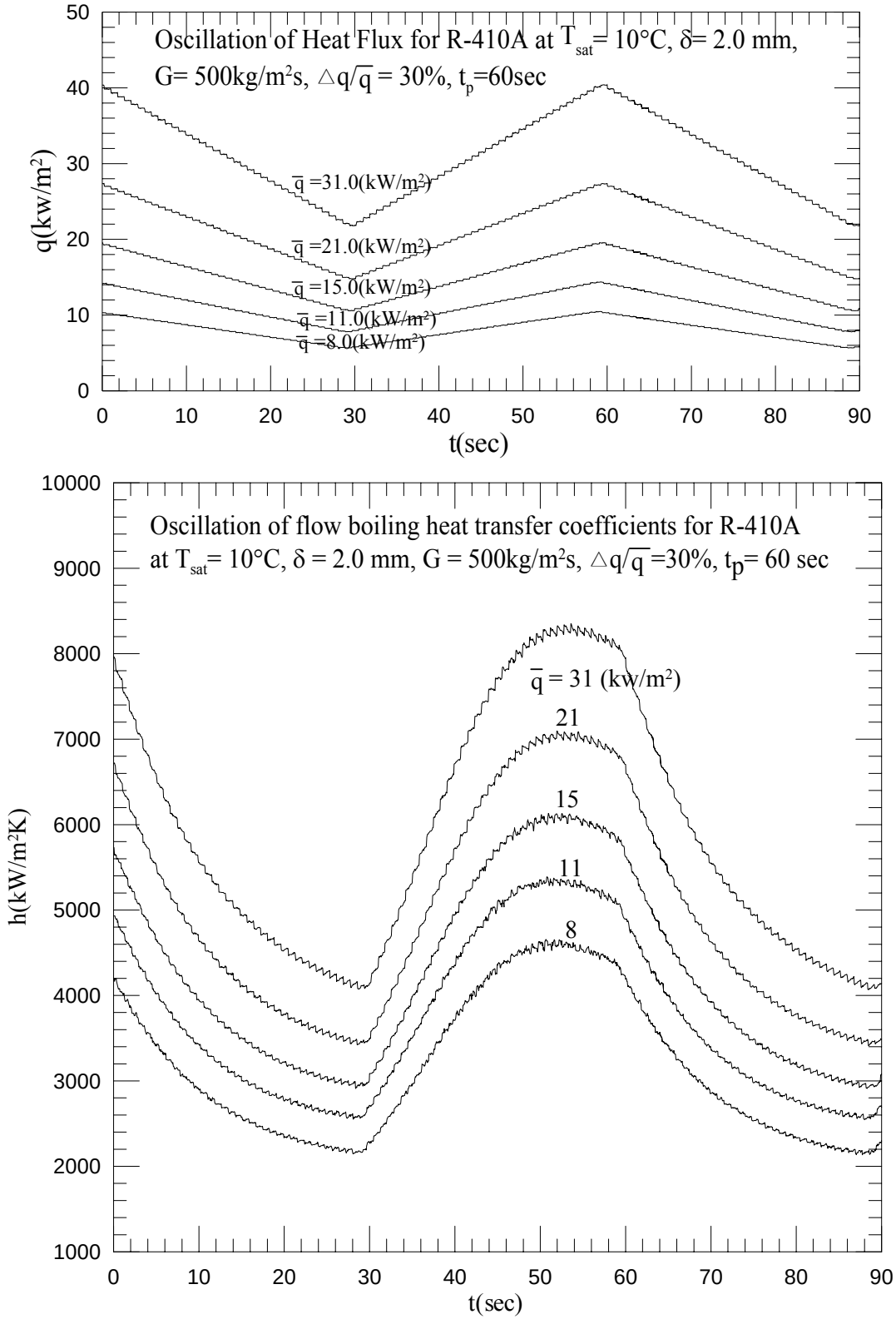


Fig. 9.18 Time variations of imposed heat flux and heat transfer coefficient in time periodic saturated flow boiling of R-410A at T_{sat} = 10℃, δ = 2.0mm, t_p = 60 sec and G = 500kg/m²s with $\Delta q/\bar{q} = 30\%$.

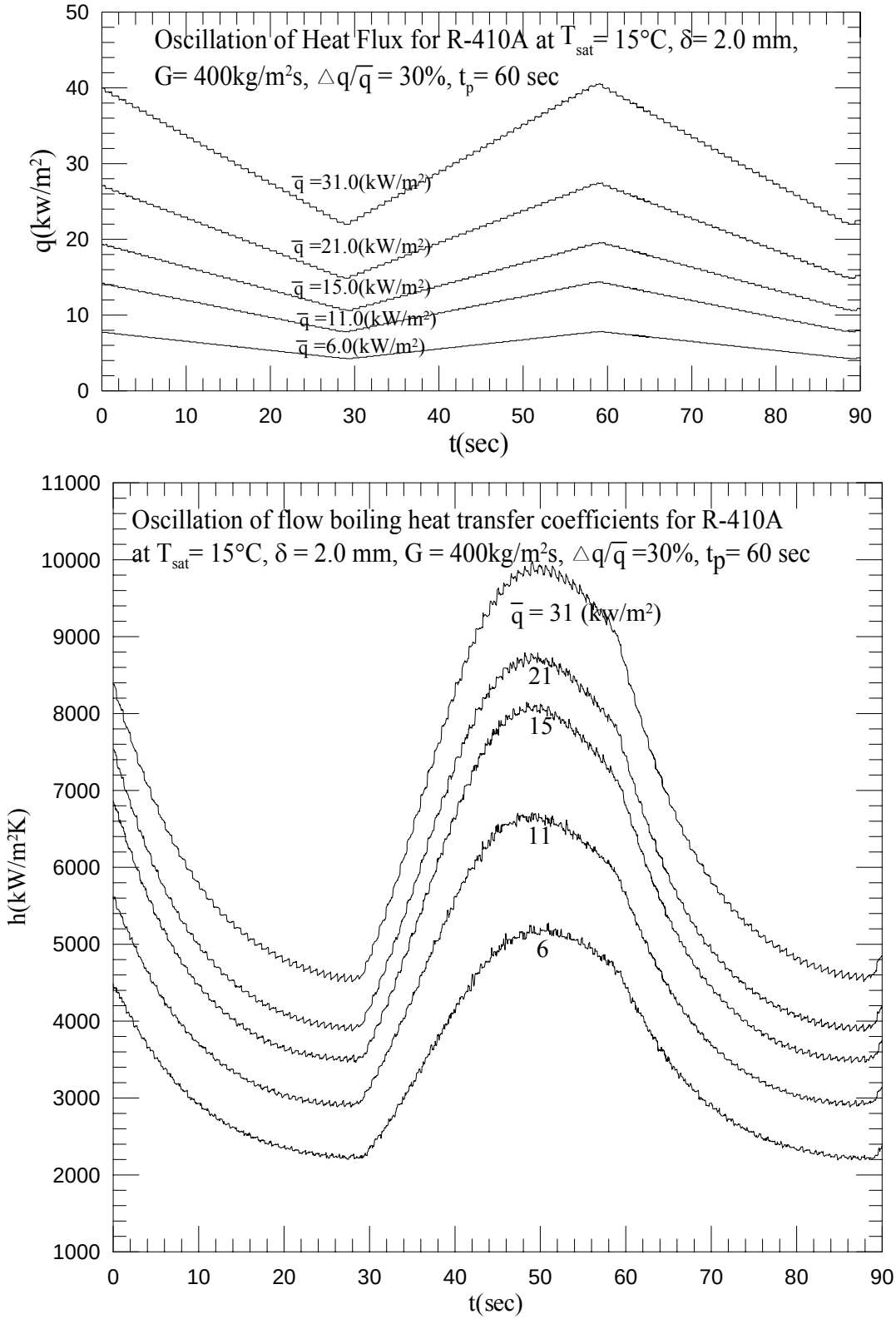


Fig. 9.19 Time variations of imposed heat flux and heat transfer coefficient in time periodic saturated flow boiling of R-410A at T_{sat} = 15℃, δ = 2.0mm, t_p = 60 sec and G = 400kg/m^{2}s with $\Delta q/\bar{q} = 30\%$.

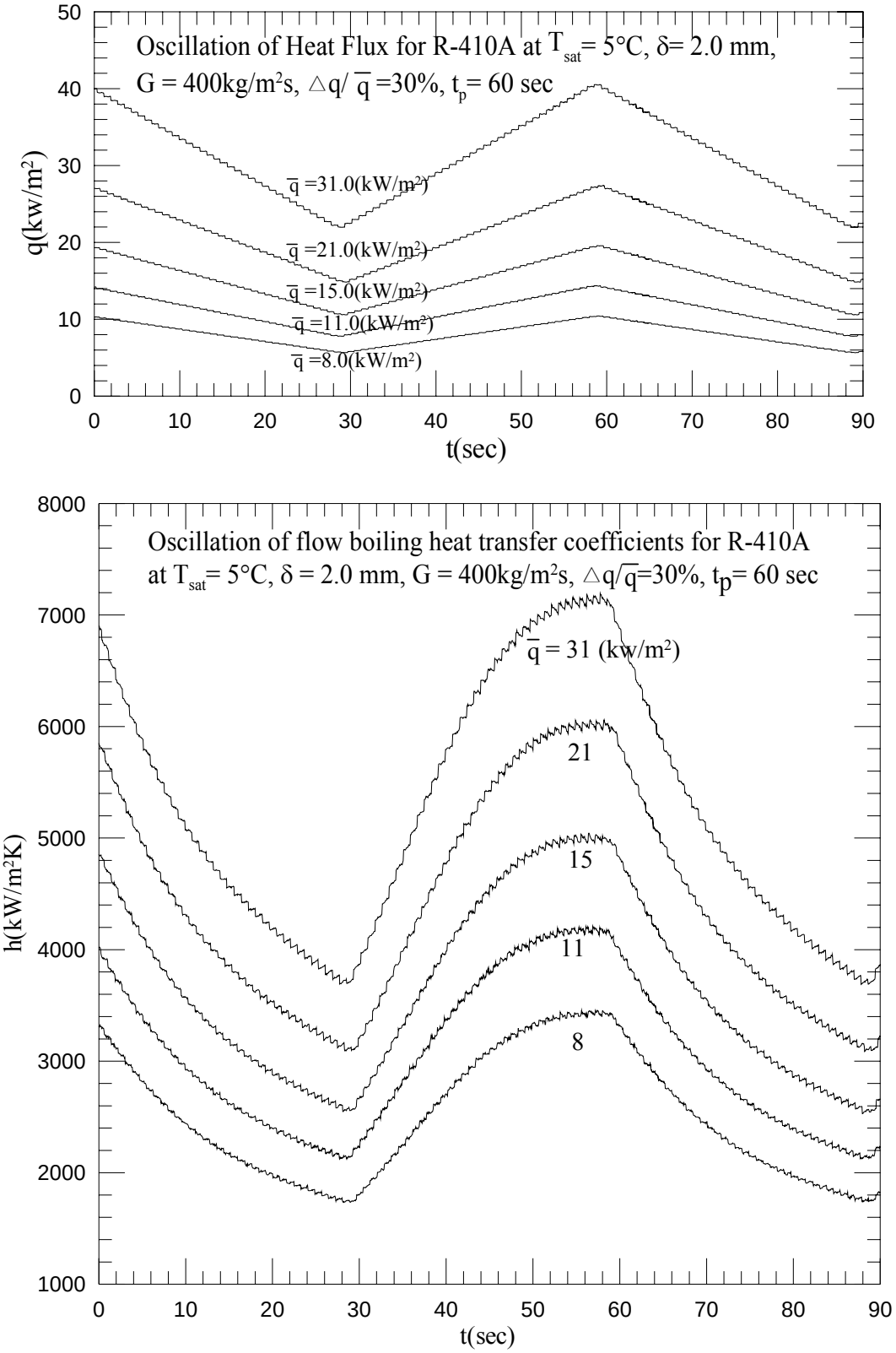


Fig. 9.20 Time variations of imposed heat flux and heat transfer coefficient in time periodic saturated flow boiling of R-410A at T_{sat} = 5℃, δ = 2.0mm, t_p = 60 sec and G = 400kg/m²s with $\Delta q/\bar{q} = 30\%$.

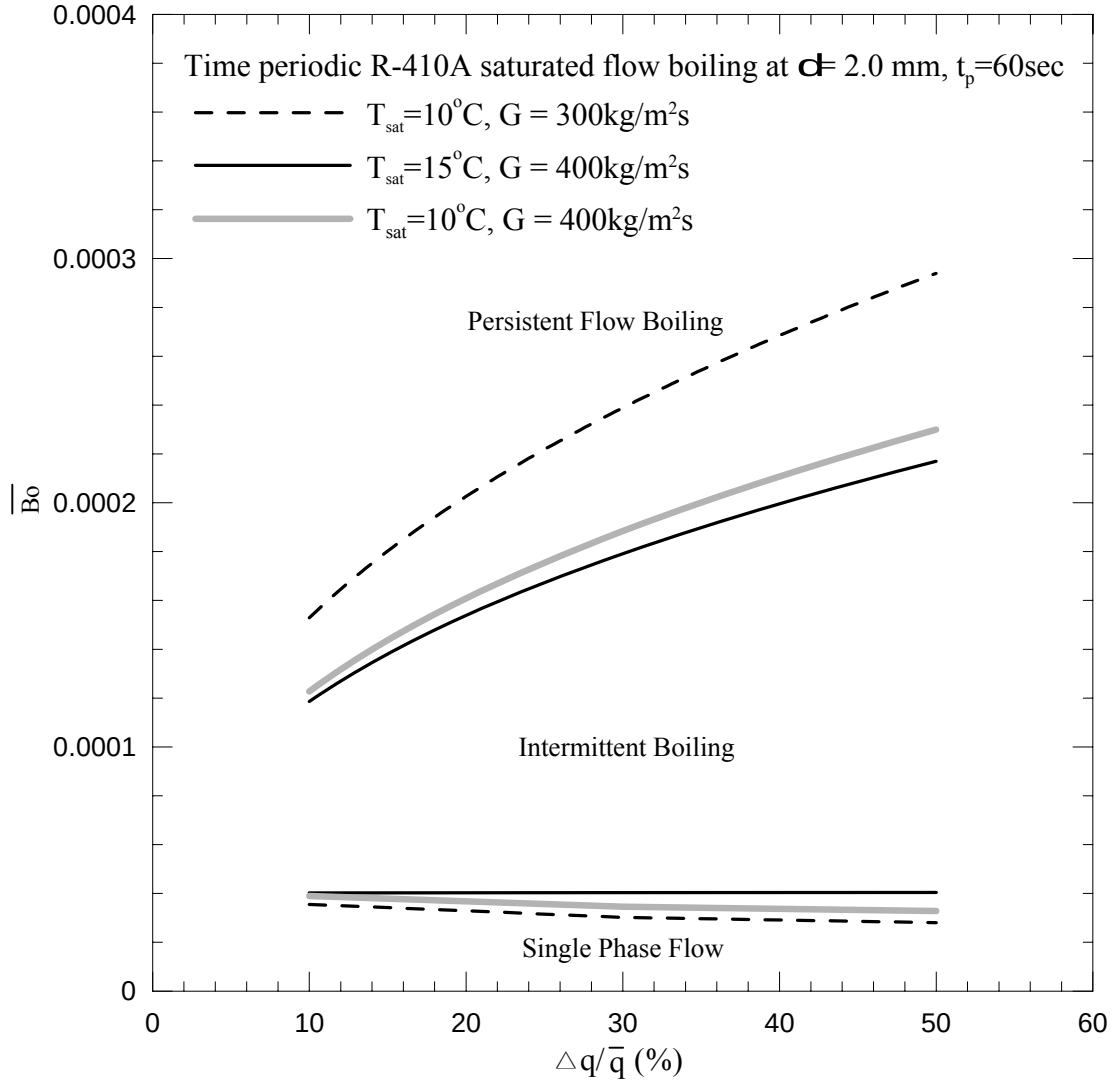


Fig. 9.21 Flow regime map for time periodic R-410A flow boiling regimes at δ =2mm and t_p = 60 sec for various saturated temperatures and mass fluxes.

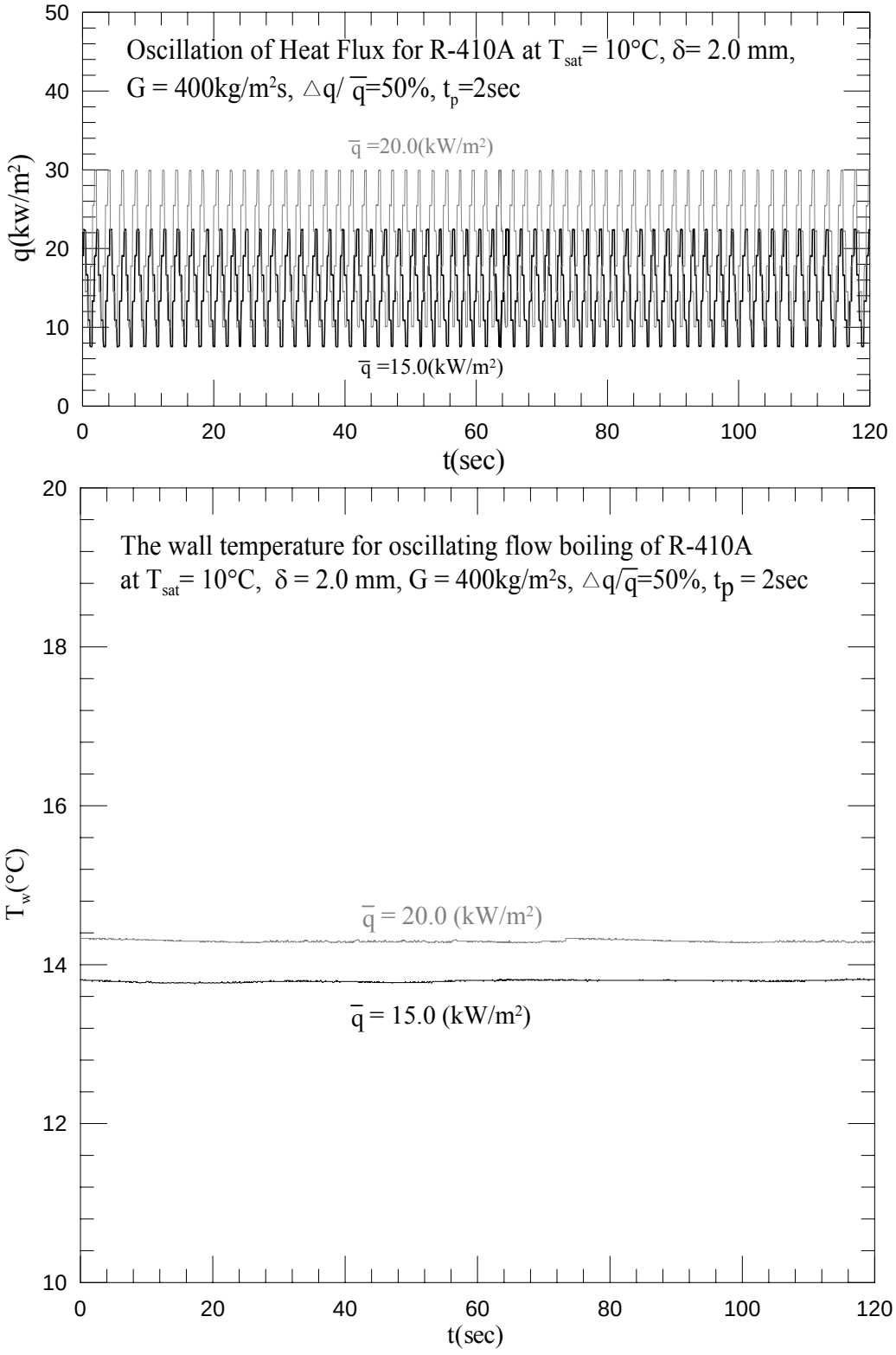


Fig. 9.22 Time variations of imposed heat flux and wall temperature at z = 80 mm for t_p = 2 sec.

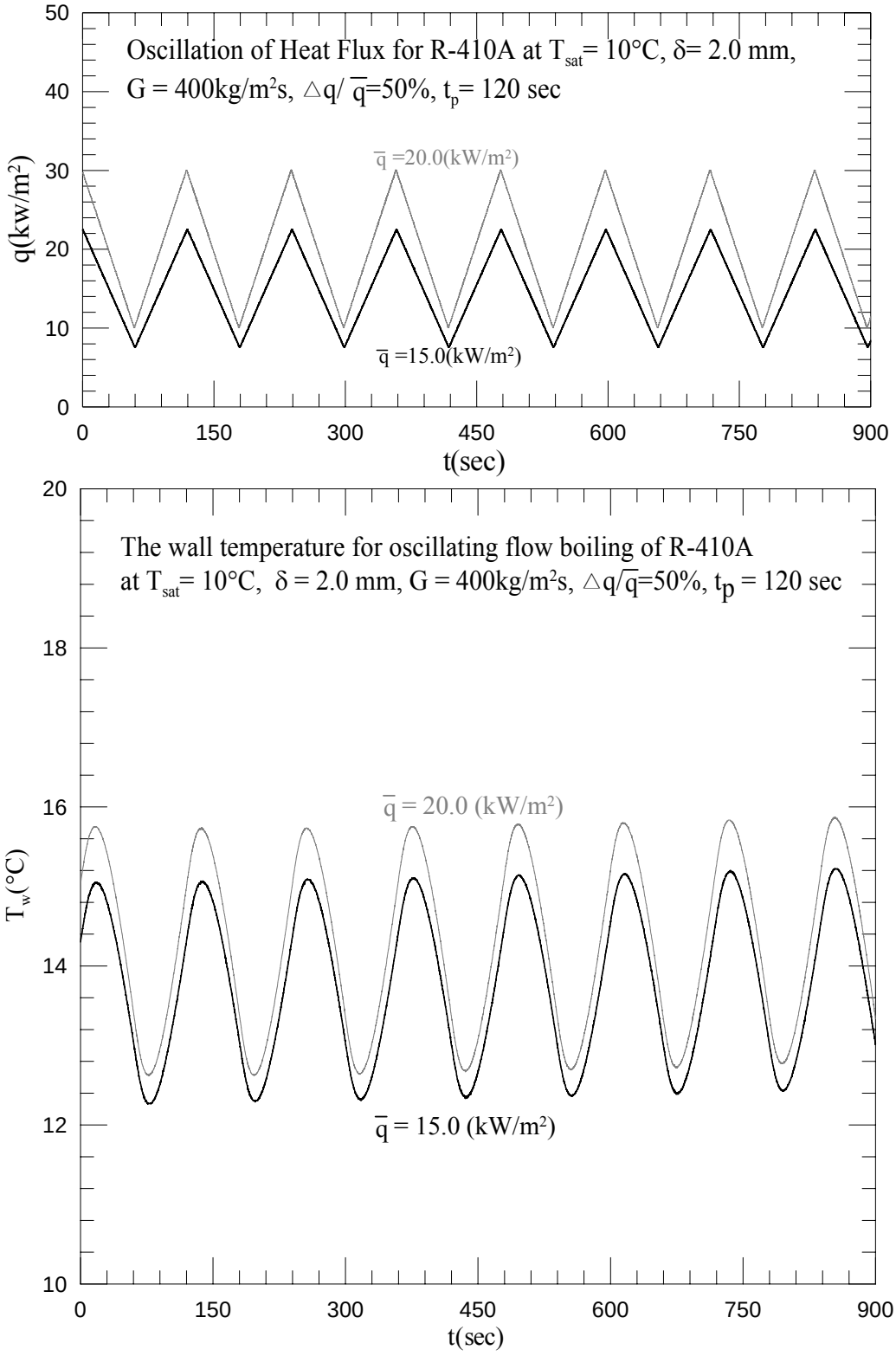


Fig. 9.23 Time variations of imposed heat flux and wall temperature at z = 80 mm for t_p = 120 sec.

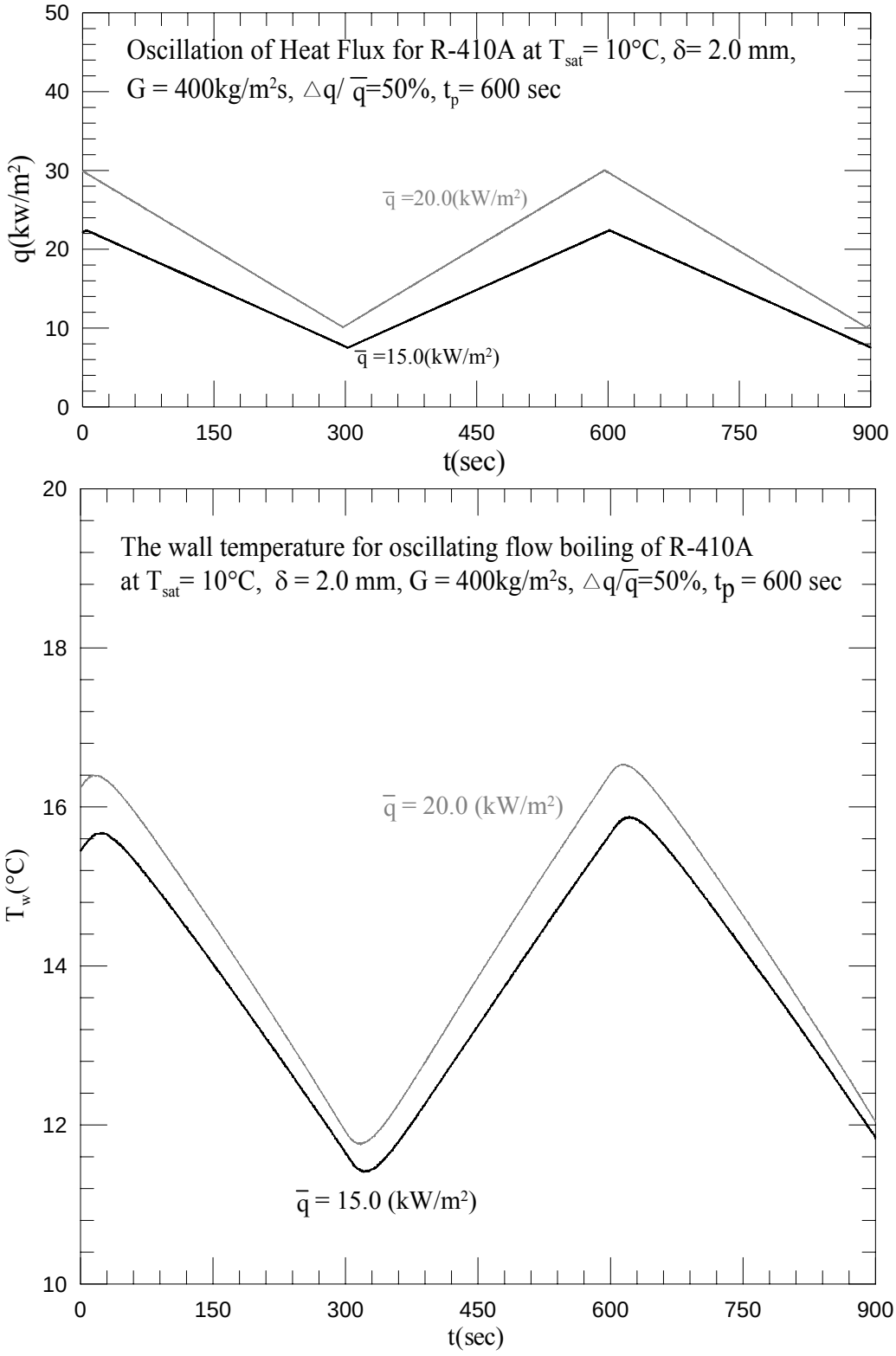


Fig. 9.24 Time variations of imposed heat flux and wall temperature at z = 80 mm for t_p = 600 sec.

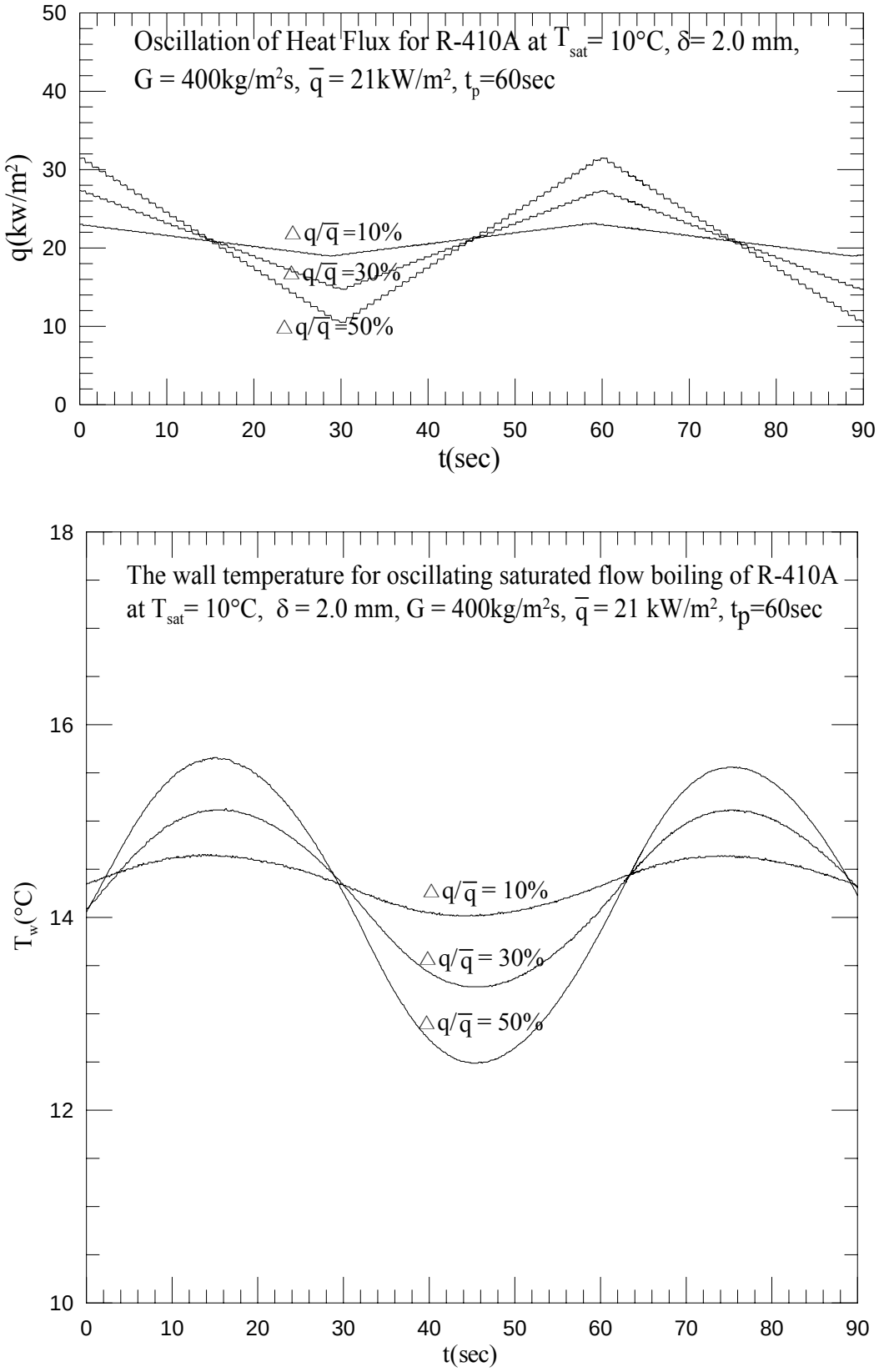


Fig. 9.25 Time variations of imposed heat flux and wall temperature at z = 80 mm for various $\Delta q/\bar{q}$.

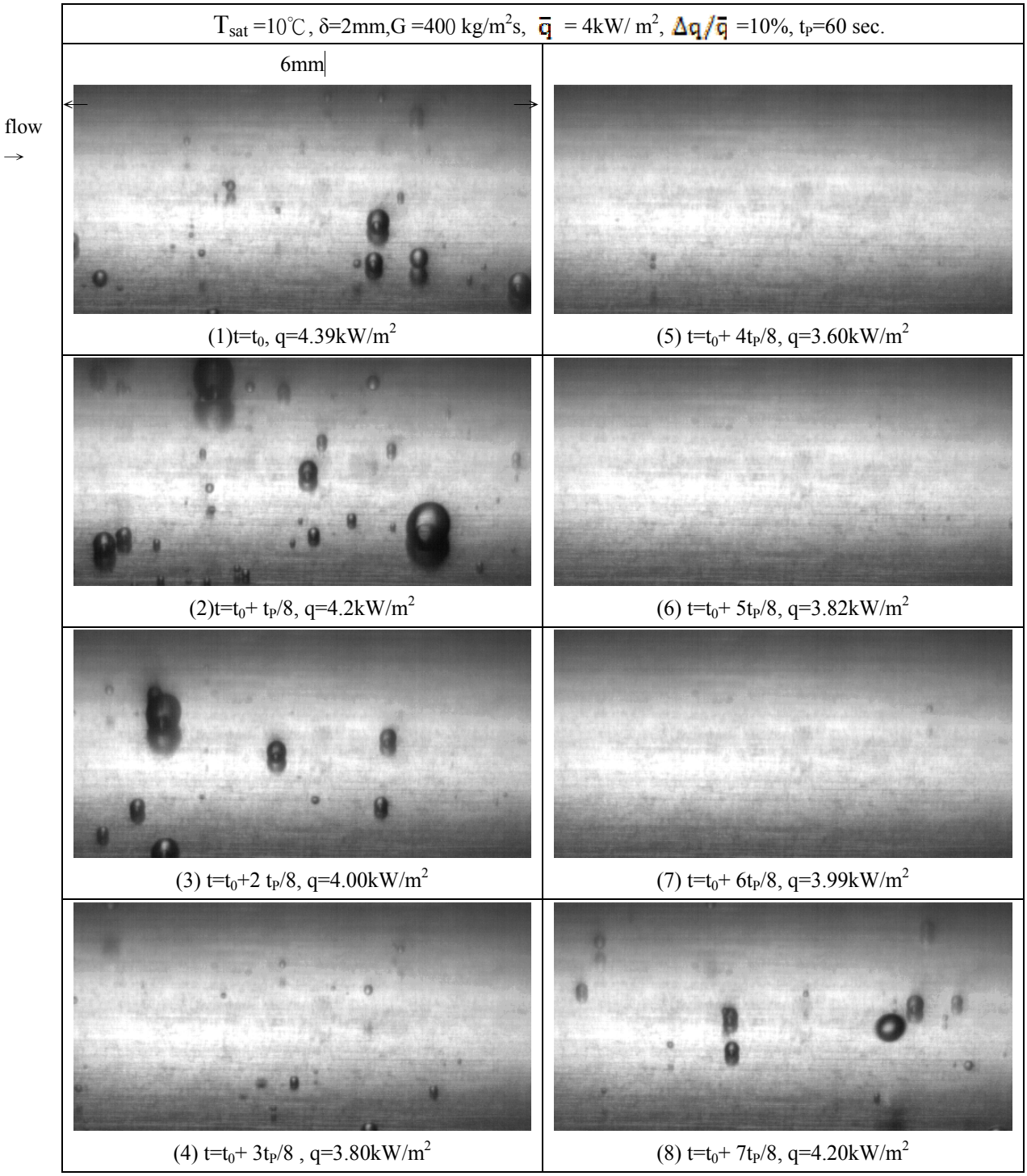


Fig. 9.26 Photos of time periodic intermittent flow boiling of R-410A at selected time instants in a typical periodic cycle at T_{sat} =10℃, G = 400 kg/m²s, δ =2.0mm and t_p= 60 sec for $\bar{q}$ = 4kW/m², $\Delta q/\bar{q}$ = 10%.

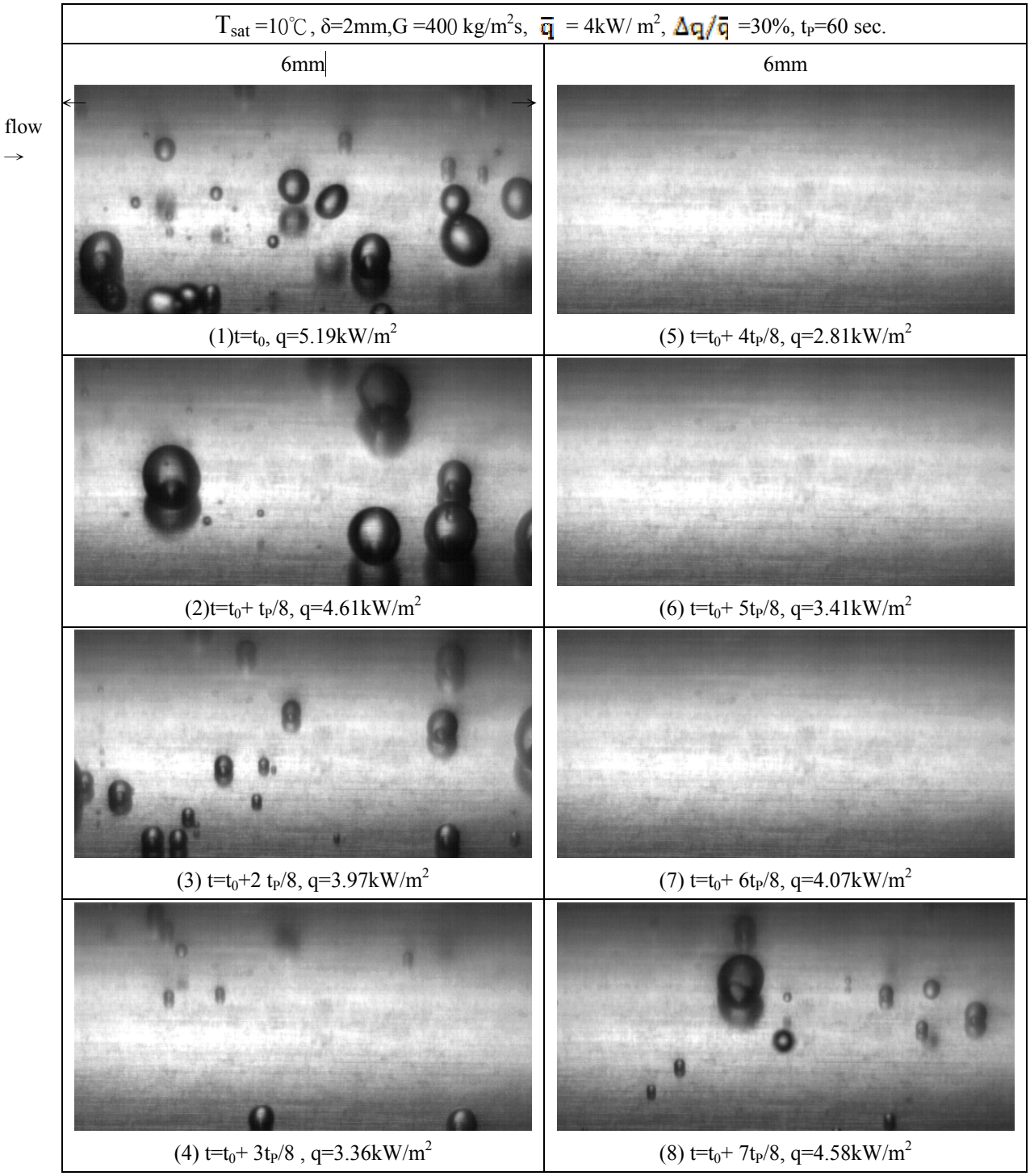


Fig. 9.27 Photos of time periodic intermittent flow boiling of R-410A at selected time instants in a typical periodic cycle at T_{sat} =10℃, G = 400 kg/m^{2}s, δ =2.0mm and t_p= 60 sec for $\bar{q}$ = 4kW/m^2, $\Delta q/\bar{q}$ = 30%.

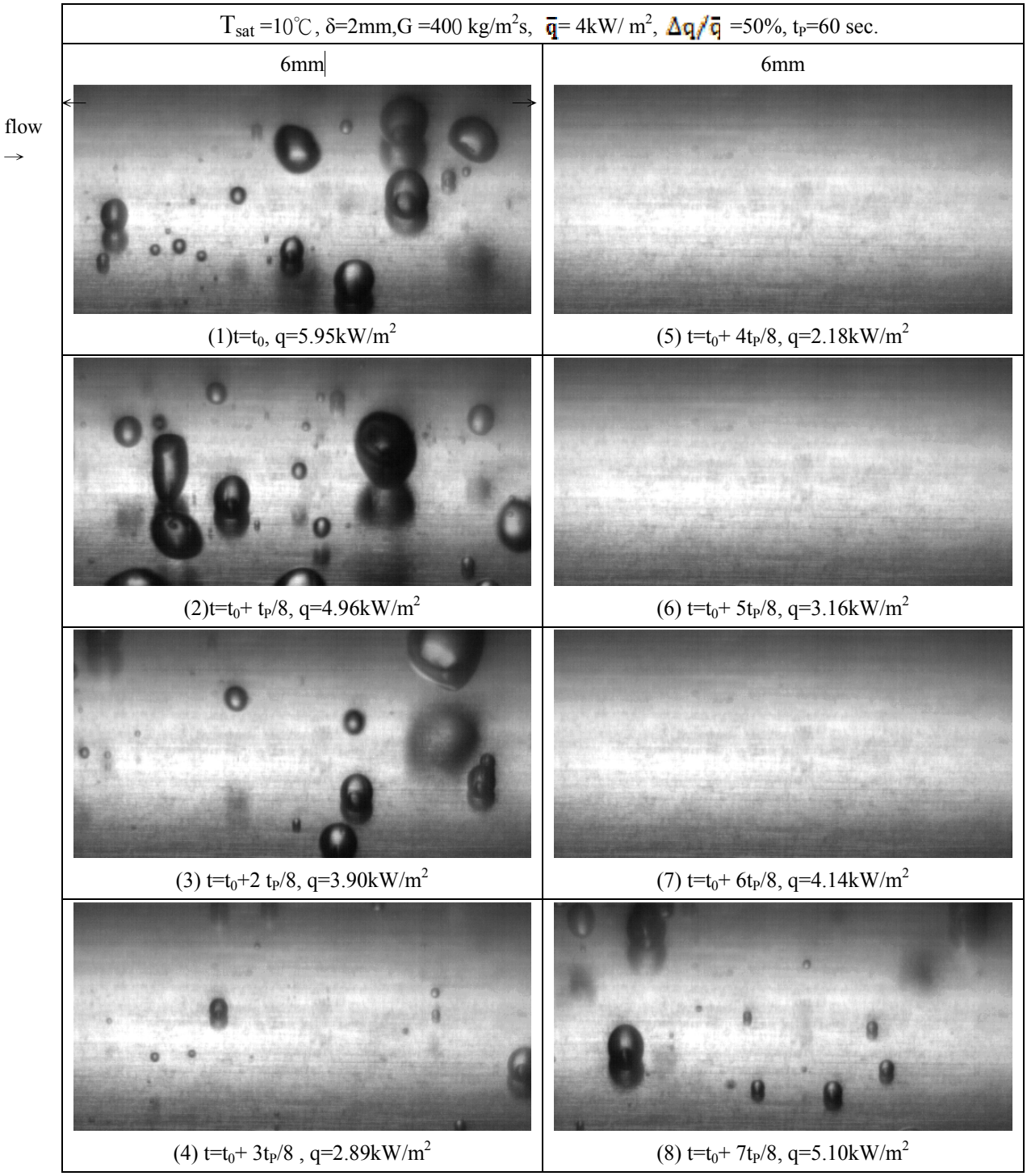


Fig. 9.28 Photos of time periodic intermittent flow boiling of R-410A at selected time instants in a typical periodic cycle at T_{sat} =10℃, G = 400 kg/m²s, δ =2.0mm and t_p= 60 sec for $\bar{q}$ = 4kW/m², $\Delta q/\bar{q}$ = 50%.

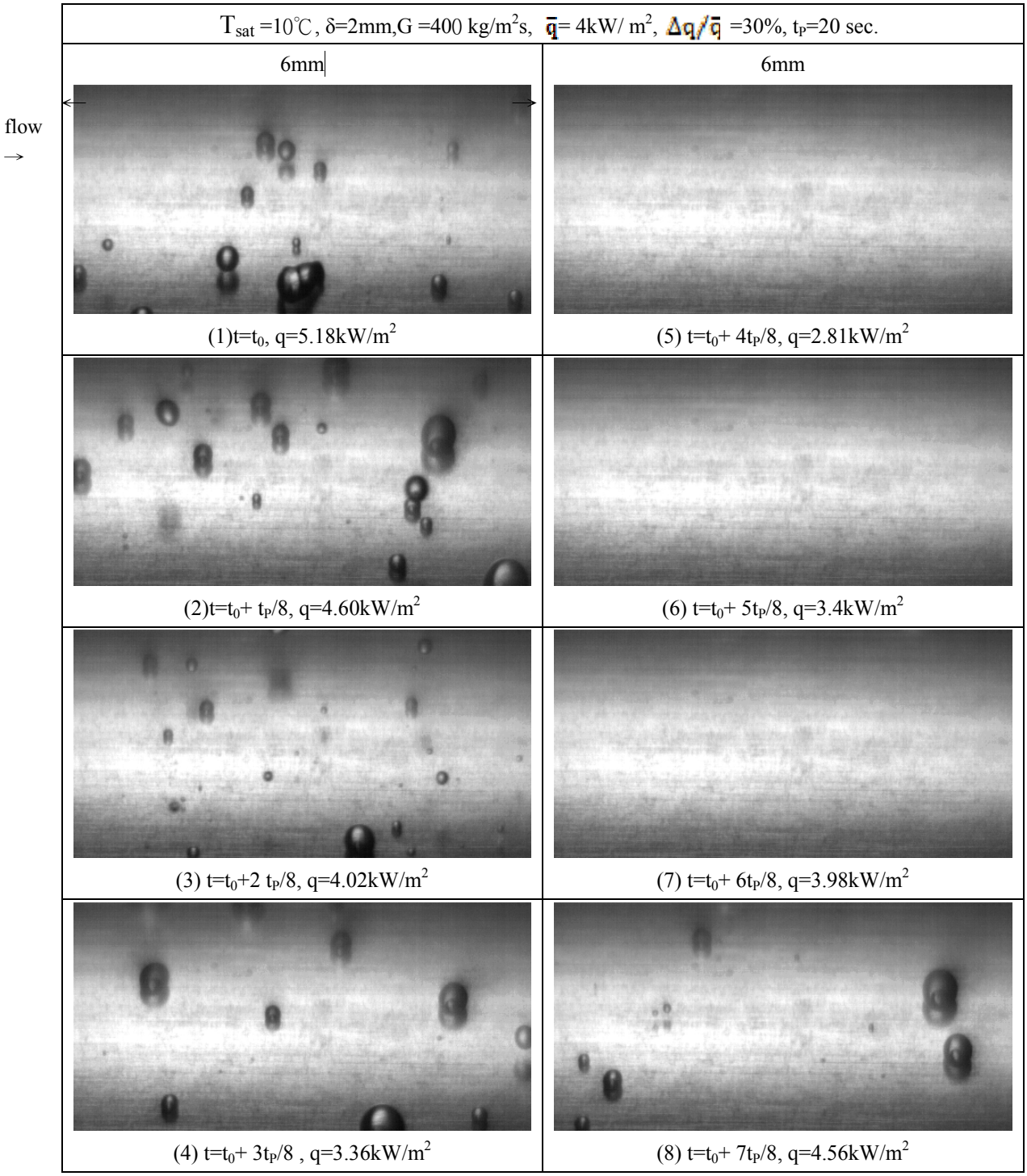


Fig. 9.29 Photos of time periodic intermittent flow boiling of R-410A at selected time instants in a typical periodic cycle at T_{sat} =10℃, G = 400 kg/m²s, δ =2.0mm and t_p= 20 sec for $\bar{q}$ = 4kW/m², $\Delta q/\bar{q}$ = 30%.

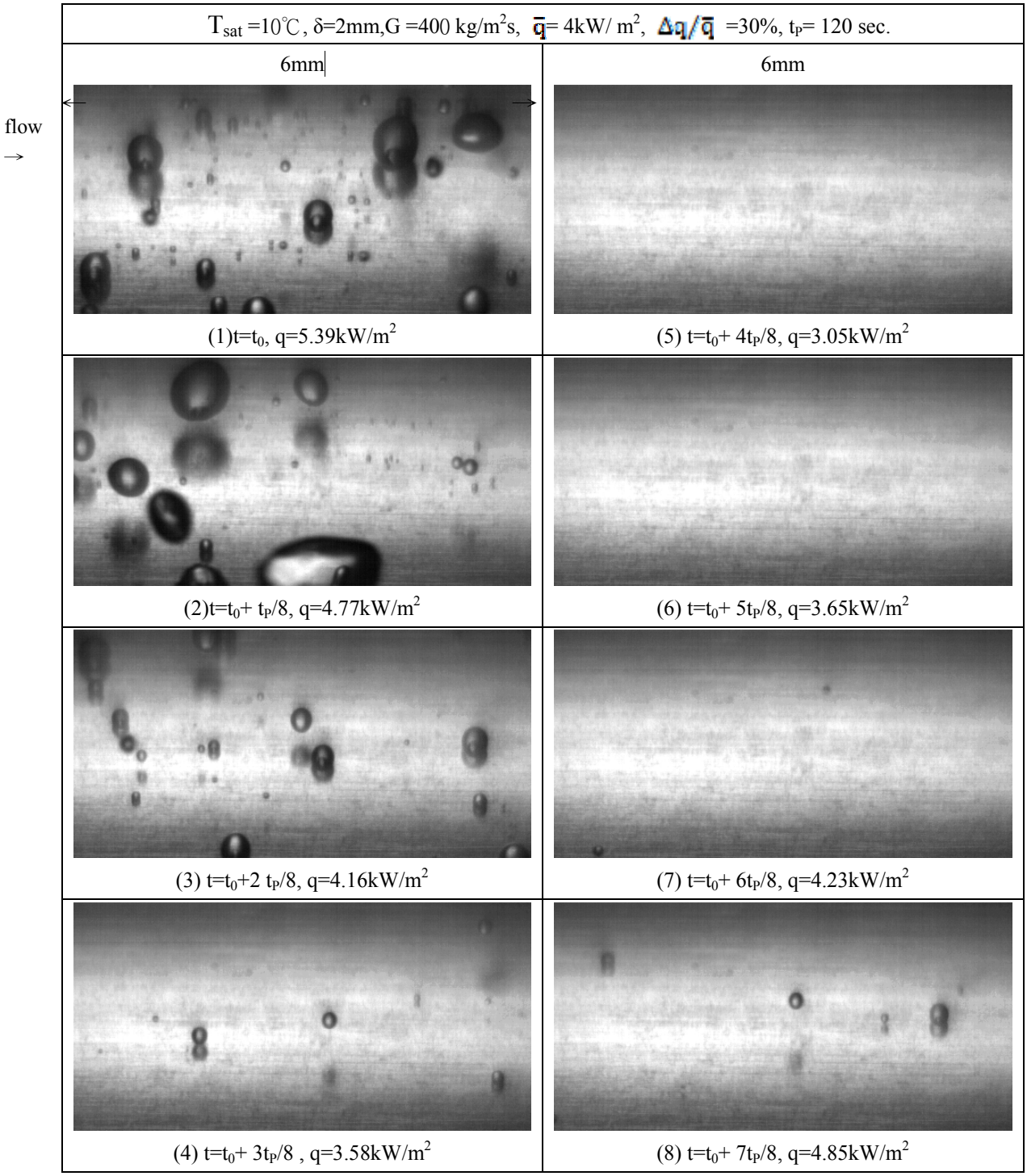


Fig. 9.30 Photos of time periodic intermittent flow boiling of R-410A at selected time instants in a typical periodic cycle at T_{sat} =10℃, G = 400 kg/m²s, δ =2.0mm and t_p= 120 sec for $\bar{q}$ = 4kW/m², $\Delta q/\bar{q}$ = 30%.

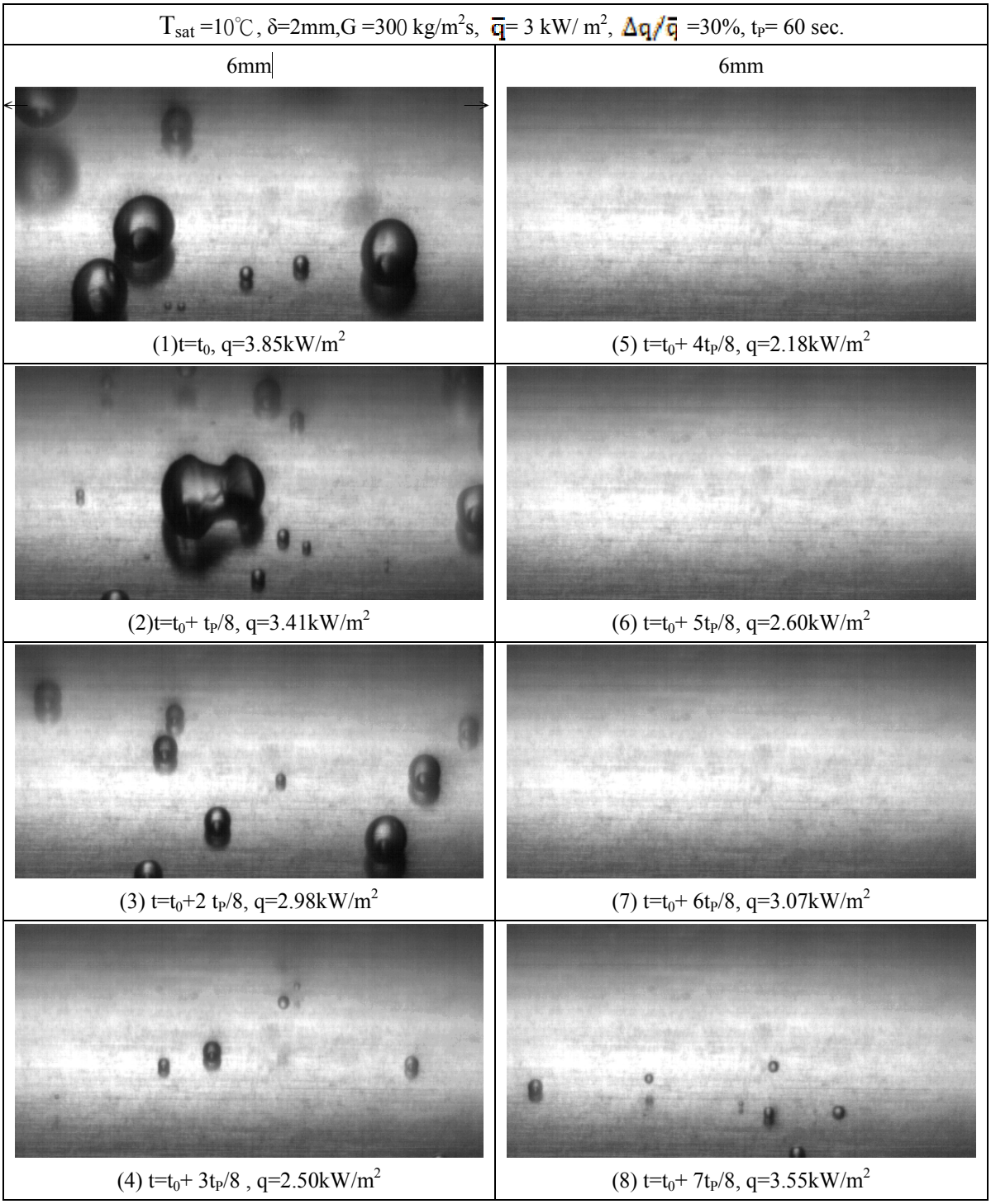


Fig. 9.31 Photos of time periodic intermittent flow boiling of R-410A at selected time instants in a typical periodic cycle at T_{sat} =10℃, G = 400 kg/m²s, δ =2.0mm and t_p= 60 sec for $\bar{q}$ = 3kW/m², $\Delta q/\bar{q}$ = 30%.

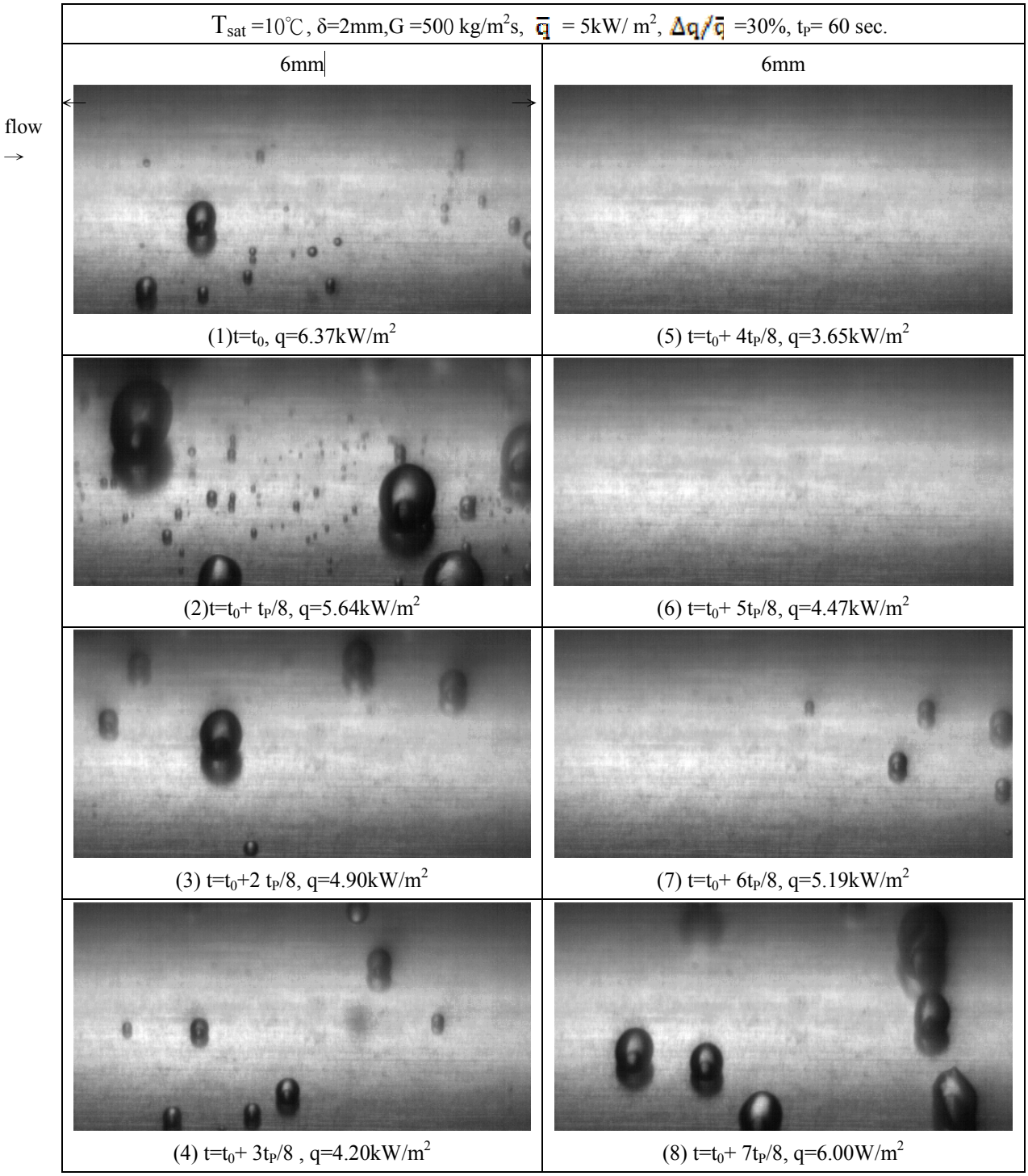


Fig. 9.32 Photos of time periodic intermittent flow boiling of R-410A at selected time instants in a typical periodic cycle at T_{sat} =10℃, G = 400 kg/m²s, δ =2.0mm and t_p= 60 sec for $\bar{q}$ = 5kW/m², $\Delta q/\bar{q}$ = 30%.

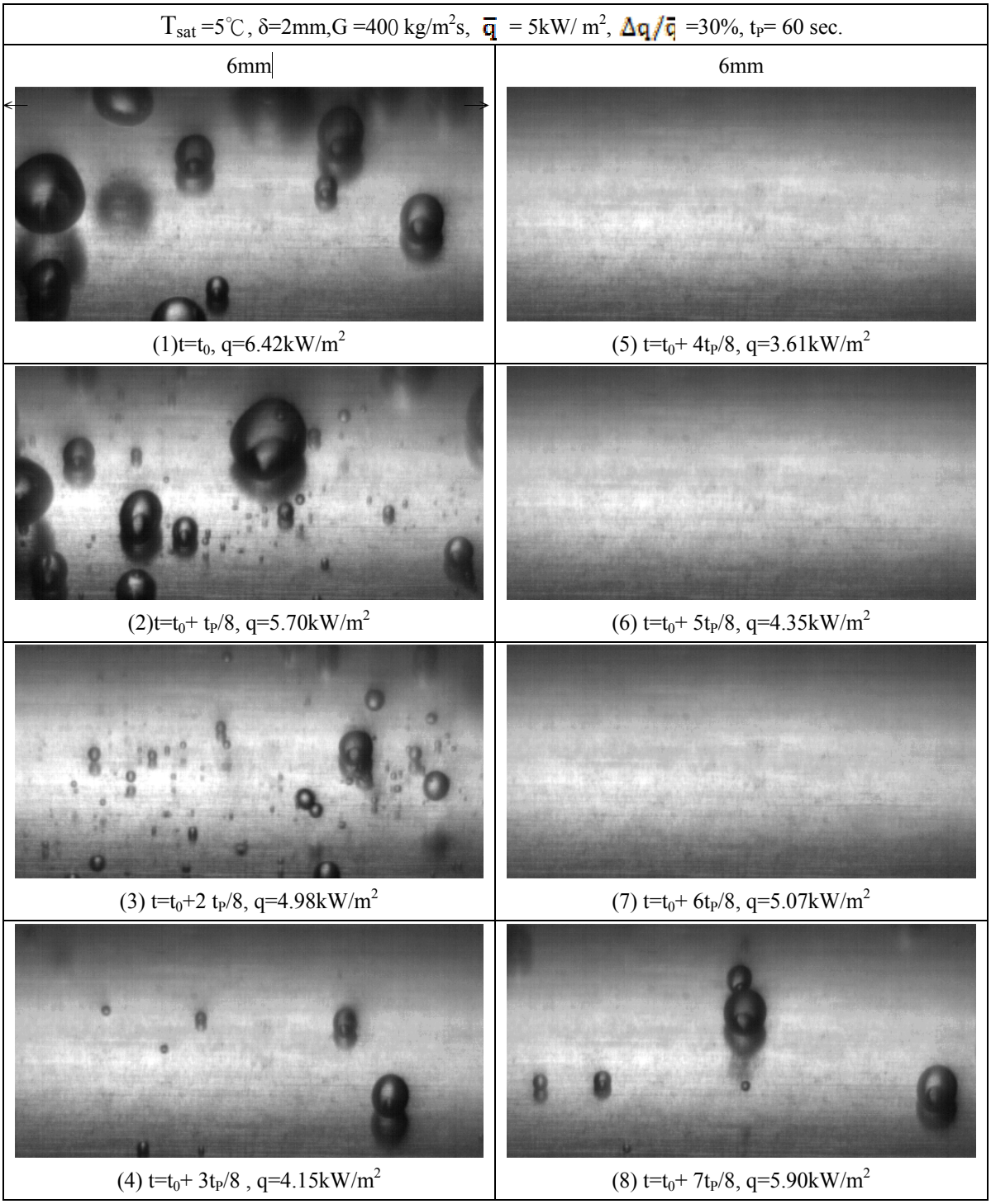


Fig. 9.33 Photos of time periodic intermittent flow boiling of R-410A at selected time instants in a typical periodic cycle at T_{sat} = 5℃, G = 400 kg/m²s, δ =2.0mm and t_p= 60 sec for $\bar{q}$ = 5kW/m², $\Delta q/\bar{q}$ = 30%.

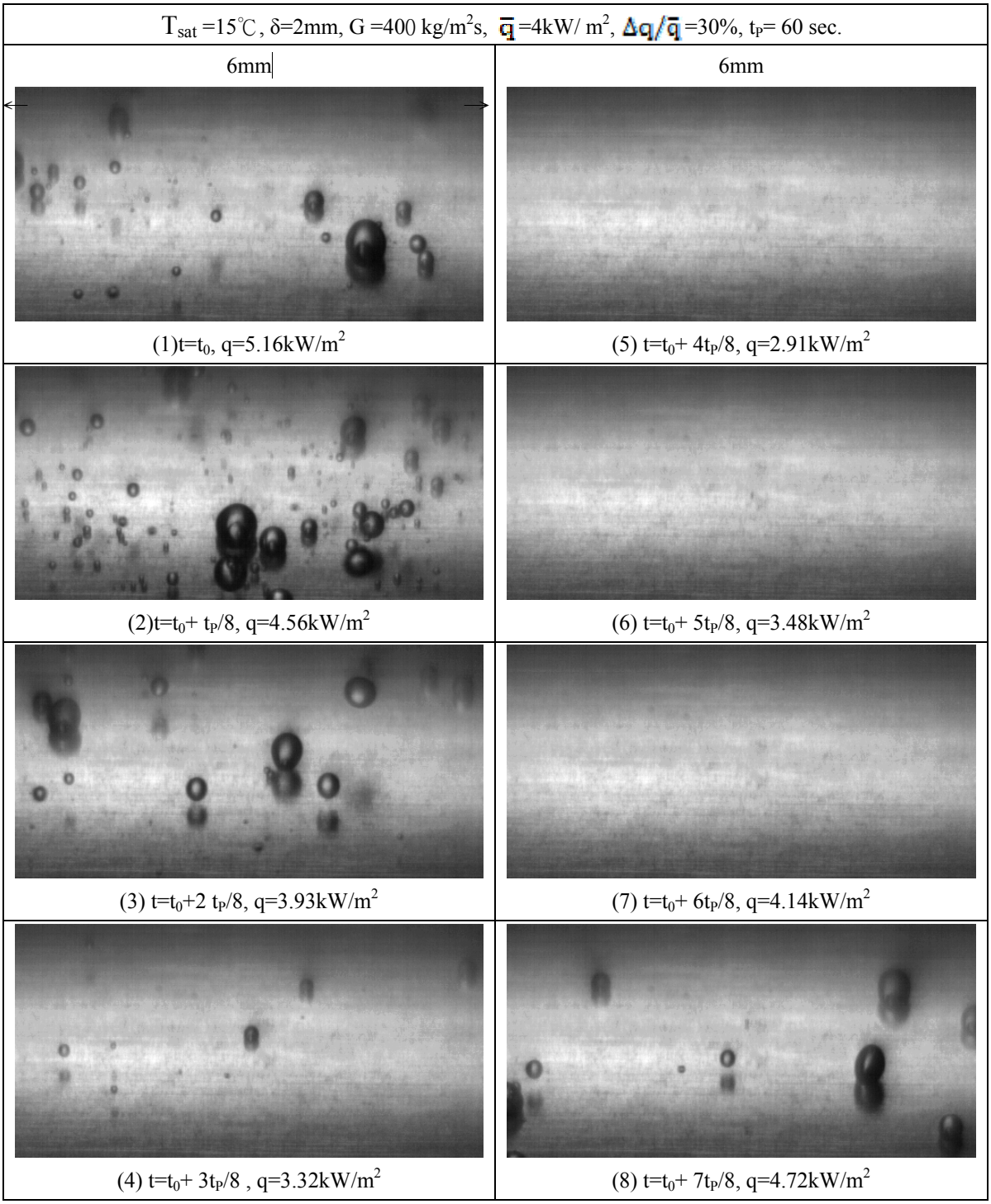


Fig. 9.34 Photos of time periodic intermittent flow boiling of R-410A at selected time instants in a typical periodic cycle at T_{sat} = 15℃, G = 400 kg/m²s, δ =2.0mm and t_p= 60 sec for $\bar{q}$ = 4kW/m², $\Delta q/\bar{q}$ = 30%.

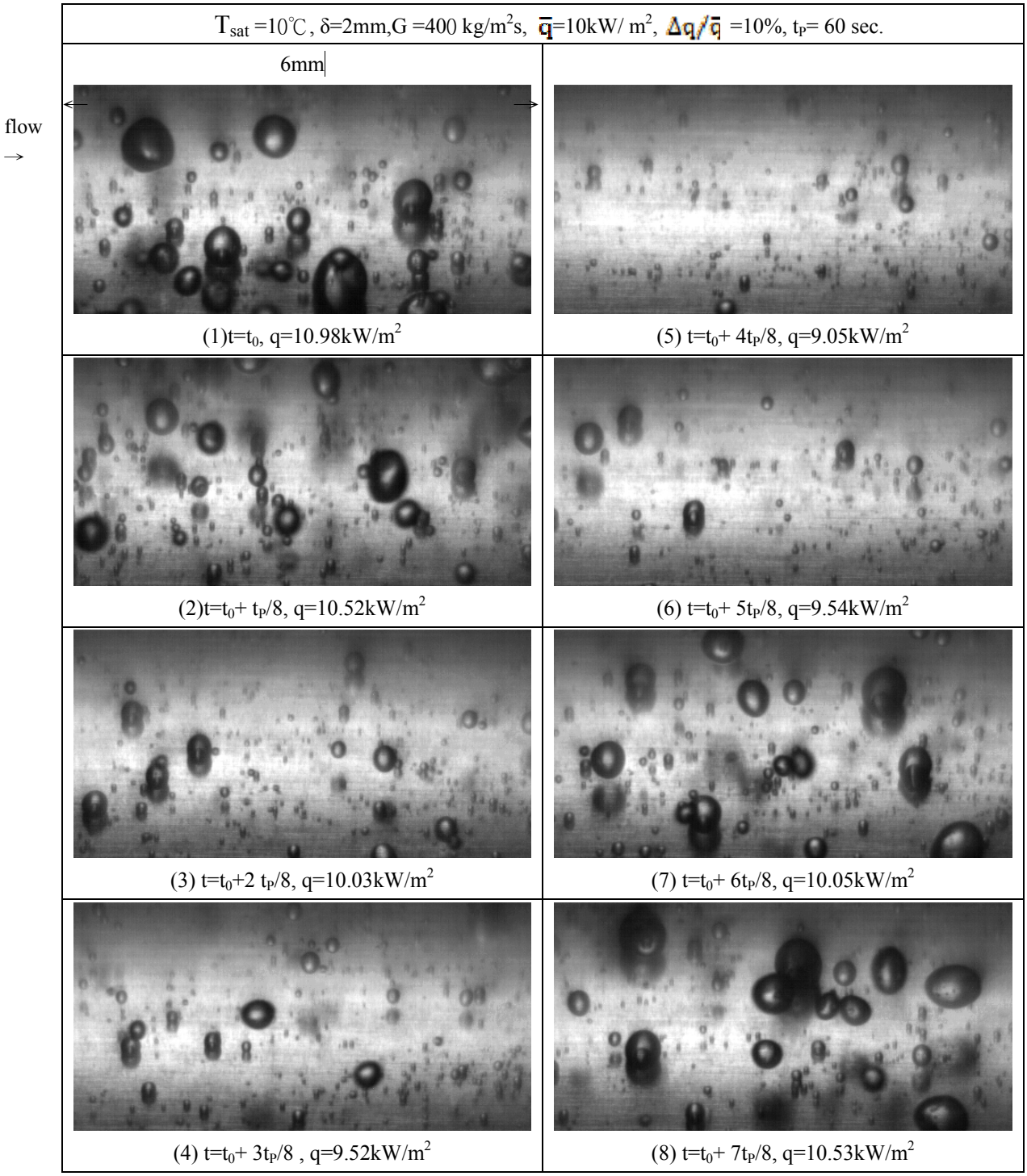


Fig. 9.35 Photos of time periodic saturated flow boiling of R-410A at selected time instants in a typical periodic cycle at T_{sat} =10℃, G = 400 kg/m²s, δ =2.0mm and t_p= 60 sec for $\bar{q}$ = 10kW/m², $\Delta q/\bar{q}$ = 10%.

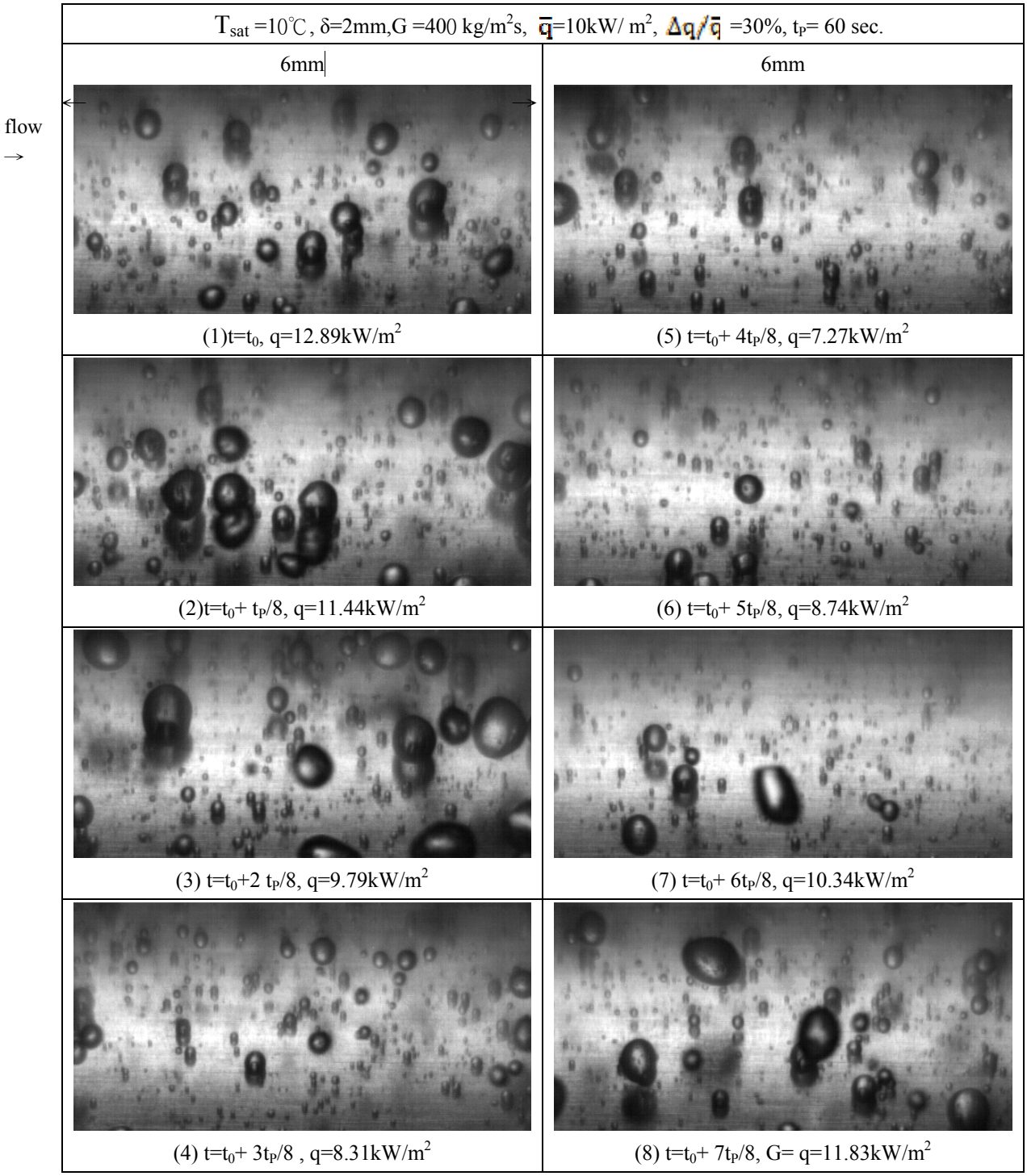


Fig. 9.36 Photos of time periodic saturated flow boiling of R-410A at selected time instants in a typical periodic cycle at T_{sat} =10℃, G = 400 kg/m²s, δ =2.0mm and t_p= 60 sec for $\bar{q}$ = 10kW/m², $\Delta q/\bar{q}$ = 30%.

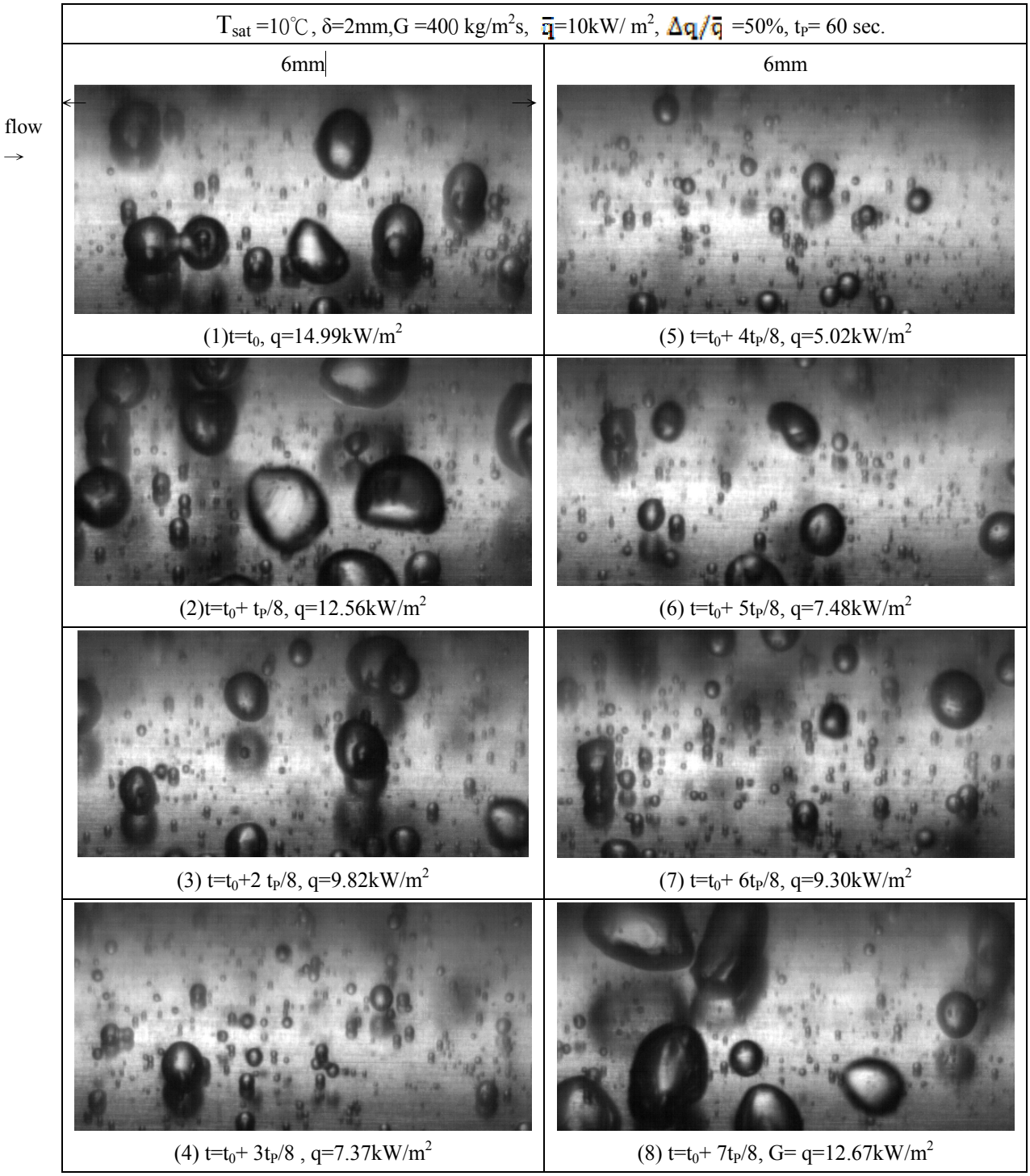


Fig. 9.37 Photos of time periodic saturated flow boiling of R-410A at selected time instants in a typical periodic cycle at T_{sat} =10℃, G = 400 kg/m²s, δ =2.0mm and t_p= 60 sec for $\bar{q}$ = 10kW/m², $\Delta q/\bar{q}$ = 30%.

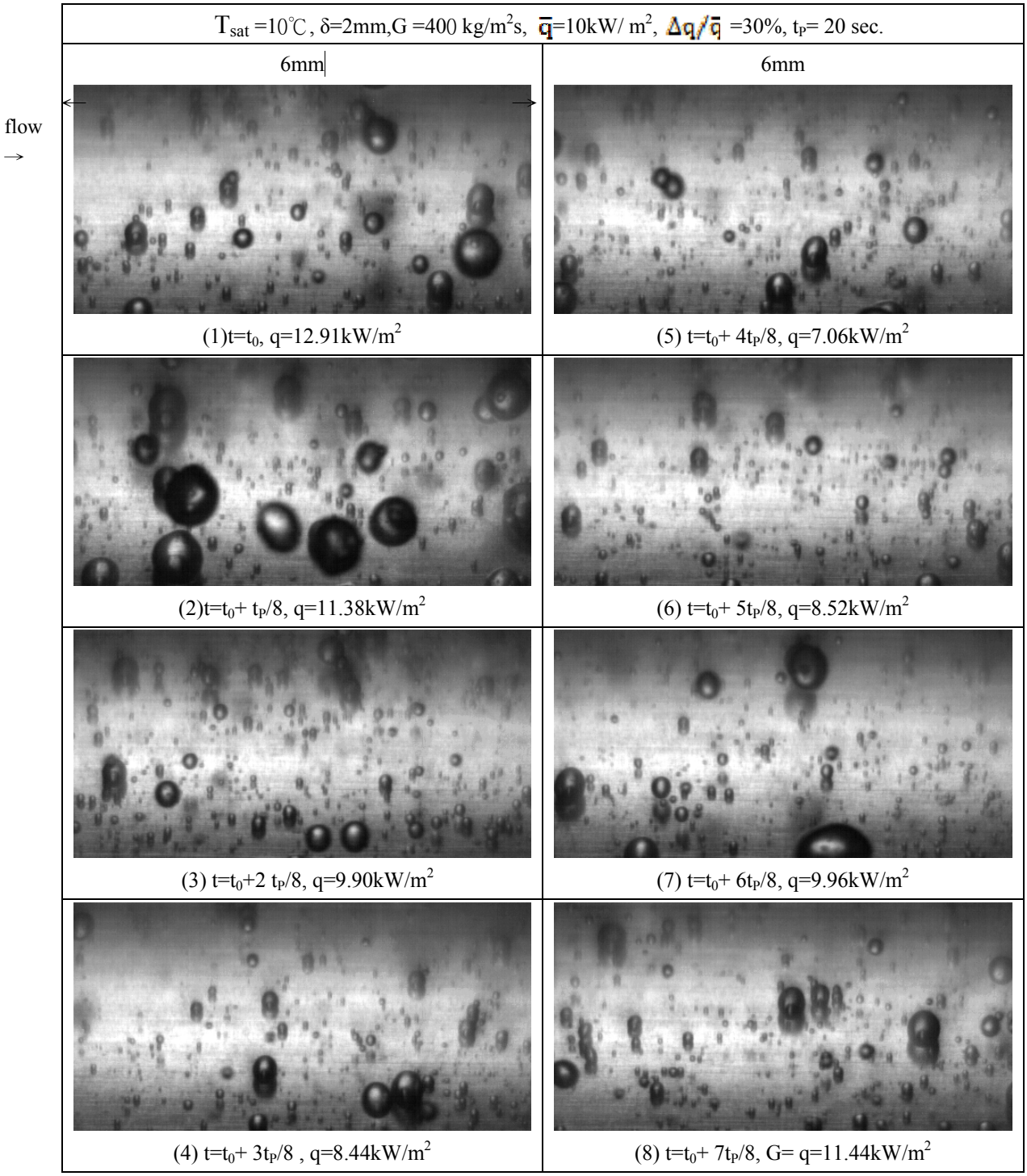


Fig. 9.38 Photos of time periodic saturated flow boiling of R-410A at selected time instants in a typical periodic cycle at T_{sat} =10℃, G = 400 kg/m²s, δ =2.0mm and t_p= 20 sec for $\bar{q}$ = 10kW/m², $\Delta q/\bar{q}$ = 30%.

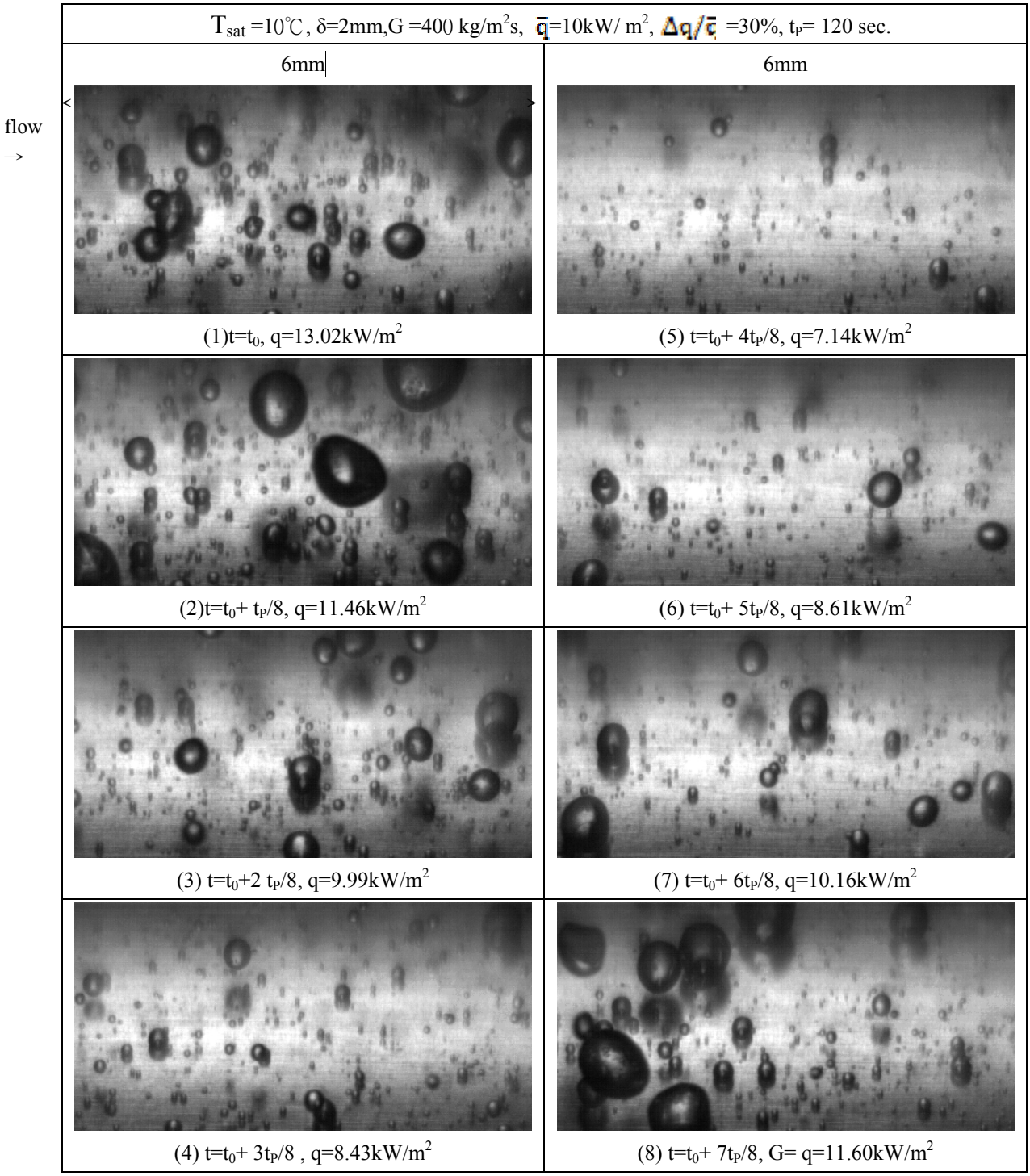


Fig. 9.39 Photos of time periodic saturated flow boiling of R-410A at selected time instants in a typical periodic cycle at T_{sat} =10℃, G = 400 kg/m²s, δ =2.0mm and t_p= 120 sec for $\bar{q}$ = 10kW/m², $\Delta q/\bar{q}$ = 30%.

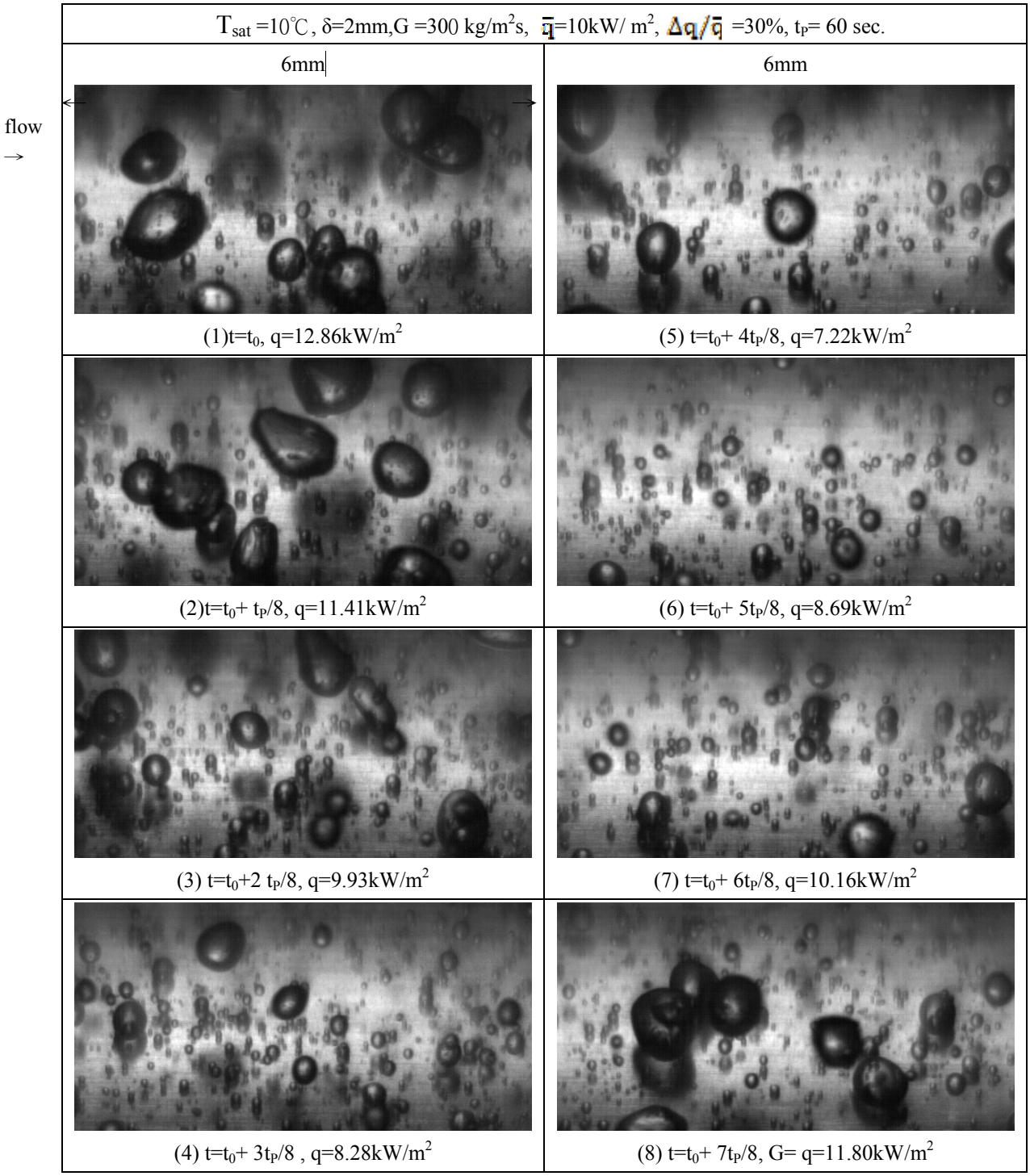


Fig. 9.40 Photos of time periodic saturated flow boiling of R-410A at selected time instants in a typical periodic cycle at T_{sat} =10℃, G = 300 kg/m²s, δ =2.0mm and t_p= 60sec for $\bar{q}$ = 10kW/m², $\Delta q/\bar{q}$ = 30%.

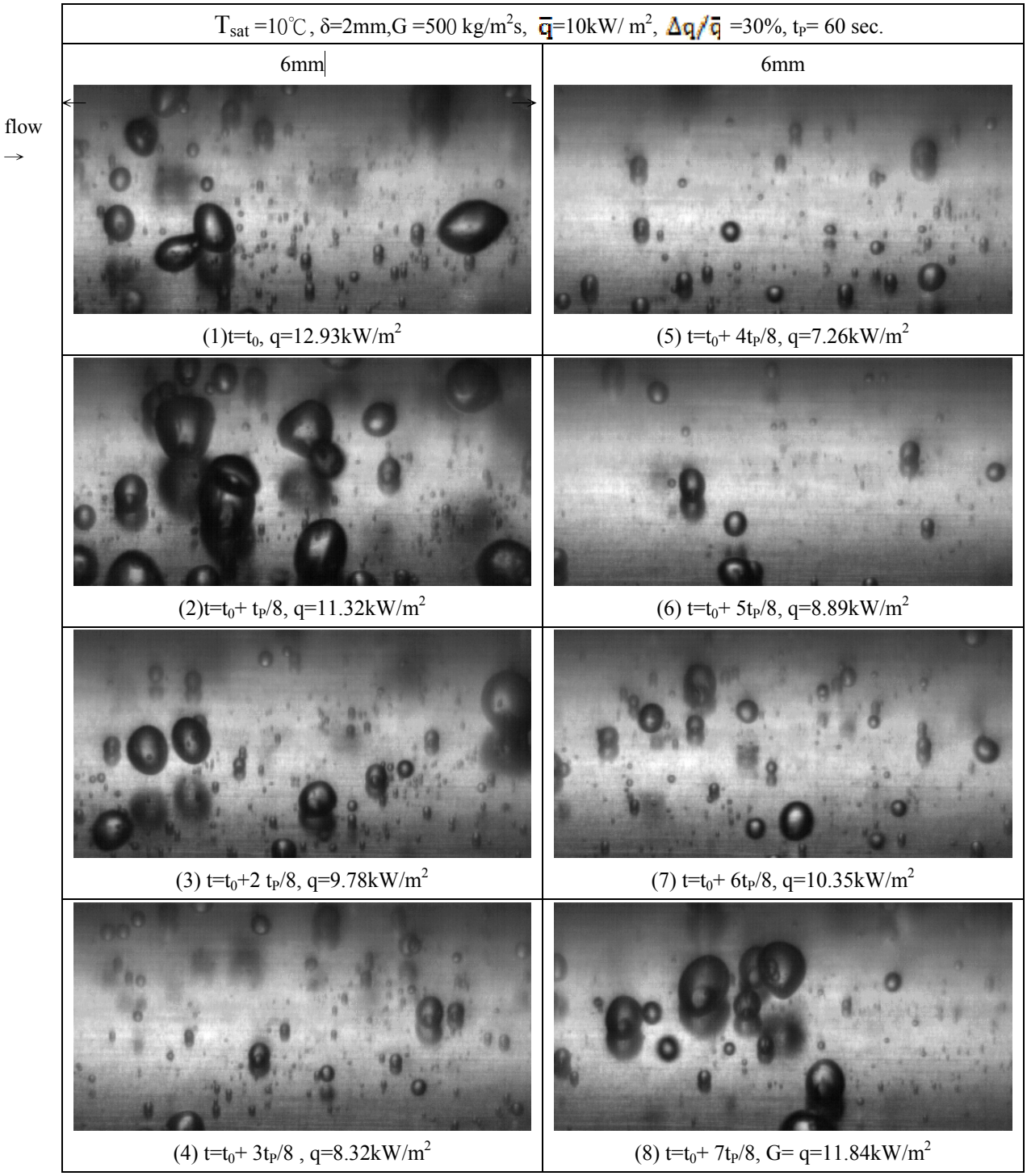


Fig. 9.41 Photos of time periodic saturated flow boiling of R-410A at selected time instants in a typical periodic cycle at T_{sat} =10℃, G = 500 kg/m²s, δ =2.0mm and t_p= 60sec for $\bar{q}$ = 10kW/m², $\Delta q/\bar{q}$ = 30%.

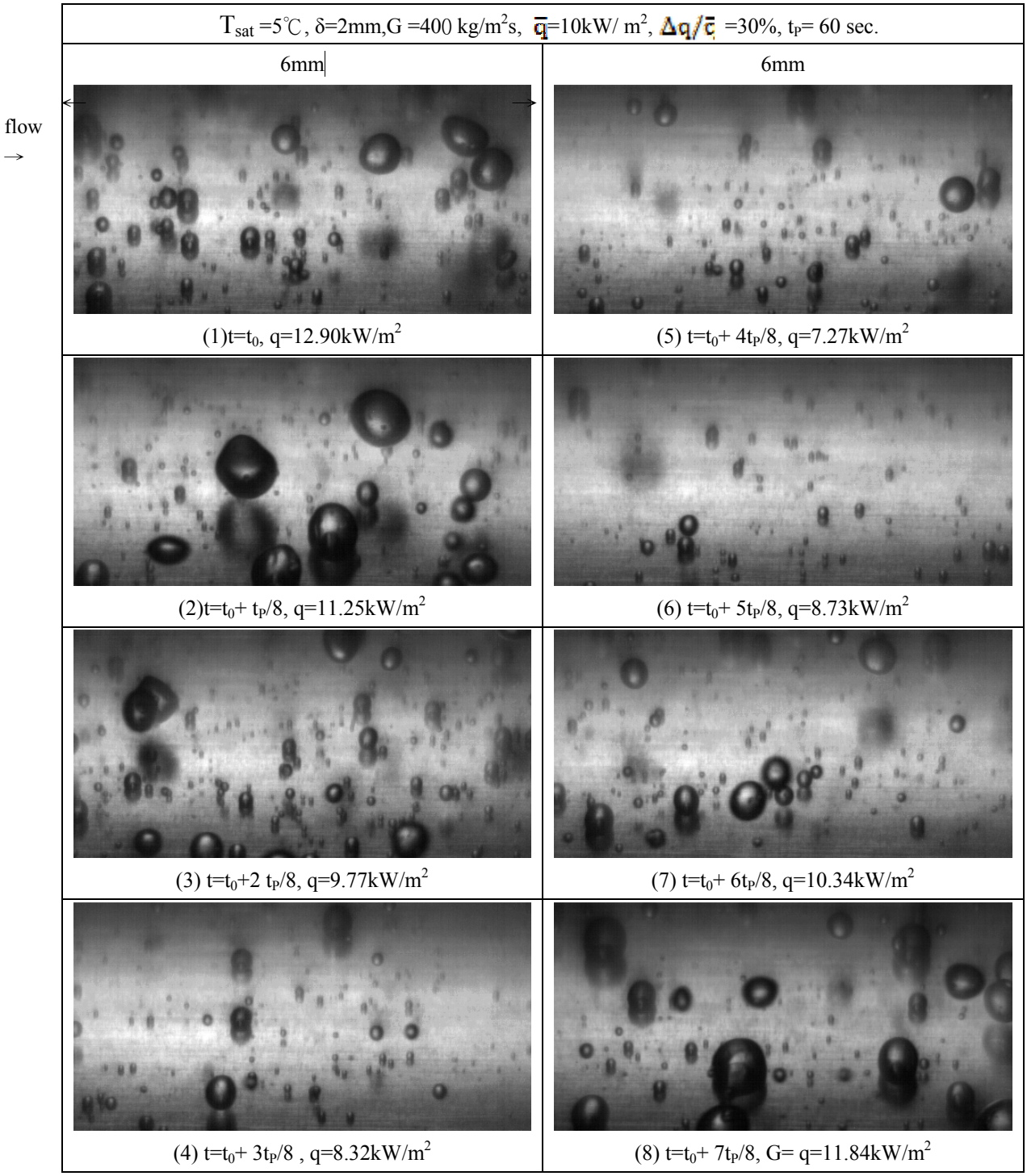


Fig. 9.42 Photos of time periodic saturated flow boiling of R-410A at selected time instants in a typical periodic cycle at T_{sat} = 5℃, G = 400 kg/m²s, δ =2.0mm and t_p= 60sec for $\bar{q}$ = 10kW/m², $\Delta q/\bar{q}$ = 30%.

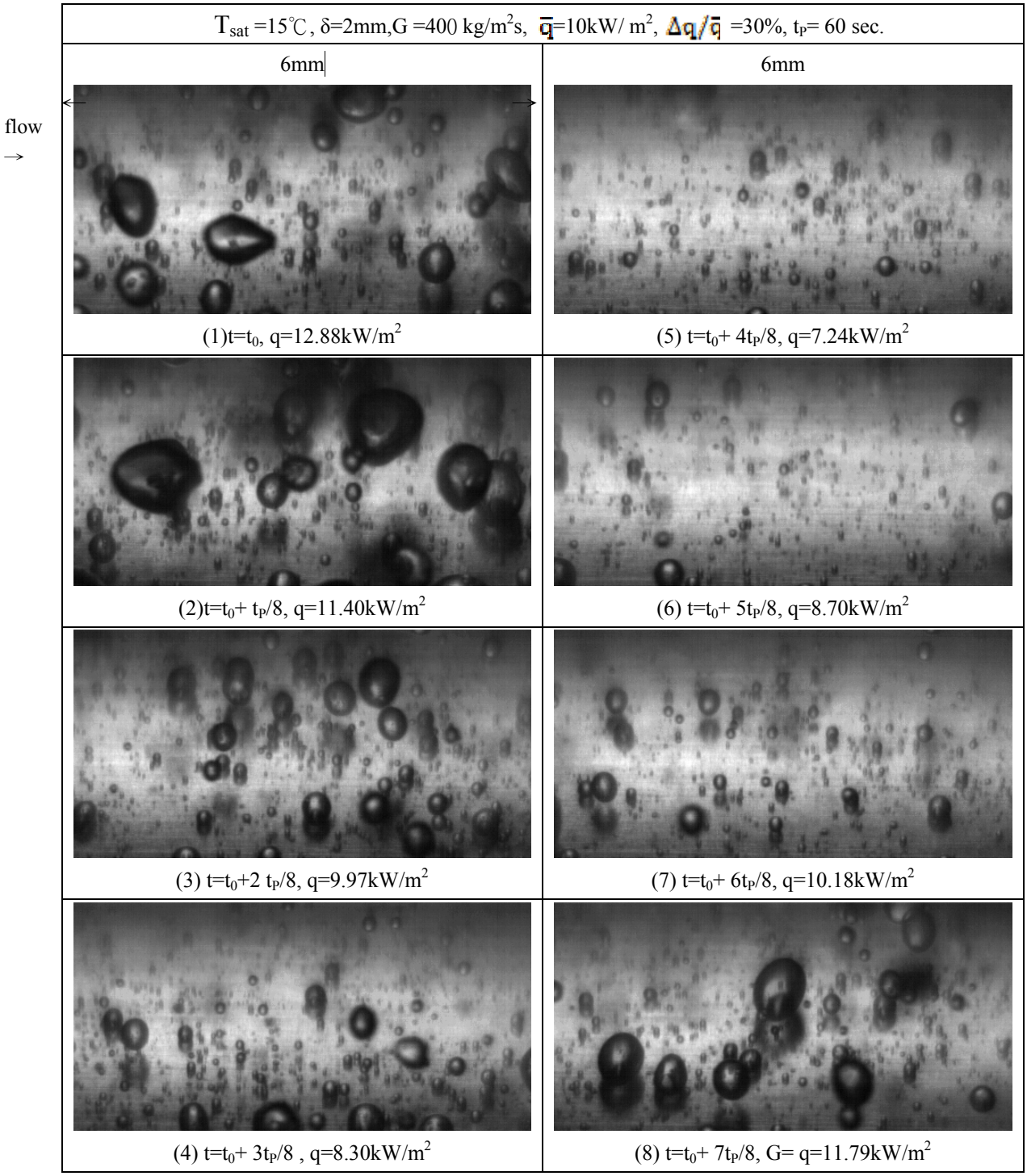


Fig. 9.43 Photos of time periodic saturated flow boiling of R-410A at selected time instants in a typical periodic cycle at T_{sat} =15℃, G = 400 kg/m²s, δ =2.0mm and t_p= 60sec for $\bar{q}$ = 10kW/m², $\Delta q/\bar{q}$ = 30%.

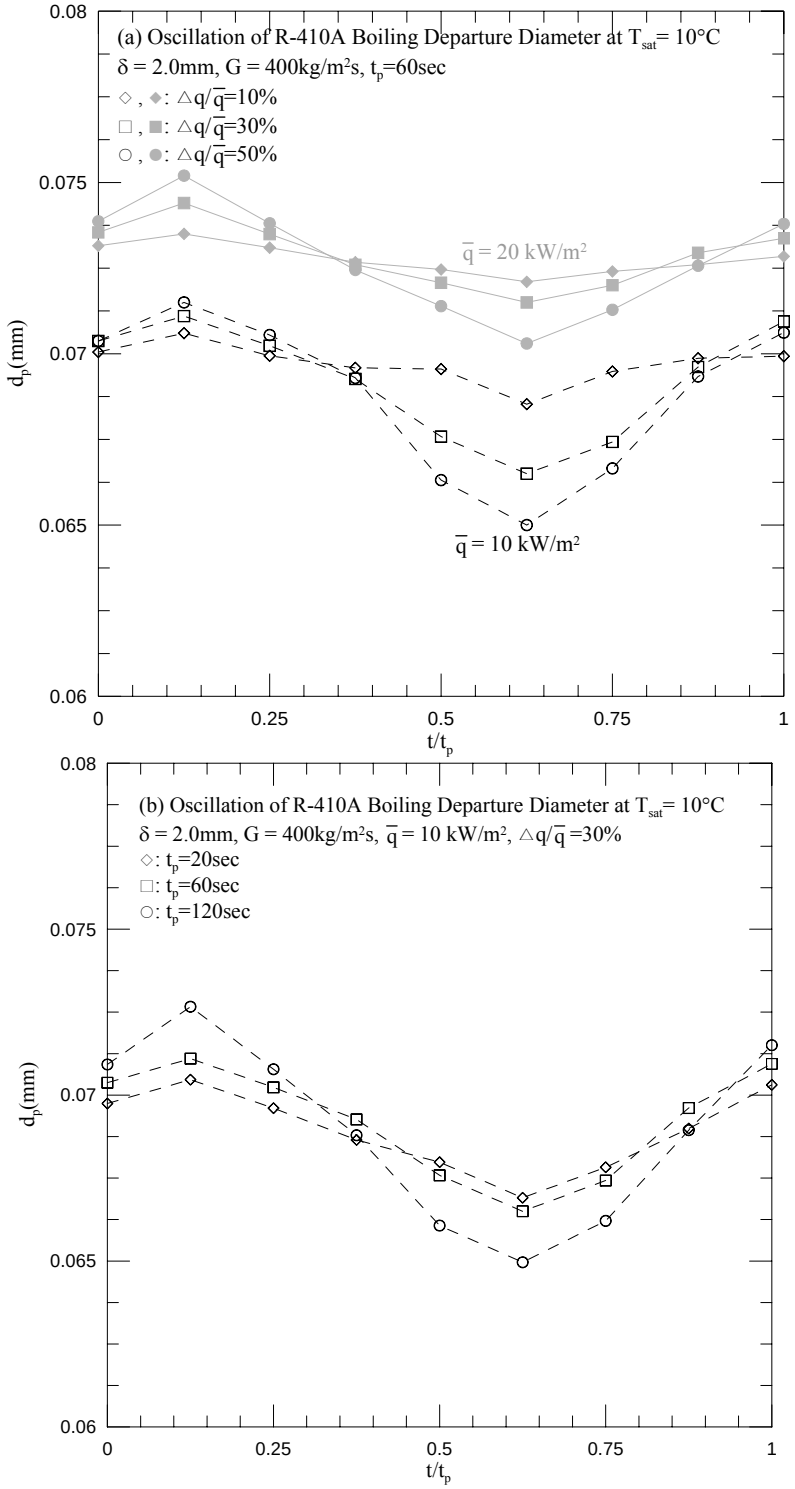


Fig. 9.44 Time variations of mean bubble departure diameter in time periodic saturated flow boiling of R-410A for $\bar{q} = 10\,\mathrm{kW/m^2}$ at $T_{sat} = 10\,^{\circ}\mathrm{C}$, G = 400 kg/m²s and δ =2.0mm for (a) various $\Delta q/\bar{q}$ at t_p = 60 sec and (b) various t_p at $\Delta q/\bar{q}$ = 30%.

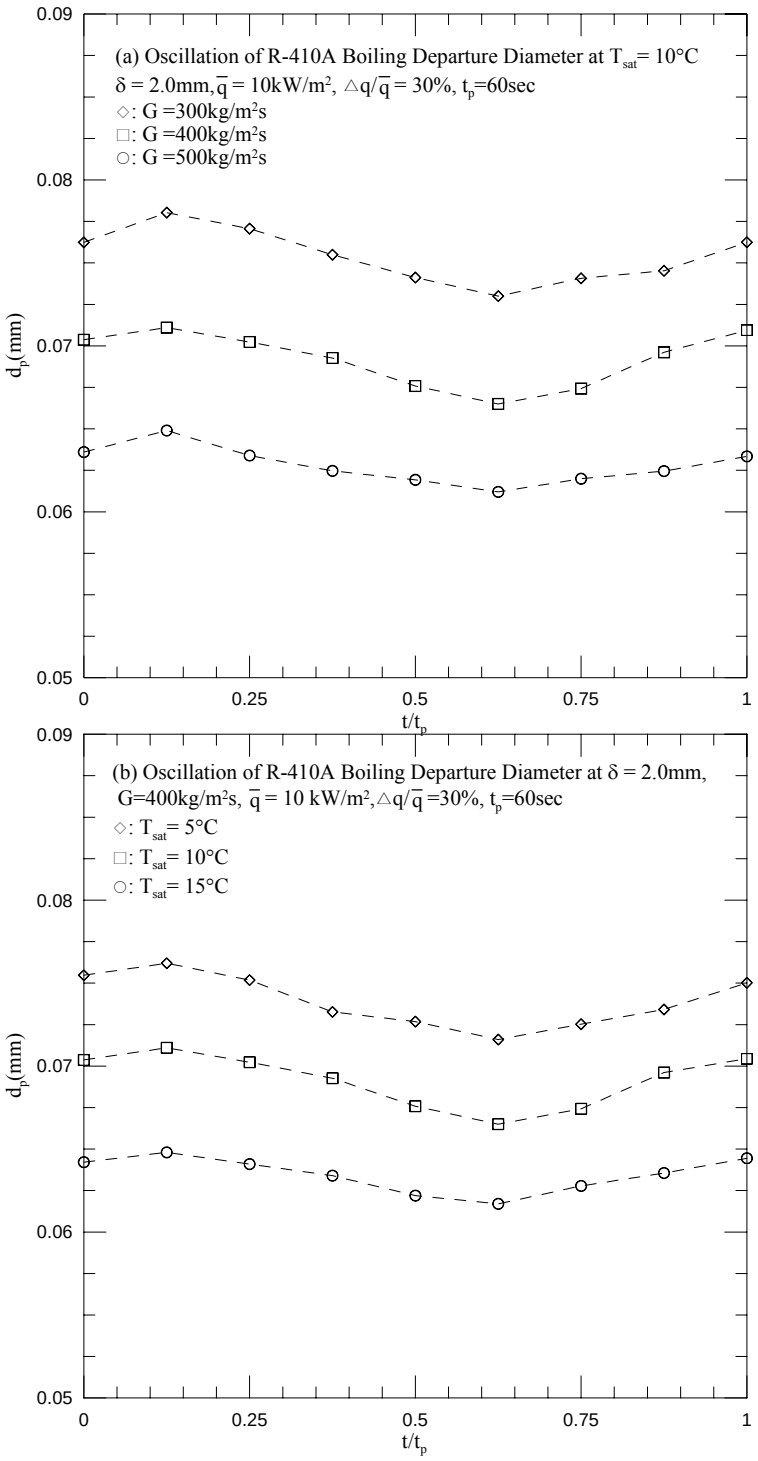


Fig. 9.45 Time variations of mean bubble departure diameter in time periodic saturated flow boiling of R-410A for $\bar{q}$ = 10 kW/m^2 at $\Delta q/\bar{q}$ = 30%, t_p = 60 sec and δ =2.0mm for (a) various G at T_{sat} = 10 °C and (b) various T_{sat} at G = 400 kg/m^{2}s.

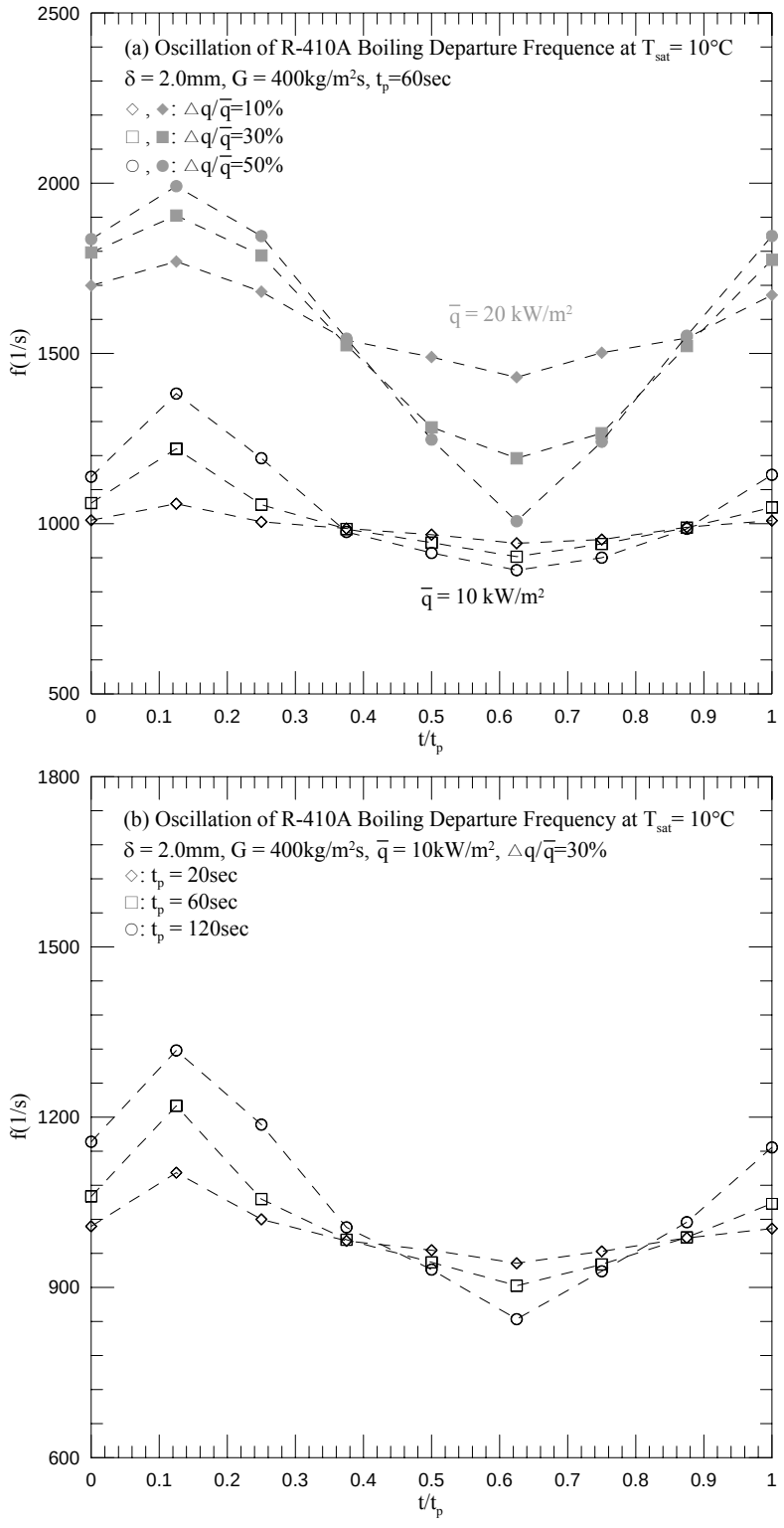


Fig. 9.46 Time variations of mean bubble departure frequency in time periodic saturated flow boiling of R-410A for $\bar{q} = 10\,kW/m^2$ at T_{sat}=10 °C , G = 400 kg/m^{2}s and δ =2.0mm for (a) various $\Delta q/\bar{q}$ at t_p = 60 sec and (b)

various t_p at $\Delta q/\bar{q}$ = 30%.

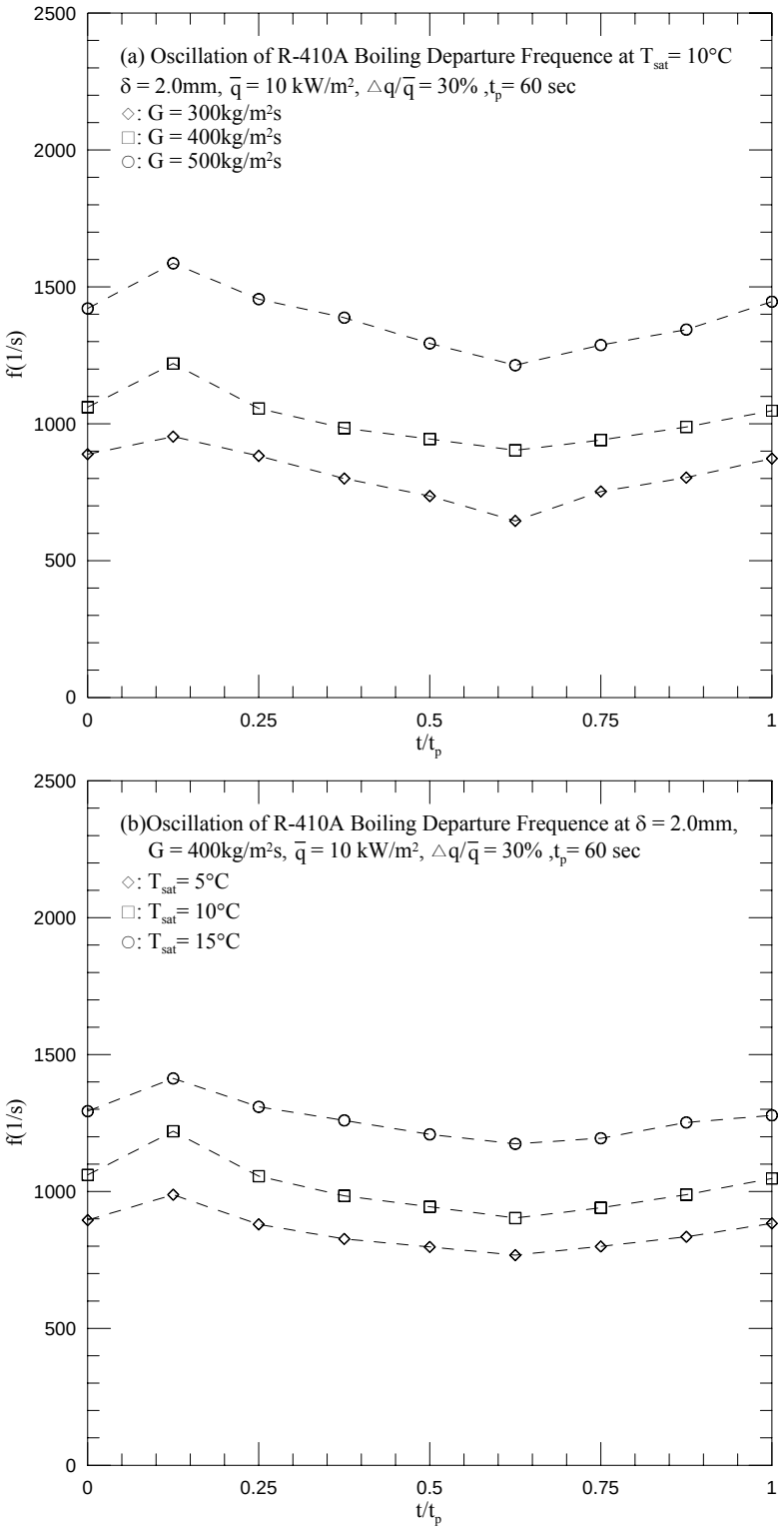


Fig. 9.47 Time variations of mean bubble departure frequency in time periodic saturated flow boiling of R-410A for $\bar{q}$ = 10 kW/m^2 at $\Delta q/\bar{q}$ = 30%,

t_p = 60 sec and δ =2.0mm for (a) various G at T_{sat} = 10 °C and (b) various T_{sat} at G = 400 kg/m^{2}s.

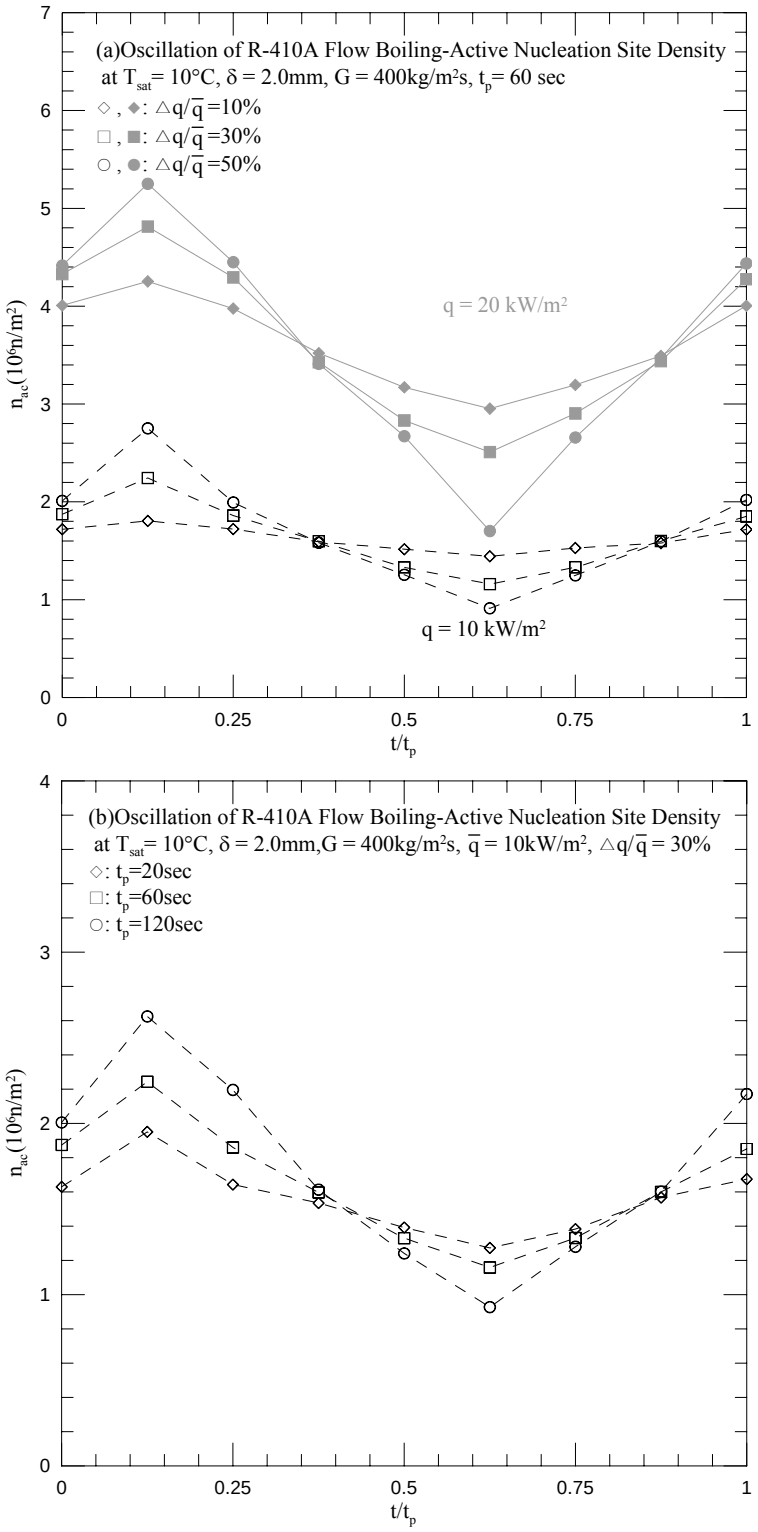


Fig. 9.48 Time variations of mean active nucleation site density in time periodic saturated flow boiling of R-410A for $\bar{q}$ = 10 kW/m^2 at T_{sat} =10 °C , G =

400 kg/m^{2}s and δ =2.0mm for (a) various $\Delta q/\bar{q}$ at t_p = 60 sec and (b) various t_p at $\Delta q/\bar{q}$ = 30%.

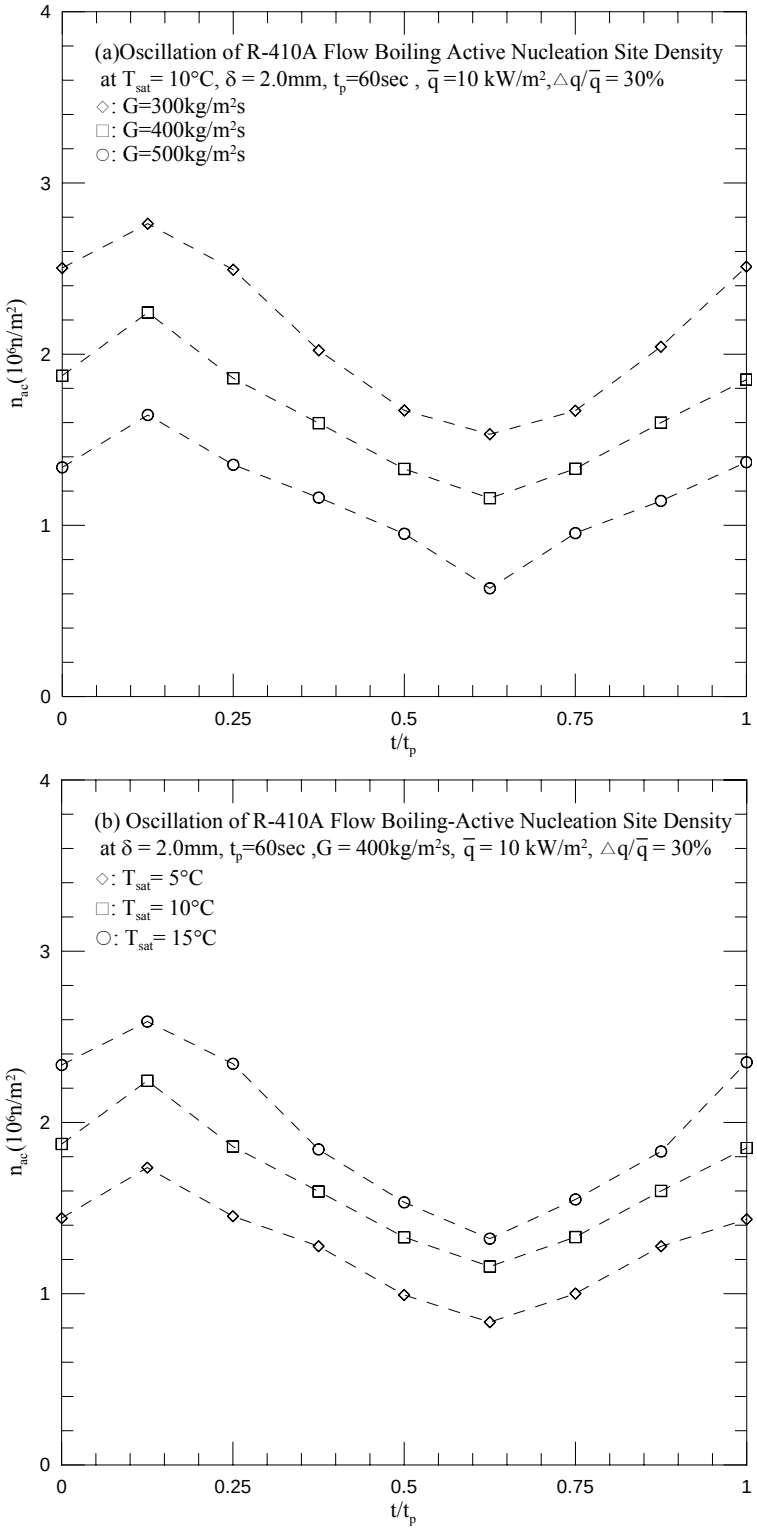


Fig. 9.49 Time variations of mean bubble departure frequency in time periodic saturated flow boiling of R-410A for $\bar{q}$ = 10 kW/m^2 at $\Delta q/\bar{q}$ = 30%,

t_p = 60 sec and δ =2.0mm for (a) various G at T_{sat} = 10 °C and (b) various T_{sat} at G = 400 kg/m^{2}s.

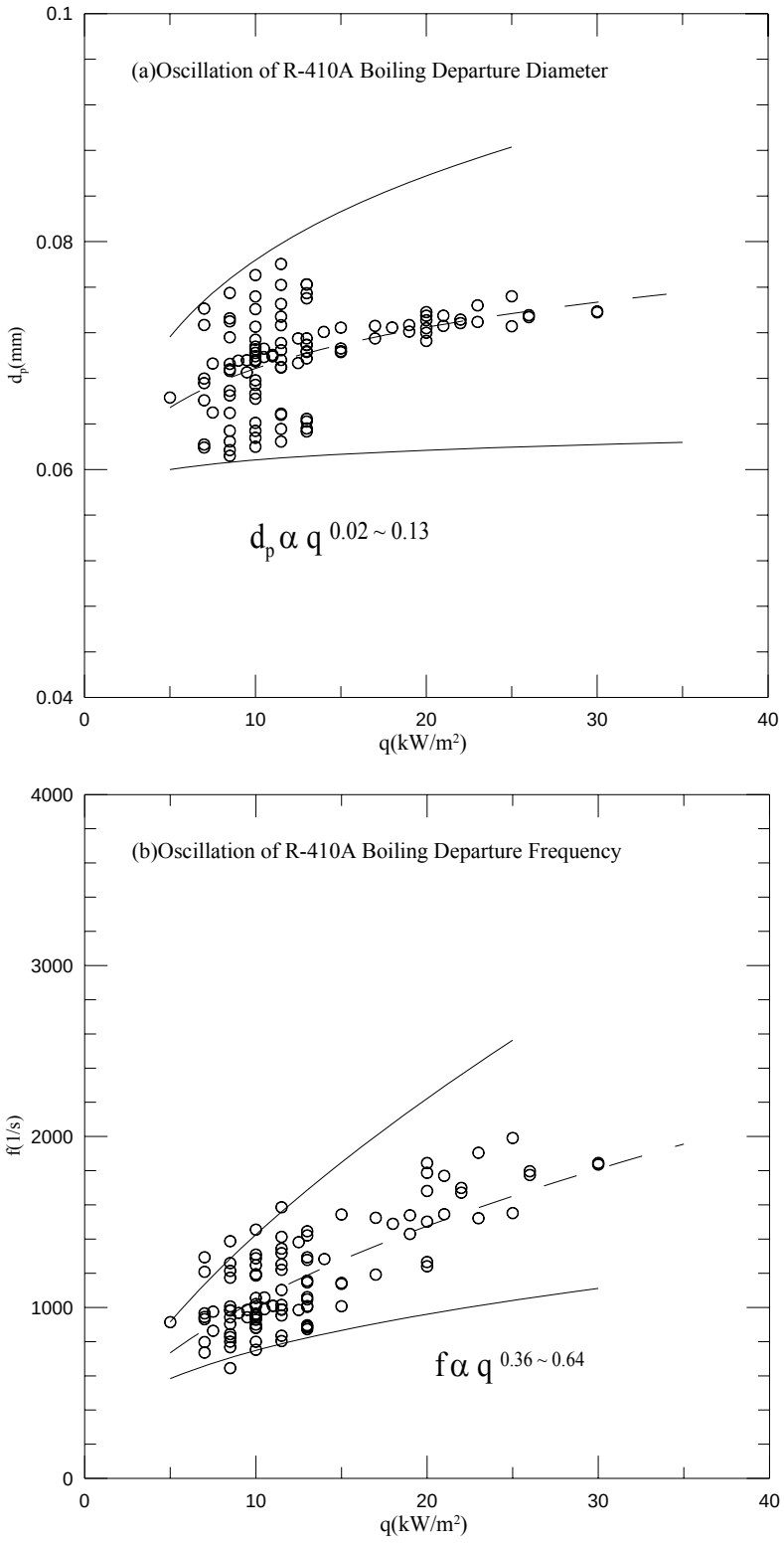


Fig. 9.50 Variations of bubble departure diameter (a), departure frequency (b), and active nucleation site density (c) with heat flux for time-periodic

saturated flow boiling of R-410A.

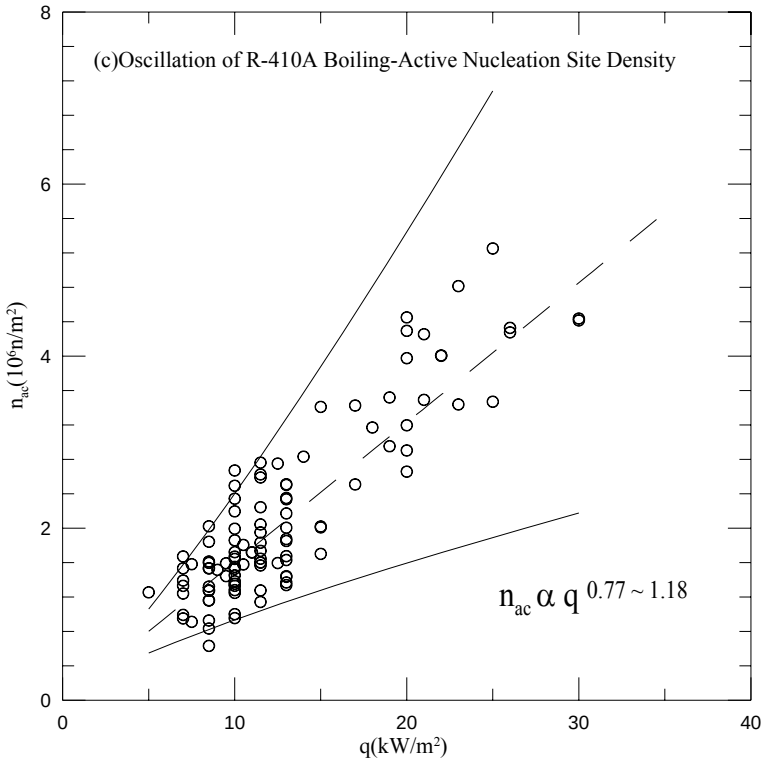


Fig. 9.50 continued

CHAPTER 11

TRANSIENT OSCILLATORY SATURATED FLOW BOILING OF FC-72 OVER A SMALL HEATED COPPER PLATE

The experimental results obtained in the first part of this study are presented here to illustrate how the imposed heat flux oscillation in the form of rectangular waves affects the transient oscillatory saturated flow boiling heat transfer of FC-72 over the small heated circular copper flat plate flush mounted on the bottom of a horizontal rectangular channel. The present experiments are carried out for the FC-72 mass flux G fixed at 300 and 400 kg/m^2s for the time-average imposed heat flux $\bar{q}$ varied from 0.1 W/cm^2 to 10 W/cm^2. Besides, the amplitude of the heat flux oscillation $\triangle q$ is set at 10%, 30% and 50% of the average heat flux. In addition, the period of the heat flux oscillation t_p is fixed at 10, 20 and 30 seconds. The coolant FC-72 in the test section is at a slightly subatmospheric pressure of 99KPa with T_{sat}=55 °C. In the following , the effects of the experimental parameters including G, $\bar{q}$, $\triangle q/\bar{q}$ and t_p on the transient FC-72 saturated flow boiling heat transfer performance will be examined in detail. The heat transfer performance is presented mainly in terms of the time variations of the space-average surface temperature of the copper plate and the space-average boiling heat transfer coefficient. The conduction time scale t_1 is estimated by considering a slab of the characteristic length L_c (thickness) subject to a constant heat input at one of its surface at certain time instant and t_1 is the duration for the other surface to begin to feel the heat input. According the thermal diffusion speed, $t_1 \approx L_c^2/\alpha_w$. The time scale for bubble growth or departure is t_2 which can be approximated by $d_p/[\frac{\sigma g(\rho_l-\rho_v)}{\rho_l^2}]^{\frac{1}{4}}$. Finally, the time constant of the present boiling on the copper surface t_c is obtained by measuring T_w for both single-phase and boiling conditions. The results are shown in Figs. 11.135 for a step increase in the imposed heat flux and

increase in the mass flux.

11.1 Single-phase Liquid Convective Heat Transfer

Before beginning the two-phase flow boiling experiments, steady single-phase convective heat transfer experiments are conducted for liquid FC-72 flow over the copper plate heated by a constant heat flux in the rectangular channel. The measured space-average heat transfer coefficient for single-phase convection from the heated copper surface to the coolant is compared with the correlation proposed by Gersey and Mudawar [6]. Their correlation is

$$\overline{Nu}_L = 0.362 \cdot Re_L^{0.614} \cdot Pr^{1/3} \tag{11.1}$$

where

$$Re_L = \frac{G \cdot L}{\mu_l} \tag{11.2}$$

$$\bar{h}_{l\varphi} = \frac{K_l}{L} \overline{Nu}_L \tag{11.3}$$

Their correlation is based on the experimental data procured from the same liquid and same flow configuration as the present data and the comparison is shown in Fig. 11.1 for the dimensional and dimensionless heat transfer coefficients. The results indicate that our data are in good agreement with their correlation.

It should be mentioned that all of the working fluid properties used in reducing the data for Fig. 11.1 from Equations (11.1) – (11.3) are calculated at the coolant inlet temperature. The copper plate diameter is chosen as the characteristic length in defining the Reynolds number Re_L and average Nusselt number $\overline{Nu}_L$ because of its significant effect on the heat transfer performance [6].

11.2 Stable and Time-average Saturated Flow Boiling Curves and Heat Transfer Coefficient

It is of interest to compare the time-average data deduced from the present transient flow boiling heat transfer measurement with that from the stable flow boiling in which the imposed heat flux does not vary with time. The results from this comparison are shown in Figs. 11.2 - 11.6 by presenting the boiling curves for various G, $\triangle q/\overline{q}$ and t_p. Note that for each stable boiling curve at a given coolant mass flux the mean temperature of the copper plate increases with the imposed heat flux. When the imposed heat flux is increased gradually to a certain value, the temperature of the copper plate is slightly higher than T_{sat} but no bubble nucleation on the heated copper plate is observed. Heat transfer in the flow completely results from single-phase forced convection. A continuing increase of the heat flux to a certain higher value, the boiling curve is characterized by a sharp increase in the surface heat flux for a small rise in the temperature of the copper surface when the bubbles begin to appear on the copper surface. We define this phenomenon as onset of nucleate boiling (ONB). The reason causing the sharp increase in the slope of the boiling curve is due to a significant increase in the surface heat transfer by the boiling processes when ONB occurs. It is also noted from the stable and time-average boiling curves that beyond ONB the coolant mass flux only has slight effects on the boiling curves, suggesting that the surface heat transfer is mainly dominated by the fully developed nucleate boiling. Besides, at a higher G the required heat flux for ONB is higher and this implies that more energy is needed for the vapor to nucleate from the heated plate since the residence time of the coolant on the heated surface is shorter. The results also suggest that the time-average boiling curves are not noticeably affected by the amplitude and period of the heat flux oscillation. A close inspection of the boiling curves, however, reveals that for the time varying imposed heat flux a slightly higher q_{ONB} is required to

initiate bubble nucleation.

The results for the variations of the time-average $\bar{h}_{2\phi,sat}$ with the time-average surface heat flux presented in Figs. 11.7-11.11 manifest that the heat flux oscillation amplitude and period show negligible influences on the time-average flow boiling heat transfer coefficients. However, for a given coolant mass flux the time-average boiling heat transfer coefficient increases substantially with the mean imposed heat flux.

11.3 Transient Saturated Flow Boiling Heat Transfer Characteristics

The transient boiling heat transfer characteristics for the FC-72 flow over the heated copper plate resulting from the imposed temporal heat flux oscillation are illustrated by presenting the time variations of the space-average heated surface temperature T_w and heat transfer coefficient $h_{2\phi}$ for various G, $\bar{q}$, $\triangle q/\bar{q}$ and t_p. First, the measured time variations of T_w for the limiting cases of constant G and q are shown in Fig. 11.12. These data indicate that the fluctuations of the average heated surface temperature with time for various $\bar{q}$ are relatively small. The saturated boiling in the flow for $\triangle q=0$ can be regarded as at a statistically stable state.

Next, the measured heat transfer data for the cases with the imposed heat flux oscillating noticeably in time are examined. The results given in Figs. 11.13–11.21 for G=300 kg/m^{2}s indicate that significant temporal oscillations in the space-average heated surface temperature occur even at a small amplitude of the heat flux oscillation with $\triangle q/\bar{q} = \pm 10\%$. For clear illustration the measured imposed heat flux oscillations with time are also shown in these figures. Note that the temporal oscillation of the heated surface temperature is more or less like a sinusoidal wave and it is also periodic in time and is at the same frequency as the imposed heat flux oscillation. Besides, at a higher mean imposed heat flux, the heated surface temperature oscillation is stronger for the

same $\triangle q/\overline{q}$ for a short t_p of 10 and 20 seconds. However, at a longer t_p of 30 seconds the amplitude of the heated surface temperature oscillation varies non monotonically with the mean imposed heat flux(Figs. 11.19-11.21). Moreover, the heated surface temperature oscillates in a larger amplitude for a larger $\triangle q/\overline{q}$ and/or a longer t_p. It should be mentioned here that even for the single-phase forced convection with $\overline{q} < \overline{q}_{ONB}$ the heated surface temperature exhibits some temporal oscillation. A close inspection of the data shown in Figs. 11.13-11.21 further reveals that the temporal increase of T_w following the step rise in the imposed heat flux experiences some delay. And the delay is slightly longer for a lower mean imposed heat flux, suggesting the response of the heated plate temperature to a step change in q is faster at a higher $\overline{q}$. Similar time delay in the T_w oscillation is also found for a step decrease in q. This time delay in T_w obviously results from the thermal inertia of the heated copper plate. Besides, the time lag in the T_w oscillation is shorter for a longer t_p. Similar trend is noted from the data shown in Figs. 11.22-11.30 for a higher G of 400 kg/m^{2}s. Finally, the quantitative data evaluated from the above results are summarized in Tables 11.1 and 11.2 for the oscillation amplitudes of the space-average heated surface temperature and the relative time lag of T_w for various cases tested here.

The corresponding time variations of the space-average flow boiling heat transfer coefficient affected by the imposed heat flux oscillation are also shown in Figs. 11.13–11.30. The results manifest that the flow boiling heat transfer coefficients also oscillate periodically in time and is at the same frequency as the q oscillation. At a higher mean imposed heat flux and for a larger amplitude of the imposed heat flux oscillation, the boiling heat transfer coefficient oscillates stronger.

11.4 Intermittent Boiling

It is of interest to note in the visualization of the boiling flow over the heated copper

plate that for the mean imposed heat flux only slightly above the heat flux corresponding to ONB for the stable boiling, intermittent boiling appears. More specifically, in a typical periodic cycle for given refrigerant mass flux and amplitude and period of the heat flux oscillation bubble nucleation in the heated plate is first seen at a certain time instant after the imposed heat flux is raised to the high level. We have a start of boiling in the flow. Since then the boiling process continues. But after some period following the sudden reduction of the imposed heat flux to a lower level, bubble nucleation disappears and the boiling stops. The above process of intermittent boiling is repeatedly seen in the flow. To be more clear, we indicate the time instants at which boiling starts and stops in Figs. 11.13 – 11.30 for the cases with the presence of the intermittent boiling. Note that at a higher mean imposed heat flux the onset of boiling is earlier and the termination of boiling is later.

A close inspection of the data presented in Figs. 11.13 – 11.30 further reveals that the heat flux for the onset of nucleate boiling for the present transient heating conditions can be significantly higher than that for the stable boiling. Besides, the heat flux for the disappearance of boiling can be much lower than that for the ONB in the stable boiling. It is worth noting that for a higher $\triangle q/\overline{q}$ and/or a longer t_p boiling persists at a heat flux well below q_{ONB} for the stable boiling. Besides, for the present imposed time varying heat flux the heated plate temperature at ONB can be noticeably above or below that for the ONB in stable boiling.

11.5 Effects of Heat Flux Oscillation at Very Short and Long Periods

Due to the thermal inertia of the copper plate, it takes a finite amount of time for the plate to respond to the imposed heat flux oscillation. This in turn causes a time lag in the temporal variations of the space-average temperature of the heated plate, as illustrated above. This time lag becomes longer relative to t_p at a shorter period of the heat flux

oscillation (Tables 11.1 and 11.2). Is it possible that the plate is not able to respond to a fast heat flux oscillation at very small t_p and we have a stable boiling on the plate? This possibility is tested here by reducing t_p to 4 seconds, which is the shortest t_p we can attain in the present experimental facility. The data from this test are shown in Figs. 11.31 and 11.32. These results do indicate that even at a very high imposed heat flux with $\bar{q}$=6.08W/cm^2 and a large $\triangle q/\bar{q}$ of 50% the oscillation amplitude of T_w is only about 0.26^{o}C at t_p=4 seconds(Fig. 11.31(a)). This small amplitude of the T_w oscillation is very close to the background thermal disturbances and the boiling approaches that at steady state. For the lower $\triangle q/\bar{q}$ of 10% and 30% the boiling is essentially at steady state for t_p= 4 seconds.

Then, the time response of the copper plate subject to a very slow heat flux oscillation is explored. The measured data for the temporal variations of the space-average heated surface temperature for selected cases with t_p=60, 120 and 180 seconds are shown in Figs. 11.33 and 11.34. The results for t_p=180 seconds indicate that for the cases with high $\bar{q}$ and low $\triangle q/\bar{q}$ the heated plate temperature at either half cycle of high heat flux level at $\bar{q}+\triangle q$ or low heat flux level at $\bar{q}-\triangle q$ gradually levels off and nearly approaches a steady state value corresponding to the heat flux at that half cycle. Besides, the nearly stable T_w is also very close to that in stable boiling shown in Fig. 11.2.

11.6 Bubble Characteristics

To elucidate the above transient saturated flow boiling heat transfer characteristics, the data for the bubble characteristics of FC-72 obtained from the present flow visualization are examined in the following. The photos taken from the top view of the boiling flow in a small region around the geometric center of the heated surface for various coolant mass fluxes and imposed heat fluxes are shown in Figs. 11.35 - 11.89 for the transient saturated flow boiling. At first, the bubble characteristics for the limiting

cases of constant imposed heat fluxes are illustrated by the photos in Fig. 11.35. It is noted in the flow visualization and the results in Fig. 11.35 that the vapor bubbles begin to appear as the heated surface temperature exceeds the boiling incipient superheat. In the beginning, tiny bubbles are observed in the active nucleation sites. The bubbles grow and then detach from the heated surface with certain mean bubble departure diameters. As the imposed heat flux increases, more bubbles are generated on more active nucleation sites and more bubbles detach from the heated surface. Besides, the detached bubbles tend to merge into larger bubbles. Note that the large bubbles become distorted and elongated as they slide on the heating surface. Moreover, at a higher mass flux the bubbles are smaller and the bubble coalescence is less significant.

Next, the bubble characteristics in the transient flow boiling are illustrated by presenting the photos of the boiling flow at eight selected time instants in a typical periodic cycle in Figures 11.36-11.53 for the cases with the presence of the intermittent boiling for the mean imposed heat flux slightly above that for ONB in the stable boiling. In these figures the symbol " $t=t_o$ " signifies the time instant at the beginning of a periodic cycle in the statistical state. The results clearly indicate that in the first half of the cycle with the copper plate subject to a constant low heat flux level of $\overline{q}-\triangle q$, the number and size of the bubbles at first diminish noticeably with time. Note that the bubbles cease to nucleate from the heated surface at a certain time instant near $t_0+3t_p/8$ and boiling stops completely. Then in the second half of the periodic cycle after the imposed heat flux is raised to the high level of $\overline{q}+\triangle q$ at $t_o + t_p/2$ the plate temperature increases gradually. As the superheat of the plate exceeds certain critical limit at certain later time instant near $t_0+3t_p/4$ bubbles start to nucleate from the heated surface. The precise instant of time at which onset of nucleate boiling occurs depends on $\overline{q}$, t_p and $\triangle q/\overline{q}$. Beyond ONB the number and size of the bubbles increase drastically.

The photos of the boiling flow for the cases with the mean imposed heat flux well above the heat flux at the ONB for the transient saturated boiling are presented in Figs. 11.54 – 11.89. At these higher $\bar{q}$ we have persistent boiling in the flow. The results indicate that in the first half of the periodic cycle with the imposed heat flux at the low level of $q-\triangle q$, the bubble population decreases with time and the bubbles are smaller. The opposite is the case in the second half of the cycle with the imposed heat flux at the high level of $q+\triangle q$. A number of big bubbles are seen in these photos. They are formed from the merging of small bubbles. These changes in the bubble characteristics are more significant at a higher amplitude of the heat flux oscillation and at a higher mean imposed heat flux.

To quantify the bubble characteristics, the measured data for the time variations of the space-average bubble departure diameter and frequency and active nucleation site density in a typical periodic cycle are given in Figs. 11.90 – 11.134 for various coolant mass fluxes, amplitudes and periods of the imposed heat flux oscillations, and mean imposed heat fluxes.

The results in Fig. 11.90(a) for $\triangle q=0$ indicate that the mean size of the bubbles departing from the copper plate is somewhat smaller for the mass flux raised from 300 to 400 kg/m^{2}s in the stable flow boiling. It reflects the fact that the coolant at a higher mass flux and hence at a higher speed tends to sweep the bubbles more quickly away from the heating surface. Now as the imposed heat flux oscillation is at a low amplitude of 10%, the bubble departure diameter varies slightly with time (Figs. 11.90(b) – (d)). More specifically, the size of the departing bubbles decreases in the first half of the periodic cycle in which the heat flux is at the low level of $\bar{q}-\triangle q$. While in the second half of the cycle an opposite process is noted since the imposed heat flux is maintained at the high level of $\bar{q}+\triangle q$. Besides, at a higher imposed heat flux the departing bubbles are larger.

Similar trend is noted in Figs. 11.91 and 11.92 for higher $\triangle q/\bar{q}$ of 30% and 50%. Comparing the results in Fig. 11.90 with Figs. 11.91 and 11.92 indicates that at the larger amplitude of the heat flux oscillation the effects of the imposed heat flux on the bubble departure diameter are somewhat stronger. Similar trend is noted in Figs. 11.93-11.95 for a higher coolant mass flux of 400 kg/m^{2}s. The effects of the coolant mass flux on the time variations of d_p are further illustrated in Figs. 11.96 – 11.98. Moreover, an increases in the period of the heat flux oscillation causes a larger variation of the bubble departure diameter with time (Figs. 11.99 – 11.104).

Next, the data for the variations of the space-average bubble departure frequency with time for various cases are shown in Figs 11.105 – 11.119. In the stable flow boiling the increase in the bubble departure frequency with the imposed heat flux and coolant mass flux is clearly seen (Fig. 11.105(a)). The increase of f with G is ascribed again to the higher drag on the bubbles attaching to the heated surface by the liquid coolant moving at a higher speed for a higher G. This in turn, causes an earlier departure of the bubbles from the surface, resulting in a higher departure frequency. For a oscillation heat flux the bubbles depart from the heated surface at a decreasing rate in the first half of the periodic cycle in which the imposed heat flux is at the low level. Apparently, in the second half of the cycle in which the imposed heat flux is at the high level the bubble departing rate increases. It should be pointed out that the time variations of the bubble departure frequency are stronger for a longer period and a higher amplitude of the imposed heat flux oscillation and for a higher mean imposed heat flux. But the effects of the coolant mass flux on the time variation of the bubble departure frequency are relatively milder. Obviously, the bubble departure frequency is higher for a higher G..

Finally, the space-average active nucleation site density on the heated surface affected by the imposed heat flux oscillation is illustrated in Figs 11.120 – 11.134. The results in Fig. 11.120(a) indicate that in stable flow boiling the active nucleation site

density increases substantially with the imposed heat flux. But the increase is rather mild for the mass flux reduced from 400 to 300 kg/m^{2}s. Note that in the transient flow boiling the active nucleation site density decreases with time in the first half of the periodic cycle in which the imposed heat flux is at the low level. The reverse process appears in the second half of the cycle in which the heat flux is at the high level. At a longer period and a higher amplitude of the heat flux oscillation and at a higher mean imposed heat flux the temporal variations of N_{ac} is stronger. Besides, at a lower coolant mass flux the time variations of N_{ac} is slightly larger. A boiling regime map to delineate various states of the present transient saturated flow boiling is shown in Fig. 11.136.

11.7 Correlation Equations

According to the present experimental data, an empirical correlation for the space-average bubble departure diameters in the FC-72 stable saturated flow boiling on the heated circular copper flat plate flush mounted on the bottom of the rectangular channel estimated from the present flow visualization is proposed as

$$\frac{d_p}{\sqrt{\sigma/g\cdot\Delta\rho}} = \frac{0.2\cdot(\rho_l/\rho_v)^{0.6}\cdot Bo^{0.35}}{Re_D^{\,0.04}} \quad \text{for stable flow boiling}$$

(11.4)

where Re_D and Bo are the Reynolds and Boiling numbers, respectively, They are defined as

$$Re_D = \frac{G\cdot D}{\mu_l} \tag{11.5}$$

$$Bo = \frac{q''}{G\cdot i_{lv}} \tag{11.6}$$

Figures 11.135 show that the present experimental data fall within ± 20 % of the correlation given in Equation (11.4). In addition, an empirical equation is provided to

correlate the data for the space-average bubble departure frequency as

$$\frac{f \cdot d_p}{\mu_l/\rho_l \cdot D_h} = 0.52 Re_D^{1.32} \cdot Pr^{0.75} \cdot Bo^{0.68} \quad \text{for stable flow boiling} \tag{11.7}$$

Figures 4.136 reveal that the present experimental data for $f \cdot d_p$ can be correlated with the deviation less than ± 20 % by the above equation. Moreover, an empirical correlation for the space-average active nucleation site density in the FC-72 saturated flow boiling deduced from the present flow visualization is proposed as

$$N_{ac} \cdot d_p^{\,2} = -0.065 + (85 \cdot Bo^{0.84} \cdot Re_D^{-0.12}) \quad \text{for stable flow boiling} \tag{11.8}$$

The comparison in Figs. 11.137 shows that the present experimental data fall within ± 30 % of the correlation given in Equation (11.8). Finally, the total heat flux input to the stable boiling flow q_t is considered to be roughly composed of two parts: one resulting from the bubble nucleation q_b and another due to the single phase forced convection q_c. Thus

$$q_t = q_b + q_c \tag{11.9}$$

Here q_b and q_c can be individually calculated from the quantitative data for the bubble characteristics examined in section 4.6 and single-phase liquid forced convection as

$$q_b = \rho_v \cdot V_v \cdot f \cdot N_{ac} \cdot i_{lv} \tag{11.10}$$

where ρ_v is the vapor density, V_v is the vapor volume of the mean departing bubble defined as $\frac{4\pi}{3}(\frac{d_p}{2})^3$, f is the space-average bubble departure frequency, N_{ac} is the space-average active nucleation site density, i_{lv} is the enthalpy of vaporization, and

$$q_c = E \cdot h_{l\phi} \cdot \Delta T_{sat} \tag{11.11}$$

where E is an enhancement factor added to account for the agitating motion of the bubbles which can enhance the single-phase liquid convection heat transfer. From the experimental data, E can be empirically correlated as

$$E = 4.5 \cdot N_{conf}{}^{0.5} \cdot Fr_l^{0.15} \cdot (1 + 280 \cdot Bo)^{1.8} \quad \text{for stable flow boiling} \tag{11.12}$$

here Fr_l is the Froude number and N_{conf} is the Confinement number. They are respectively defined as

$$N_{conf} = \frac{(\sigma/g \cdot \Delta\rho)^{0.5}}{D_h} \tag{11.13}$$

and

$$Fr_l = \frac{G^2}{\rho_l{}^2 \cdot g \cdot D_h} \tag{11.14}$$

where g is the acceleration due to gravity, D_h is the hydraulic diameter of the test section, and ΔT_{sat} (= T_w - T_{sat}) is the wall superheat. The results shown in Figure 11.138 indicate that the present data can be correlated with the deviation less than $\pm 25\%$ by the empirical correlation given in Equations (11.9) - (11.14).

Table 11.1 Amplitudes of heated surface temperature oscillation and time lag in transient oscillatory saturated flow boiling for various imposed heat fluxes and amplitudes and periods of the heat flux oscillation at G = 300kg/m^{2}s.

$\Delta q/\bar{q}$	G = 300kg/m^{2}s			
	Period t_p(sec)	$\bar{q}$ (W/cm^2)	ΔT_w (K)	t_l/t_p
±10%	10	0.80	0.18	0.15
		2.51	0.31	0.13
		4.31	0.43	0.09
		6.14	0.52	0.072
	20	0.82	0.32	0.0385
		2.48	0.51	0.0345
		4.32	0.52	0.0235
		6.14	0.55	0.018
	30	0.80	0.51	0.0173
		2.49	0.88	0.0156
		4.25	0.69	0.0106
		6.04	0.68	0.0083
±30%	10	0.80	0.42	0.149
		2.49	0.79	0.131
		4.30	0.88	0.09
		6.16	0.95	0.07
	20	0.82	0.65	0.0365
		2.50	1.45	0.0325
		4.37	1.57	0.0225
		6.20	1.64	0.0175
	30	0.79	0.83	0.016
		2.44	2.44	0.0146
		4.18	1.69	0.0103
		5.90	1.74	0.008
±50%	10	0.81	0.52	0.148
		2.50	1.04	0.128
		4.34	1.43	0.088
		6.10	1.73	0.068
	20	0.83	0.86	0.0365
		2.51	2.44	0.032
		4.41	2.51	0.0225
		6.19	2.88	0.017
	30	0.77	1.21	0.016
		2.38	3.91	0.0133
		4.11	3.18	0.01
		5.81	3.29	0.0076

Table 11.2 Amplitudes of heated surface temperature oscillation and time lag in transient oscillatory saturated flow boiling for various imposed heat fluxes and amplitudes and periods of the heat flux oscillation at G = 400kg/m^{2}s.

$\Delta q/\bar{q}$	G = 400kg/m^{2}s			
	Period t_p(sec)	$\bar{q}$ (W/cm^2)	ΔT_w (K)	t_l/t_p
±10%	10	0.82	0.13	0.143
		2.51	0.24	0.128
		4.32	0.35	0.093
		6.13	0.41	0.072
	20	0.83	0.26	0.035
		2.52	0.67	0.031
		4.33	0.70	0.0235
		6.14	0.76	0.018
	30	0.81	0.36	0.015
		2.49	0.84	0.0136
		4.27	0.71	0.0103
		6.06	0.79	0.008
±30%	10	0.83	0.24	0.141
		2.53	0.58	0.126
		4.33	0.94	0.091
		6.11	1.02	0.071
	20	0.83	0.65	0.0345
		2.54	1.98	0.0305
		4.35	2.13	0.0245
		6.21	2.08	0.0185
	30	0.79	0.83	0.0146
		2.45	2.59	0.0133
		4.17	2.18	0.01
		5.95	2.24	0.008
±50%	10	0.81	0.54	0.137
		2.54	1.19	0.123
		4.34	1.49	0.09
		6.10	1.75	0.069
	20	0.84	1.32	0.033
		2.54	3.31	0.0295
		4.38	3.41	0.0215
		6.23	3.36	0.017
	30	0.79	1.43	0.0133
		2.42	4.32	0.012
		4.10	3.87	0.0093
		5.81	3.86	0.0073

CHAPTER 12

CONCLUDING REMARKS

12.1 Concluding Remarks

We have carried out experiments to unravel the refrigerants R-134a, R-407C and R-410A and dielectric coolant FC-72 time periodic flow boiling heat transfer characteristics (including subcooled and saturated boiling and evaporation heat transfer) and associated bubble characteristics in a horizontal narrow annular duct due to an imposed flow rate or heat flux oscillation. The effects of the refrigerant saturated temperature, inlet subcooling, vapor quality, gap size, and mean level, amplitude and period of the mass flux or heat flux oscillation on the temporal boiling heat transfer characteristics have been examined in detail. A summary of the major findings from the present results is given in the following.

12.1.1 Concluding remarks for mass flux oscillation

(1). The time-average boiling curves and heat transfer coefficients for the time periodic saturated and subcooled flow boiling and evaporation of refrigerants R-134a, R-407C and R-410A and dielectric coolant FC-72 are not affected to a noticeable degree by the amplitude and period of the refrigerant mass flux or imposed heat flux oscillation.

(2). For the mass flux oscillation the resulting heated pipe wall temperature, bubble departure diameter and frequency, and active nucleation site density also oscillate periodically in time and at the same frequency as the mass flux oscillation. Data also show that the oscillation amplitude of the wall temperature gets larger for a longer period and a larger amplitude of the mass flux oscillation. Besides for a larger amplitude of the mass flux oscillation, stronger oscillations in the bubble characteristics, such as d_p, f and n_{ac}, are noted. But f and n_{ac} are only slightly affected by the period of the mass flux oscillation. A short time lag in the heated wall temperature oscillation is also noted. Moreover, the bubbles become smaller and more dispersed when the refrigerant mass flux increases with time. The opposite processes take place for a decreasing refrigerant mass flux. Furthermore, reductions in the size of the departing bubbles and in the active nucleation site density and augmentation in the bubble departure frequency result in the time duration the mass flux is rising. When the mass flux is sinking the opposite processes occur.

(3). For the mass flux oscillation the resulting heated pipe wall temperature and evaporating flow pattern also oscillate periodically in time and at the same frequency as the mass flux

oscillation. Experiments also show that the resulting oscillation amplitudes of the wall temperature get larger for a longer period and a larger amplitude of the mass flux oscillation. A significant time lag in the wall temperature oscillation is also noted. Moreover, at the intermediate vapor quality changes in the evaporating flow patterns between that dominated by the nucleation bubbles and liquid film take place cyclically. Furthermore, after the time lag the heated pipe wall temperature decreases and the evaporation heat transfer gets better as the mass flux decreases in the first half of the periodic cycle. In the second half of the cycle in which the mass flux increases the opposite processes occur. These unusual changes of the heating surface temperature and heat transfer coefficient with the mass flux oscillation are attributed to the strong effects of the mass flux oscillation on the state of the refrigerant at the duct inlet and hence on the changes of the vapor quality and liquid film thickness in the evaporating flow.

(4). Increases in the bubble departure size and active nucleation site density at decreasing refrigerant mass flux overwhelms the bubble departure frequency. This in turn causes an increase in the latent heat transfer and a drop in the heated wall temperature in the boiling flow at decreasing G, opposite to that in the single-phase flow.

(5). When the imposed heat flux over the heated surface is close to the heat flux corresponding to that for the onset of stable flow boiling, intermittent flow boiling appears. But the intermittent flow boiling exists in narrow ranges of the experimental parameters in the subcooled flow boiling. Flow regime maps and empirical correlations are given to delineate the boundaries separating different flow regimes in the annular duct for both saturated and subcooled flow boiling.

(6). The temporal variations of the heat transfer coefficient and associated bubble characteristics in the time periodic refrigerants R-134a, R-407C and R-410A and dielectric coolant FC-72 subcooled flow boiling affected by the refrigerant mass flux oscillation qualitatively resemble those for the time periodic saturated flow boiling. Some differences do exist. An increase in the inlet liquid subcooling results in stronger oscillations in the boiling heat transfer coefficient and heated surface temperature.

12.1.2 Concluding remarks for heat flux oscillation

(1). In the refrigerants R-134a, R-407C and R-410A and dielectric coolant FC-72 time periodic flow boiling subject to the imposed heat flux oscillation, the heated pipe wall temperature, bubble departure diameter and frequency, and active nucleation site density also oscillate periodically in time and at the same frequency as the heat flux oscillation. Experiments also show that the resulting oscillation amplitudes of the heated surface temperature and heat

transfer coefficient and bubble parameters, such as d_p, f and n_{ac}, get larger for a longer period and a larger amplitude of the imposed heat flux oscillation and for a higher mean imposed heat flux. An increase in the inlet liquid subcooling results in stronger oscillations in the boiling heat transfer coefficient and heated surface temperature. Moreover, a significant time lag in the heated copper duct surface temperature oscillation is also noted, which apparently results from the thermal inertia of the copper duct. The nondimensional time lag, defined as the ratio of the time lag to the period of the imposed heat flux oscillation, is longer at a lower mean imposed heat flux and a shorter period and for a larger amplitude of the imposed heat flux oscillation when its amplitude is below 30%. Furthermore, the bubbles become smaller and more dispersed after the time lag when the imposed heat flux and heated wall temperature decrease with time. The opposite processes take place at increasing heat flux. Finally, reductions in the size of the departing bubbles, the bubble departure frequency and active nucleation site density result in the time duration the heat flux is sinking. When the heat flux is rising the opposite processes occur.

(2). For the heat flux oscillation the resulting heated pipe wall temperature and evaporating flow pattern also oscillate periodically in time and at the same frequency as the heat flux oscillation. Experiments also show that the resulting wall temperature oscillation is stronger for a longer period and a larger amplitude of the imposed heat flux oscillation and for a higher mean imposed heat flux. A significant time lag in the heated surface temperature oscillation is also noted, which apparently results from the thermal inertia of the copper inner pipe. The nondimensional time lag, defined as the ratio of the time lag to the period of the imposed heat flux oscillation, is longer at a lower mean imposed heat flux and a shorter period. Moreover, at the intermediate vapor quality changes in the evaporating flow patterns between that dominated by the nucleation bubbles and by the liquid film take place cyclically. Furthermore, after the time lag the heated pipe wall temperature decreases and the evaporation heat transfer gets worse as the heat flux decreases in the first half of the periodic cycle. In the second half of the cycle in which the heat flux increases the opposite processes occur. These changes of the heating surface temperature and heat transfer coefficient with the heat flux oscillation are attributed to the strong effects of the heat flux oscillation on the changes of the vapor quality and liquid film thickness in the evaporating flow.

(3). The effects of the heat flux oscillation at extremely short and long periods have been explored. Due to the existence of the thermal inertia of the heated copper duct, the resulting heated surface temperature does not oscillate with time and is close to that in the stable boiling at an extremely short period of the imposed heat flux oscillation. But the oscillation

amplitude of the heated surface temperature gets noticeably stronger for an extremely long period of the imposed heat flux oscillation.

(4). When the imposed heat flux over the heated surface is close to the heat flux corresponding to that for the onset of stable flow boiling, intermittent flow boiling appears. But the intermittent boiling exists in narrower ranges of the experimental parameters in the subcooled flow boiling. Flow regime maps and empirical correlations are also given to delineate the boundaries separating different boiling flow regimes in the annular duct.

Finally during the present study four articles have been published in the International Journal of Heat and Mass Transfer up to this point. They are included here for more detailed reference of the boiling of R-134a, R-407C and R-410A in an annular duct and FC-72 in a rectangular duct.

1. C.A. Chen, W.R. Chang, K.W. Li, Y.M. Lie, T.F. Lin, Subcooled flow boiling heat transfer of R-407C and associated bubble characteristics in a narrow annular duct, International Journal of Heat and Mass Transfer 52 (2009) 3147-3158.

2. C.A. Chen, C.Y. Lee, T.F. Lin, Experimental study of evaporation heat transfer of R-134a in a narrower annular duct, International Journal of Heat and Mass Transfer 53 (2010) 2218-2228.

3. C.A. Chen, W.R. Chang, T.F. Lin, Time periodic flow boiling heat transfer of R-134a and associated bubble characteristics in a narrow annular duct due to flow rate oscillation, International Journal of Heat and Mass Transfer 53 (2010) 3593-3606.

4. W.R. Chang, C.A. Chen, J.H. Ke, T.F. Lin, Subcooled flow boiling heat transfer and associated bubble characteristics of FC-72 on a heated micro-pin-finned silicon chip, International Journal of Heat and Mass Transfer 53 (2010) 5605-5621.

REFERENCES

1. S. G. Kandlikar, and W. J. Grande, Evolution of microchannel flow passages-thermohydraulic performance and fabrication technology, Heat Transfer Engineering, 24(1)(2003)3-17.

2. P. A. Kew and K. Cornwell, Correlations for the prediction of boiling heat transfer in small-diameter channels, Applied Thermal Engineering 17(1997)705-715.

3. Y. Y. Hsieh, Y. M. Lie and T. F. Lin, Saturated flow boiling heat transfer of refrigerant R-410A in a horizontal annular finned duct, International Journal of Heat and Mass Transfer, 50(2007)1442-1454

4. C. C. Wang, W. T. Shieh, Y. J. Chang, An experimental study of convective boiling of refrigerants R-22 and R-410A, ASHRAE Trans. 121 (1998) 1144-1150.

5. T. Ebisu, K. Torikoshi, Heat transfer characteristics and correlations for R-410A flowing inside a horizontal smooth tube, ASHRAE Trans. 121 (1998) 556-561.

6. Y. Fujita, Y. Yang and N. Fujita, Flow boiling heat transfer and pressure drop in uniformly heated small tubes, Proceedings of the Twelfth International Heat Transfer Conference 3(2002)743-748.

7. F. C. Hiseh, K. W. Lin, Y. M. Lie, C. A. Chen, and T. F. Lin, Saturated flow boiling heat transfer of R-407C and associated bubble characteristics in narrow annular duct, International Journal of Heat and Mass Transfer, 51 (2008) 3763-3775.

8. Y. M. Lie and T. F. Lin, Saturated flow boiling heat transfer and associated bubble characteristics of R-134a in a narrow annular duct, International Journal of Heat and Mass Transfer 48(25-26)(2005)5602-5615.

9. Y. M. Lie and T. F. Lin, Subcooled flow boiling heat transfer and associated bubble characteristics of R-134a in a narrow annular duct, International Journal of Heat and Mass Transfer, 49 (2006) 2077-2089.

10. Z. Y. Bao, D. F. Fletcher and B. S. Haynes, Flow boiling heat transfer of Freon R11 and HCFC123 in narrow passages, International Journal of Heat and Mass Transfer 43(18)(2000)3347-3358.

11. T. N. Tran, M. W. Wambsganss and D. M. France, Small circular- and rectangular-channel boiling with two refrigerants, International Journal of Multiphase Flow 22(1996)485-498.

12. S. G. Kandlikar and M. E. Steinke, Flow boiling heat transfer coefficient in

minichannels – correlation and trends, Proceedings of the Twelfth International Heat Transfer Conference, vol.3(2002)785-790.

13. H. Oh, M. Katsuta and K. Shibata, Heat transfer characteristics of R134a in a capillary tube heat exchanger, Proceedings of 11th International Heat Transfer Conference, Vol. 6,1998, pp.131-136.

14. C. P. Yin, Y. Y. Yan, T. F. Lin, and B. C. Yang, Subcooled flow boiling heat transfer of R-134a and bubble characteristics in a horizontal annular duct, International Journal of Heat and Mass Transfer, 43 (2000) 1885-1896.

15. C. A. Chen, W. R. Chang, K. W. Li, Y. M. Lin, and T. F. Lin, Subcooled flow boiling heat transfer of R-407C and associated bubble characteristics in a narrow annular duct, International Journal of Heat and Mass Transfer, 52 (2009) 3147-3158.

16. O. Comakli, S. Karsli, and M. Yilmaz, “Experimental investigation of two phase flow instabilities in a horizontal in-tube boiling system,” Energy Conversion and Management 43 (2002) 249-268

17. S. Kakac, T. N. Veziroglu, M. M. Padki, L. Q. Fu, and X. J. Chen, “Investigation of Thermal Instabilities in a Forced Convection Upward Boiling System,” Experimental Thermal and Fluid Science 3 (1990) 191-201.

18. Y. Ding, S. Kakac, and X. J. Chen, “Dynamic Instabilities of Boiling Two-Phase Flow in a Single Horizontal Channel,” Experimental Thermal and Fluid Science 11 (1995) 327-342.

19. Q. Wang, X. J. Chen, S. Kakac, and Y. Ding, “Boiling Onset Oscillation : a new type of Dynamic Instability in a Forced-Convection Upflow Boiling System,” International Journal of Heat and Fluid Flow 17(1996) 418-423

20. M Ozawa, H Umekawa, Y Yoshioka and A Tomiyama, Dryout under oscillatory flow condition in vertical and horizontal tubes : experiments at low velocity and pressure conditions, International journal of heat and mass transfer, 36 (1983) 4076-4078.

21. I. Kataoka, A. Serizawa and A. Sakurai, “Transient Boiling Heat Transfer Under Forced Convection,” International Journal of Heat and Mass Transfer 26 (1983) 583-595.

22. S. Lin, P.A. Kew and K. Cornwell, “Two-Phase Heat Transfer to a Refrigerant in a 1mm Diameter Tube,” International Journal of Refrigeration 24 (2001) 51-56.

23. P. R. Mawasha and R. J. Gross, “Periodic Oscillations in a Horizontal Single Boiling

Channel with Thermal Wall Capacity," International Journal of Heat and Fluid Flow 22 (2001) 643-649.

24. P. R. Mawasha, R. J. Gross, and D. D. Quinn, "Pressure-Drop Oscillations in a Horizontal Single Boiling Channel," Heat Transfer Engineering 22 (2001) 26-34.

25. K. Cornwell and P. A. Kew, Boiling in small parallel channels, Energy Efficiency in Process Technology, P.A. Pilavachi, Elsevier Applied Science, London, 1993, pp. 624-638.

26. R. Situ, Y. Mi, M. Ishii and M. Mori, Photographic study of bubble behaviors in forced convection subcooled boiling, International Journal of Heat and Mass Transfer 47(2004)3659-3667.

27. G. E. Thorncroft, J. F. Klausner and R. Mei, An experimental investigation of bubble growth and detachment in vertical upflow and downflow boiling, International Journal of Heat and Mass Transfer 41 (1998) 3857-3871

28. S. G. Kandlikar, "Bubble Nucleation and Growth Characteristics in Subcooled Flow Boiling of Water," National Heat Transfer Conference HTD-Vol. 342 4 (1997) 11-18

29. S. H. Chang, I. C. Bang and W. P. Baek, A photographic study on the near-wall bubble behavior in subcooled flow boiling, International Journal of Thermal Science 41(2002)609-618.

30. Victor H. Del Balle M. and D. B. R. Kenning, Subcooled flow boiling at high heat flux, International Journal of Heat and Mass Transfer 28(10)(1985)1907-1920

31. R. Maurus, V. Ilchenko and T. Sattelmayer, Automated high-speed video analysis of the bubble dynamics in subcooled flow boiling, International Journal of Heat and Fluid Flow 25(2004)149-158.

32. T. Okawa, T. Ishida, I. Kataoka and M. Mori, An experimental study on bubble rise path after the departure from a nucleation site in vertical upflow boiling, Experimental Thermal and Fluid Science 29(2005)287-294.

33. J. C. Chen, A correlation for boiling heat transfer to saturated fluids in convective flow, Ind. Engng. Chem. Proc. Des. Dev. 5(1966)322-329.

34. F. W. Dittus and L. M. K. Boelter, Heat transfer in automobile radiator of the tube type, Publication in Engineering, University of California, Berkley, 2(1930)250.

35. K. E. Gungor and R. H. S. Winterton, A general correlation for flow boiling in tubes and annuli, International Journal of Heat and Mass Transfer 29(1986)351-358.

36. Z. Liu and R. H. S. Winterton, A general correlation for saturated and subcooled flow boiling in tubes and annuli, based on a nucleate pool boiling equation, International Journal of Heat and Mass Transfer 34(1991)2759-2766.

37. W. Zhang, T. Hibiki and K. Mishima, Correlation for flow boiling heat transfer in mini-channels, International Journal of Heat and Mass Transfer 47(2004)5749-5763.

38. G. M. Lazarek and S. H. Black, Evaporative heat transfer, pressure drop and critical heat flux in a small vertical tube with R-113, International Journal of Heat and Mass Transfer, 25(7)(1982)945-960.

39. S. G. Kandlikar, A general correlation for two-phase flow boiling heat transfer coefficient inside horizontal and vertical tubes, Journal of Heat Transfer 102(1990)219-228.

40. S. G. Kandlikar, A model for predicting the two-phase flow boiling heat transfer coefficient in augmented tube and compact heat exchanger geometries, Journal of Heat Transfer 113(1991)966-972.

41. S. G. Kandlikar and P. Balasubramanian, An extension of the flow boiling correlation to transition, laminar, and deep laminar flows in minichannles and microchannels, Heat Transfer Engineering 25(2004)86-93.

42. S. W. Churchill and H. H. S. Chu, Correlating equations for laminar and turbulent free convection from a horizontal cylinder, International Journal of Heat and Mass Transfer 18(1975)1049-1053.

43. S. J. Kline and F. A. McClintock, Describing uncertainties in single-sample experiments, Mech. Eng. 75(1)(1953)3-12.

44. V. Gnielinski, New equations for heat and mass transfer in turbulent pipe and channel flow, International Chemical Engineering 16(2)(1976)359-368.

45. C. A. Chen, Time periodic flow boiling heat transfer of refrigerant R-134a in a horizontal annular duct due to flow rate or heat flux oscillation, Ph.D thesis, National Chiao Tung University, Hsinchu, Taiwan (2010).

可供推廣之研發成果資料表

☐ 可申請專利　☐ 可技術移轉　　日期：__年__月__日

國科會補助計畫	計畫名稱：冷媒流量和熱通量振盪引起之暫態新冷媒和 FC-72 流動沸騰研究 計畫主持人：　林清發　教授 計畫編號：NSC 96-2221-E-009-133-MY3　學門領域：機械熱流
技術/創作名稱	
發明人/創作人	
技術說明	中文： （100~500 字）
	英文：
可利用之產業及可開發之產品	
技術特點	
推廣及運用的價值	

※　1. 每項研發成果請填寫一式二份，一份隨成果報告送繳本會，一份送　貴單位研發成果推廣單位（如技術移轉中心）。

※　**2. 本項研發成果若尚未申請專利，請勿揭露可申請專利之主要內容。**

※　3. 本表若不敷使用，請自行影印使用。